Terms and Conditions of Use of Digitised Theses from Trinity College Library Dublin

Copyright statement

All material supplied by Trinity College Library is protected by copyright (under the Copyright and Related Rights Act, 2000 as amended) and other relevant Intellectual Property Rights. By accessing and using a Digitised Thesis from Trinity College Library you acknowledge that all Intellectual Property Rights in any Works supplied are the sole and exclusive property of the copyright and/or other IPR holder. Specific copyright holders may not be explicitly identified. Use of materials from other sources within a thesis should not be construed as a claim over them.

A non-exclusive, non-transferable licence is hereby granted to those using or reproducing, in whole or in part, the material for valid purposes, providing the copyright owners are acknowledged using the normal conventions. Where specific permission to use material is required, this is identified and such permission must be sought from the copyright holder or agency cited.

Liability statement

By using a Digitised Thesis, I accept that Trinity College Dublin bears no legal responsibility for the accuracy, legality or comprehensiveness of materials contained within the thesis, and that Trinity College Dublin accepts no liability for indirect, consequential, or incidental, damages or losses arising from use of the thesis for whatever reason. Information located in a thesis may be subject to specific use constraints, details of which may not be explicitly described. It is the responsibility of potential and actual users to be aware of such constraints and to abide by them. By making use of material from a digitised thesis, you accept these copyright and disclaimer provisions. Where it is brought to the attention of Trinity College Library that there may be a breach of copyright or other restraint, it is the policy to withdraw or take down access to a thesis while the issue is being resolved.

Access Agreement

By using a Digitised Thesis from Trinity College Library you are bound by the following Terms & Conditions. Please read them carefully.

I have read and I understand the following statement: All material supplied via a Digitised Thesis from Trinity College Library is protected by copyright and other intellectual property rights, and duplication or sale of all or part of any of a thesis is not permitted, except that material may be duplicated by you for your research use or for educational purposes in electronic or print form providing the copyright owners are acknowledged using the normal conventions. You must obtain permission for any other use. Electronic or print copies may not be offered, whether for sale or otherwise to anyone. This copy has been supplied on the understanding that it is copyright material and that no quotation from the thesis may be published without proper acknowledgement.

NEW BIOCHIPS FOR A THREE-DIMENSIONAL STUDY OF TRANSENDOTHELIAL LEUKOCYTE MIGRATION

A thesis presented to the University of Dublin for the degree of Doctor of Philosophy

Stéphanie Toetsch

Supervisors

Professor Yuri Volkov – Department of Clinical Medicine

Professor Igor Shvets – School of Physics

Ph. D 2011

DECLARATION

I declare that the present work has not previously been submitted as an exercise for a degree at this or any other University. It consists entirely of my own work, except where references indicate otherwise.

The library of Trinity College Dublin may lend or copy this thesis on request.

Stéphanie Toetsch

ABSTRACT

An important step in the inflammatory response is the recruitment of leukocytes into tissues through the endothelial cells which line blood vessels. Transendothelial migration (TEM) is the result of a multistep cascade in which chemoattractant gradients mediate the migration of leukocytes through the endothelial wall and into the underlying tissue.

The leukocyte transendothelial migration is a small part of the processes that comprises the immune system. However cell migration through the endothelium plays a role in the progression of diverse diseases, such as cancer metastasis and atherosclerosis, or physiological processes, such as embryonic morphogenesis and wound healing. It is necessary to understand the mechanisms of this migration in order to establish, through research, how to support, supplement and improve its function.

Consequently there are numerous *in vitro* assays which attempt to mimic chemotactic gradients. The majority of these assays have limitations as they take place in the absence of flow with no precise control over the concentration of the chemokine gradient. However, in recent times the design of the standard chemotaxis assay has been reconsidered in order to incorporate modern microfluidic platforms, computer controlled flow devices and cell tracking software. Assays under fluid flow which use biochips have provided data highlighting the importance of shear stress on cell attachment and migration towards a chemokine gradient. However, the *in vivo* environment is much more complex than that which is found in conventional cell assay chambers and 2-dimensional biochips. To reproduce realistic *in vivo* conditions, microfluidic biochips must present an environment capable of replicating the release of a chemokine gradient from tissues through the endothelium, such as occurs at sites of inflammation.

The aims of this thesis are to a) develop an engineered microenvironment for leukocyte migration studies closely imitating physiological conditions, b) generate an equivalent of natural chemokine gradient in a tissue-mimicking matrix and c) assess the migration

of leukocytes towards a gradient of chemokine in real time under precision controlled flow conditions.

We developed and comprehensively evaluated four prototypes of new microfluidic biochips designs. We have concluded that these designs were not entirely suitable for sophisticated chemotactic assays. However, considering the complexity of the challenges involved across physics, engineering and immunology, we believe the work presented here will be of considerable significant interest to those who take up the challenge to create ever more realistic biochip.

ACKNOWLEDGEMENTS

In science, Luck is not taking into account to explain a process, a mechanism or an observation. However, I have to say that without Luck I could not have finished and presented such a challenging work!

I was lucky because the people I was working with, from the first moment until the end of my work, encouraged me and listened to me even when I felt that I would never have enough strength to finish what I had started.

First, I would like to thank Professor Dermot Kelleher, Director of the Institute of Molecular Medicine, for the great chance to join his high-level research group.

I would like to express my appreciation to my both supervisors for giving me such a great opportunity to work in a multidisciplinary field. Professor Yuri Volkov helped me to understand the intricacies of biological processes which were mainly unknown to me. His patience during the past four years and his availability whenever I knocked on his door were a real encouragement to me. Professor Igor Shvets introduced me to the incredible field of microfluidic biochips and gave me the chance to express my creativity. I would also like to express my gratitude to Dr Aideen Long for her advice about researches but also life.

The Luck also came from the unlimited support of the post-docs of our lab. I would like to express my special thanks to Dr Peter Olwell who was always there to listen to my (also unlimited) questions and doubts. Without his belief in me, I would have been back in my country long time ago. Dr Anthony Davies is another key person in "my story" who took part in my rescue when I had deep doubts! The energetic Dr Adriele Prina-Mello helped me with his positive waves (seriously!), but more specifically with his broad knowledge in physics. Dr Eugene Dempsey was not directly involved in my research project, but was as much supportive as if he was part of it!

Special thanks go to Ruchika. Since I have known her, she has been another key person who has always been there to listen to me or... laugh at me! And that was exactly what I

needed from time to time! And when I was homesick, Danijela was the one who understood the difficulty of being far from my "home sweet home". Many thanks go to Jen for her help with the confocal microscope and her ever good mood, to Fifi for being a great friend and many more "sweet" persons such as the flawless Anne-Marie, the untiring Mike, the coolest ever Dara, the lovely Ruth, the nanoparticles Gosia, the discrete but unforgettable Stephen Paul, and all the girls from the lab beside ours: Sinead, Seónadh, Avril, Seow Theng, Antje, Emily, Deirdre, Mary and "umbilical cords" Martina! Many thanks to the Cellix Ltd team, especially to Dmitry and Frank who were "really" patient with my questions in physics.

Then, we have all the "indescribable" labmates: from our "spagnol" (Ramon) who left us for a bit of sun back in his hometown Madrid to our break dancer Steve, or the facebooker Kunal. Special "hello" to Connla!

Sincere thanks go to my friends with whom I shared this experience, here and abroad, this constant support was really important to me and was an immense resource of energy.

Finally, I would like to thank and express my infinite gratitude to my family for encouraging me and also for standing for my fears, doubts and frustrations about my work, my homesickness, and the life! This constant support was an immeasurable resource of energy and comfort. I deeply thank them.

I am lucky for having shared such challenging scientific experience but also life experience with all these unforgettable persons.

I would like to acknowledge my funding source: the Science Foundation of Ireland.
I would also like to acknowledge Trinity Trust for its generous contribution towards the Travel Grants which supported my attendance at the SBS Conference in Montreal.

Special acknowledgements go to Dr Prina-Mello for the simulation he made with the COMSOL software, to Martina Gogarty who isolated umbilical cords for the culture of HUVEC cells and to Jennifer Conroy for the assays with the confocal microscope.

PUBLICATION AND PRESENTATIONS

Journal Publication

Stephanie Toetsch, Peter Olwell, Adriele Prina-Mello, Yuri Volkov. 2009. The evolution of chemotaxis assays from static models to physiologically relevant platforms. *Integrative Biology*, **1**, 170-181.

Poster Presentations and Awards

Stephanie Toetsch, Peter Olwell, Eugene Dempsey, Dermot Kelleher, Dmitry Kashanin, Frank O'Dowd, Igor Shvets, Yuri Volkov. 2007. New biochips for a 3-D study of transendothelial leukocyte migration. *13th Society for Biomolecular Sciences exhibition and conference*, April 2007, Montreal, Canada.

Awarded as Best Poster 2007.

Stephanie Toetsch, Peter Olwell, Eugene Dempsey, Dermot Kelleher, Dmitry Kashanin, Frank O'Dowd, Igor Shvets, Yuri Volkov. 2007. New biochips for a 3-D study of transendothelial leukocyte migration. *10th Annual Meeting of the Institute of Molecular Medicine*, October 2007, Dublin, Ireland.

Awarded as the 3rd Best Poster 2007.

Adriele Prina-Mello, Stephanie Toetsch, Peter Olwell and Yuri Volkov, Next generation chemotaxis assays. From static models to physiologically relevant platforms. *Lab-on-a-chip, European Congress,* May 2009, Stockholm, Sweden.

Trinity Trust Travel Grant Award, March 2007.

TABLE OF CONTENTS

LIST OF ABBREVIATIONS

APC: antigen presenting cell

AOI: area of interest

BSA: bovine serum albumine

CAM: cell adhesion molecule

CAD: computer-aided design

cP: centiPoise

CCD: charged coupled device

CD: cluster of differentiation

DNA: deoxyribonucleic acid

DMSO: dimethyl sulfoxide

DMEM: Dulbecco's modified eagle medium

EEO (agarose): electroendosmosis

EB/AO: ethidium bromide/acridine orange

EGTA: ethylene glycol tetraacetic acid

EDTA: ethylenediaminetetraacetic acid

ECM: extracellular matrix

FBS: fetal bovine serum

Fc region: fragment crystallizable region

FCS: fetal calf serum

Fmlp: formyl-methionyl-leucyl-phenylalanine

g: units of gravity

GAM: goat anti-mouse

HAT: hypoxanthine aminopterin thymidine

HUT78: human T-cell lymphoma cell line

ICAM-1: intercellular adhesion molecule-1

IgSF: immunoglobulin superfamily

IL-2: interleukine 2

IL-8: interleukine 8

kDa: kilo Dalton

LFA-1: leukocyte function associated molecule 1

NaCl: sodium chloride

MHC: major histocompatibility complex

MEMS: micro-electromechanical systems

MTD: migration testing distance

MW: molecular weight

PAMP: pathogen-associated molecular patterns

PBL: peripheral blood lymphocytes

PBS: phosphate buffered saline

PHA: phytohaemagglutinin

PDMS: polydimethylsiloxane

PMMA: polymethylmethacrylate

PLL: poly-L-Lysine

ROI: region of interest

rpm: round per meter

SME company: small-to-medium company

SDF-1α, CXCL12: stromal cell-derived factor 1α

TCR: T-cell receptors

TLR: toll-like receptors

TNF-α: tumour necrosis factor-α

UV: ultraviolet

VCAM-1: vascular cell adhesion molecule-1

VLA-4: very late antigen-4

w/v: weight/volume

1 Introduction

1.1 General overview

The recruitment of leukocytes into tissues through the endothelial cells which line blood vessels is an essential first step in the inflammatory response. Multiple biochemical signals are required to direct this process[1, 2] which is relevant for all instances of inflammation[3, 4]. Transendothelial migration (TEM) is the result of a multistep cascade in which different events culminate in the successful migration of a leukocyte through the endothelial wall and into the underlying tissue (Fig. 1-1). The first step (a) is the margination of leukocytes in free flowing blood to the endothelial wall after which they make contact with the endothelial cells and begin rolling on the surface of the endothelium. This rolling is mediated by selectin ligands expressed on the surface of the endothelial cells. Selectins form weak bonds with carbohydrate ligands on the surface of leukocytes. These bonds are rapidly broken and reformed as the leukocytes are pushed along by the flow of blood giving the impression that they are rolling on the surface of the endothelium.

Cytokines are small signalling proteins that are known to induce the high affinity state of certain integrin receptors on leukocytes. Cytokines also stimulate the expression of matching integrin ligands on endothelial cells, which further slow leukocytes down (b). Cytokines, which are a family of proteins and peptides, also allow cells to communicate with each other[5-18]. Leukocytes which are adhered to the vessel wall (c) are stimulated to migrate across the endothelium into the tissues via a gradient of chemotactic cytokines termed "chemokines" (d)[19]. Leukocytes reach the tissue interstitium then bind to the extracellular matrix through a set of specific expressed integrins[20].

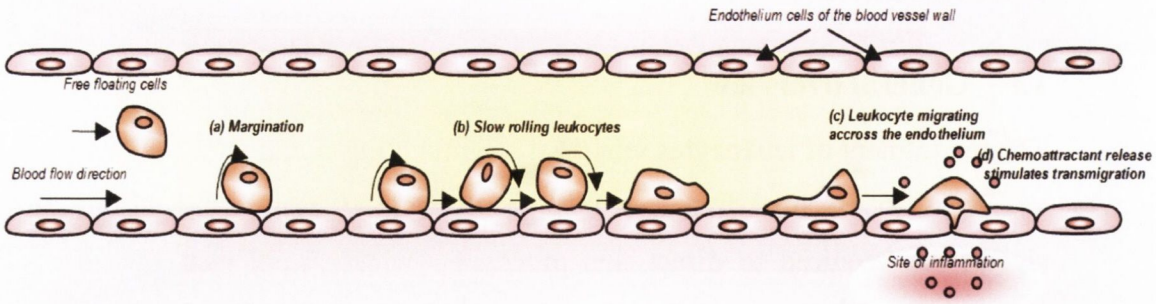

Figure 1-1: Model of multistep leukocyte adhesion cascade resulting in transendothelial migration. First step is the initial attachment of free floating leukocytes which lead to the margination (a). Interactions between endothelium integrins and cells ligands induce the slowing down of leukocytes (b) which further results in leukocytes migration across the endothelium (c) due to a gradient of chemokines (d).

Due to the essential role of leukocytes in inflammation, defects in leukocyte function often result in a decreased capacity for an inflammatory response with subsequent vulnerability to infection. Therefore, the leukocyte adhesion cascade is an important area of study for developing methods to control inflammation by modulating or blocking leukocyte adhesion to the endothelium. Likewise, the development of anti-inflammatory drugs is largely dependent on research into inflammation using *in vitro* model systems and *in vivo* microcirculation studies.

1.2 Experimental procedures

In past years, many *in vitro* studies[21] (e.g. Boyden chamber, Dunn chamber) have shown the important role of the release of chemokines in leukocyte homing. These assays had significant limitations as experiments were performed in static environments without any shear stress; this is in contrast to *in vivo* conditions where cells are continually exposed to shear stress in flowing blood. New assays, based on the micro-electromechanical systems (MEMS), utilizing continuous-flow microfluidic biochips have been proposed to overcome these limitations. Human capillaries are mimicked within 2-dimensional (2D) microfabricated channels in which continuous flow of cells and flow of chemokines are dispensed thanks to a microfluidic pump system. Cells are then free to migrate in 2D (only x-y axis) toward the gradient of chemokines.

However, it is necessary to keep in mind that in the *in vivo* milieu, the leukocyte adhesion cascade is not taking place in a smooth environment as is the case in the channel of a microdevice. In the human body, the leukocytes and other blood cells circulate within blood vessels. Capillaries are the thinnest vessels represented by a one-layer of endothelium that enables exchange of nutrients and chemical substances between the blood and the tissues. Arteries and veins are named the conduit vessels since they carry the blood away from and back towards the heart. Their anatomies exhibit a three-layer structure (endothelium, smooth muscle cells and connective tissue).

Thus, the anatomy of blood vessels and the morphology of the cells composing their endothelium layer are different, depending on their function. Therefore, high endothelial venules are distinguished from regular venules by their cuboidal cells opposed to the squamous cells found in regular venules.

Therefore, the interface between the lumen and the underlying tissue is not a linear or flat surface, instead it presents a continually changing topography difficult to simulate in a model system. Epoxy resin casts of inflamed and non inflamed blood vessels confirm this[22]. Hence, the generic structure of a standard venule is used as a model for our study instead of focusing on one specific type of blood vessels bearing specialised endothelial cells and other differentiating characteristics (Fig. 1-2).

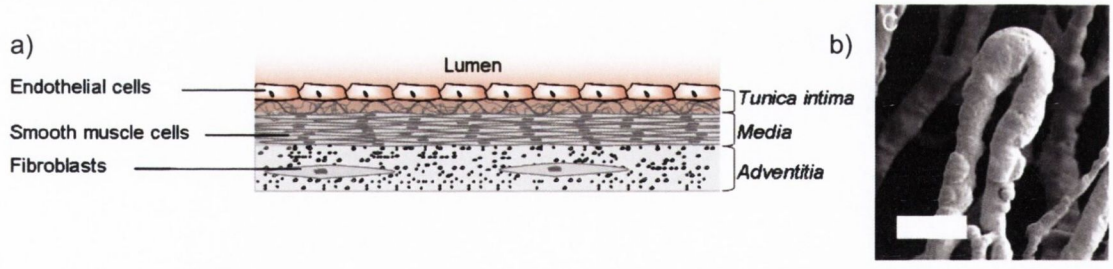

Figure 1-2: a) Generic schematic model of the human blood vessel wall (venule). The inner layer is called *tunica intima*. It is structured by a pavement of endothelium maintained by a layer of internal elastic lamina. The middle layer called *media* layer is made of smooth muscle cells and elastic tissue. The outer layer is the *adventitia* mainly composed of connective tissue and fibroblasts. b) Scanning electron photograph representing the microcirculatory topology[22] (bar = 50 µm).

Thus, the diffusion of chemokines from the extracellular matrix to the lumen encounters a markedly different environment to that presented by *in vitro* models to date.

1.3 Aim of this study

Current standardised microfluidic assays present a reductionist environment in which chemotaxis can be monitored. Hence, to reproduce realistic *in vivo* conditions, microfluidic biochips must present an environment capable of replicating the situation where chemokines are released in a concentration gradient from tissues through the endothelium, as occurs at the site of inflammation. Significant efforts by researchers are focused on the development of the next generation of microfluidic biochips in order to present more physiologically relevant 3D environments enabling the cells to migrate in the x, y and z axes.

The aims of this thesis are to:

- Develop an engineered microenvironment for leukocyte migration studies closely imitating the physiological conditions,
- Generate an equivalent of natural chemokine gradient in a tissue-mimicking matrix,
- Assess the migration of leukocytes towards a gradient of chemokine in real time under precision controlled flow conditions.

Flow chart of the experiments carried out for that project

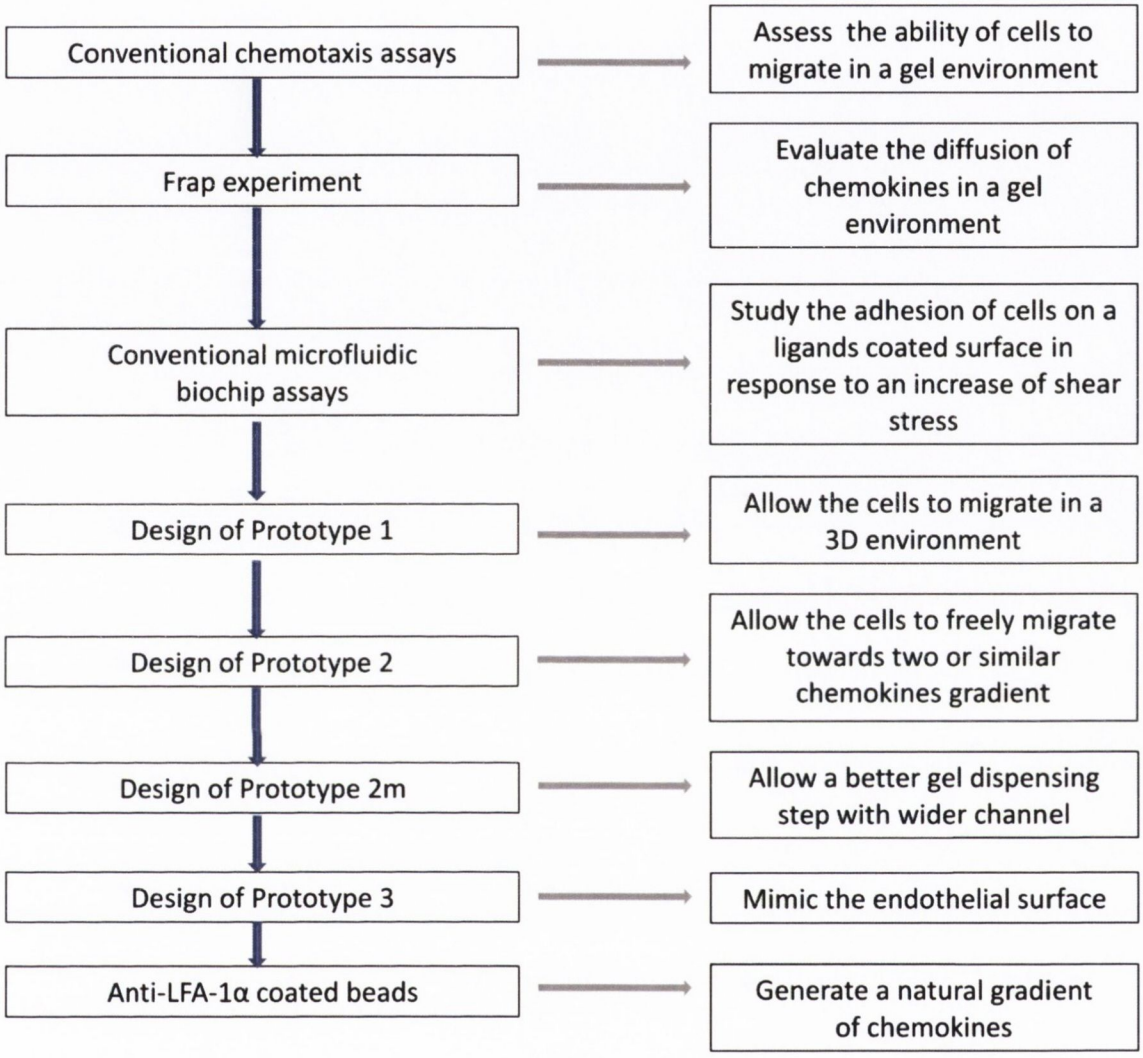

2 The function of leukocytes within the human body and technical approaches for *in vitro* investigations

2.1 Introduction

The process of inflammation is crucial for protecting the body against external infectious agents or pathogens (worm, protist, bacteria, fungi, and virus) and also against internal agents (virus, bacteria, and tumour). Some pathogens are harmless or beneficial for our system and other can cause illness. A harmful pathogen first needs to enter the body and can do that through a number of ways e.g. through the skin, via droplet infection, direct contact, contaminated food/drink, or cuts in the skin. Therefore, day-to-day events expose humans to multiple incidences where their immune system is challenged.

Human body has two main fluid-carrying systems, blood and the lymphatic system. They not only support the transport of cells and soluble factors to screen or clear infection, but also distribute and provide the energy required for the body to do its routine tasks. An adult human has approximately 5 litres of blood which flows throughout the body. All blood cells have a common lineage, originating in the bone marrow from the pluripotent stem cells through a process called hematopoiesis. Through this process, stem cells are differentiated into three types of cells: erythrocytes (red blood cells), leukocytes (white blood cells), and thrombocytes (platelets). Leukocytes are subdivided into neutrophils, lymphocytes (B cells and T cells), monocytes, eosinophils and basophils. The lymphoid system transports the fluid called lymph via lymphatic vessels that interact with the blood system to drain fluid from the tissues. It also distributes immune cells, such as lymphocytes throughout the body.

It is necessary to understand the mechanisms of immune system in order to establish, through research, how to support, supplement and improve its function. The transendothelial migration (TEM) is a small but essential element of the total immune function. Cell migration through the TEM mechanism plays a critical role in the progression of many diseases, such as cancer metastasis and atherosclerosis, or physiological processes, such as embryonic morphogenesis and wound healing. Assays developed in this area to date have enabled investigation of the different steps of the

TEM, observing each step in isolation. However, the existing assays are approaching a point where they are no longer sufficient to answer "the next questions": for example, can the leukocytes migrate without the action of external chemical cues? Are there key signals generated *in vivo* which are not present in existing *in vitro* assays? For this reason it is necessary to develop new experimental platforms for the study of TEM.

2.2 Basic cell structure: an introduction

Cells are found in any living organism providing structural and functional properties of the surrounding environment. There are two types of cells: eukaryotic and prokaryotic cells. Prokaryotic cells are believed to be the precursor of living organisms on Earth because of their capacity to live in inhospitable conditions such as extremes of temperature, pH, and radiation. They are usually unicellular and can be found in a variety of organisms including human. The presence of a nucleus in eukaryotic cells and their large size differentiated them from prokaryotic cells. The most familiar eukaryotic cells are found in animals and plants presenting a complex subcellular organization.

Humans have an estimated 10^{14} cells of different types such as skin cells, stomach cells, liver cells, brain cells, eyes cells, and many more. They have different abilities and functions depending on their nature. Figure 2-1 shows the compartments and the components of a simplified cell system.

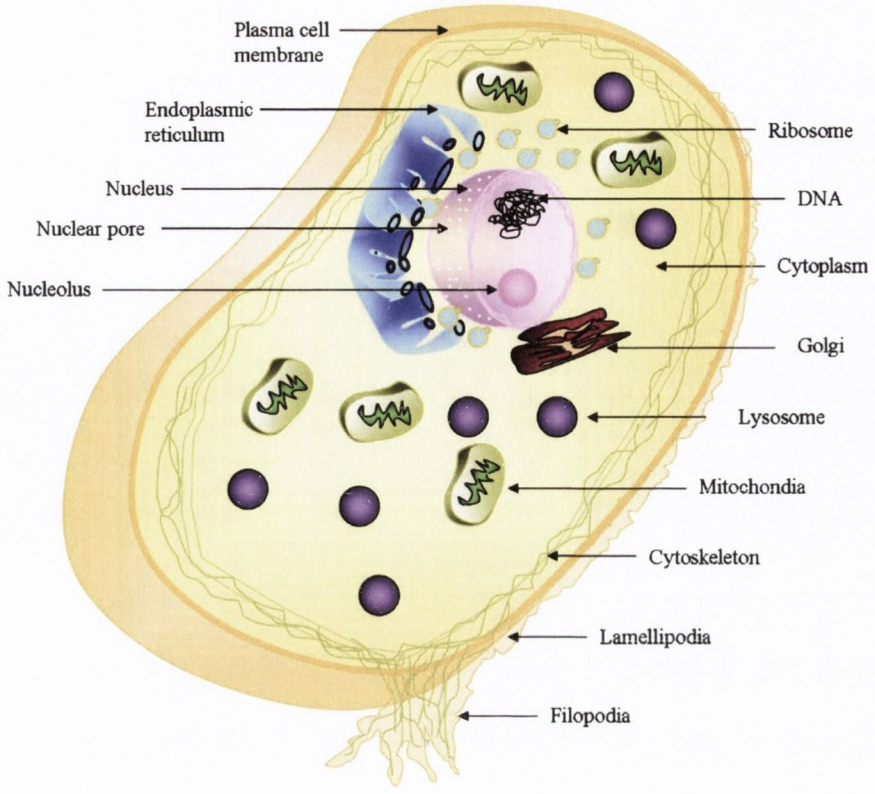

Figure 2-1: Diagram of eukaryotic or animal subcellular components. A cell is composed of flexible cell membrane that exhibits on its surface proteins involved in cell signalling. The cytoskeleton is part of the cell membrane and enables the locomotion of the cells via filament protrusions (e.g. lamellipodia, filopodia). Within the cell is found the genetic code deoxyribonucleic acid (DNA) inside the nucleus which manages protein synthesis. This synthesis is also performed by organelles (ribosome, mitochondria, lysosome, endoplasmic reticulum and Golgi apparatus).

The plasma membrane of a cell separates its interior from its surrounding milieu. It is selectively permeable and regulates the movement of water, nutrients and waste into and out of the cell. The cell membrane is a flexible lipid bilayer (mainly phospholipids) that supports on its surface different proteins involved in cell signalling. The genetic code that coordinates protein synthesis is confined in the nucleus. Protein synthesis is also carried out by organelles such as ribosome, mitochondria, lysosome, endoplasmic reticulum and Golgi apparatus. Each of these have different role in the day-to-day functioning of the cell. The free volume inside the cell contains a gel-like material, the cytoplasm. It maintains in suspension the in-cell components where metabolic pathways occur (e.g. transport and diffusion of proteins in and out of the cell). A network of long protein filament (actin filaments, intermediate filaments and microtubules) extending throughout the cytoplasm is called the cytoskeleton. This dictates the shape of the cell

and permits cell locomotion via dynamic formation of cytoplasmic protrusions, such as lamellipodia and filopodia. This locomotion essentially relies on the association of the motor protein myosin with actin. This interaction is a key step for the crawling movements and polarization of cells.

2.3 Immune system

The immune system is the body's defence system, protecting the organism against pathogens and other infectious organisms. Through a cascade of mechanisms that first includes the identification of hostile organisms, the immune response leads to the neutralization of the threat to the organism.

The human immune system has two components: innate (or non-specific immunity) and adaptive (or acquired immunity). The innate immune response is an immediate defence against infection. Leukocytes are part of the innate immune system which includes phagocytes (macrophages, neutrophils, dendritic cells), mast cells, basophils, eosinophils, and natural killer cells. Macrophages and dendritic cells are mature monocytes that phagocytose by engulfing and ingesting foreign bodies. This phagocytic process can be followed by the presentation of digested proteins on the surface of the cells that informs other immune cells of the nature of the invader. These types of cells are identified as antigen presenting cells (APC) such as dendritic cells, macrophages, and B cells. Signalling proteins called cytokines are also released through these immune responses, promoting recruitment and activation of immune cells. Natural killer cells are cytotoxic that means they kill infected cells by injecting molecules inducing cell apoptosis. They are activated in response to macrophage-derived cytokines. Neutrophils are also phagocytes but they are the first immune cells to arrive at a site of infection directed by chemotactic cytokines.

A second line of defence, the acquired immune system, comes into play at the later stages of the organism's immune response. Cells associated with the acquired immune system are capable of recognising specific pathogens after one or multiple exposure to it. A process of immunological memory is activated after the first response to the same pathogen. Leukocytes such as B lymphocytes and T lymphocytes are the major cells of adaptive immune system. The adaptive immune system can be activated via signals

produced as a result of the innate immune response, and also through a process known as antigen presentation (Fig. 2-2).

These complex but efficient mechanisms that control the immune system have varying modes of action. It has been shown that mechanisms from one system can be influenced by the other, such as activation of adaptive cells by cytokines produced by innate cells. That is why most studies of the immune system are artificially simplified and divided into several steps in order to isolate each parameter that influences cells reaction in the immune response.

2.4 Activation and recruitment of immune cells

Immature lymphocytes B-cells and T-cells originate from hematopoietic stem cells in the bone marrow. Only B-cells mature there while T-cells become mature in the thymus. T-cells and B-cells that are mature but not activated are called naïve cells.

B-cells represent an essential component of the adaptive immune system. They can be differentiated into plasma B-cells and memory B-cells. Once they have been exposed to antigens, they become fully activated and are responsible for the production of antibody molecules. Antibodies are proteins found in blood, lymph and throughout the body designed to recognise and neutralise foreign bodies.
T-cells are a class of lymphocytes involved in the control of cell-mediated immunity. There are different types of T-cells: helper T-cells, cytotoxic T-cells, memory T-cells, regulatory T-cells, and natural killer T-cells. Although they all have specific functions in the immune responses, their activation processes are developed on the similar scenario.

The process of T-cell activation relies on the binding of T-cell receptors (TCR) to a small peptide presented by the major histocompatibility complex (MHC) on the surface of antigen presenting cells. These peptides result of the internalization and the digestion of an antigen by B-cells, macrophages or dendritic cells. The combination of peptides/MHC further binds to a mature T-cell receptor. The expression of a co-stimulatory molecule found on the MHC complex is also required for activation of T-cells via its binding to T-cell receptor. If only one binding occurs in the absence of the

second binding, it results in an anergy and no specific immune response is displayed in the body. However, in the case of both signals, T-cells become fully activated and start secreting cytokines.

Toll-like receptors (TLR) found on innate cells are also a key step in the production of cytokines, they recognise what is called the pathogen-associated molecular patterns (PAMP) found on pathogens. This complex promotes the proliferation and secretion of effector molecules and enables the immune system to recognise self cells and non-self cells. This is an important step in the development of the phenomenon of immunological memory.

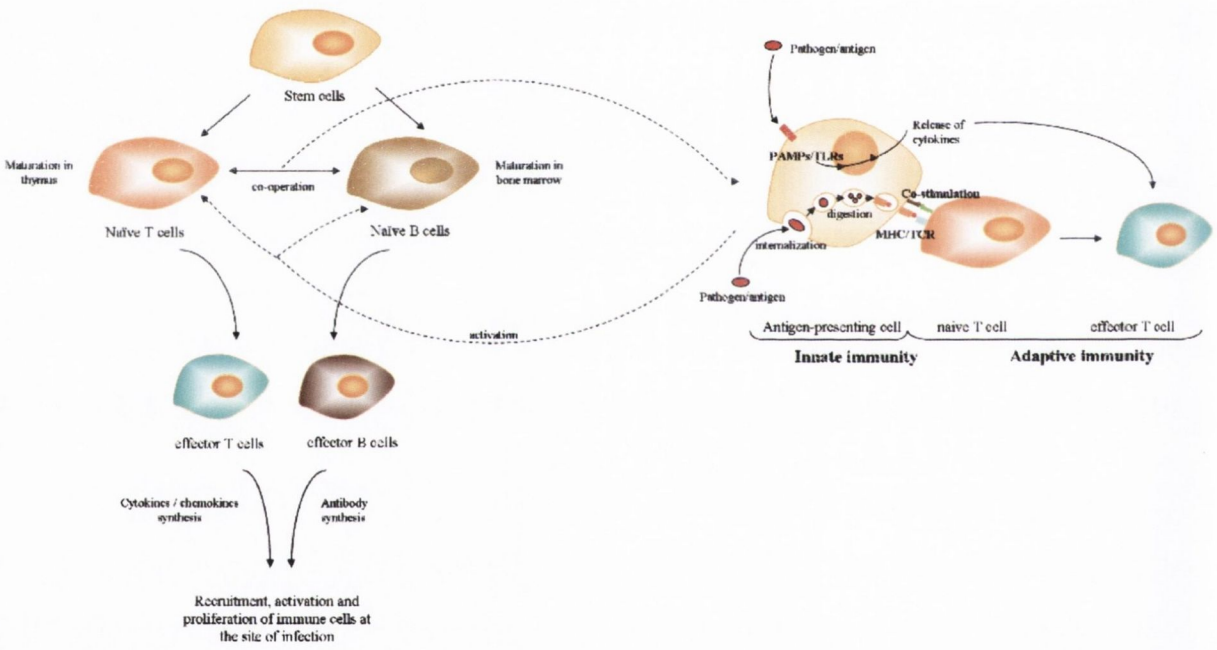

Figure 2-2: Schematic drawing showing the activation of innate and adaptive immune cells. Stem cells are the origins of naïve lymphocytes B-cells and T-cells. The maturation of naïve T-cells and B-cells takes place in the thymus and in the bone marrow respectively. Activation of naïve T-cells (adaptive immunity) occurs when they are stimulated via their bindings to antigen-presenting cells (innate immunity). B-cells become activated when they have been exposed to antigens. Innate and adaptive immune cells are activated by co-operation and co-stimulation between the immune cells.

The activation and recruitment of effector cells at the site of infection relies on a cascade of intertwine events, whereby one cytokine stimulates its target cells to release additional cytokines. A gradient of cytokines is formed and can be diffused in the blood flow and tissue. However cytokines are mostly effective at a short-distance and each cytokine is specific to particular cell-surface receptor(s). There are different types of cytokines such as lymphokines, interleukins and chemokines. Lymphokines are produced by lymphocytes in particular T-cells while interleukins are produced by T-cells but also macrophages. Chemokines are chemotactic cytokines that are often released in response to interleukins. They chemotactically guide cells of both the innate and acquired immune system. The structure of chemokine can be CC that means it has two adjacent amino-acid cysteine (abbreviated C), CXC with an amino acid represented by "X" between the two CC, CX_3C with three amino acids between the CC pattern, and the last one is C structure with cysteine at both beginning and end of the molecule.

The impact of cytokines on leukocytes can be synergistic[23] which means that a combination of cytokines could increase T-cells stimulation more than the additive effects of such cytokines when used singularly. Individual cytokines can have different effects on cells (pleotropy[24]) such as tumour necrosis factor-alpha (TNF-α) which can enhance cell adhesion molecule and cytokine expression but can also cause cell death of tumour cells. Another effect of cytokine secretion can be the suppression of its own effect by feedback inhibition[25].

In this study we have focused on the subclass of cytokines with chemotactic activities, or chemokines.

2.5 Leukocyte locomotion

The key functional characteristic enabling leukocytes to reach their ultimate target is their locomotion. The basic mechanism for cells to circulate in the body is through the fluid systems (blood and lymph vessels). The process of migration occurs when cells are attached to the vessel wall in opposite to free flowing cells that circulate in the fluid systems. Only cells that first adhered to the substrate are able to migrate into the tissue. Therefore, the homing process relies on what is called substrate dependent locomotion.

Cell adhesion is supported by integrin receptors that bind to ligands of the substrate. Integrins activation is triggered by chemokines. Integrins exhibit multiple conformations: a low-affinity and a high-affinity binding. Changing in conformation of integrins is mediated through cellular stimulation often called "inside-out" signalling. This refers to the exchange of information inside and outside of the cells. Several studies suggest that the low-affinity reveals a bent conformation while the high-affinity exposes an extended conformation[26].

Once cell integrin receptor binds to its specific ligands, cells are further capable of crawling on the substrate thanks to intra cellular rearrangement. This is thought to be the result of three coordinated reorganization and involves numerous different proteins.

Actin is a globular protein; its monomeric form called G actin polymerizes to form long filamentous polymers (F actin) with a diameter of around 7 nm. Myosin II is a motor protein that drives movement along F actin responsible of actin-based motility.

Cell crawling is initiated when cross-linked subunits actin interact with myosin and polymerized actin filament. This interaction generates protrusions such as lamellipodia or pseudopodia[27], and promotes adhesion of the leading edge of the cell to the substratum. The adhesion at the front of the leading edge of the cell is firmer than at its rear. The cytoplasmic reorganization such as the contraction of the actin/myosin network leads to the advance of the nucleus by traction force[28]. The nucleus is translocated forward and the adhesion to substratum at the trailing edge of the cells is reduced allowing the release/retraction of the trailing edge.

2.6 Leukocyte adhesion molecules

In the leukocyte transendothelial process, the migration of the cells is relying on different intra and extra cellular parameters. It has been shown that cells crawl when they are first activated allowing them to adhere to the substratum. A wide range of cell adhesion molecules (CAM) is known to promote the interaction between cell-cell and cell-extracellular matrix. These molecules are proteins and are found on the surface of the cells embedded in the plasma membrane or in the cytoplasm, this is why they are called transmembrane receptors. A molecule that binds to a specific receptor is a ligand.

Bindings of similar CAM is a homophilic binding, while bindings of different CAM is a heterophilic binding.

There are four different families of receptor that allow the binding of the cells to the surrounding environment or other cells. The immunoglobulin superfamily (IgSF) is a large group of CAM that includes cell surface antigen receptors, antigen specific receptors and diverse cytokine receptors. IgSF molecules are either homophilic which means they bind to another identical cell molecules or heterophilic which is a non-identical binding.

Some important IgSF involved in the TEM process are:

- ICAM-1 (ICAM-2 and 3): intercellular adhesion molecule-1 (-2 and -3),
- VCAM-1: vascular cell adhesion molecule-1,
- PECAM-1: platelet-endothelial cell adhesion molecule-1.

Integrins are heterodimers that means they have two distinct chains called the alpha and the beta subunits. Two main functions of the integrins are the attachment of the cells to the extracellular matrix (ECM) and the signal transduction from the ECM to the cell ("inside-out signalling").

Cadherins are described as homophilic CAM that are calcium (Ca^{2+}) dependant such as E-cadherins (epithelial-cadherins). The cadherin family presents different class depending on the structure of the cadherin molecules. Cadherins within one class would stick one to the others. Therefore, cadherins are important between cells within a tissue because they ensure that cells are bound together.

The selectin family binds to heterophilic CAM and is Ca^{2+} dependant. Selectins are essential in the interaction between leukocytes (lymphocytes, neutrophils) and the vascular endothelium. Selectins are divided in three family members depending on where they are found, for example: E-selectin for endothelial, L-selectin for leukocyte, and P-selectin for platelet.

2.7 Typical cell culture conditions

Cells that are directly isolated from tissues or from blood are known as primary cells. They have a limited lifetime with the exception of some cells derived from tumours. However, tumours cells undergo senescence as they replicate and over time they can lose their capacity to proliferate. Consequently cell lines with the ability to proliferate indefinitely have been developed. Some cells grow in suspension as opposed to adherent cultures. Cells isolated from blood can usually be grown in suspension. These cells are able to grow to a higher density than adherent cells. Most adherent cells derived from tissue such as endothelial cells require a substrate to attach to. Therefore, the density of the adherent cells in culture is limited by the size of the surface where they grow.

Cells are cultured in media in tissue vessels such as flasks with various sizes and surface coatings. Cell culture takes place under controlled conditions (pH, temperature) in a sterile environment with a supply of nutrients for growth. Regulation of pH and temperature is typically carried out in a cell incubator that allows the maintenance of cells in an atmosphere of 5 % CO_2 at 37 °C. Chemical buffering (HEPES, sodium bicarbonate) can also be used to balance the pH of a cell culture. In that case, there is no need to incubate the cells in 5 % CO_2 environment.

Media for cell culture needs to be enriched with nutrients which are analogous to those found in the body. The composition of the media varies with the nature of the cells. In general, cells need a source of energy such as carbohydrates (glucose, galactose…), amino acids (L-glutamine) or salts (sodium pyruvate). Other important source of nutrients is certain alkaline minerals such as calcium and magnesium that enable acid-alkaline balance in the body but also regulate integrin conformation. They are found in the form of ions (Cl^{2+}, Mg^{2+}) and are flowing in and out of the cell membrane through the ion channels. These ions are usually in competition because of their similar valences. They also have an impact on the adhesive and migratory activities of many cell types[29], especially the ion Mg^{2+}. Therefore, EGTA and EDTA are reagents that are commonly used to chelate the ion Ca^{2+} in presence of Mg^{2+}.

The most common growth factors used is the serum that is a complex mix of albumin. Fetal bovine serum (FBS) is usually added to the cell culture medium. Contamination in the culture of bacteria is avoided by carrying out all manipulations under a bio-safety hood and antibiotics can also be added to the media such as penicillin and streptomycin.

Cells that are cultured in media need to be regularly split in order to avoid the process of apoptosis, or natural death, which occurs when cell density becomes too high. The split step is also mentioned as passaging. Depending on the cells, their protein expressions differ with the number of passages. Cells in suspension are split by diluting a small volume of cells into a larger quantity of fresh media. For the adherent cultures, cells are attached to the surface and needed first to be detached with an enzyme solution such as Trypsin-EDTA. Fresh media is then added to a small amount of cells.

2.8 Conventional chemotactic assays

As explained above, a gradient of cytokines such as chemotactic cytokines can regulate multiple cell activities, for instance cell activation and cell recruitment at the site of inflammation. Therefore, different chemotactic assays have been developed to study the influence of chemokines on cells.

One of the most commonly used migration assays is the Boyden chamber/Transwell assay (Fig. 2-3). This system is used to quantify the migration of cells exposed to different chemokine concentrations. The chamber contains two compartments separated by a microporous filter (with commonly used pore sizes between 2 μm to 12 μm) through which cells migrate. The relevant chemoattractant solution is placed in the lower chamber to create a chemotactic gradient while leukocytes are incubated in the upper chamber. The cells need to squeeze between the pores of the filter. In some cases, endothelial cells are grown on the membrane to replicate the *in vivo* environment. The advantage of the Boyden Chamber is that it facilitates the observation of the effect of chemokines on cells, allowing analysis of both chemokinetic (speed at which cells migrate) and chemotactic effects (direction in which cells migrate). One of the limitations of the Boyden chamber is that there is no reliable way to sustain the chemokine gradient. In a matter of hours the chemokine becomes homogeneously diffused in the upper chamber and the cells will no longer migrate through the pores.

Another limitation with a Boyden Chamber type assay is that there is no possibility to incorporate the effects of shear stress on the cells under investigation.

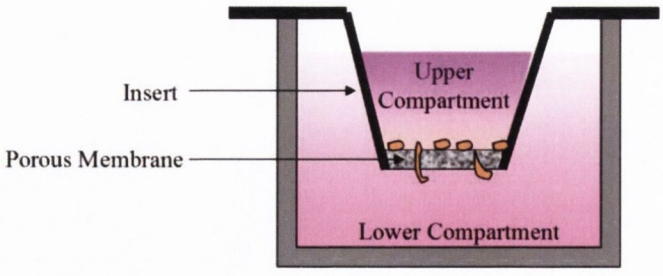

Figure 2-3: Illustration of the Boyden Chamber assay. The chamber consists in two compartments separated with a porous membrane in which cells can migrate through. The lower compartment is filled with a chemoattractant solution creating a gradient by natural diffusion in the upper compartment which contains the cells. The gradient generated allows the cells to migrate through the porous membrane into the lower compartment.

The agarose[30] or Dunn chamber assays are examples of other standard chemotaxis assays which have been used to show the importance of chemokine gradients by evaluating leukocyte motility dependent on the concentration of specific chemokines. These static experimental systems are implemented predominantly to estimate the ability of particular cells to migrate towards a gradient of chemokines. However, they all have the same disadvantage; the cells are incubated in static conditions and not under hemodynamic shear stress conditions, as would be found *in vivo*.

2.9 Micro-electromechanical systems

Micro-electromechanical systems (MEMS) technology was developed in the 1950s[31-37]. MEMS were facilitated by the development of microfabrication techniques[38-41] which were utilised in the design of the micro-electronic components (e.g. transistor, integrated circuit)[42-44]. During the 1990s the novel aspects of MEMS were used to combine the mechanical and electronics micrometer elements on a common substrate. The size of these devices was so technologically attractive that, subsequently, many diverse areas of research became interested in miniaturisation such as chemistry, biology, bioengineering and physics. Chemical reagents and markers for biomedical studies can be very costly and large volumes of each reagent were previously necessary for each experiment. This is why miniaturisation is a cost effective solution since it

reduces the total sample volume from millilitre to nanolitre and maximise the usable surface area on which the reaction is carried out. It was seen as a means of miniaturising the laboratory. A subset of the MEMS devices appeared in the latter part of the 80s termed "lab-on-a-chip". A wide range of novel mechanical systems emerged utilising new MEMS influenced designs which utilise low volume liquid handling devices[45-50] and biochip platforms[37, 51-53]. There were a significant number of advantages in using these designs from the point of view of cost and time. For example, multiple parts of the same assay can be run in sequence; additionally, replicates can be included and run in parallel[54-57]. Biochips can be applied to various fields of medical research including immunology, genomic and proteomic research, as well as pharmacology and toxicology.

In the earliest biochip designs that utilised the effects of biological shear, the architecture of the channels had square cross-sections which precluded laminar flow. More recent advances in soft polymer lithographical processing and design comprised of channels with rounded cross-sections which are better suited for enabling laminar flow. Now, after half a century since the original development of MEMS technology, designs are more advanced and processes of microfabrication are better understood (Fig. 2-4). As a consequence of this, the layout of a biochip can rapidly be redesigned and that design can be subsequently manufactured with much more ease and at a lower cost. Soft polymer and MEMS technologies can be used for chemotaxis assays and allow detailed dissection of disease processes at the cellular level in a disposable biochip.

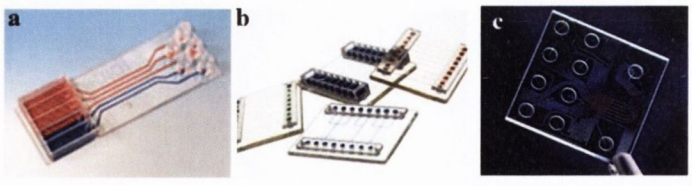

Figure 2-4: Examples of commercially available microfluidic biochips. (a) μ-Slide V from the μ-Slide family chip of IBIDI GmbH (Germany) for parallel immunoassays. (b) Different designs of Cellix biochips (Ireland). Each chip contains enclosed microcapillaries that can be coated with different antibodies. (c) Lab-on-a-chip of Agilent (Santa Clara, CA) with a network of channels and wells enabling sample handling, mixing, and dilution.

2.10 Microfabrication of a biochip

The architecture of a biochip relies on the process of fabrication used to develop its structure, but also on the materials employed[36]. Laser ablation (excimer, CO_2), microlithography (X ray, E beam, photolithography) or microfabrication (wet etching, dry etching, contact printing) are the most common processes used over the past few decades[41, 58, 59]. A batch of materials is used as primary material or substrate such as glass, quartz, epoxy, polymethylmethacrylate (PMMA), polydimethylsiloxane (PDMS), silicone, polyimide and gels[38, 60, 61]. New techniques are constantly tested for development of precise patterns for example laser beam (pulsed or continuous) enables fast and accurate microfabrication.

In our study, we focused on the process of microlithography, and more precisely the photolithography. This microfabrication technique presents different steps for the development of channels network on a chip. These steps can vary depending on the desired architecture of the chip.

First, the pattern of the device is designed using computer-aided design (CAD) software. A blueprint of the chip is then produced and transferred to a photoresist material such as epoxy (e.g. SU8) to manufacture a photoresist mask. Such materials have different characteristics and their photoresist performance varies with their viscosity, their nature (positive or negative photoresist) and their sensitivity to exposure radiation. The structure of a photoresist after light or radiation exposure is modified; it can be polymerized or photosolubilised. A mask is usually generated using an electron beam (e-beam) and is made of borosilicate or quartz glass covered with a layer of chrome and photoresist. The quartz plate is then developed and the chrome is etched, creating the photomask. A cheaper method to develop a mask is to print the mask on paper.

The substrate of the chip needs to be free of dust particles (e.g. organic or inorganic materials) that could affect the substrate bond strength and could further cause defects in the patterns. Therefore, any contaminations are removed using a solvent treatment technique (e.g. methanol). The next step is the spin-coating of a photosensitive material, which means that a uniform layer of this material is deposed on top of the cleaned

substrate. The thickness of the layer relies on the parameters set for the spin-coating process but also on the photoresist material chosen.

When a soft baking has been proceeded to remove the solvent contained in the photoresist, the coated substrate is next exposed to specific radiation. This creates a latent pattern in the resist layer that is further developed (via developing solution) to produce the final three-dimensional relief image.

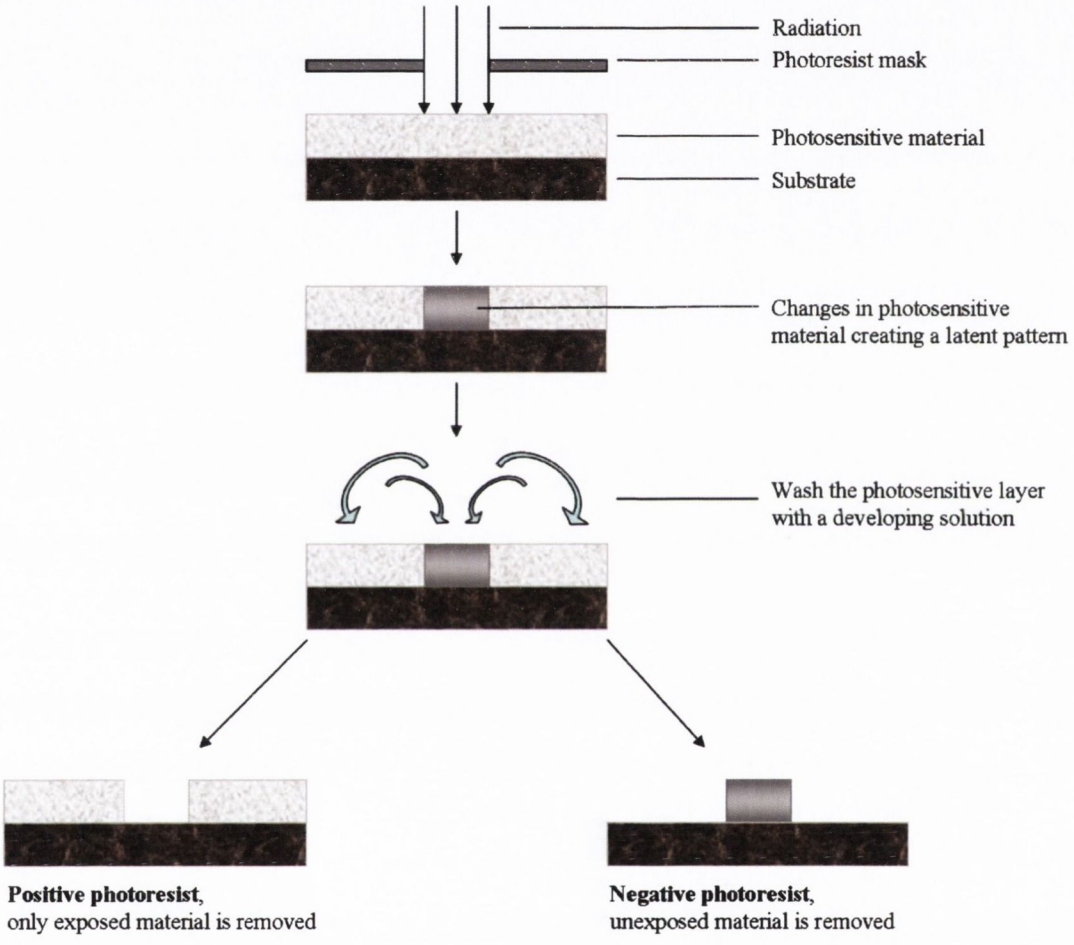

Figure 2-5: Schematic representation of the photolithographical process used for the microfabrication of biochips. A substrate is recovered with a photosensitive material. A mask describing the pattern desired is used to change the property of the photosensitive layer via radiation. Photosensitive layer is washed and the pattern on the substrate is developed.

A plasma treatment is further carried out to provide increased wettability and biocompatibility for surface adhesion (e.g. cells, proteins).

2.11 Microfluidic platforms

Microfluidic biochips are typically made to mimic human capillaries using a specific channel network. These systems are essential for the study of basic cell signalling related phenomena, such as T-cell chemotaxis,[62, 63] bacterial chemotaxis,[64, 65] morphogenesis,[37, 66] and regulation of gene expression[67, 68]. Channels are usually coated with proteins present in extracellular matrix or endothelial cells.

A continuous flow with varying shear stresses can be applied in closed-channels using a precisely controlled microlitre injection or dispensing system[37, 47, 48, 69, 70]. The advantage of such systems is that the control of the gradient of chemokines in these channels is predictable, reproducible and easily quantified[71, 72]. There are limited reports in the literature on the microfluidic devices where tunable concentration gradients can be produced. The gradient of chemokines in such dual channel microfluidic biochips is created not by physiological means but by the exogenous addition of the chemokine of choice,[71] by alternating gradients,[73] or by natural diffusion between two continuous flows[69]. This is a disadvantage, as it does not mimic physiologically relevant chemokine concentrations or patterns of their release. Even if the surface of the channel is coated with extracellular proteins, it still cannot imitate either the diffusion of chemokines from the tissue at the site of inflammation, or the leukocyte migration through the endothelium. One attractive design option is to grow a confluent layer of endothelial cells on a coated channel. Then, a continuous flow of cells is dispensed over the endothelial cells and the adhesive properties of these cells on the endothelial layer can be observed using standard microscopic procedures[74].

In a recent review, Keenan and Folch[21] have summarised the technical aspects of current microfluidic biochips in which a gradient of chemokines can be mechanically controlled. The designs which are now possible using advanced computer-aided design, moulding and manufacturing techniques are limited only by the creativity of researchers. Both biologists and physicists have focused on improving microfluidic biochips, this cross disciplinary collaboration is essential for the successful creation of new model systems. The advantage of this complimentary research is clear and many of the interesting innovative designs described below have come from this interdisciplinary approach.

2.12 Theory of microcapillary flow

The mechanisms of fluid flow in a complex are depending on the nature of the flow but also on the environment in which it flows through. In the human body, the blood circulates through a channel network such as arteries, arterioles, veins or capillaries. The arterial blood pressure maintains the flow and the surrounding environment under physiologic conditions and is regulated by the pumping action of the heart. It has previously been shown that the vessel walls are not linear and rigid but are covered with rough endothelial cells and are elastics.

Therefore, it is important to understand the complexity of the *in vivo* milieu from a physical point of view in order to be familiar with the terms that are used for developing artificial networks.

- What is a fluid?

A fluid is defined as a substance that is continuously deformed due to the application of a shear stress (τ).

- Shear stress:

A shear stress (τ) is defined as a stress component applied on a material (e.g. fluid). For example, a shear stress on a fluid between two infinite plates causes its deformation under a certain shear rate (*du/dy*). It is then related to fluid viscosity (μ): $\tau_{yx} = \mu\, du/dy$

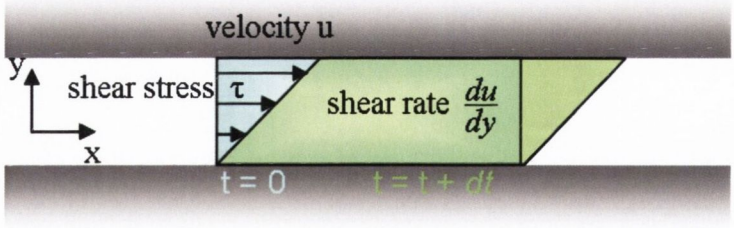

Figure 2-6: Illustration of the response of a fluid to shear stress applied between two infinite plates. The drawing shows that the fluid is deformed when a shear stress τ is applied.

- Viscosity:

The viscosity (η) of a fluid is determined as the resistance of a fluid to deformation under shear stress.

- Nature of fluid:

A fluid can be characterized depending on its behaviour under shear stress conditions. A Newtonian fluid is defined such as shear stress is directly proportional (or linear) to shear rate, whereas the relation between shear stress and shear rate of a non-Newtonian fluid is non linear. Therefore, flowing water (Newtonian fluid) comparing to flowing blood (non-Newtonian fluid) would not flow on the same manner within a system.

- Flow regime:

Laminar flow is characterized by smooth straight line motion at a velocity independent from time. While turbulent flow is defined as stochastic and irregular fluctuations in the flow motion with a velocity dependant in space and time.

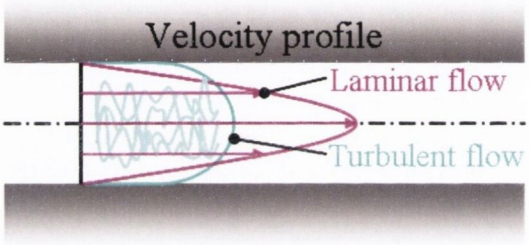

Figure 2-7: Illustration of the velocity profile of a flow depending on its nature. The drawing shows the difference of the velocity profile between laminar flow (straight layers) and turbulent flow (irregular layers).

- Reynolds number:

The dimensionless Reynolds number (Re) is used to classify the flow whether it is laminar (Re < 2300, viscous forces are dominant) or turbulent (Re > 2300, inertial forces are dominant). It is defined as the ratio of inertial forces (vρ) to viscous forces (η/L) and is evaluated by using the following equation:

$$\mathrm{Re} = \frac{\rho \cdot v \cdot L}{\eta} \qquad \text{Equation 2-1}$$

where ρ is the density of the fluid, η the viscosity, v the velocity and L the maximum between the width and the depth of the channel.

2.13 Physiological range of shear stress

Under different physiological conditions blood vessels are subjected to differing shear stresses. Shear stress is defined as the tangential force per unit area that is exerted by the flowing fluid on the surface of the conduit tube. Shear stress is a potent facilitator of integrin conformational changes during leukocyte arrest on blood vessels and antigen-presenting cells[75]. The magnitude of shear stress is proportional to the velocity gradient near the tube wall, i.e. it is dependent on the speed of the flowing blood. Shear stress is expressed in dyne per cm^2 (dyn/cm^2). The physiological range of shear stresses varies considerably depending on the type of vessel and its inflammatory state (Table 2-1), typically more than 10 dyn/cm^2 in arteries and 1 dyn/cm^2 to 5 dyn/cm^2 in postcapillary venules[76]. The physiological range of shear stresses for leukocyte recruitment close to the postcapillary venules is usually around 1 to 6 dyn/cm^2 [77, 78].

Cell type	Shear stress (dyn/cm^2)	Surface/coating assay	Assay conditions	References
Vascular endothelial cells	10-100	-	*in vivo*	79
	0.6-22	Gelatin	*in vitro*	80
Hepatocytes	<2	Collagen type I	*in vivo*	79
Mouse embryonic stem cells	6.5-16	Collagen type I	*in vitro*	79, 81
Human umbilical vein endothelial cells (HUVECs)	4-25	Gelatin Collagen type I/III	*in vitro*	79, 82, 83
Bovine/Porcine aortic endothelial cells (BAEC-BAEC)	4- 25	Fibronectin Collagen type I	*in vitro*	74, 79
HeLa cells	4-25	-	*in vitro*	79
Chinese hamster ovary (CHO)	2-25	von Willebrand factor	*in vitro*	84
Leukocytes	0.5-10	HUVEC monolayer Fibronectin HUVECs	*in vitro*	85, 86, 87
Neutrophils	0.72 to 6.2	Human fibrinogen	*in vitro*	78

Table 2-1: Table presenting the shear flow conditions for different type of cells in microfluidic biochip or *in vivo* milieu (modified from Kim *et al.*[79])

Different model systems have shown mechanisms of leukocyte transmigration and described the multistep paradigm for leukocyte recruitment[88-90]. However, recently substantial evidence has been accumulated highlighting the impact of shear stress[91-93] on the induction and enhancement of T cell migration. In that work, shear stress was applied to the cells which would encounter physiological flow and response differences were detected[85, 94]. Due to these innovative *in vitro* methods, leukocyte capture and subsequent rolling are known to be mediated by shear stress[77, 95-97]. Transendothelial migration has been reproduced *in vitro* using these biochip designs highlighting the hitherto unknown importance of shear stress in transmigration due to its ability to modulate the activity of many of the cell bound proteins and their ligands involved in the extravasation process[69, 70, 98-100].

2.14 Tools for analysis and interpretation

There is a wide variety of image analysis software packages available to researchers. These can be used to assess and quantify the morphometric parameters of cells. The commonly used and relevant packages[69] are ImageJ (National Institute of Health), ImagePro (MediaCybernetics), Volocity (ImproVision), Cell (Olympus), Analysis Pro (Analysis), MetaMorph (Molecular Devices). Many of these applications emerged from researchers and spin out companies, for example CellTrek from the University of Virginia. Such software applications are now *de rigueur* in labs which need to track multiple fast-moving cells over a selected area for a fixed time period. Cell-tracking software is necessary for the compilation and analysis of the masses of data which results from any experiment which involves the tracking of cells in a flow environment. Some software packages are also used for mathematical modelling of proposed chip designs to approximate their expected efficacy[69, 77].

It is beneficial to have mathematical modellings of a continuous flow of cells concurrent with the data which describes the diffusion of a gradient of chemokines, correlating to the experimental data obtained. It enables the researcher to anticipate the movement of the chemokine gradients in response to the flow and thus aids in the rationalisation of the design. MATLAB® (from Mathworks) is one of the most powerful software packages for numerical computing and modelling. As many non-programmers have to work with these packages, the utilization of this kind of software

has become easier and more accessible to a wider range of users. Thus, the interface of the software has become more intuitive over time. COMSOL Multiphysics® (previously femlab, from ComsolLab) is a fully developed Matlab platform integrated in a user-friendly Finite Element Analysis (FEA) Graphic User Interface (GUI). COMSOL extensively covers the majority of advanced multiple physics applications in a modular software package; among these there are dedicated modules for fluidodynamics problems. The user friendly interface of this package effectively removes all programming steps from the design process to the post-processing simulation.

2.15 Methods to generate a natural gradient of chemokines

Natural chemotactic cytokines (chemokines) can be obtained from bacteria or eukaryotic cells[101]. More precisely, they can be derived from freshly isolated leukocytes, connective tissue cell cultures or malignant cell lines. Alternatively, recombinant chemokines can be produced. To stimulate the cells and keep them activated, cells need to be induced with endogenous (cytokines) or exogenous (bacterial, viral) agents[102].

Conventional assays such as Boyden chambers allow the incubation of cells (e.g. leukocytes) in presence with cytokines to stimulate and enhance cells secretion of chemokines. The supernatant is then isolated and screened using a technique called enzyme-linked immunosorbent assays (ELISA). This technique is used to detect and identify the presence of an antibody or an antigen in a supernatant. Chromatography techniques are used to purify and isolate the natural chemokines.

Chemokines can also be secreted by endothelial cells such as human umbilical vein endothelial cells[103] (HUVECs) that have been stimulated with cytokines (e.g. TNF-α, IL-1). It has been shown that the production of chemokines by both HUVECs and leukocytes are increased when they bind to each other[104]. Therefore, the interaction between leukocytes and HUVECs is one of the key mechanisms for the release of natural chemokines.

Murphy *et al.* mimicked this interaction between activated leukocytes and endothelial ligands in an artificial manner in order to produce natural chemotactic cytokines[105]. It has previously been shown that the leukocyte function-associated antigen-1 alpha (LFA-1α) molecule is involved in leukocytes migration into the tissue at the site of infection and induces cytoskeleton rearrangement in leukocytes (e.g. T-cells) promoting cells locomotion[106]. To address the mechanism of this phenomenon, Murphy *et al.* coated protein G-sepharose beads with immobilized antibody to LFA-1α and incubated them with leukocytes in a non coated plate. They noticed that cells migrated towards the coated beads suggesting that the interaction between anti-LFA-1α and cells integrin mediated the release of chemokines (e.g. MIP-1α and MIP-1β). This was validated by neutralizing antibodies to MIP-1α and MIP-1β that further inhibited cells migration.

Such natural ways of generating a gradient of chemokines in an engineered environment could be used as alternative methods to the pump-assisted approach of gradient establishing in microfluidic platforms.

2.16 Diffusion and transport of particles in the human body

The natural movement of particles within a system makes them to move from a higher concentration area to a lower concentration area. This is possible due to the random molecular motion also called diffusion. This mixing creates a gradient of concentration over the time until reaching a homogeneous concentration at an infinite time.

In biology, the diffusion of particles through the cell membrane or the tissue is fundamental for the transport of nutrients in and out of the cells or to clear the body of waste substances. The diffusion of cytokines is also a primordial process in the body mediating immune responses. Therefore, techniques have been developed in order to understand and observe the basic mechanisms of different nature of transports in the body. Ultrasound waves are commonly used for the imaging of the blood transport in vessels (e.g. optical Doppler tomography). Magnetic resonance angiography is another imaging technique for the visualization of flowing blood in vessels.

However, for the imaging at a cellular level, other techniques have been widely used for the study of molecule mobility through cell membrane or tissue involving fluorescent

markers. For example, fluorescence correlation spectroscopy (FCS) is a technique that uses correlation analysis to characterize the dynamics of weak fluorescent signals[107] such as binding of protein to its environment. The measurement of the fluorescence intensity and its temporal decay is related to the diffusion speed of the molecules and the diffusion coefficient of the particles (e.g. proteins) can be calculated.

The fluorescence loss in photobleaching[108] (FLIP) is another technique based on the fact that repeatedly photobleached area in a matrix gives information about molecules transport within this matrix. If the fluorescence of the area bleached is continuously recovered until total loss of it, it means that non-bleached molecules are free to diffuse in the matrix. Thus, it can give an idea on how molecules are bind to their environment.

The fluorescence recovery after photobleaching[109] (FRAP) technique is widely used to track dynamic behaviour of molecules in living cells. A fluorescent labelled area is bleached for a short period of time and stopped to monitor the fluorescent recovery of the bleached area. Large amount of protocols of FRAP experiments are available and one can be carried out using the beam from a confocal laser scanning microscope.

The previous techniques are used to obtain quantitative information of the particle studied such as its hydrodynamic radius or its diffusion coefficient within a matrix.

Therefore, the progression of a gradient of chemokines within a system relies on the characteristic of the chemokines used and also on the environment in which they evolve in. Using FRAP technique is a reliable technique to evaluate the characteristic of diffusivity of particles through a specific environment (e.g. gel).

3 Efficacy of existing chemotactic assays

Chemotactic assays are *in vitro* experimental tools for the evaluation of cell migration. The migratory ability of cells is assessed by detecting the response of cells towards a gradient of a chemotactic factor. The response of cells to a gradient is quantified in two ways: the rate of cell movement and the directional orientation of the movement. Conventional *in vitro* assays are widely carried out in different environments such as in matrices composed of gel[110, 111] (e.g. collagen, agarose), filters with variable pore size (Boyden chamber), or plate chambers (Dunn chamber, parallel plate chamber[77]).

These assays enable the determination of qualitative and quantitative responses of cells towards a chemotactic gradient. A qualitative response refers to the behaviour of cells in presence of chemokines, whether they are reacting to these molecules or not. Thus, the observation of what is happening to the cells is directly visualized and evaluated using microscopy and image acquisition. A quantitative response refers to the analysis of cells locomotion, more precisely to the quantification of the rate of the cell movement as well as the direction in which cells are migrating. The response of the cells is also visualized using microscopy[112] and, again, images are acquired, but additional measures are generated using image analysis software.

Specialised software is used for multiple tasks e.g. image enhancement for further visualization of details on images; image processing such as the classification of objects, the automatic count or track of objects on images and also mathematical calculation such as Fourier Transform for image filtering or reconstruction. These computation tools are useful for the analysis of biological images. In the case of chemotactic assays, the response of cells to chemokines can be estimated and quantified.

The aim of the present research is to advance the development of a physiological environment for the cells within an implemented chemotaxis assay. This environment should present similar characteristics to the *in vivo* environment. It includes mechanical stress on cells to mimic the blood flow and also a channel network that imitates the vessel structure found in tissues. The diffusion of chemokines occurs through the

different layers of the tissue (Fig. 1-2) which is usually mimicked *in vitro* using gels such as agarose, collagen, and many more.

Therefore, assays under-agarose[30] present a straightforward approach to observe cell responses within a gel scaffold. The protocol for these assays have been widely used and described in literature[113] (and later in this chapter). Briefly, two wells are punched in the gel at a distance of 5 mm from each other; cells and chemotactic solution are dispensed in separate wells. The gradient of chemokine is diffused through the gel allowing the cells to migrate along this gradient. The time for cells to migrate the distance between the two cells usually takes up to 4 hours.

The study of cells in Dunn chamber[114] is an alternative method to study migrating cells towards a gradient of chemokine. This chamber consists in 2 ring-wells one filled with an inert solution (e.g. phosphate buffer saline) and the other with a solution of chemokine, both separated by a 1 mm wide bridge. Cells are seeded on a cover slide places upside down on the chamber. This method allows the observation of the response of cells towards the chemotactic gradient generated on a shorter distance than under agarose assay and within a reduced time of incubation (2 hours).

Therefore, before developing new assays, it is first necessary to evaluate the behaviour of cells in conventional chemotactic assays and to get a clear understanding of the efficacy and limitations of the existing approaches. Under agarose assays were used to study the cells within a gel environment and the Dunn chamber was used to evaluate the cell responses on a short distance (1 mm). The experimental data obtained were analysed using Image-Pro software.

3.1 Materials and methods

3.1.1 Cells isolation and culture

Neutrophil isolation: Blood (20 ml) was collected from healthy volunteers into sterile heparinized Vacutainer® tubes (Becton Dickinson, U.K.). Whole blood was gently mixed with 6 % dextran in 0.9 % NaCl in a 4:1 ratio in a 50 ml tube. This step causes the red blood cells to clump and sediment to the bottom of the container. After 45 min

of incubation at 37 °C and 5 % CO_2, the leukocyte-rich supernatant was removed and gently layered on top of a Lymphoprep gradient (Fresenius Kabi Norge, Norway) and centrifuged for 30 min at 400g at 4 °C. As the neutrophils sediment to the bottom, the supernatant was discarded and the neutrophil pellet was washed twice in 10 ml of phosphate buffered saline (PBS) and centrifuge at 400g at 4 °C for 5 min. The cell pellet was then resuspended in 3 ml of distilled water and 1 ml of erythrocyte lysing solution (3.6 % NaCl) was added. The neutrophils were then counted on a haemocytometer and 2 x 10^6 cells/ml was resuspended in PBS (Gibco, Invitrogen, Ltd, UK).

The purity of the isolation of neutrophils was assessed by staining the cells with a fluorescent dye Hoechst 33342 which stains DNA thereby enabling to visualize cell nuclei. Therefore the typical segmented nucleus of neutrophils could be observed. Simultaneously, cell viability assays were performed.

PBL isolation and culture: Peripheral blood lymphocytes (PBL) were isolated from buffy coats obtained from healthy volunteers from the Irish Blood Transfusion Service (National Blood Centre, James's Street, Dublin 8). Buffy coats were diluted with PBS in a ratio 1:3 in a 250 ml container. In 50 ml tubes, a volume of 30 ml of diluted blood was layered onto 15 ml of Lymphoprep gradients (Fresenius Kabi Norge, Norway). The preparation was centrifuged at 1200g for 20 min at 4 °C. The buffy layer (Fig. 3-1) was removed and centrifuged at 1500 rpm for 5 min and resuspended and washed twice in RPMI 1640 supplemented with FCS (10 %), penicillin (100 U/mL), streptomycin (100 µg/mL), L-glutamine (2 mM). When lymphocytes were washed twice, they were resuspended in RPMI 1640 serum free medium in a 175 cm^3 flask at a concentration of 1-2 x 10^6 cells/ml for 2h. This step allows the separation of adherent cells such as monocytes or platelets from lymphocytes. Lymphocytes in suspension were then centrifuged at 1500 rpm at room temperature for 5 min and resuspended at 2 x 10^6 cells/ml and activated with phytohaemagglutinin (PHA) at a concentration of 1 µg/ml. After three days, cells were centrifuged at 1500 rpm for 5 min and resuspended in complete medium at a concentration of 1-2 x 10^6 cells/ml. Cells were cultured for ten days and activated every 2 days with 20 ng/ml of interleukine-2 (IL-2). After ten days, routine check of cells migratory capability was performed using anti-LFA-1 antibody. PBL could be maintained in culture for approximately 7 days.

An "activation buffer"[115] was prepared for the experiment involving the migration of PBL on a surface coated with ICAM-1 or VCAM-1. The buffer consisted in 20 mM HEPES, 2 mg/ml glucose, 5 mM $MgCl_2$, 1 mM EGTA, the pH of the final solution was 7.2. A "washing buffer" was used to wash cells from the culture medium. This buffer also consisted in 20 mM Hepes and 2 mg/ml glucose but was not supplemented with magnesium and calcium.

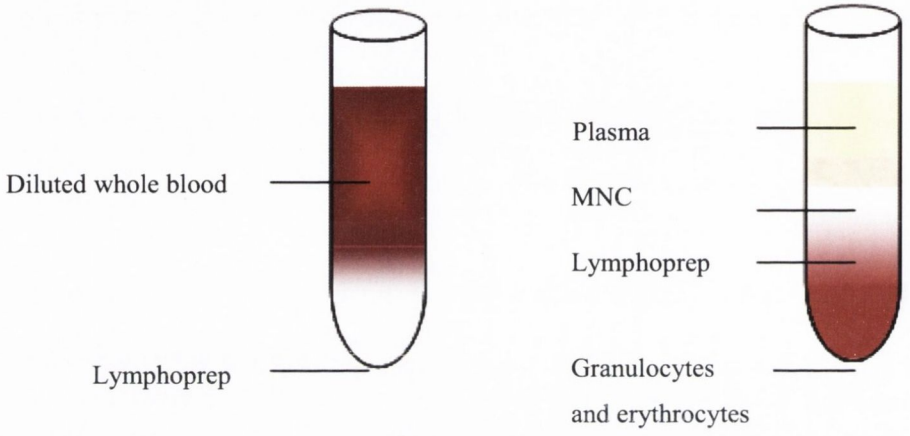

Figure 3-1: Procedure of isolation of peripheral blood lymphocytes (PBL) from buffy coats. Diluted buffy coat (1:3 in PBS) was dispensed on 15 ml of lymphoprep in 50 ml tube and centrifuge at 1200g for 20 min at 4 °C (left drawing). After centrifugation, mononuclear cells (MNC) containing PBL were collected for further purification (right drawing).

HUT78 culture: T lymphoma cells line 78 (HUT78) were cultured in RPMI 1640 medium supplemented with L-glutamine (2 mM), Hepes buffer (1 M), sodium bicarbonate (1.5 g/l), sodium pyruvate (1 mM), glucose (4.5 g/l), penicillin/streptomycin (5 ml), 8% FCS.

3.1.2 Biological reagents for chemotactic assays

Stromal Cell-Derived Factor 1α (SDF-1α, CXCL12)[116] is a chemoattractant for T lymphocytes and monocytes purchased from Sigma-Aldrich (Ireland). It is a member of α-CXC chemokine family and its molecular weight is around 8 kDa. It was used at a concentration of 100 ng/ml.

Interleukine-8 (IL-8)[117] is also called monocyte-derived neutrophil chemotactic factor (Sigma-Aldrich, Ireland). It belongs to the chemokine α-CXC family and has a molecular weight of 8.4 kDa. It presents a chemotactic activity *in vitro* for T cells and was used at a concentration of 100 ng/ml.

Formyl-methionyl-leucyl-phenylalanine (FMLP)[117] is a synthetic chemotactic peptide affecting the orientation and movement of leukocytes. FMLP mimics the activity of bacterially-derived peptides. It was used for the activation of neutrophils at a concentration of 1 ng/ml.

The antibody LFA-1α reacts with the alpha chain of LFA-1 the CD11a/CD18 integrin heterodimer presents on human T-lymphocytes[118]. A vial of 1 ml contained purified antibody in PBS with 0.1 % BSA and 0.02 % sodium azide (Monosan, Netherlands). A range of concentration of anti-LFA-1α was used for the routine check of cells polarization. Dilution in PBS from 0.5:100 up to 10:100 was performed.

Bovine serum albumin (BSA)[119] is a single polypeptide isolated from bovine blood plasma that contains albumin. Albumins are a group of acidic proteins which occur plentifully in the body fluids and tissues of mammals. BSA is routinely used in biology to inhibit cell attachment to surfaces. It is diluted in PBS at a concentration of 2 %.

3.1.3 Staining reagents

The fluorescent stain Hoechst 33342 was used for labelling nuclear DNA in order to visualize the nuclei of live neutrophils. It is used at a concentration of 5 µg/ml. Cells (20 µl - $1x10^6$ cells/ml) are dispensed on a cover glass in a 6 well plate and incubated for 10 min at 37 °C and 5 % CO_2. This step allowed cells to stick onto the cover glass. Cells were washed twice with PBS in order to remove any non-attached cells and Hoechst stain was dispensed on top of the cells and incubated for 5 min. Additional wash was performed before dispensing prewarmed medium on top of cells. Hoechst is excited by ultraviolet (UV) light at around 350 nm and emits a blue fluorescence light at around 461 nm.

Ethidium bromide/acridine orange (EB/AO) solution (1 %) was used to evaluate cells viability. Acridine orange was excited at a wavelength of 500 nm and its green fluorescence emission was at 526 nm, while ethidium bromide was excited at 510 nm to get an orange fluorescence emission at 595 nm. Viable cells take up acridine orange and appeared green when observed under fluorescent microscope, whereas non-viable cells take up ethidium bromide and appeared orange.

3.1.4 Characteristics and preparation of the agarose gel

Agarose[120] is a polysaccharide obtained from agar that forms a gel when the temperature of aqueous agarose solution cools down. Agarose gel is a viscoelastic material which means that it exhibits both viscous and elastic characteristics when undergoing deformation. The viscosity of a material relies on its response when being deformed by a shear stress. The elasticity of a material also relies on its response to a mechanical deformation under stress but its particularity is that when the stress is stopped the material returns to its original shape. The geometrical measure of that deformation is the strain. Therefore, a viscoelastic material exhibits time dependant strain or time dependant deformation. In other terms, the stiffness of the agarose gel would increase with gel concentration.

Agarose gel is widely used for chemotactic assays because it has little or no effect on live cells. Ultra-pure agarose (Pronadisa, Madrid, Spain) with a low gel point (31 °C for a 0.5 % gel and 39 °C for 2 % gel) was used to create an inert matrix in which cells were dispensed. The melting point of an agarose solution of 0.5 % and 2.5 % is 85 °C and 88 °C respectively. The gel was formed by diluting agarose in distilled water in 50 ml tube and was vortexed gently. With the lid of the tube loosely attached, the agarose solution was heated in a microwave for about 5 s and vortexed at high speed for 5 s. This was repeated until the agarose was totally dissolved. The liquid agarose was then dispensed on the bottom of a well and cooled down at room temperature to gelify. A concentration range (weight/volume, w/v) of 0.1 % up to 2 % was used to study the impact of the gel concentration on cells mobility.

3.1.5 Assays for investigation of the polarity of cells

PBL cells were tested before each experiment in order to assess their capacity of polarization. A 96-well plate was coated with goat anti-mouse (GAM, dilution 1:200 in PBS). The plate was kept overnight at 4 °C and washed twice with PBS. The plate was then coated with anti-LFA-1α antibody (range of dilution 1:200 to 1:10 in PBS) for 1 hour at 37 °C and washed twice with PBS. The preliminary coating with GAM enabled the presentation of anti-LFA-1α to the cells in the appropriate orientation, with antigen (LFA-1) binding sites facing away from the substrate towards the surface of the cells. Cells were dispensed onto the coated surface at a concentration of 15 000 cells per well and incubated for 30 min at 37 °C. Polarization of cells was observed under an inverted Nikon microscope and the pictures were acquired using ImageQ software. PBL cells polarity was compared to the polarization of HUT78 cells that were dispensed on the coated surface using the same protocol that for PBL. HUT78 cells were used because they are known to develop high polarity when they are stimulated with immobilized antibody to LFA-1α[121].

Polarization of PBL was also tested on human recombinant ICAM-1-Fc and VCAM-1-Fc chimeric proteins[2, 122]. Both ligands are known to have an important role in leukocyte rolling during the leukocyte homing process. For this experiment, the surface was first coated with anti-human IgG (Fc specific) at a dilution of 1:1000 in PBS. This step enabled the presentation of ICAM-1 or VCAM-1 to the cells in a proper spatial orientation, with the Fc fragment oriented towards the support substrate and receptor-binding sites facing outwards. A titration of ICAM-1 and VCAM-1 (0 µg/ml, 1 µg/ml, 2.5 µg/ml and 5 µg/ml) was performed to determine the optimised concentration for cell polarization. A volume of 100 µl of 0.5 x 10^6 cells/ml was dispensed in each well and incubated for 30 min.

3.1.6 Image-Pro-based analysis

The quantification of the capacity of the cells to polarize on a substrate was processed by analysis of the microscopic cell images using Image-Pro software. The images obtained from the Dunn chamber and the under agarose assays were also processed using this software and the method used is explained in each respective section (§ 3.1.7 and § 3.1.8).

The images acquired with ImageQ software were opened in the main window of Image-Pro. The intensity level of each image was edited to enhance the contrast between the background of the image and the cells. The correction of the image intensity was carried out manually by changing the range of the intensity (Fig. 3-2). The background was also flattened to enhance this contrast.

However, the variability in the quality of the images could present artefacts restraining further image processing. For example, the background of the image may not be flattened enough and the intensity of the image might vary considerably across the image, mostly at the edges of the image. Therefore, an area of interest (AOI) was chosen in the middle of the image in order to minimise artefacts (Fig. 3-2).

Figure 3-2: Example of image analysis using Image-Pro software. An area of interest (AOI) of the digitally taken microscopic image was selected (white square) and the range of the intensity of the image was set (right panel) to adjust the contrast between the background of the image and the contour of the cells.

Filters were applied on the area of interest to measure various parameters of the selected objects. The purpose was to assess the ability of the cells to polarize on a coated substrate to establish the best concentration of the coating. To simplify, the longer the shape of the cell was the better the polarization was. Therefore, the filters selected were the Area, the Axis (major), and the Aspect. As it is shown on figure 3-3, the filter Area measured the area of an object. If an object presents a porous surface (hole), there is an option to measure only the area without the hole. There was no need to take into

account this option as the type of the objects we measured presented no holes. The filter Axis (major) measured the length of the major axis of the selected object and the filter Aspect measured the ratio between the major and the minor axis of the objects. For the last two filters, the software used a simplified model of the filtered object that was equivalent to an ellipse.

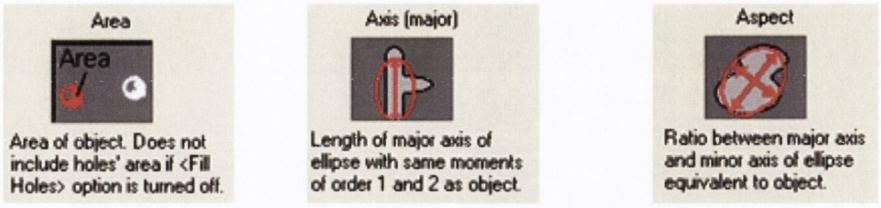

Figure 3-3: Algorithm of filter selection in Image-Pro application. Each microphotograph of cells was processed using the filters Area, Axis (major) and Aspect which take into account the shape of the object filtered.

The objects were screened on each image depending on the range of each filter. In our case the target objects (to be included in analysis) were the cells and the unwanted objects were for example artefacts from the background or dust particles (Fig. 3-4).

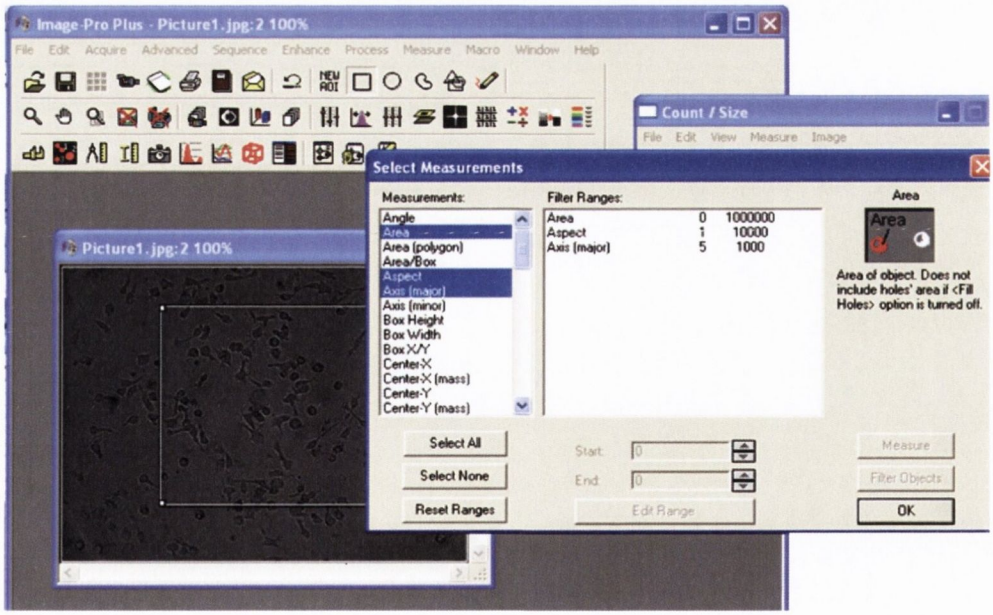

Figure 3-4: Example of the experimental acquisition and process window in Image-Pro software. Experimental acquisition window in the background with the selected area showing polarized cells that have been processed by Image-Pro with the Area, Aspect and Axis (major) as chosen object filters. These settings enabled to discriminate between the desired objects to be included in calculation from the unwanted structures (i.e. dust particles, background artefacts).

Once all the parameters were set, the filtered objects were observed using the Count/Size dialog box. The contour of the cells that were in the range set was displayed in red (Fig. 3-5).

Figure 3-5: An example of a result of cells screened on an experimental acquisition in Image-Pro using the filters (Area, Aspect, Axis). The cells that fitted in the range of the filters were outlined in red.

The data obtained using each filter were visualized in the Data box in Image-Pro and subsequently exported to an Excel sheet for further analysis. The filter that was linked to the polarization ability of the cells was the filter Axis (major).

3.1.7 Migration of cells under an agarose gel

The assay using agarose gel[30, 110] was used to observe the response of a population of cells to one or more chemoattractant sources. A 12-well cell culture plate was filled with 500 µl of agarose mixture. A concentration range of agarose was tested from 0.1 % to 2 % to study the influence of the composition of the gel on the cells mobility. Three reservoirs separated from each other by 5 mm were punched into the agarose plate with a 500 µl pipette. (Fig. 3-6). Chemoattractant solution (100 µl) was dispensed in one well, while cells (100 µl) were dispensed into the central well. In the third well, 100 µl of PBS was dispensed as a control. The diffusion of the chemokine solution generated a

chemotactic gradient from the reservoir containing the chemoattractant solution to the well containing cells.

Therefore, the cells were in the situation where in one side they could detect a gradient of chemokine, while in the other side they had no particular signal due to the neutrality of the PBS. Hence, in the same well, the chemotactic experiment was run in parallel to the control assay.

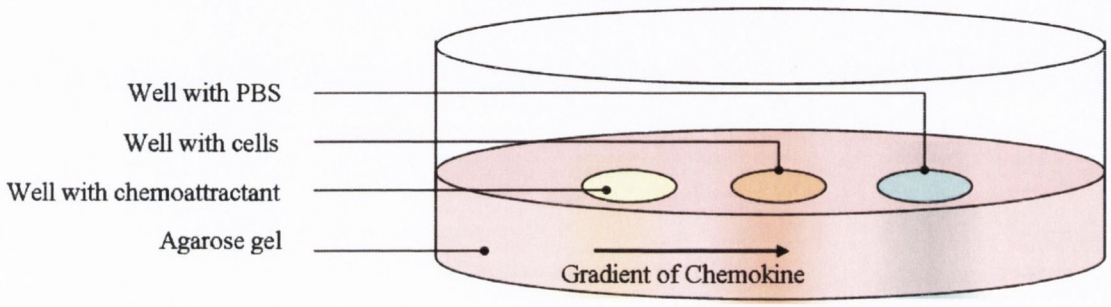

Figure 3-6: Schematic illustration of the under agarose assay setup. Three reservoirs were punched in the agarose gel and were filled with PBS (control), cells and the chemoattractant solution. The gradient of chemokines was diffused from the chemoattractant reservoir to the reservoir that contained the cells.

Once cells were dispensed in the well, we let them to settle down for 10 min. Pictures of each well were taken after that at t=0 and t=4h using ImageQ software. The acquired pictures were then opened in Image-Pro. The filters previously described in section 3.1.6 were used to select each cell. The filter named Centre-X was also chosen to give the position of each cell across the image (in arbitrary units). The data obtained in Image-Pro were exported into an Excel sheet. The image was divided into 6 segments of equal size. The total length of the 6 segments represented 400 μm. The mean number of cells across the image was displayed for each segment.

3.1.8 Generation of chemokine gradient in the Dunn chamber

The behaviour of cells subjected to a linear concentration gradient of chemoattractant was observable in the Dunn Chemotaxis Chamber (Hawksley DCC100). The Dunn chamber consists of two ring wells separated from each other with a 1 mm wide bridge. When a cover glass is placed on top of the wells, the chamber was designed such as a

20 µm gap separates the bridge from the cover glass. This gap allows the diffusion of solution along the bridge (Fig. 3-7).

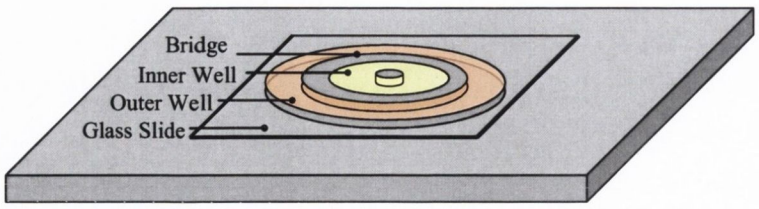

Figure 3-7: Scheme of the Dunn chamber DCC100 Hawskley. Cells were seeded on the glass slide and placed upside down on top of the chamber. The two ring reservoirs were separated by a 1 mm wide bridge. The outer well was filled with chemoattractant solution and the inner well with PBS. The gradient of chemokines was induced from the outer well to the inner well through the 20 µm gap.

A glass slide was immerged in 2 % BSA solution for 5 min at room temperature and washed twice with PBS. Neutrophils were cultured on BSA-coated glass slide for 1h at 37 °C. Then, the glass slide seeded with cells was inverted onto the chamber. The inner well of the chamber was filled with PBS which represented the gradient concentration of C = 0 %. While the outer well of the chamber was filled with the chemoattractant IL-8 which represented the gradient concentration of C = 100 %. The gradient in the chamber was set after 30 min and the chemotaxis assay was recorded for a time lapse of 2 hours on an inverted microscope.

The images collected from ImageQ were analyzed with Image-Pro software using the same filters previously explained (§ 3.1.6). The tool "Track object" was subsequently selected and each filtered cell was tracked over the period of the record. The coordinates of each track was then normalized in an Excel sheet.

3.2 Results

3.2.1 Analysis of the viability of the cells

Neutrophils were isolated and used on the day of their isolation. The quality of the isolation was evaluated by staining the cells with the Hoechst dye to observe the nucleus morphology. It is shown on figure 3-8 that isolated neutrophils presented a

segmented nuclear structure that is the typical nuclear morphology of neutrophils. The cells were also stained with EB/AO to observe viable and non-viable cells under microscope. Neutrophils were counted on a haemocytometer and the yield of neutrophils isolation was estimated around 90%.

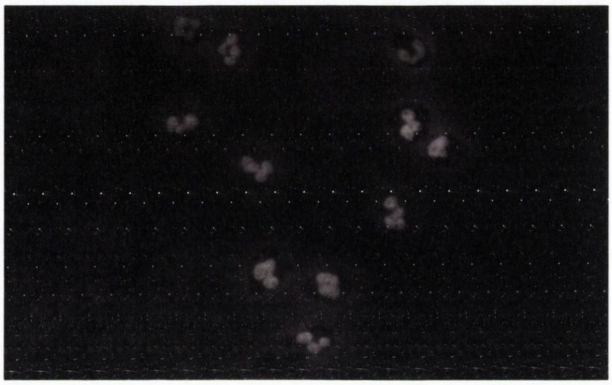

Figure 3-8: Fluorescence photograph of the nuclear morphology of neutrophils stained with Hoechst dye. Visualization under UV light permitted to observe the segmented nuclear structure that is typical of neutrophils nuclear shape.

Cultured cells such as PBL and HUT78 cells were tested on anti-LFA-1α. The figures 3-9 present the behaviour of cells to different concentrations of anti-LFA-1α. A titration from 1:200 up to 1:10 was done for both cells. Control on plastic with no specific coating was done to compare cells morphology.

The pictures showing the polarization of PBL and HUT78 on anti-LFA-1α were analyzed using Image-Pro software to quantify the morphology of the cells depending on the coating of the substrate. The same protocol was applied to the pictures showing the polarization of PBL on VCAM-1 and ICAM-1.

For each picture, the data displayed came from the filter "Axis (major)" that described the total length of the tracked cells. Experiments were duplicated (n = 3) and standard error of the mean was displayed on each graph.

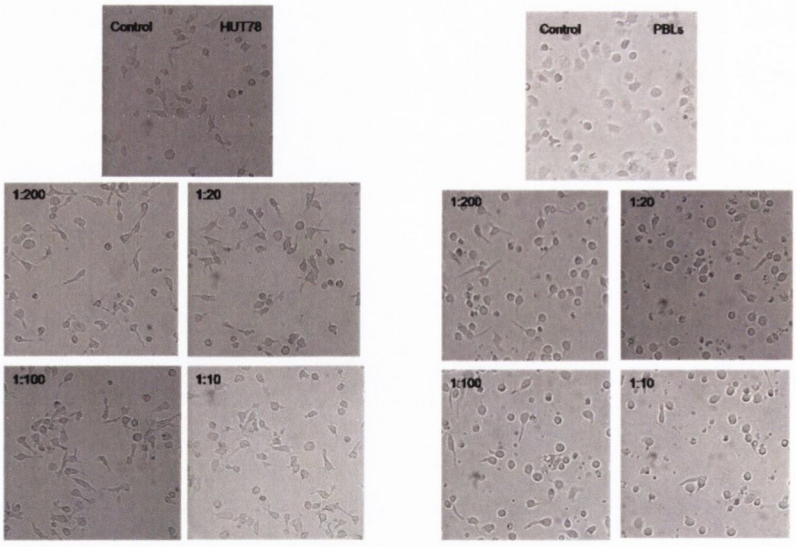

Figure 3-9: Lymphoma cell line HUT78 and peripheral blood lymphocytes (PBL) polarization in response to LFA-1α cross-linking. The microphotographs show cells of cultured lymphoma HUT78 (left panel) and PBL (right panel) acquiring locomotory behaviour reflected in their polarisation response to immobilized LFA-1α antibody on the plastic surface. Concentrations of immobilized antibody are indicated on each microscopic panel.

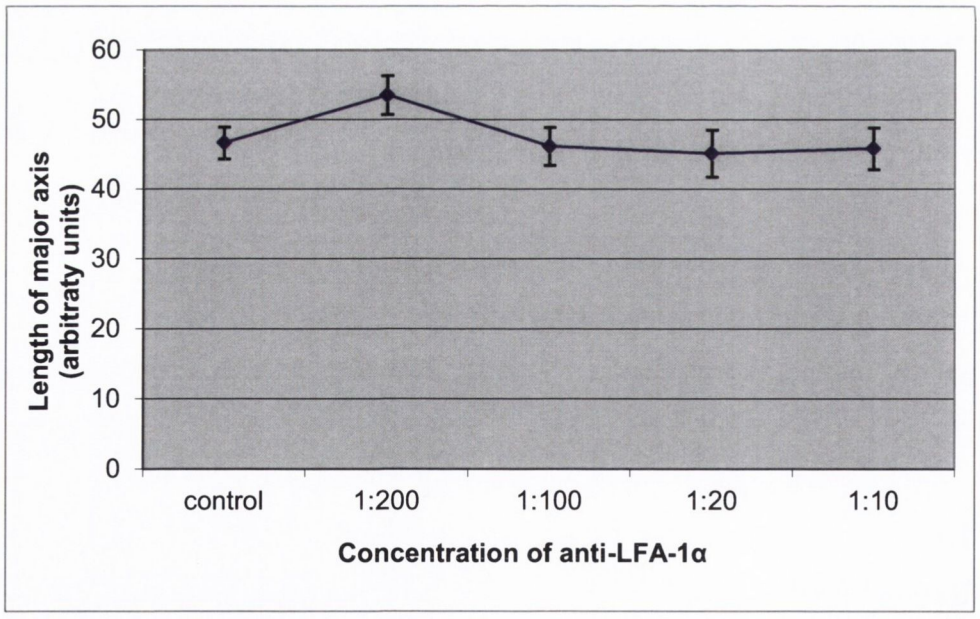

Graph 3-1: Polarization of PBL cells on several dilutions of LFA-1α antibody immobilized on the bottom of a 96-well plate. PBL were incubated on the coated surface for 30 min at 37 °C. Pictures of the cells taken with an inverted microscope were analyzed with Image-Pro software using the filter "Axis (major)". Cells dispensed on a substrate coated with anti-LFA-1α at a concentration of 1:200 displayed the most elongated shape. Results are the mean ± S.E.M. of three independent experiments.

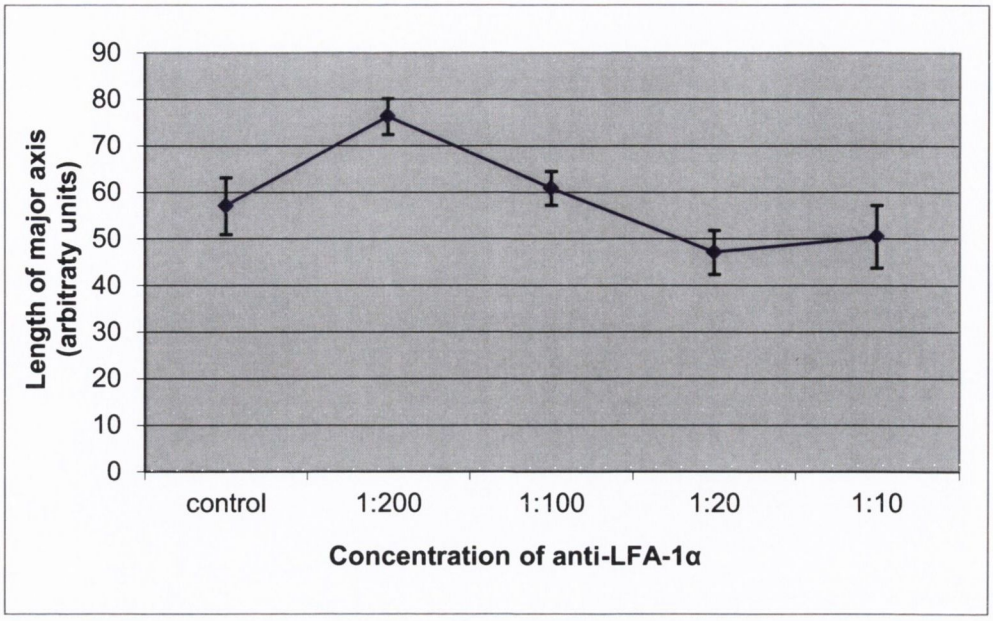

Graph 3-2: Polarization of HUT78 cells on several dilutions of LFA-1α antibody immobilized on the bottom of a 96-well plate. HUT78 were incubated on the coated surface for 30 min at 37 °C. Pictures of the cells taken with inverted microscope were analyzed with Image-Pro software using the filter "Axis (major)". The pick on the graph shows that the morphology of the cells was the most elongated at the concentration of 1:200 of anti-LFA-1α. Results are the mean ± S.E.M. of three independent experiments.

It has been found that both PBL and HUT78 present a highest length of the major axis with a concentration of anti-LFA-1α of 1:200.

A titration of endothelial ligands coated on the surface of a 96-well plate was also carried out (Fig. 3-10). A plate was coated with ICAM-1 and VCAM-1 at a concentration of 1 μg/ml, 2.5 μg/ml and 5 μg/ml.

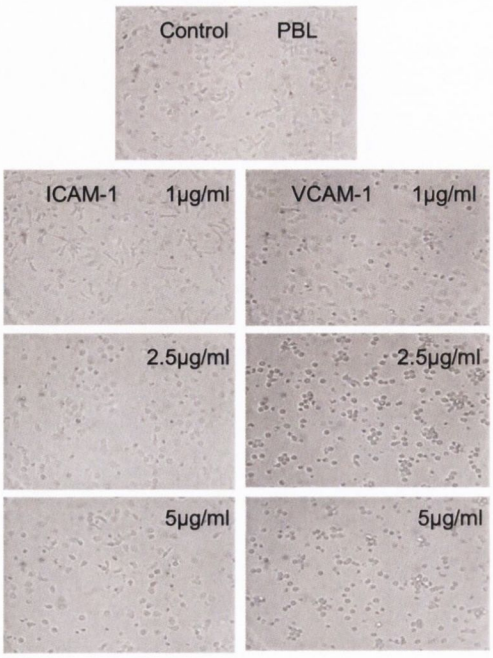

Figure 3-10: Peripheral blood lymphocytes (PBL) polarization in response to ICAM-1 and VCAM-1. Representative microphotographs show PBL cells acquiring motile phenotypes reflected in their polarisation response to immobilized ICAM-1 (left panel) and VCAM-1 (right panel) on the plastic surface. Concentrations of immobilized ligands are indicated on each microscopic panel.

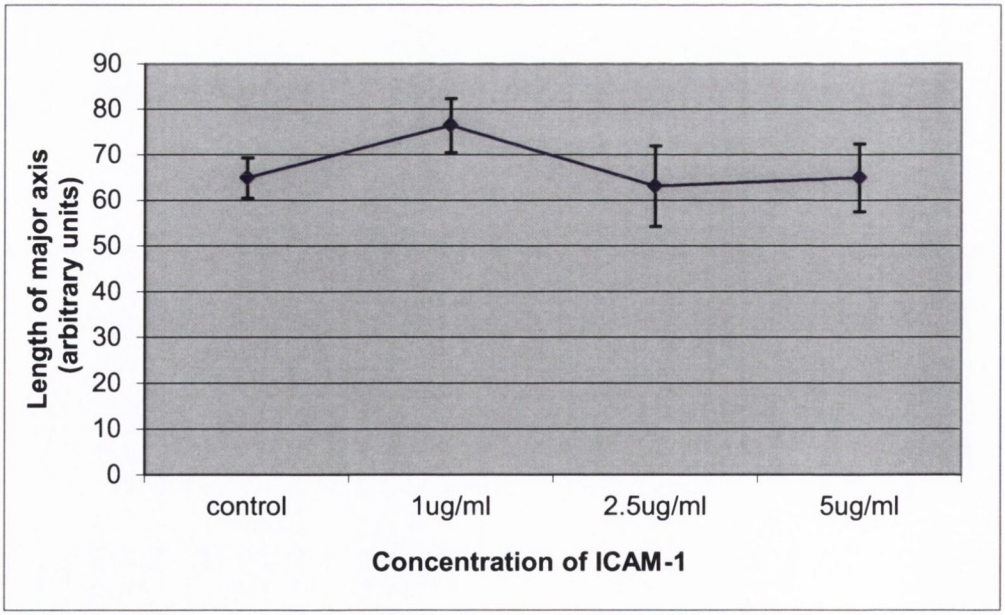

Graph 3-3: Polarization of PBL cells on several dilutions of ICAM-1 immobilized on the bottom of a 96-well plate. PBL were incubated on the coated surface for 30 min at 37 °C. Pictures of the cells captured with the microscope were analyzed with Image-Pro software using the filter "Axis (major)". The pick on the graph shows that the morphology of the cells was the most elongated at the concentration of 1µg/ml of ICAM-1. Results are the mean ± S.E.M. of three independent experiments.

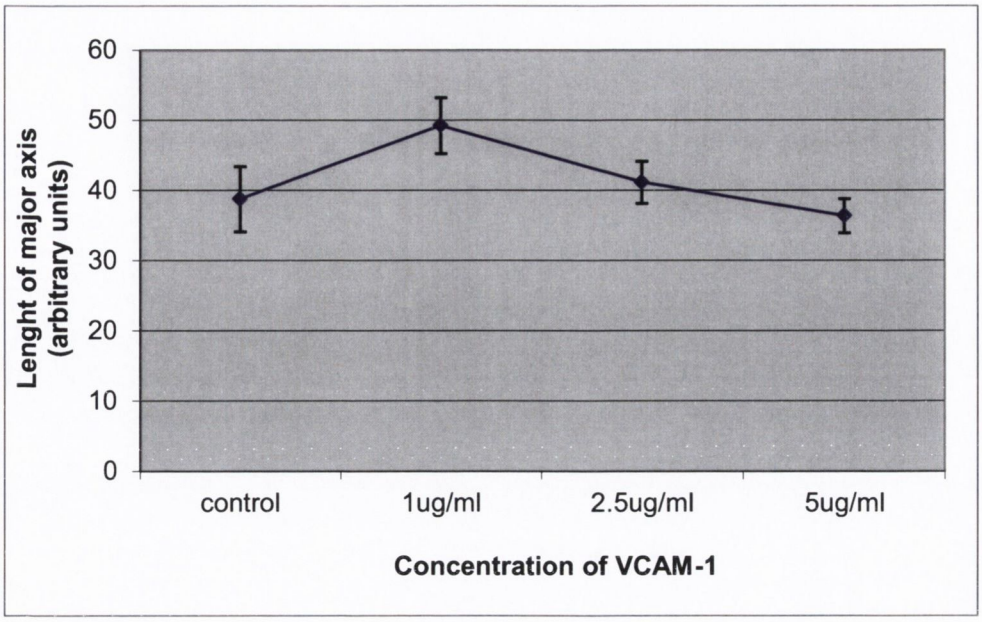

Graph 3-4: Polarization of PBL cells on several dilutions of VCAM-1 immobilized on the bottom of a 96-well plate. PBL were incubated on the coated surface for 30 min at 37 °C. Pictures of the cells captured with the microscope were analyzed with Image-Pro software using the filter "Axis (major)". The pick on the graph shows that the morphology of the cells was the most elongated at the concentration of 1 µg/ml of VCAM-1. Results are the mean ± S.E.M. of three independent experiments.

We have established that PBL exhibit a greater polarization when they are seeded on a substrate coated with 1 µg/ml of VCAM-1 as well as 1 µg/ml of ICAM-1.

3.2.2 Chemotactic responses of cells within a gel environment

The following graphs show the quantification of the migration of PBL cells towards a gradient of chemokine (CXCL-12) or PBS in an under-agarose assay. Each image acquired on the microscope at t=0 and t=4h was divided into 6 equal segments which represent a total distance of 400 µm. The mean number of cells across the image was displayed for each segment.

At time t=0 the amount of cells in each segment was similar in both experiments. At time t=4h, cells migrated in the direction of the diffusion of chemokine at a maximum rate of 1.6 µm/min. This caused a clearly defined cell scattering over the substrate which is demonstrated on graph 3-5. The responses of the cells to the gradient of PBS over 4 hours were negligible in comparison to the responses of the cells that migrated towards the chemoattractant gradient (graph 3-6).

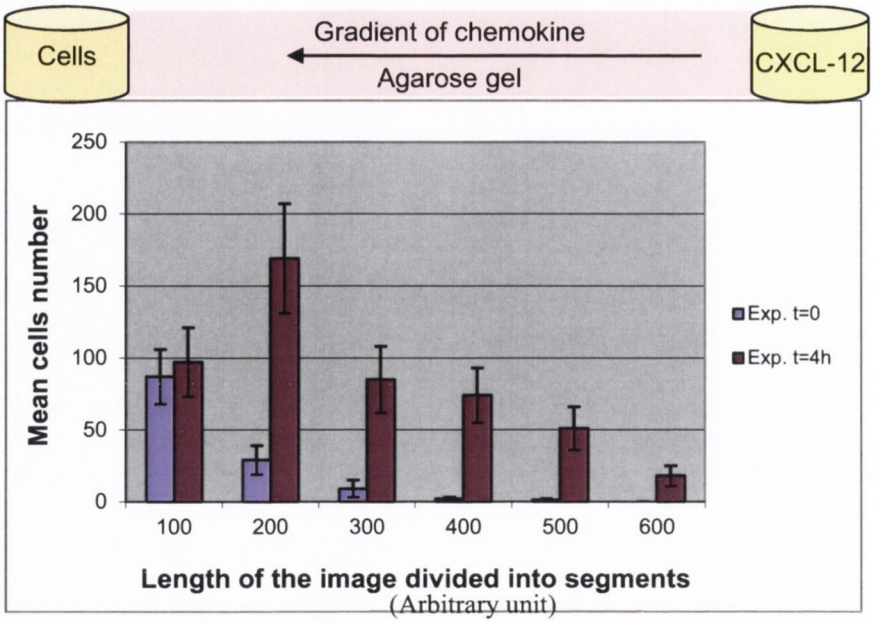

Graph 3-5: Quantification of the migration of PBL cells towards a gradient of CXCL-12 in an under-agarose assay. Each image acquired on the microscope was segmented into 6 equal segments. Results are the mean ± S.E.M. of three independent experiments. The mean cells number are displayed for each segments at time t=0 and t=4h. The results of the experiments show that after 4 hours the cells were migrating towards the gradient of chemokines.

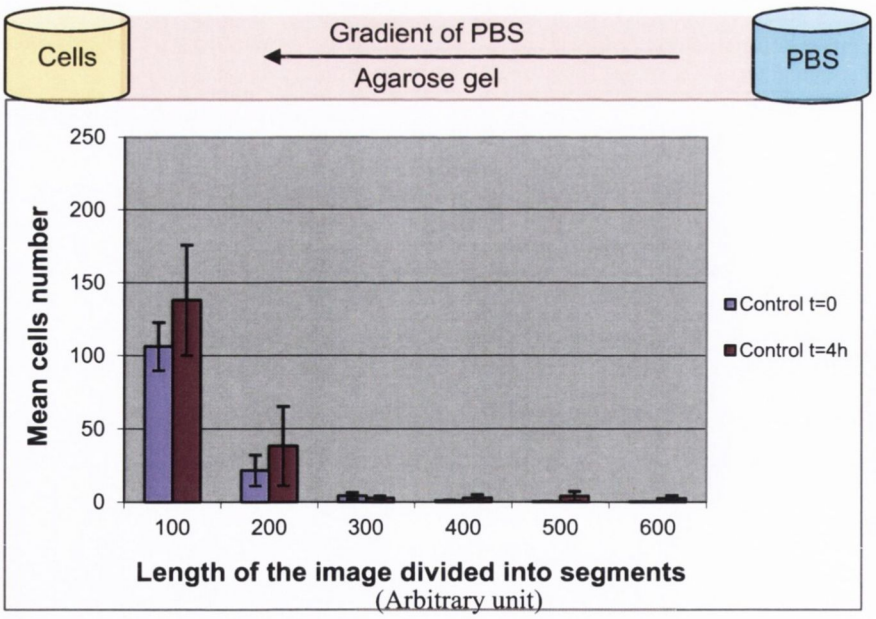

Graph 3-6: Quantification of the migration of PBL cells towards a gradient of PBS in an under-agarose assay. Each image acquired on the microscope was segmented into 6 equal segments. The mean cells number are displayed for each segment at time t=0 and t=4h. Results are the mean ± S.E.M. of three independent experiments. The results of the experiments show that after 4 hours the responses of the cells to the gradient of PBS were negligible.

However, it was noticed that the cells were not able to migrate the total distance between two reservoirs. The most probable explanation of this phenomenon is that once the gradient was diffused and the concentration became homogeneous, the cells were not stimulated by chemokines anymore.

3.2.3 Responses of the cells to a short-term chemotactic gradient

The Dunn chamber was used to observe the migration of neutrophils towards a gradient of chemokines (IL-8). Neutrophils were used because they are known to respond more rapidly to a gradient of chemokines compared to the PBL[123].

The migration of neutrophils was tracked using Image-Pro. Normalization of each track was implemented in order to have all the starting positions of the cells at the origin of the axes on the graph. Nine tracks of cells were randomly picked up from three independent assays. The readout of the graph was becoming overcomplicated if more cells than nine were picked up. Results are shown on graph 3-7 and 3-8.

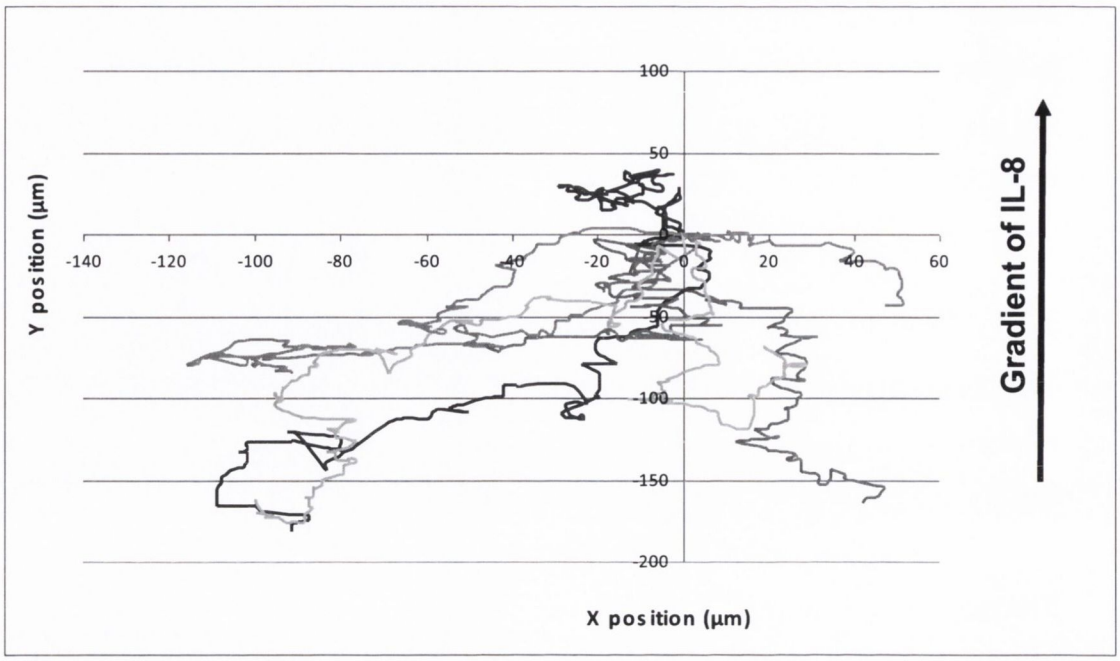

Graph 3-7: Migration of neutrophils in response to a gradient of IL-8 in a Dunn chamber. The gradient is indicated on the graph by an arrow on the left side. The tracks of neutrophils were processed using Image-Pro. The results of the experiments show that the cells migrated over 2h in the direction of the diffusion of chemokines.

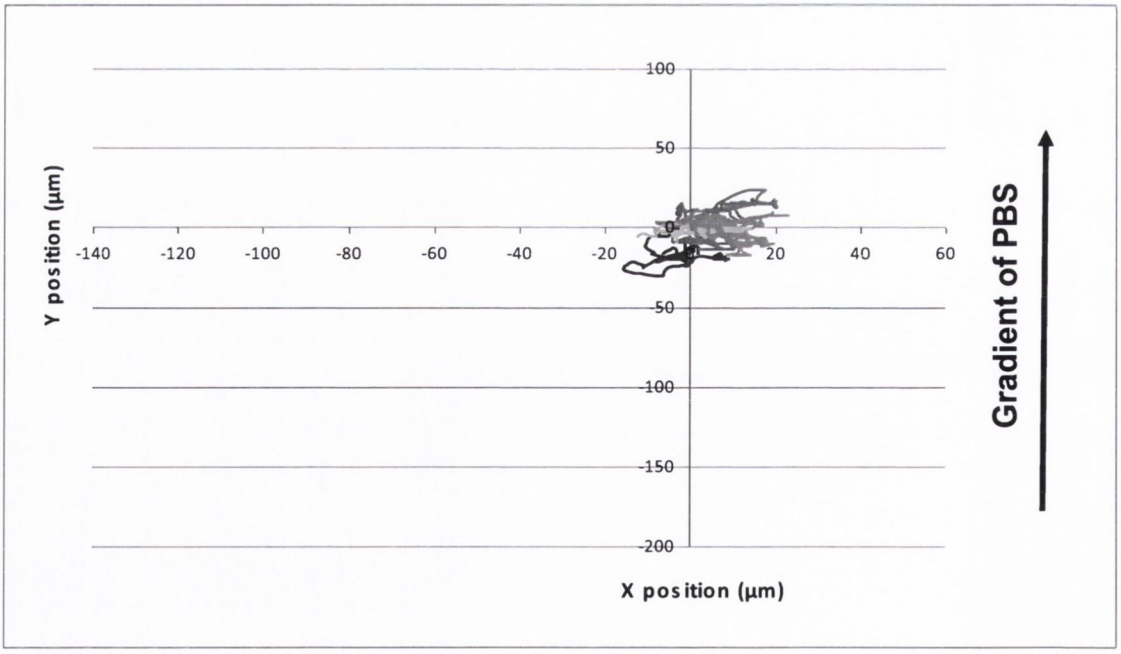

Graph 3-8: Migration of neutrophils in response to a gradient of PBS in a Dunn chamber. The gradient is indicated on the graph by an arrow on the left side. The tracks of neutrophils were processed using Image-Pro. The results of the experiments over 2h show that the cells randomly migrated close to their initial positions and not exclusively towards the gradient of PBS.

It is shown on graph 3-7 that neutrophils migrated towards the gradient of IL-8 (50 ng/ml) over 2 hours at a maximum rate of 1 μm/min, whereas the cells in presence of a PBS gradient randomly migrated close to their initial positions.

3.3 Discussion

Conventional chemotactic assays have been used in order to evaluate and observe the responses of cells to different chemokines. In the under-agarose setting, the cells were placed in the central reservoir while the chemokine and the buffer solution (PBS) were dispensed in the adjacent reservoirs (Fig. 3-6). The advantage of this configuration of reservoirs was that within the same well we observed both the response of the cells towards a gradient of chemokine and the control response. Therefore, the cells had the choice to respond to the chemoattractant solution or to the PBS solution that were diffused on each side of the well containing the cells. The chemotactic gradient in such setting supported the migration of cells over 4 hours. The configuration of the under agarose assay did not allow the cells to migrate the migration testing distance (MTD) of 5 mm between the two reservoirs mainly because once the chemokines had fully diffused within the gel and the concentration gradients were consequently annihilated, cells were not exposed to the chemotactic stimuli anymore and no directed migration occurred. The under-agarose assay also provided essential information on the characteristic of the agarose gel. The higher the concentration of the agarose solution was, the more viscous the gel was and therefore the quicker the solution turned into gel. In other terms, the viscosity of agarose solutions during gelation was dependent on the temperature. An agarose solution of 2 % starts its gelation at a higher temperature[124] (≈ 50 °C) than a solution of 1 % (≈ 40 °C). Many proteins of mammalian tissues start denaturing over 40 °C[125], thus agarose 2 % could not be used, as its gel point would not allow the introduction of chemokines into the gel without the risk of partially denaturing them. What is more, concentrations of agarose below 0.5 % were not viscous enough to enable the punching of reservoirs in the gel. Thus, if agarose gel was to be used in the biochip as a matrix enabling efficient chemokine diffusion, only agarose at 0.5 % and 1 % concentrations would be suitable.

The Dunn chamber assay was used to assess the ability of cells to move towards a gradient of chemokines as it incorporated a migration testing distance of 1 mm that was significantly shorter than the 5 mm MTD in under agarose assays. A fast sustained

diffusion of chemokines was established in this chamber and cells seeded on the cover slip could rapidly move along the gradient which was fully established over 30 min. However, the diffusion of chemokines from one side of the bridge (Fig. 3-7) to the other side occurred from liquid to liquid (chemokine solution to PBS solution), and not from a gel to a liquid such as would be likely found in the *in vivo* situation, for example, from the vascular tissues (solid) to the blood flow (liquid). Therefore, an attempt was made to fill the outer reservoir with gel enriched with chemokine and to assess the capacity of the cells to migrate towards the resulting generated gradient. But the Dunn chamber setup did not enable the diffusion from gel to liquid mainly because of the system limitations. Specifically, when working with liquid in both ring reservoirs, once the cover glass was placed on top of the chamber a balance between the two liquids naturally occurred. Conversely, with a gel, it was more difficult to create a balance because the gel would not diffuse through the bridge.

These two assays were appealing due to their relative simplicity, cost effectiveness and rapid setup. However, they have not been used subsequently for further chemotactic experiments because their experimental conditions were not reflecting the physiological *in vivo* milieu. Indeed, cells that were maintained in Dunn/agarose conditions for at least 2 hours could not respond in the same manner as *in vivo* situation, as multiple physiologically encountered factors were missing (e.g. shear flow and 3D oriented migration). In addition, in the under-agarose assay large volumes (millilitres) of agarose gel were dispensed in a well whereas smaller volumes (microlitres) would be dispensed within a biochip environment. The manipulation of agarose gel when working with biochip would be different than when working in well plates. Microlitres of gel would gelify quicker than millilitres because of the faster gel cooling. Therefore, the temperature environment when dispensing the gel in biochips was expected to be crucial.

One of the key objectives of these preliminary assays was to determine a concentration range in which cells were capable of migration in 2D environment. However, the established exact concentration of chemokines could not be subsequently applied to a biochip platform because the biochip environment would present more complex experimental conditions than within under-agarose assays, such as the application of shear stress. Indeed, the diffusion of chemokines in a biochip could be affected by the

shear stress[126] applied in the channels. Therefore the concentration gradient could vary from the under agarose assay and would have to be adjusted accordingly.

The ability of cells to polarize on the surfaces coated with ligands such as ICAM-1 and VCAM-1 was studied to establish the optimised concentration where cells exhibit a higher polarity reflecting cell locomotory potential. That was important for further experiments in a biochip environment where the flowing cells would be exposed to the immobilized ligands on the surface of the channel. The coating of the channel would allow the cells to attach and subsequently migrate towards a gradient of chemokine.

The quality of T-cell isolation proved to be a crucial integral step influencing the outcome of chemotactic assays. The motility of cells was largely dependent on cell viability in the preparations. As the isolation of the cells had to be done on a weekly basis, the cell isolation was established as a routine procedure. This routine manipulation permitted to reduce the time for the PBL extraction from buffy coat from 20 min to 10 min, thereby reducing potential stress on cells during the isolation. That resulted in an increase of cell viability by 20 % and thus an improved yield of the cell isolation.

An important aspect of the work presented in this chapter was also the analysis of results via Image-Pro software for image processing. This was as important as the optimization of the isolation of cells and of the concentration of the chemokine. The image analysis with this software permitted to evaluate the responses of cells to a substrate coated with different reagents (anti-LFA-1α, ICAM-1, VCAM-1). Image-Pro provided a useful and rapid methodology to convert qualitative observation into quantitative results.

4 Evaluation of the diffusion of molecules through a matrix

Molecular diffusion is defined as the transfer of molecules from an area of higher concentration (C_2) to an area of lower concentration (C_1) by random molecular motion. The molecules gradually mix which creates a gradient. Therefore, the concentration is also gradually changing and we can say that a concentration gradient is created. The concentration of molecules is dissipated and becomes homogeneous at an infinite time (t_∞) as it is depicted on figure 4-1.

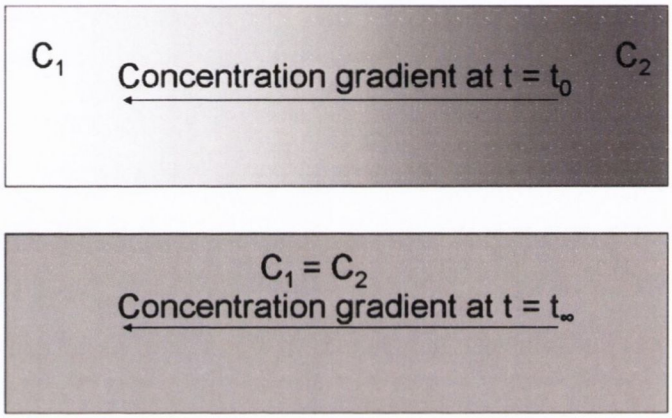

Figure 4-1: Illustration of the diffusion of molecules in a matrix. Molecules diffuse from the more concentrated area C_2 to the less concentrated area C_1 (top panel) creating concentration gradients across the matrix. The concentration of molecules becomes homogeneous over time (bottom panel).

Different types of diffusion are described in the literature[127], such as the atomic diffusion (diffusion at the atomic scale), Brownian motion (random motion of molecules in liquid or gas) and osmosis (diffusion of a solvent through a semi-permeable membrane e.g. cell membrane). For each of these, different physical laws are applicable depending on the matrix (nature of the milieu) where the molecules are[128].

The parameter that describes the ability of a molecule to diffuse in a matrix is called the coefficient of diffusion[129] and is expressed in cm^2/s. The coefficient of diffusion varies with the experimental conditions such as the temperature and pressure[130].

In this study, the gradient of molecules (i.e. chemokines) created by diffusion within a matrix (i.e. gels) was one of the key elements of the whole study. Prior to expose cells

to a gradient of chemokines released from a matrix in a biochip setting, the characteristics of diffusion of the chemokines within each gel needed first to be defined.

Three gels were used: agarose gel, collagen and extracellular matrix (ECM) gel. The agarose gel was used as it had previously been reported to be suitable for chemotactic assays (Chapter 3). Collagen is a fibrillar protein and is one of the components of connective tissues and can be used as a gel. The gel formed can be used for multiple biological applications such as a thin layer on tissue-culture surfaces to enhance cell attachment or as a gel to study cell invasion into collagen scaffold[131] or to promote cell expression and function[132]. The extracellular matrix is the defining feature of most connective tissues in the human body[72]. It is mainly composed of proteins such as collagen, laminin, fibronectin and polymers called glycosaminoglycans (heparin sulphate, hyaluronic acid and others) that provide structural support to the cells. The agarose, collagen and ECM gels have been extensively used previously[133-136] and are widely accepted by scientists for their biocompatibility.

Diverse methods are available to enable the researchers to observe, analyze and quantify the diffusion of molecules in a matrix. These include such methods as fluorescence resonance energy transfer (FRET),[112] fluorescence lifetime imaging (FLIM),[137] and fluorescence after photobleaching (FRAP)[138]. One of the most common of these is FRAP using a confocal microscope. This technique has been used for decades and is now a routine method used for the evaluation and study of the diffusion coefficient of molecules principally because most research group can avail of the confocal microscope facilities[126].

However, before applying the FRAP technique for the evaluation of the diffusion of molecules within the selected matrices, it is essential to understand the underlying mechanisms of this method. That would facilitate further evaluation and interpretation of the coefficient of diffusion obtained.

4.1 Materials and methods

4.1.1 Theoretical basis of fluorescence recovery after photobleaching

The 'fluorescence recovery after photobleaching' (FRAP) technique[71, 126] was used to define the diffusion coefficient of chemokines within the following gels: agarose, ECM, collagen. Fluorescent molecules that have the same molecular weights as the chemokines used for chemotactic assays are incorporated into the gels. When the sample is observed under the microscope, the fluorescent molecules of an unbleached area are in equilibrium. Bleaching a fraction of the fluorescent molecules in a region of interest (ROI) disturbs this equilibrium. Under optimal conditions the recovery kinetics is dependent only on the mobility of the investigated molecule and partial fluorescence recovery can be observed (Fig 4-2).

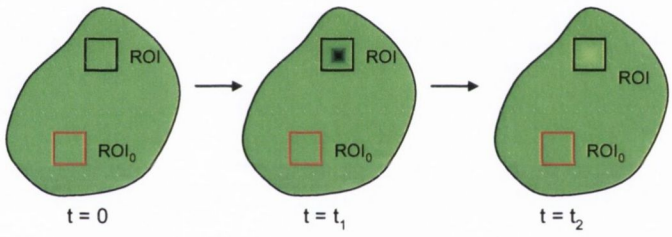

Figure 4-2: Schematic representation of the diffusion of molecules in a fluorescence recovery after photobleaching (FRAP) experiment. Fluorescent molecules in the sample are in equilibrium at time t=0. A region of interest (ROI) is bleached at time t_1. The fluorescence recovery occurs by diffusion of fluorescent molecules into the ROI over time ($t_2 > t_1$). A region of interest away from the bleaching area (ROI_0) was selected for further data processing (i.e. correction of the background of the image acquired).

The branch of physical sciences that explains the basis of the fluorescence recovery phenomenon is quantum mechanics. In the quantum mechanics terms, the macroscopic behaviour of any systems or matter relies on their behaviours at an atomic scale i.e. the behaviour of molecules, atoms, and electrons. A molecule is composed of at least two atoms and is electrically stable. An atom is the basic unit of matter consisting of a central nucleus surrounded by a cloud of negatively charged electrons. Electrons reside in the atomic orbital which presents different energy levels or electronic states which are described by the Jablonski diagram[139] (Fig. 4-3). An important intrinsic property of an electron is its spin direction S, which corresponds to its dynamic angular position

(spin -½, spin +½) within the molecule which is directly linked to its energy state. The ground state refers to the electronically stable state (S_0) and the excited states are named depending on the level where the electrons are such as singlet state (S_1, S_2 … S_n) or triplet state (T_1, T_2 … T_n). In a singlet state, all electrons in the molecule are spin-paired so S=0 (an electron at -½ and another at +½). In a triplet state, one set of electron are unpaired S=1 (an electron at +½ and another at +½). The transition between those states involves absorption or emission of photons (basic unit of light).

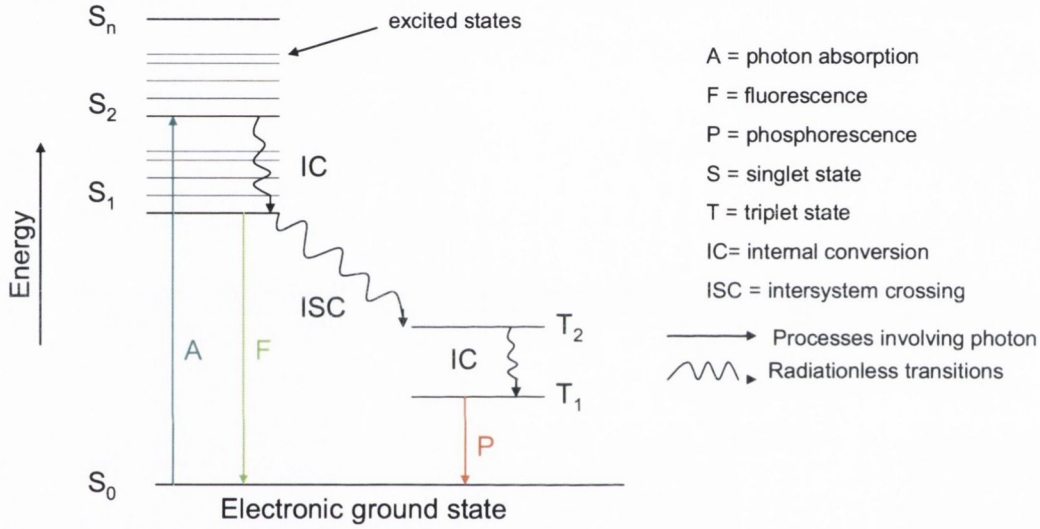

Figure 4-3: A Jablonski diagram representing electronic states of a molecule. The diagram shows the different routes by which an excited molecule can return to a stable state. A molecule is excited when it absorbs a photon (A) which disturbs the electronic equilibrium of the molecule. The energy level of a molecule depends on the configuration of its electrons (singlet S, triplet T). To relax to an electronic stable state (ground state), the excess of energy of an excited molecule can be internally converted (IC) via radiationless transitions. These transitions can be subsequently followed by the emission of a photon which is the principle of fluorescence (F) or a transition between singlet state to triplet state called intersystem crossing (ISC) can take place. The relaxation from triplet state results in a post-illumination of a photon which is called phosphorescence (P).

Therefore, from a quantum mechanics point of view the absorption of light by a molecule (e.g. fluorophore) elevates electrons from the ground state to an excited state which presents a higher energy. Different intra-molecular redistributions of energy are possible to allow the molecule to return to the electronic ground state. For instance, the

excess of energy of an excited molecule can be internally converted (IC) to further relax from the excited state to the ground state by emission of a photon; this is the principle of the fluorescence. Another transition called the intersystem crossing (ISC) occurs when the spin of an excited singlet state reversed, leaving the molecule in an excited triplet state. The lifetime of the excited triplet state (up to 10 s) is longer than an excited singlet (10^{-5} to 10^{-8} s) and is chemically more reactive. Therefore, more time is needed for the excited electron to relax from a triplet state to the ground state than from a singlet state. This is observed by the post-illumination emission of a photon which is called phosphorescence. An alternative phenomenon can occur during the relaxation of the triplet state which is the interaction between a fluorophore molecule and another molecule (e.g. oxygen) that produces irreversible covalent modifications[140, 141]. These modifications lead to the bleaching of the fluorophore molecules[142] which is the principle of the process called the photobleaching. Some molecules would only partially be bleached whereas some other would irreversibly be bleached[143]. That depends on the fluorophore molecule and its interaction with the matrix but also on the intensity of the laser beam focused on the area to bleach. It is important to choose a fluorescent dye that can be irreversibly photobleached (e.g. FITC-dextran). In these circumstances, the fluorescence recovery of a bleached area of a fluorescent sample would only depend on the random motion of unbleached molecules and not on the self-recovery fluorescence of the bleached molecules. Depending on the sample studied, this random motion of unbleached molecule can result from the diffusion of molecules, the binding to other molecules, or the transport processes, but overall it provides the information on the behaviour of the molecules within the matrix[144].

Therefore, considering that the FITC-dextran can be irreversibly photobleached, if a fluorescence recovery occurs it means that the molecules are able to diffuse within the gels. If no fluorescence recovery is observed, that could be explained by molecular interactions between the fluorophore molecules and the molecules composing the gels and in this case, the employ of these gels for our study would be impossible and other matrices should be considered.

4.1.2 Evaluation of the diffusion coefficient

When an area of a sample containing fluorophore molecules is bleached, a fluorescence recovery curve I(t) is obtained (Fig. 4-4). The following empirical formula from Ellenberg *et al.* introduces the diffusion coefficient D:

$$I(t) = I_{final}(1 - \frac{w^2}{w^2 + 4\pi Dt})^{1/2} \qquad \text{Equation 4-1}$$

where I_{final} is the plateau level, w is the width of the bleached spot and t the time.

The diffusion coefficient D of the investigated molecule can be measured *via* the halftime of the fluorescence recovery ($t_{1/2}$). This coefficient reflects the mean squared displacement explored by the molecule through a random walk[129] over time.

Images of the FRAP assays were acquired with the Zeiss Meta LSM 510 confocal microscope. Any images acquired from electronic devices (e.g. confocal microscope[145]) contain background signal of various intensity, such as detector readout noise[146], autofluorescence (medium, glass) or artefacts from pixel saturation. Therefore, the background signal of each image was corrected by subtracting the measurement collected for each time step from an area away from the bleached region (ROI_0), which had been manually selected prior to the image acquisition.

To compare different graphs obtained for each experiment, the average prebleach fluorescence intensity values were normalized to one by dividing the intensities of all time points by the average prebleach intensity. The initial fluorescence intensity plateau on the curve I(t) corresponded to the pre-bleach intensity. Mobile fraction (F_m) of fluorescent probes and immobile fraction (F_i) could be determined from this curve (Fig 4-4).

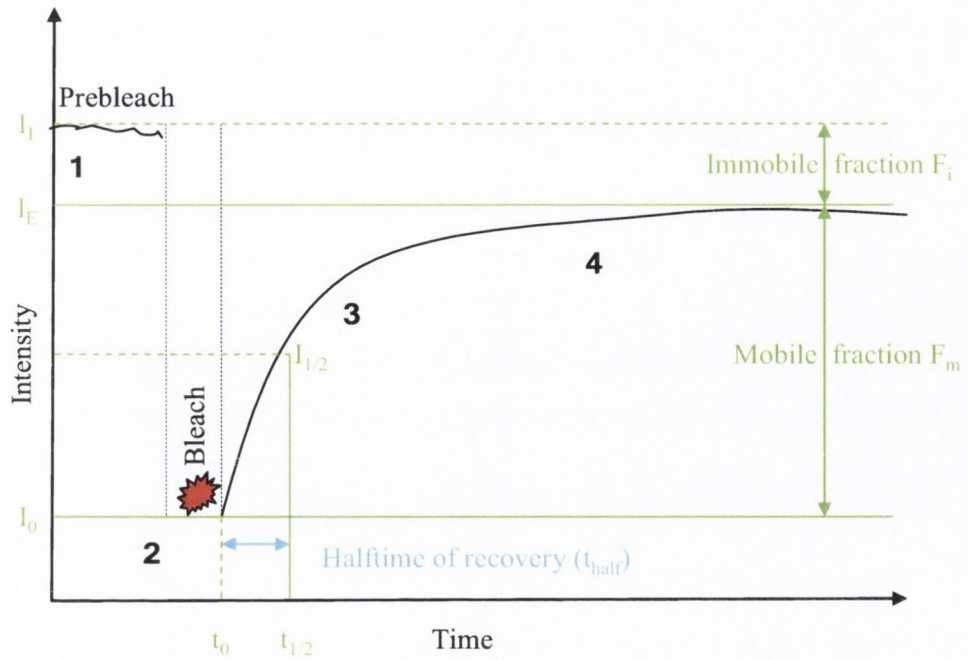

I_I: initial intensity

I_0: intensity at timepoint t_0 (first photobleach intensity)

$I_{1/2}$: half recovered intensity ($I_{1/2}$= (I_E-I_0) / 2)

I_E: endvalue of the recovered intensity

$t_{1/2}$: halftime of fluorescence recovery to $I_{1/2}$ ($t_{1/2} - t_0$)

Mobile fraction F_m = (I_E – I_0) / (I_I-I_0)

Immobile fraction F_i =1 – Fm

Figure 4-4: Representation of the results of a FRAP experiment. The graph shows the variation of the fluorescence intensity with the time during a FRAP assay. A fluorescence baseline intensity (I_I) is recorded before the photobleaching occurs (1). After the bleach (2), the fluorescence drop to a minimum of intensity (I_0) and unbleached molecules start to diffuse into the ROI, hence the increase of fluorescence (3). A fluorescent recovery threshold is reached (I_E) when a flat line is obtained (4). Experimental graphs permit to evaluate the fraction of mobile (F_m) and immobile fluorescent molecules (F_i) but also the halftime of fluorescence recovery ($t_{1/2}$) of the ROI which is directly linked to the ability of molecules to diffuse within a matrix.

For qualitative determination of the recovery dynamics a first approximation can be done using the following exponential equation.

$$I(t) = A.(1-e^{-t\tau}) \qquad \text{Equation 4-2}$$

where I is the fluorescence intensity, A is the endvalue of the recovered intensity (I_E), τ is the fitted parameter which is related to the half-time $t_{1/2}$, and t is the time after the bleaching pulse. After determination of τ by fitting the above equation to the recovery curve the corresponding halftime of the recovery can be calculated with the following formula:

$$t_{1/2} = \frac{\ln 2}{\tau} \qquad \text{Equation 4-3}$$

4.1.3 FRAP settings

Fluorescent dextran, which has a molecular weight analogous to chemokines of around 10 kDa such as CXCL-12 or IL-8, was used as a model to estimate the predicted rates of diffusion of these chemokines in gels. Agarose, collagen and ECM gel were mixed with FICT-dextran at a concentration of 5 mg/ml. A volume of 10 µl of this mixture was dispensed on a glass slide and a cover glass was placed on top of the sample to homogeneously spread the sample on the glass slide. The slide was then ready to be observed using confocal microscopy.

FRAP experiments were performed on a Zeiss Meta LSM 510 confocal system based on a Zeiss Axiovert inverted microscope using 63x oil immersion lens. An argon laser at full intensity at 488 nm was selected for the excitation of FITC-dextran fluorophore. The laser was focused in the region of interest and a prebleached image series were first acquired at low intensity illumination to measure the fluorescence intensity prior to the disturbance of the equilibrium caused by bleaching. The bleaching of the ROI was continued at higher intensity illumination and finally stopped to acquire a series of postbleached images which would exhibit the fluorescence recovery in the ROI.

The chemokine diffusion coefficient (D) was determined by comparing $t_{1/2}$ measured in the gels of different composition (ECM, agarose, collagen) to that in similar size droplet

of saline containing 5 mg/ml FITC-dextran with known diffusion coefficient of 8.0×10^{-7} cm^2/s.

4.1.4 Protocol for the preparation of the sample of gels

Dextran labelled with fluorescein isothiocyanate (FITC) with a molecular weight of 10 kDa was purchased from Sigma-Aldrich (Ireland). This fluorescent dye was chosen because of its molecular weight that was close to the chemokines used for chemotactic assays: IL-8 and SDF-1α. A stock solution of 100 mg/ml of FITC-Dextran in phosphate buffered saline (PBS) was prepared. It was then dispensed in the gel to obtain a final concentration of 5 mg/ml. When that dye was excited at 492 nm, its green fluorescence emission was around 518 nm.

The agarose gel was prepared as it has previously been described in chapter III and was used at a concentration of 1 % and 0.5 %. The FITC-dextran was introduced in the agarose solution and vortexed for 5 s. A volume of 10 µl of this solution was dispensed on a cover glass and turned into gel when its temperature cooled down at 20 °C.

Extracellular matrix (ECM) gel is isolated from Engelbreth-Holm-Swarm murine sarcoma (Sigma-Aldrich, Ireland). This gel is mainly composed of laminin, collagen type IV, heparin sulphate proteoglycan and entactin. It presents a final protein concentration of 8-12 mg/ml. The gel was stored at -20 °C and before use was thawed overnight at 2-8 °C. ECM turned into gel within 5 minutes at 20 °C. Therefore all materials used to manipulate ECM gel needed to be cool down at 4 °C. FITC-dextran was mixed with the gel at 4 °C and 10 µl of this solution was dispensed on a cover glass and allowed to turn into gel at room temperature.

Collagen is a fibrous structural protein which is found in most supportive tissues, connective tissues and border between tissues in the body. It is a major component of the extracellular matrix, making the structure of fibres or membranes. Bovine collagen, Type-1 purchased from Biosciences (Bedford, MA) at a concentration of 3 mg/ml turned in gel when its pH was brought to neutrality using the following procedure. A neutralized isotonic collagen solution was prepared by mixing 8 parts of chilled collagen solution to one part of 0.01 M sodium hydroxide (NaOH) and 1 part of 10X phosphate buffered saline. The pH of the solution was assessed by pH paper and

adjusted to 7.4±0.2 using 0.1 M hydrochloric acid (HCl). The diluted material could be used right away or stored at 2-8 °C for several hours. Before gelation at 37 °C for 10 min, collagen was mixed with FITC-dextran and dispensed on a cover glass.
The cover glass with each solution was incubated at room temperature in a humidification chamber to avoid dehydration of the samples.

4.2 Results of the FRAP experiments of diverse gels

Series of images acquired during a FRAP experiment (Fig. 4-5) show the evolution of the fluorescence intensity of a region of interest (ROI). In this example, a bleached area in a sample of PBS labelled with FITC-Dextran fully recovered by the diffusion of unbleached molecules into the ROI.

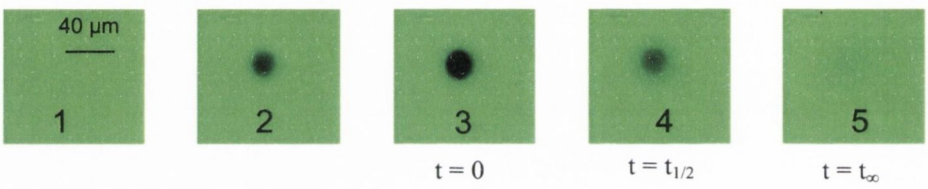

Figure 4-5: Example of experimental acquisitions of the fluorescence recovery of a bleached area obtained during a FRAP experiment. A droplet of FITC-Dextran mixed in PBS was dispensed on a cover glass. The first panel shows the fluorescence intensity of the sample before the bleach. When the laser is focused on the region of interest (ROI) of the sample at a high intensity, fluorescent molecules became photobleached (panels 2-3). Fluorescence recovery of the ROI (panels 4-5) indicates that unbleached molecules diffused into the ROI.

The fluorescence recovery curves I(t) were obtained for each matrix investigated: PBS, ECM, agarose gels (0.5 %, 1 %) and collagen. The microscope software enabled the mathematical processing of the fluorescence intensity value at each timepoint and the curves I(t) acquired for each assay permitted to directly obtained the halftime ($t_{1/2}$) for the half fluorescence recovery in the matrices which was determined by resolving the equation 4-3 and the results are reported in table 4-1.

Knowing the coefficient of diffusion of the FITC-Dextran (MW: 10 kDa) in PBS[147] and its $t_{1/2}$ from the FRAP assay, it was possible to estimate the diffusion coefficient of each

gel by comparing the $t_{1/2}$ of similar size droplet of FITC-dextran in PBS and $t_{1/2}$ of FITC-dextran in gels[71, 126].

Matrix	τ (s)	$t_{1/2}$ (s)	Coefficient of diffusion (10^{-7} cm^2/s)
PBS	1.55±0.18	0.50±0.08	8.00*
ECM	2.15±0.25	0.35±0.05	5.56±0.7
Collagen	2.06±0.12	0.34±0.02	5.48±0.3
Agarose 0.5 %	2.86±0.44	0.27±0.03	4.27±0.5
Agarose 1 %	3.15±0.20	0.23±0.02	3.60±0.2

Table 4-1: Summary table of data obtained in FRAP experiments. The fitted parameter τ obtained from the fluorescence recovery curves for each matrix (PBS, ECM, collagen, agarose 0.5 %, agarose 1 %) is reported in the table. The halftime $t_{1/2}$ (s) was calculated for each matrix using equation 4-3 and their diffusion coefficients (cm^2/s) were estimated. Results are the mean ± S.E.M. of three independent experiments. * Data from literature[71, 126].

4.3 Discussion

FRAP experiments were carried out to evaluate the coefficient of diffusion of the chemokines (IL-8, CXCL-12) within a gel environment. FITC-dextran was used as a fluorescent marker and was mixed in PBS, ECM gel, collagen and agarose gel (0.5 % and 1 %). That marker was chosen because it would react in a similar manner than the chemokines (used in chemotactic assays) due to its analogous molecular weight. FITC-dextran was also chosen because it could be totally photobleached. Therefore, the fluorescence recovery of a bleached area was possible only because of the diffusion of unbleached molecules within the sample.

The half-time obtained for each matrix from the fluorescence intensity curve I(t) enabled the study of the behaviour of the fluorescent molecules within different environments. According to the faster rate of diffusion of unbleached molecules into the bleached area in the PBS sample than the rate of diffusion of the fluorescent molecules in gels, the freedom of movement of the fluorescent molecules in a liquid is higher than in a gel. This is explained by the physical characteristics of gels that are described as

porous materials. The structure of a gel relies on networks of cross-linked polymer chains in which "pore size" is a defining parameter. A pore is the void space in a solid matrix, where the void may be filled with air or liquid. Therefore, molecules in a porous material have less freedom of movement than in a liquid such as in PBS and would thus diffuse in a slower manner. This is why the difference between the rate of diffusion of the FITC-dextran in each gel and in the PBS was significant.

The slower coefficient of diffusion was the agarose gel at 1 % and the faster coefficient of diffusion was obtained in ECM gel. These coefficients are directly linked to the porosity of each matrix. Therefore an agarose 1 % presented a narrower porosity than an agarose 0.5 %, a collagen, or than an ECM gel[148]. Therefore, different rates of diffusion of chemokines could be generated in a biochip setting which would give the opportunity to assess the most suitable gel for chemotactic assays.

The diffusion coefficient of each gel was essential to determine because it directly gave information on the motion of molecules. It was clear that negligible interactions with the matrix molecules and the fluorescent molecules occurred because a fluorescence recovery in the bleached area was observed. Therefore, the FITC-dextran molecules were able to diffuse in the gels. That was important to know for the subsequent advanced experiments in which chemokines would diffuse from a gel milieu in a channel network. The capacity of the gel to release the chemokines in the channel network in the presence of a shear flow had to be first mathematically justified. Therefore, knowing the coefficient of diffusion of each gel allowed us to process further simulations of the diffusion of molecule within the different architecture of the biochips designed.

5 Chemotactic assays within microfluidic biochips

The biochip application area became popular and evolved in the last decades from plate based tests to devices which fit on less than a square centimetre called "lab-on-a-chip"[149, 150]. Indeed, a complete "laboratory" with miniaturised and integrated systems can be created on a chip such as miniaturised mixers[151], diffusion chambers[40], integrated electrodes[40], pumps[57], valves[57] and more. When these chips are used to study the behaviour of fluids at the micrometre scale they are named microfluidic biochips. The miniaturisation of a laboratory to a small device exhibits several advantages such as the decrease of reagent consumption, the cost per analysis, and the time for each analyse. These biochip platforms also allow researchers to increase the quality of their data thanks to more controllable process parameters. This is possible because a biochip provides an environment wherein repetitive tasks are automated which consequently minimises any human intervention and manipulations. Therefore, data are more reproducible, significant and reliable. These chips are adopted and applied in multiple areas[54, 152-155] such as clinical diagnostics, bio-defence, genomics, environmental monitoring and chemotactic assays.

Most of the current microfluidic biochips used for chemotactic assays designed to study, for example, inflammation processes are manufactured in such a way that cells flow on the surface of a flat defined chamber[156] such as a capillary microchannel[69]. Chemical reagents in solution (i.e. chemokines[69], nanoparticles[157]) and cells are directly dispensed into the channel under controlled flow rate condition. Real-time imaging of the responses of cells to chemical reagents can be performed under inverted microscope. The design of this type of biochip allows the cells to migrate in both the x and y axes but not along the z axis which means that the freedom of movement of cells is restricted to a fully planar system as shown in figure 5-1.

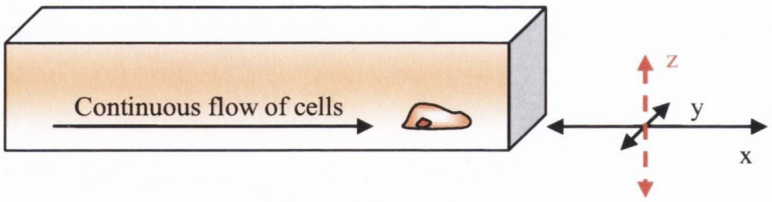

Figure 5-1: Schematic illustration showing a conventional close channel with a cell movement in its allowed two degrees of freedom. Drawing shows the mobility of the cells flowing along the flat channel (x-y plane).

However, the cells homing in response to a diffusion of chemokines (i.e. during the process of inflammation) in the body is not taking place in a simple 2-dimensional plane and smooth milieu such as found in currently commercially available biochip designs. In fact, chemokines are diffused from and through the wall tissues into the blood flow (Fig. 1-1 and 1-2) which means that in order to provide an *in vitro* model which is closer to the *in vivo* homing conditions, it is necessary to release the chemokines not only in the main channel of a chip but also from the surroundings (*e.g.* wall tissues). Therefore, the novel biochip designs had to include the followings:

- a constant cell flow rate (e.g. physiological regime),
- an environment in which cells can freely move on all their three degrees of freedom,
- a release of chemokines that mimics the diffusion from and through the wall tissues.

Therefore, one of the main purposes in this study is to reproduce *in vitro* the generation of a gradient of chemokines to trigger the cellular activation and migration towards the gradient. Thus, the *in vitro* experimental environment which will mimic the *in vivo* tissues will be generated by a matrix such as a gel. The main channel of the device will contain the flow of cells. The matrix enriched with chemokines will be connected to the main channel on the same plane or underneath to create a 3D support in which cells will be free to migrate.

The design of biochips is a real challenge for both engineers and biologists because the current biological models, for example of homing process, as previously explained, need to be more exhaustive; hence the novel designs will be more complex. The development of new biochip platforms depends on the knowledge of the engineers in

computer-aided design[158] (CAD). Several software packages (e.g. Auto-CAD, SolidWorks) are available to develop 2D and 3D drawings of each component which define the structure of the biochip. In addition, CAD software allows the designing of the static structure whereas other software packages (e.g. COMSOL Multiphysics®) make it possible to implement the dynamic experimental simulation of the biochip performance. COMSOL[159] is a simulation environment for numerical computing and modelling which covers all the most advanced multiple applications in physics in a modular software package (e.g. acoustic module, chemical engineering module, MEMS module); among these there are dedicated modules for fluidodynamics problems. Therefore, the use of computer-aided design software reduces the developing time, costs and allows fast additional engineering.

In this work, the preliminary biochip designing was carried out using SolidWorks software for the visualisation of the structure of the chip on a static 3D model. COMSOL (COMSOL AB, Burlington, MA) software permitted the creation of multiphysics model to study the behaviour of fluids within each design. The characteristics of the pattern of the chip were entered in COMSOL to create a 2D axisymmetrical model in which the influence of the chemokine diffusion coefficient (cf. Chapter 4) and the shear flow were fully characterised within the chip. Once the designs were achieved, Auto-CAD software was used to display the technical specifications of each structure such as the dimensions of the pattern within the chip. Once all of those steps were checked and optimised, the first prototype then was manufactured.

In this study, we developed the 2D designs as well as the dynamic simulation of the novel microfluidic biochips and the company Cellix Ltd[160] (Ireland) provided us the scientific consulting. Cellix Ltd is a spin-off SME company of Trinity College Dublin[140]. Cellix commercialised technology is based on several patented inventions in microfluidic devices and technology. They currently have several microfluidic-based chips on the market which are the results of previously successful research studies carried out in the Institute of Molecular Medicine[118] (IMM, Dublin, Ireland). By continuously developing new chip and applications, Cellix has been competitive on the market. Thus, new chip designs were developed utilising their consultancy and expertise. After the first modelling and validation phase, by CAD software, the polymeric based chips were first manufactured by Epigem[161] (United Kingdom). This

company has a substantial industrial knowledge and relevant technology to precisely manufacture a wide range of polymer based devices and templates. The chips manufactured by Epigem were then assembled by Cellix with purpose designed inlets and outlets to comply with their proprietary pump connectors (Fig. 5-10).

Once the prototypes were manufactured and tested, the chemotactic assays were performed.

5.1 Materials and methods

5.1.1 Commercially available microfluidic biochips

The standard commercially available Vena8™ biochip (Fig. 5-2) contains eight straight channels with input ports to connect the chip to the microfluidic pump and output ports from where liquid is evacuated. The dimensions of the microchannels are 400 µm (W) x 100 µm (D) x 20000 µm (L). The fluidodynamic response of any injected fluid within such biochip is evaluated by calculating the Reynolds number using the equation 2-1 (cf. Chapter 2) where the liquid is considered to be water with ρ is the density of the fluid (1000 kg/m^3), η is the viscosity (10^{-3} kg/m.s), v is the velocity (1 m/s) and L is the length of the channel (0.02 m). Therefore, the Reynolds number calculated under the above specified condition is equal to Re = 0.02; therefore the flow in such microchannel is laminar ($Re \ll 1$).

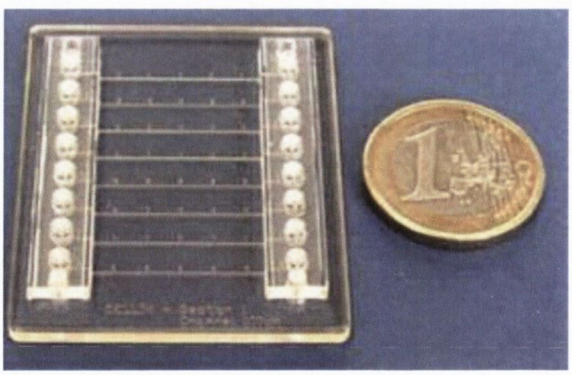

Figure 5-2: Photograph of a commercialised microfluidic biochip. Photograph shows a Vena8™ microfluidic biochip manufactured by Cellix Ltd which contains 8 channels (400 µm-100 µm-20000 µm) (Courtesy of Cellix Ltd).

Another important feature for our biological experiments is that the chips enable the adhesion of cells onto these channels in a similar manner than the adhesion of cells onto the wall tissues in *in vivo* (cf. Fig. 1-1). To achieve this, the surface of each channel was coated with leukocyte-endothelial cell adhesion protein such as ICAM-1 and VCAM-1 at a concentration of 1 µg/ml. The biochip was then kept in a humidification chamber to avoid any evaporation of the reagents and incubated at 37 °C for 2 hours. The channel was washed twice with PBS and blocked with 2 % BSA for 30 min at 37 °C and washed again twice with PBS. PBL cells at a concentration of 5 x 10^6 cells/ml were then dispensed by using the Cellix pump at various shear stresses: 0, 1, 2, 3, 4, 5, and 10 dyn/cm^2 to study the influence of shear stress on the ability of cell adherence.

5.1.2 Biochip for chemotactic assays in a 3D plan

The aim was to develop a design in which cells can migrate in the three x, y and z axes by connecting a Channel B (Ch. B) to a Channel A (Ch. A) which was underneath the Channel B (Fig. 5-3).

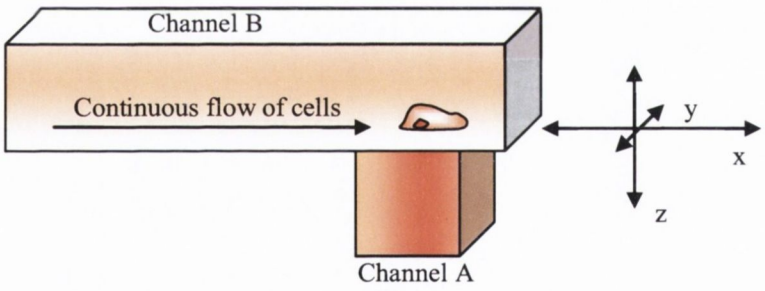

Figure 5-3: Illustration of the freedom of movement of the cells in the x, y and z axes in a novel biochip design. Channel A is connected to the Channel B and can be filled with gel and chemokines. The diffusion of chemokines will occur from the Channel A into the Channel B and cells will be free to migrate from the Channel B to the Channel A.

The software eDrawing from SolidWorks was used to develop the chip model design which is here called "Prototype 1" (Fig. 5-4).

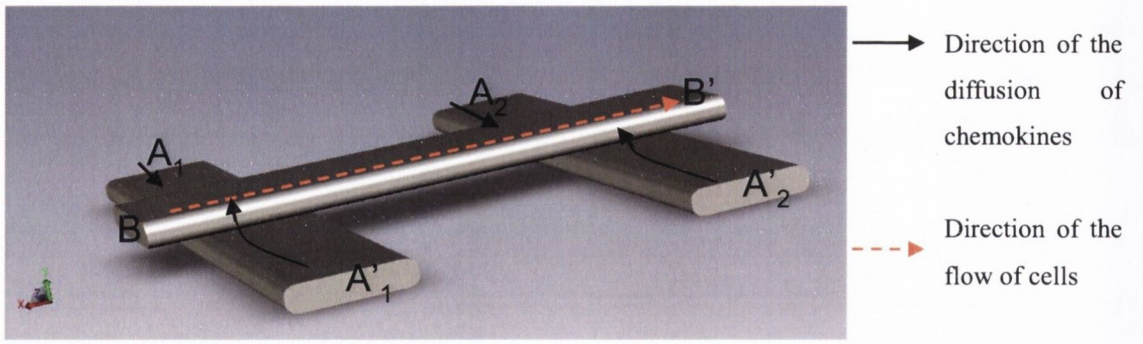

Figure 5-4: 3D schematic drawing of the novel design called Prototype 1. The model shows the Channel B which will contain the continuous flow of cells and the two perpendicular channels A_1 and A_2 which will contain the chemokines. The diffusion of chemokines into the Channel B will stimulate the migration of cells towards the gradient of chemokines generated.

With such design, the cells will continuously flow in the Channel B, while perpendicular channels A_1 and A_2 will be filled with a gel enriched with chemokines. This system was designed to avoid any constrain for the cells to migrate from the Channel B through the gel into the different Channels A containing the chemokines. Cells will have the choice to migrate towards either of the part of the Channel A: A_1, A'_1, A_2, or A'_2.

5.1.3 Mathematical model applied to the Prototype 1

For the design of the Prototype 1, the gel will first be dispensed in the Channel A_1 with the pump at a shear stress of 1 dyn/cm² (Fig. 5-5). It was necessary to estimate the volume ΔV of the gel which could seep into the Channel B while it was dispensed in the Channel A_1. Calculations were done with both water and agarose 2 % solution in order to obtain a range of volume ΔV depending on the viscosity of the solution used.

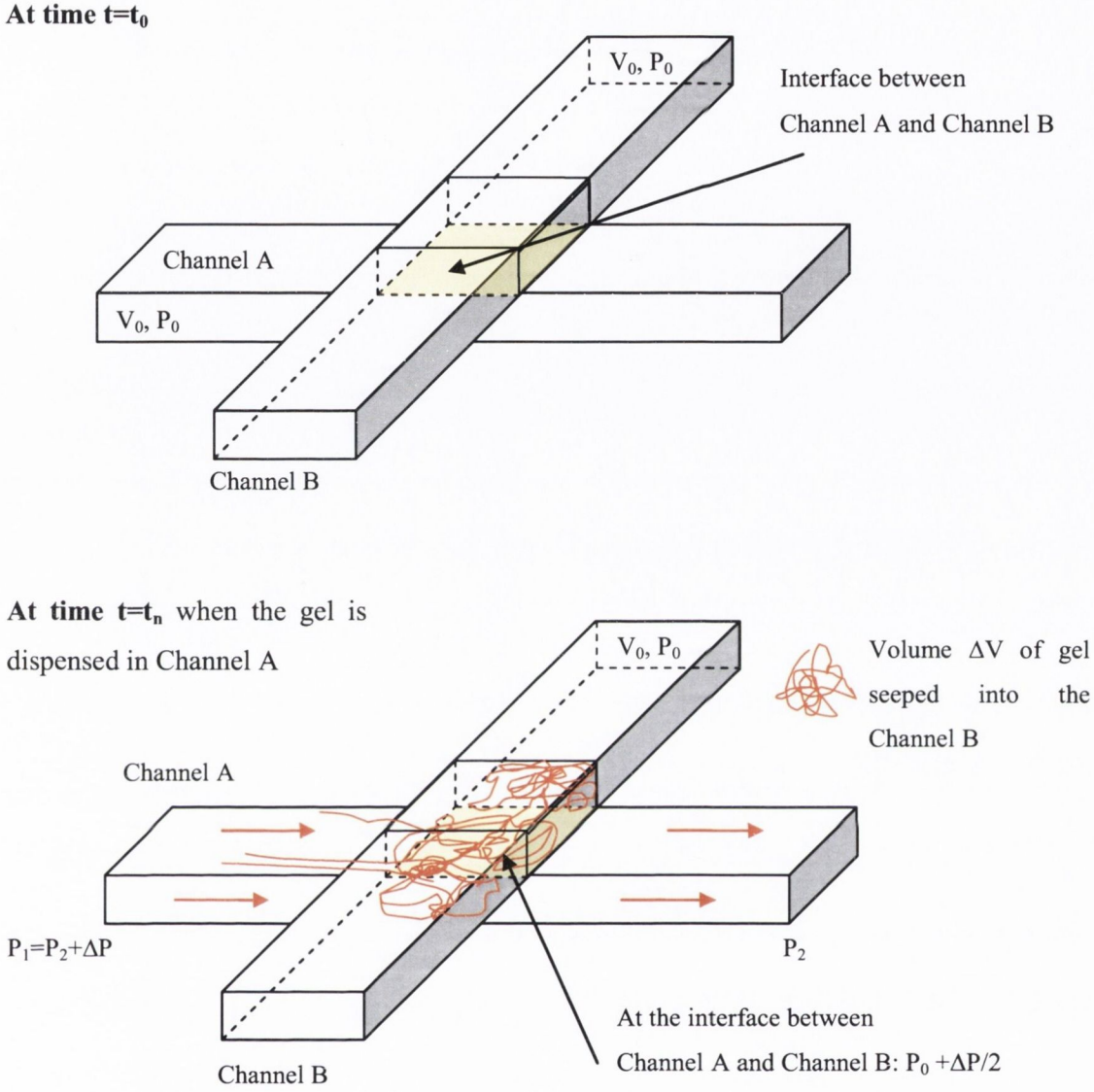

Figure 5-5: Determination of the excess of liquid in the Channel B from the gel dispensing step in the Prototype 1. It was assumed that the outlet ports of the Channel B were sealed and therefore Channel B is compared to a close system which at time $t=t_0$ has a volume of air V_0 at a pressure P_0; according to the gas law, at t_0, $P_0.V_0 = \text{const}$. When the gel is dispensed in the Channel A, a volume of liquid ΔV can seep into the Channel B. When applying a pressure P_1 at the entrance of Channel A at t_n, the pressure along the Channel A will decrease to attain P_2. The difference of pressure between P_1 and P_2 is named ΔP. The pressure in Channel B at the intersection of both channels is equal to $P_0 + \Delta P/2$.

It was assumed that:

- the temperature and the pressure were constant at t_0,
- both channels A and B have the same volume,
- both outlet ports of the Channel B were closed,
- when the pressure is dropped the gel should be set because of the low volume dispensed,
- Channel B is a closed system which contains a volume of air V_0 at a pressure P_0 at time $t = t_0$. According to the ideal gas law: $P_0V_0 = \text{const}$.

When the gel is dispensed in Channel A at time $t = t_n$, according to the conservation of mass in a closed system the volume of air in Channel B at the intersection of the two channels will be:

$$P_0V_0 = (P_0 + \frac{\Delta P}{2}) \times (V_0 - \Delta V) = \text{const} \qquad \text{Equation 5-1}$$

where ΔP is the difference of pressure between P_1 and P_2 when the gel is dispensed in the Channel A and ΔV is the volume which may enter into the top channel.
The equation above leads to:

$$\Delta V = \frac{V_0 \times \Delta P}{2P_0 + \Delta P} \qquad \text{Equation 5-2}$$

In order to calculate the volume ΔV , the difference of pressure ΔP needed first to be estimated when dispensing the gel at a shear stress of 1 dyn/cm² using the following equations. The average of fluid velocity in the microchannel (400 µm x 100 µm x 20000 µm) will be given by formula[162]:

$$Q = \frac{\tau h^2 b}{6\eta} \qquad \text{Equation 5-3}$$

with τ being the shear stress applied in the channel, h the depth of the channel, b the width of the channel and η the viscosity of the fluid.

The mean velocity Q of the fluid in the circular capillary under a limitation of laminar flow was subjected to Poiseuille's law[163]:

$$Q = \frac{\Delta P \times \pi \times D^4}{128 \times \eta \times L} \qquad \text{Equation 5-4}$$

with D being the diameter of the capillary, η the viscosity of the fluid and L the length of the capillary.

Therefore, to calculate ΔP, the previous equation led to:

$$\Delta P = \frac{Q \times 128 \times \eta \times L}{\pi \times D^4} \qquad \text{Equation 5-5}$$

The hydraulic diameter D_h is calculated when handling flow in a non-circular cross-section channel and it is defined as:

$$D_h = \frac{4 \times cross\ sectional\ area}{perimeter\ of\ channel} \qquad \text{Equation 5-6}$$

For a square cross-section channel with sidewall a and b:

$$D_h = \frac{4 \times a \times b}{2(a+b)} = \frac{2 \times a \times b}{a+b} \qquad \text{Equation 5-7}$$

Hence, it was possible to calculate the volume that could seep into the Channel B for different shear stresses during the gel dispensing step using equation 5-2. Before carrying out a chemotactic assay, the mathematical model was validated using the gel pure or mixed with FITC-dextran (5 mg/ml) dispensed into the Channel A in order to study its behaviour within the biochip.

5.1.4 T-junction biochip design

An alternative design incorporating a T-junction structure which will be further referred as "Prototype 2" was developed to connect a perpendicular channel on the same x-y plane as Channel B. This design was developed to allow the cells, flowing in Channel B, to migrate towards the gradient of chemokines generated from each branch of

Channels A (Fig. 5-6). The CAD generated model obtained with eDrawing is presented in figure 5-7.

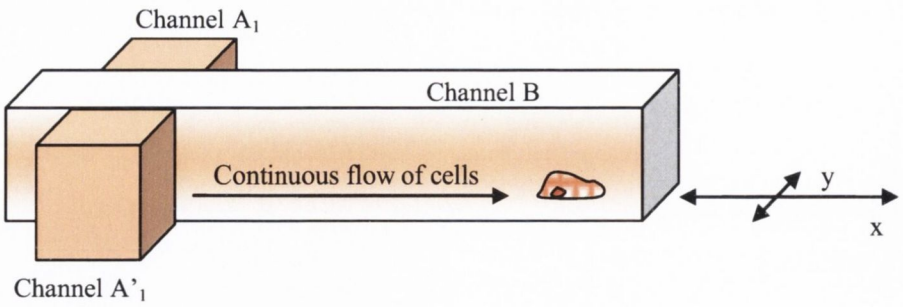

Figure 5-6: Illustration of the freedom of movement of cells in a T-junction design. The model shows that cells will be free to migrate from the Channel B to the Channels A_1 and A'_1 on a 2D plan.

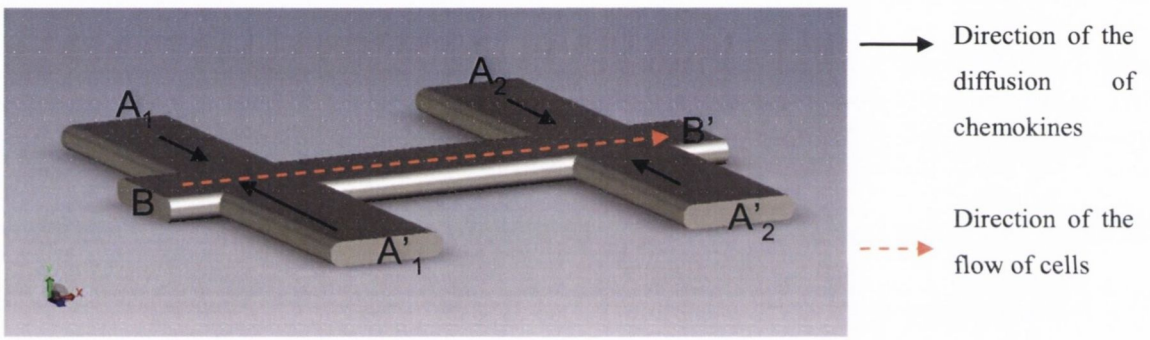

Figure 5-7: Schematic representation of Prototype 2 based on T-junction structure. The model shows the Channel B which will contain the continuous flow of cells. The diffusion of chemokines will occur from the four perpendicular channels A_1, A'_1, A_2, and A'_2. One perpendicular channel can be filled with one chemokine (e.g. SDF-1α) and the other side of the channel with another chemokine (e.g. RANTES) to study the possible potentiation of one chemokine with another.

The purpose of the T-junction design was to study the influence of two chemokines working in synergy[164] (§ 2.4). Crossed channels A_1 and A_2 can be filled with one type of chemokine (e.g. SDF-1α) and channels A'_1 and A'_2 can be filled with another chemokine (e.g. RANTES). This design presented the option to vary the relative concentrations of both chemokines to study any possible potentiation of one chemokine with another. However, experiments with the same chemokine in the four channels A_1, A'_1, A_2, and A'_2 were first tested to evaluate the validity of the design.

5.1.5 Simulation of physical phenomena in the Prototype 2

COMSOL was used to generate mathematical models describing the physical phenomena within the Prototype 2. These models were a prediction of the direction of the diffusion of the chemokines in response to the flow and thus helped in the validation of the design. Once the chip was developed, the gel pure or mixed with FITC-dextran was first dispensed into the Channels A without dispensing the cells in the Channel B in order to observe the behaviour of the gel at the intersection of both channels.

To describe the computational model, different steps have to be set: determine and simplify the geometry, specify the physics behind the problem, create the meshing of the defined geometry and finally identify all the solvers and post-processing condition for a clear convergence and accuracy on the model. The description of all the steps that lead to the simulation for the Prototype 2 are here below reported.

The geometrical definition and shape of the channels was developed by creating an axysimmetric two-rectangular subdomain (Fig. 5-8). These are representing Channel B, comprising with the flowing cells (subdomain 1) and Channel A, filled with gel and chemokines (subdomain 2). The multiphysics model choice is based on convection-diffusion equations. Convection is the transport of molecules or heat due to the movement of the surrounding molecules whereas diffusion is described as the net transport of molecules resulting from random motion. Due to the nature of the experimental design, the model conditions were set to be at constant temperature. Therefore, the governing equation was the diffusion. There, we assume the system to be at ideal condition, and therefore the equation of conservation is the main equation used for the model. In the model, the inlet of the subdomain 1 defines the conditions at the entrance of the Channel B, which means where a continuous flow of cells will be dispensed. From the experimental data, the inlet boundary was set to 1 dyn/cm^2. In order to have a degree of freedom on the model the opposite end of subdomain 1 was define as the output of the system and therefore set to be the depending variable in the model. Channel A-to-Channel B interface, where fluid mixes with the gel, was described to be linear in the model and was set to have continuous non-boundary slip condition. This defined the ideal experimental case where the gel maximum dissolution surface diffuses the chemokine along the fluid-cell channel.

The aim of the simulation was to show the dynamic of the diffusion of chemokines from the subdomain 2 to the subdomain 1, thus the coefficient of diffusion of the chemokines in each gel was also set. Following to the geometrical definition of all subdomain boundary conditions, a meshing process was carried out to refine the model and remove any possible incongruencies or irregularities in the boundaries and internal nodes. There, triangular elements without any single point solution where implemented and checked. After that, the model is solved according to the experimental conditions set in each individual element.

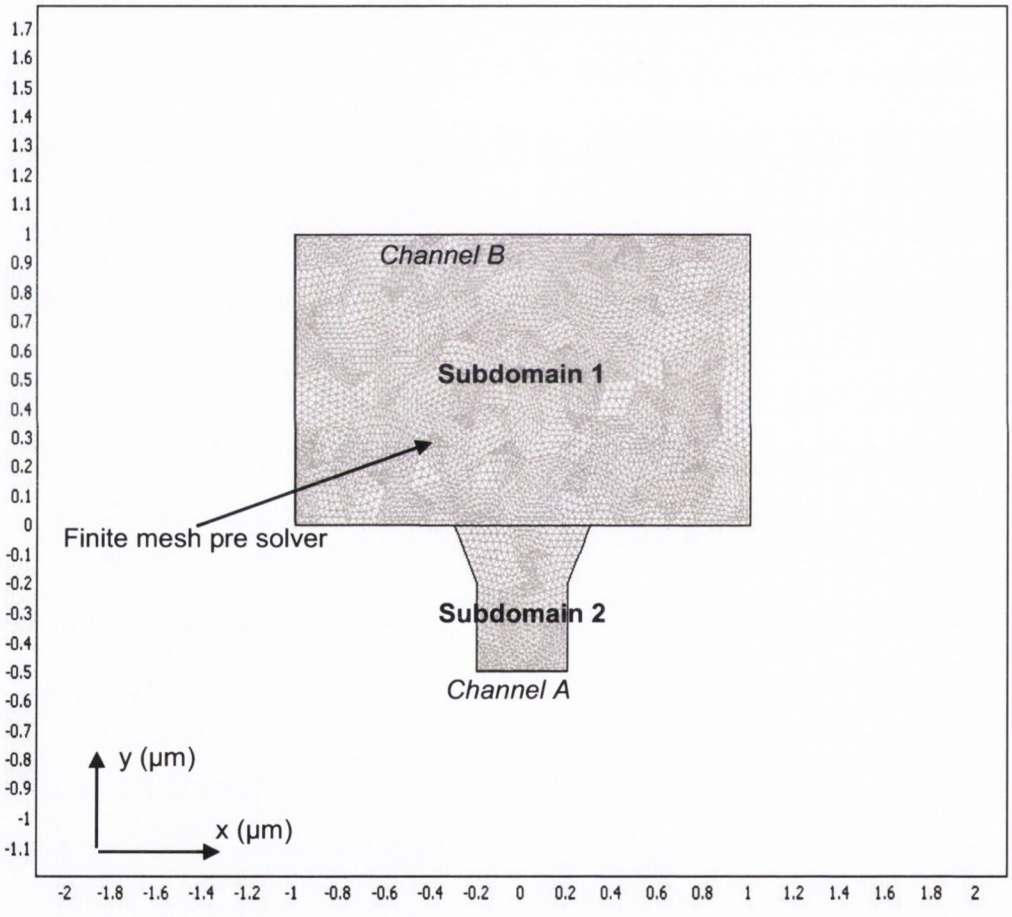

Figure 5-8: Finite element model of the Prototype 2 using COMSOL. The design of the chip is divided into two subdomains: the subdomain 1 represents the Channel B and the subdomain 2 represents the Channel A. Both subdomains are meshed accordingly.

Before carrying out a chemotactic assay, the mathematical model was validated using the gel with no chemokines in order to study its behaviour within the biochip. The gel pure or mixed with FITC-dextran (5 mg/ml) was dispensed in the Channel A.

5.1.6 3D Biochip with a membrane

Taking into account the advantages of the configurations of the Boyden chamber and the under-agarose assay (§ 2.8, § 3.1.7), two alternative designs were also considered: 1) a microfluidic channel can be created within a gel scaffold in which cells could continuously flow, and 2) a porous membrane coated with a gel introduced into a biochip setting can mimic the blood vessel wall environment. Technologically, the first design was not conceivable with the facilities available during the project. Nonetheless, a new device based on the second design was developed which consisted of two separate chips that are assembled together with a porous membrane placed between the two chips (Fig. 5-7). The surface of one chip is either flat or two channels are etched. Therefore, different configurations are possible: either two chips with both etched channels are assembled together (Prototype 3a) or two chips which the bottom chip is flat and the top chip with etched channels (Prototype 3b) are assembled together. In the Prototype 3b, either a gel can be filled on the bottom channel or chemokines can continuously flow underneath the membrane. Prototype 3b was first used to observe the response of the flowing cells to a membrane coated with cell adhesion molecules (§2.6).

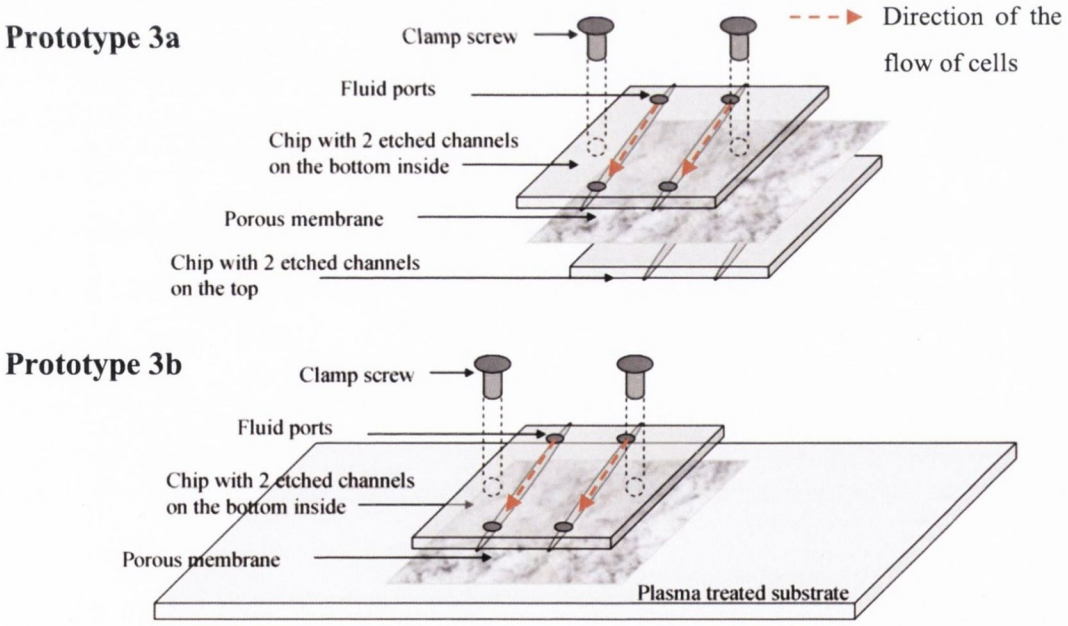

Figure 5-9: Drawings representing the design of the Prototypes 3. Either two chips with etched channels are assembled together (Prototype 3a) or one flat chip is assembled with a chip with etched channels (Prototype 3b). A porous membrane is placed between the two chips, for example, to mimic the vessel blood wall tissues. Clamp screws ensure tight contact of the chips and the resulting formation of sealed channels between them.

The Isopore® membrane (Millipore, Ireland) with 3 μm of pore size was mainly used as a barrier function between the two chips on a similar manner than the *in vivo* endothelial layer which separates the blood flow from the tissues. In addition, the porosity of the membrane makes also possible the migration of cells through it. A polycarbonate membrane was chosen due to the smooth glass-like surface which permits microscope experimental observation on the surface of the membrane. In this arrangement, the membrane was coated with fibronectin (1 mg/ml) according to the manufacturer specifications. Then, it was washed twice with PBS and placed between the two chips. Then, cells were dispensed into the channel at a shear stress of 0.5 dyn/cm^2 for 10 min.

For the observation of the cells on the membrane, the cells were stained with the green fluorescent dye CellTracker CMFDA (Invitrogen, Ireland) that readily penetrated through the membranes of live cells. Once inside the cell, this probe reacts with intracellular components to produce cells that are both fluorescent and viable for at least 24 hours after loading. This fluorescent stain features peak absorbance at 492 nm and peak emission at 517 nm. The lyophilized product was dissolved in DMSO to a stock concentration of 10 mM. The stock solution was then diluted to a final working concentration of 5 μM in serum-free medium. Cells were re-suspended in pre-warmed CellTracker dye working solution and incubated for 15 min at 37 °C. After 15 min, cells were washed twice with medium and re-suspended in pre-warmed medium and incubated for another 30 min at 37 °C before their uses in the chips.

5.1.7 Microfluidic platform and standard operating procedure

The experimental microfluidic system was composed of a Mirus Nanopump (Cellix Ltd), a heating plate, a Microscope Cage Incubator (OkoLab) and a Nikon microscope (Fig. 5-10). The chip was placed on the heated stage on the microscope. The pump was connected to the input of the chip via flexible tube. The temperature during the assay was controlled and maintained at 37 °C by the Microscope Cage Incubator and the heating plate. Sample in the channel was directly observed under the inverted microscope with different lens magnification (10x, 20x). Images were acquired with QICAM Fast 1394 digital camera (QImaging, Canada) designed for high-resolution using Qcapture software for real-time image preview and capture.

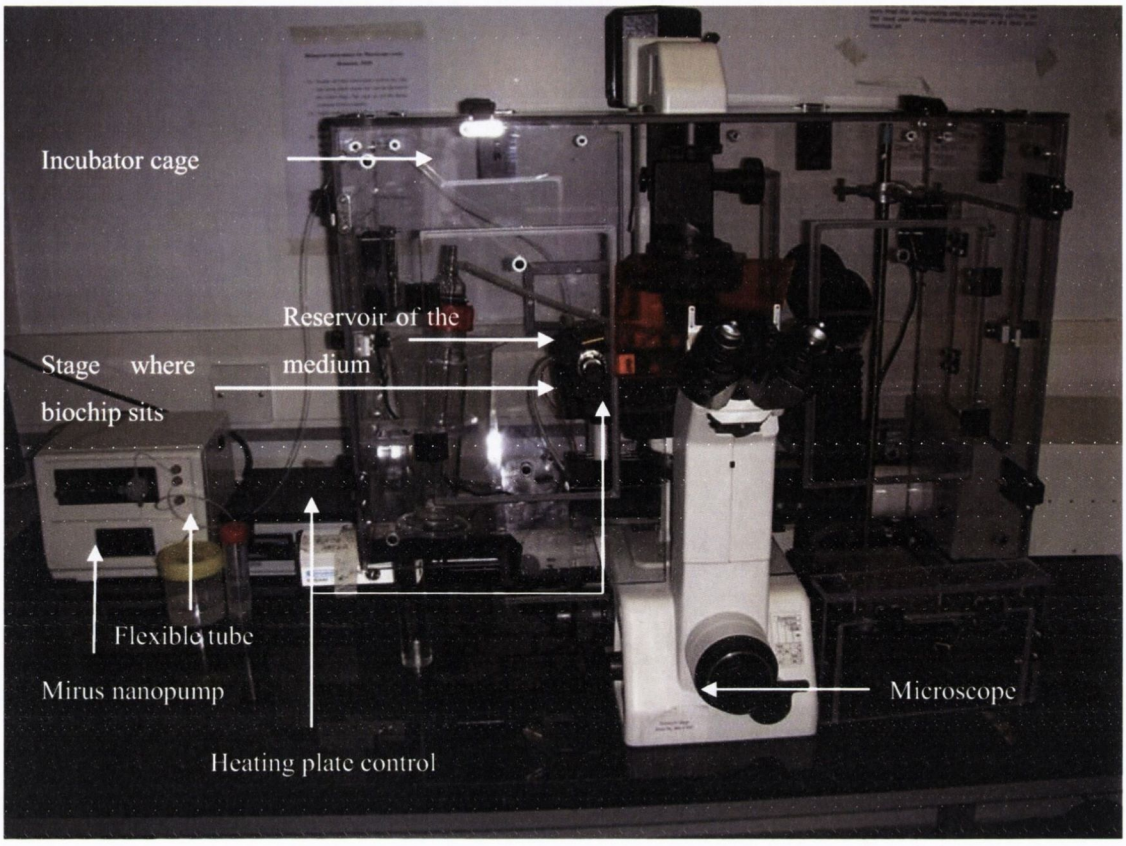

Figure 5-10: Image showing the elements composing the microfluidic platform. The microfluidic system consists of a Mirus Nanopump (Cellix Ltd), a heating plate, a microscope incubator cage (OkoLab) and a Nikon microscope. The biochip is placed on the heated stage on the microscope. The pump is connected to the inlet of the chip via a flexible tube.

Cellix's Mirus Nanopump was used to reproduce the heamodynamic shear stress in the microcapillary biochips. This high precision pumping system is designed to aspirate small sample volumes and support flow rates (100 nL/min up to 20 µL/min) within the biochip channel with a range of shear stresses from 0.05 dyne/cm² up to 20 dyn/cm² controlled by the FlowAssay software. For example, in *in vivo* conditions the range of shear stresses found in postcapillary venules is between 1 to 5 dyn/cm² and more than 10 dyn/cm² in arteries[165]. A reservoir contains the cells media that will be dispensed in the Channel B. The reservoir also enables the heating of the media at 37 °C. Depending on the experimental conditions required, the shear stress may be preset to incrementally increase during an assay. This was used in the study of cells adherence in response to a shear stress (§ 5.1.1). For the chemotactic assays, cells were dispensed into the Channel B using the pump at a shear stress of 0.5 dyn/cm² for 2 min in order to let the

cells adhere to the channel. The shear stress was then increased to 1 dyn/cm^2 for an hour experiment.

The FlowAssay software (Cellix Ltd) enables the user to execute preset protocols controlling the pump (Fig. 5.11a). Different steps need to be followed for the set up of the pump. First, the pump was initialized and the geometry of the channels used for the experiment was loaded. The pump was preliminary washed out with PBS before use.

The pump was ready for use when the washing steps were completed. Then, different steps of the protocol were optimised and subsequently executed in all experiments:

Step 1:

Wet Tip (3 µl): a drop of liquid is dispensed at the edge of the tip to avoid any formation of bubble when the liquid will be dispensed into the channel.

Step 2:

Syringe setting (6 µl): this step represents the volume of the sample that will be picked up. The concentration of cells used for the whole study was set to 5 x 10^6 cells/ml.

Step 3:

Wet Tip (3 µl): see S*tep 1*.

Step 4:

Dispense into chip/preinject cells (1.5 µl): this step was to inject the cells into the Channel B before applying any shear stress. This preinject step was to allow the gravitational cell settling at the bottom of the channel.

Step 5:

Variable Flow Rate: the value of the shear stress but also the duration for each value of shear stress was chosen depending on the experiments carried out (Fig. 5.11b).

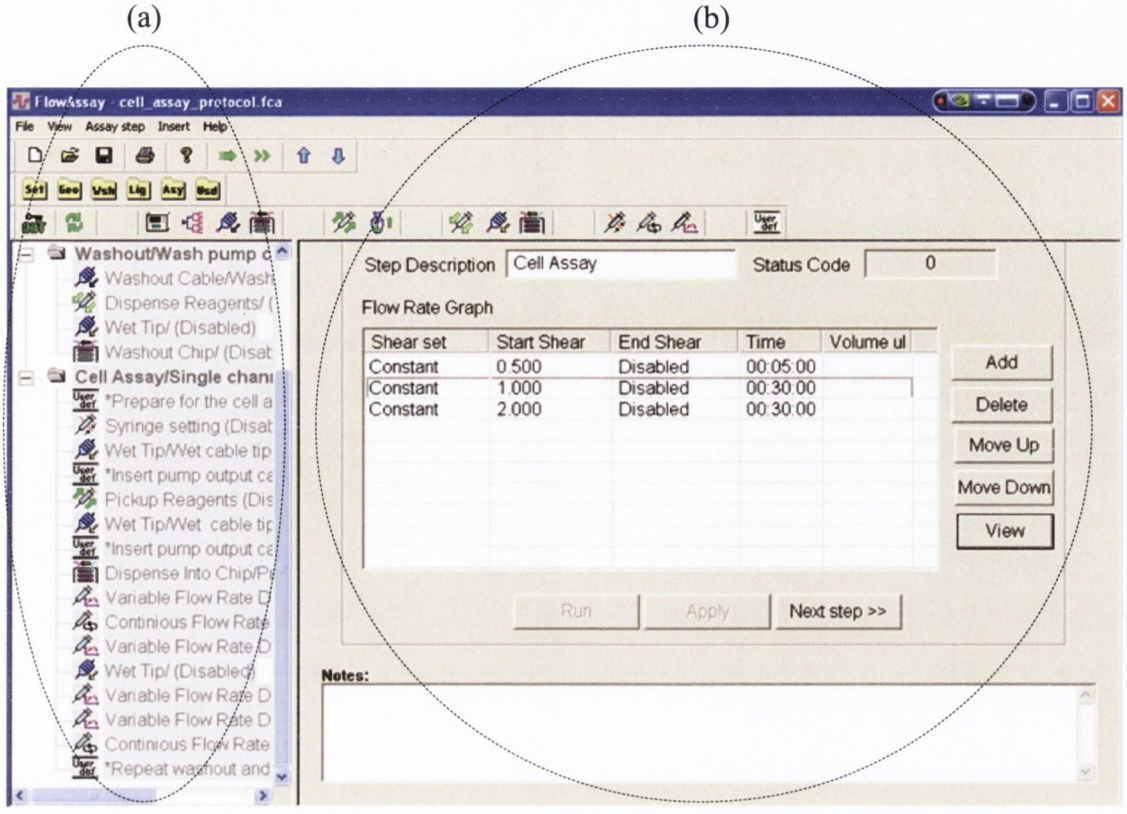

Figure 5-11: Example of the process window in FlowAssay software. Different steps of the protocol had to be followed in order to first wash out the channels and then pick up the reagent before dispensing it into the channel (a). The value of shear stresses and the duration at which the sample was dispensed were set (b) for each experiment.

During each experiment, the flow rate graph was continuously displayed showing the volume fraction of the sample dispensed into the Channel B as well as the value of the shear stress applied (Fig. 5-12). Real time imaging was performed with Qcapture software.

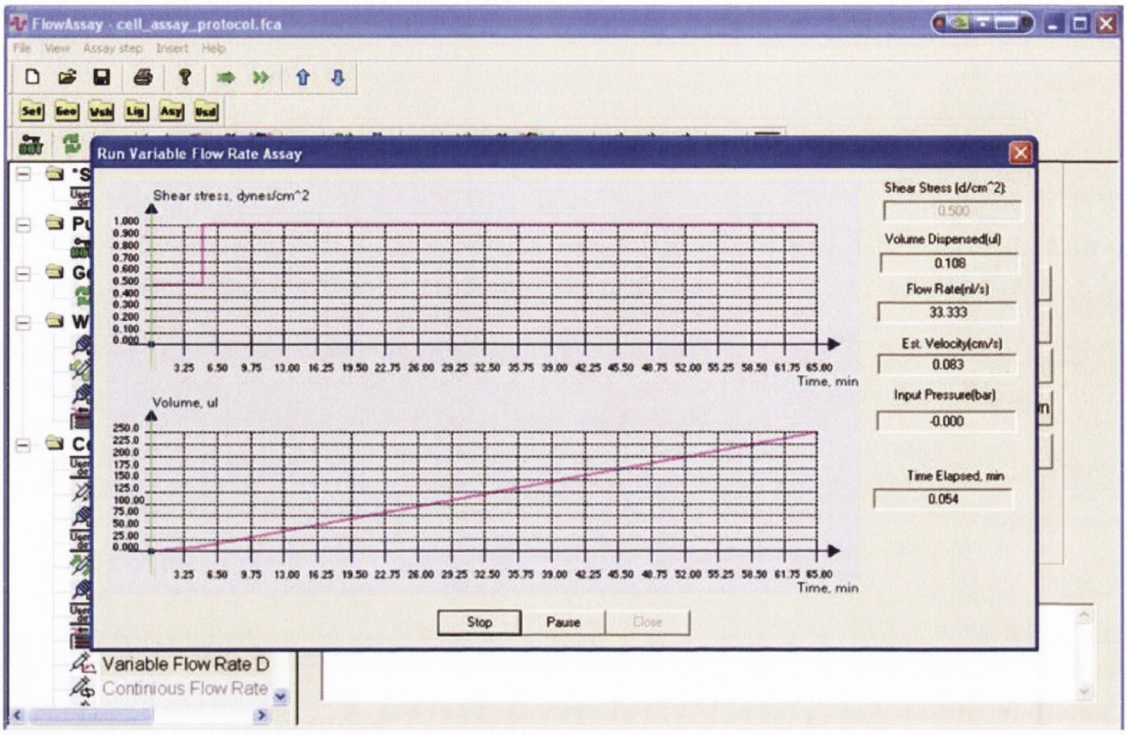

Figure 5-12: Example of a process window during a microfluidic experiment in FlowAssay software. The graph on the top of the window displays the dynamic change in the shear stress (dyn/cm^2) with the time (min) and the graph on the bottom shows the volume (µl) of the sample dispensed in the channel with the time (min).

5.1.8 Protocol of channel coating and gel dispensing in the Prototypes 1 and 2

The gel (ECM, agarose or collagen) dispensed in the Channel A in the Prototype 2 is an essential step in order to obtain a smooth surface at the intersection of both channels to ensure a laminar flow. Then, from a stock solution of the gel 10 µl only 1 µl (which is the maximum volume that can contain this channel) was pipetted out and dispensed inside the Channel A. The gels used were thermosensitive, and as expected from their properties, the lower the volume is pipetted, the quicker the gel changes its molecular organization to gelify. This is why, by pipetting out 10 µl, we minimized the effect of the temperature on the pipetted gel solution.

Due to the low melting temperature of all gels, all the preparations were performed below 4 °C temperature. In this case, ice containers were used to reduce the temperature during the mixing procedure. The chip was placed on a steel plate on ice because the plastic of the chip poorly conducts heat. According to the temperature at which agarose

becomes gel (§ 3.1.4), the chip needed to be warmed up at 40 °C on a heating plate to facilitate to dispense of the agarose solution into the Channel A.

The coating of the surface of a channel was also crucial as the chemotactic assays relied on the capacity of the cells to stick onto a homogeneous coated surface. Two protocols for coating the channels and for dispensing the gel were used in order to find the best method. Protocol A: Channel B was coated first with recombinant human ligands and then the gel was dispensed into the Channel A. Protocol B: the gel was firstly dispensed Channel A and then the Channel B was coated with recombinant human ligands.

Protocol A: Channel coating/Gel dispensing:

- the outlet ports of the Channel A were sealed with squeezed steel pins,
- the solution of ligands (10 µl) was dispensed into the Channel B,
- the chip was incubated 1h at 37 °C in the humidification chamber placed in the incubator with 5 % CO_2,
- the Channel B was washed twice with PBS (10 µl) in order to remove the solution of ligands that have not been immobilized onto the surface of the channel,
- the outlet ports of the Channel B were sealed and the outlet ports of the Channel A were unsealed,
- A volume of 10 µl of gel was pipetted and 1 µl was carefully dispensed into the Channel A. The experimental conditions depended on the gel used (see above). The chip was incubated at 20 °C for 30 min (*) to allow the gel to set.

Protocol B: Gel dispensing/Channel coating:

- the outlet ports of the Channel B were sealed with squeezed steel pins,
- 10 µl of gel was pipetted from the stock solution and 1 µl was dispensed in each Channel A at the appropriate experimental conditions depending on the gel used (see above). The chip was then incubated at 20 °C for 30 min (*) to allow the gel to set,
- the outlet ports of the Channel B were unsealed and the outlet ports of Channel A were sealed,
- the solution of ligands (10 µl) was dispensed into the Channel B,

- the chip was incubated 1h at 37 °C in the humidification chamber placed in the incubator with 5 % CO_2,
- the Channel B was then washed twice with PBS (10 µl) in order to remove the ligands that have not been immobilized onto the surface of the channel.

(*) Technical notes: at this stage, two options of chemokines incorporation into the gel were possible:

1. gel was dispensed into the Channel A and left to gelify. Subsequently, gel was soaked with chemokines for 1h at 37 °C by dispensing chemokines in the Channel B,
2. gel was directly mixed with chemokines and dispensed in the Channel A.

It was also possible to seal the outlet ports with 2 % agarose instead of the steel pin. In this case, the ports of the channels were permanently sealed because the agarose gel was too viscous to pipette it out from the outlet ports. That is why sealing the ports with agarose gel was only processed when the Channel A was first filled with the gel.

Both protocols were tried out and they both have advantages and background which are discussed in the results part (§ 5.2.3.3).

In the Prototype 1, the gel was dispensed in the Channel A with the pump. First, the two output ports of the top channel were sealed with squeezed steel pin and then 10 µl of gel was aspirated with the pump to subsequently dispense it into the Channel A. The chip was placed on ice if agarose was used or on heated stage if collagen and ECM gels were used in order to let the gel gelify during the dispensing. The solution of ligands (§ 5.1.1) was further dispensed into the Channel B and incubated 1h at 37 °C.

5.1.9 Culture of cells

PBL cells were used for this study at a concentration of 5 x 10^6 cells/ml and 6 µl were aspirated with the pump to dispense it into the Channel B. The protocol of isolation of the cells as well as the culture is detailed in the section 3.1.1.

Human umbilical vein endothelial cells (HUVEC) isolated from human umbilical cords were cultured in complete M199 media that was obtained by using the following protocol. First, 3 ml of M199 media was added to 10 000 units of heparin. A volume of 10 ml of M199 media was added to endothelial cell growth mitogen (ECGM) and 5 ml of that solution was mixed with the heparin solution. Then, the M199 media was supplemented with 5 ml of the heparin/ECGM solution, 5 ml of penicillin/streptomycin and 20 % FBS.

Tissue culture flasks were coated with 0.2 % gelatine type A porcine skin (Sigma, Ireland) to allow successful adherence of HUVEC. Gelatine was warmed up at 40 °C to permit gelatine to go into solution and 5 ml was dispensed into a T75 flask. The flask was then incubated at 4 °C for 20 min to let the gelatine turn into gel. Excess of gelatine was removed before seeding the cells.

HUVEC were used at passages 2 or 3 for the experiments as they had the highest level of CD44 expression. HUVEC cells that have reached 80 % of confluence were re-seeded on a new flask. First, the media was removed from the flask. Trypsin is used to detach the cells from the flask. However, the serum in the media contains trypsin inhibitor, therefore adherent cells were washed twice with pre-warm PBS and 5 ml of trypsin was dispensed on top of the cells and incubated at 37 °C, 5 % CO_2. The process of trypsin proteolysis was stopped after 5 min by dispensing 5 ml of complete media into the flask. Cells were counted, spin down and re-suspended in complete media for further cell culture or directly used for the experiments carried out with the Prototype 3. HUVEC in suspension (200 µl of 10 x 10^6 cells/ml) were dispensed on the bottom of the chip (Prototype 3b) and incubated for 30 min at 37 °C, 5 % CO_2 in order to let the cells to settle down and to adhere onto the surface of the chip. The non-adherent cells were then washed twice with complete medium. The adherent cells were activated with 20 ng/ml of TNF-α for 2 hours at 37 °C, 5 % CO_2. The cells were washed twice with media and the bottom of the chip was sealed with the top chip.

5.2 Results

5.2.1 Evaluation of the adherence of cells in Vena8™ channels

Vena8™ biochips from Cellix Ltd were used to assess the capacity of PBL to adhere to ICAM-1 and VCAM-1. After 2 min at 0 dyn/cm² (static), cells settled and adhered at the bottom of the channel and shear stress was gradually increased to 10 dyn/cm² (Graph 5-1).

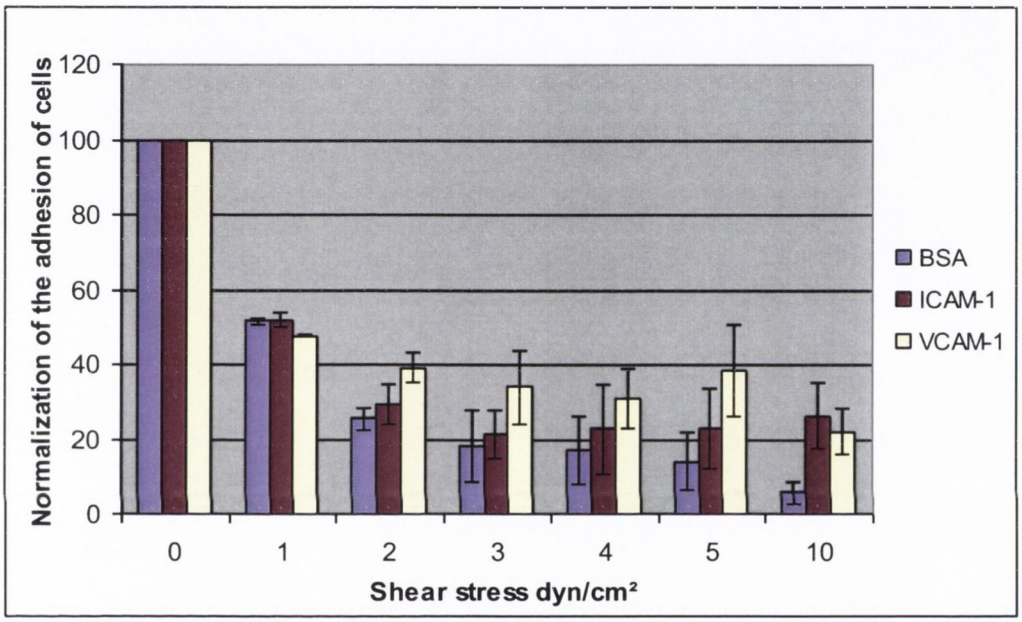

Graph 5-1: Adhesion of PBL cells on the surface of a Vena8™ channel coated with BSA, ICAM-1 and VCAM-1 in response to an increase of shear stress.

Graph 5-1 shows that 50 % of adherent cells were still attached onto the coated surface at 1 dyn/cm² whereas at higher shear stresses (10 dyn/cm²) only 20 % of the cells remain attached to the surface of the channel. This correlates with the *in vivo* cell adhesion observation which occurs at low wall shear stresses[22] (1 dyn/cm²).

Therefore, working with a channel with a surface coated with ICAM-1 and VCAM-1 will allow cells to adhere onto the channel to subsequently migrate towards the gradient of chemokines generated in the new Prototypes.

5.2.2 Results obtained using the Prototype 1

5.2.2.1 Design of the Prototype 1

The design of the Prototype 1 is presented in figures 5-13 and 5-14 where the Channel A corresponds to the sinuous line and the Channel B corresponds to the straight line. Input and output ports of each channel are on each side of the chip. The sinusoidal shape of the Channel A was done to have multiple intersections between Channel B and A to create a multiple release of chemokines.

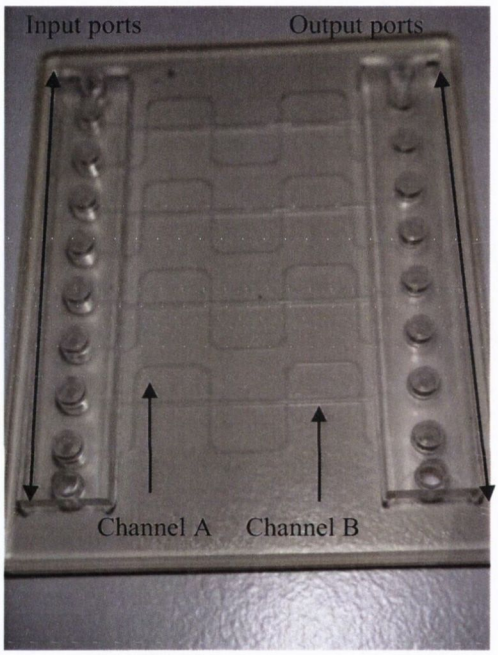

Figure 5-13: Photograph representing the Prototype 1. The sinuous channel corresponds to the Channel A which is underneath the straight Channel B. The bottom channel will be filled with gel and chemokines while the cells will continuously flow in the Channel B. The four intersections between the Channels A and B represent the sites where the chemokines will be released from the Channel A to the flowing cells.

The specifications given by Cellix Ltd for the Prototype 1 are presented below (Fig. 5-14). For each type of chip, input ports and output ports have the same properties.

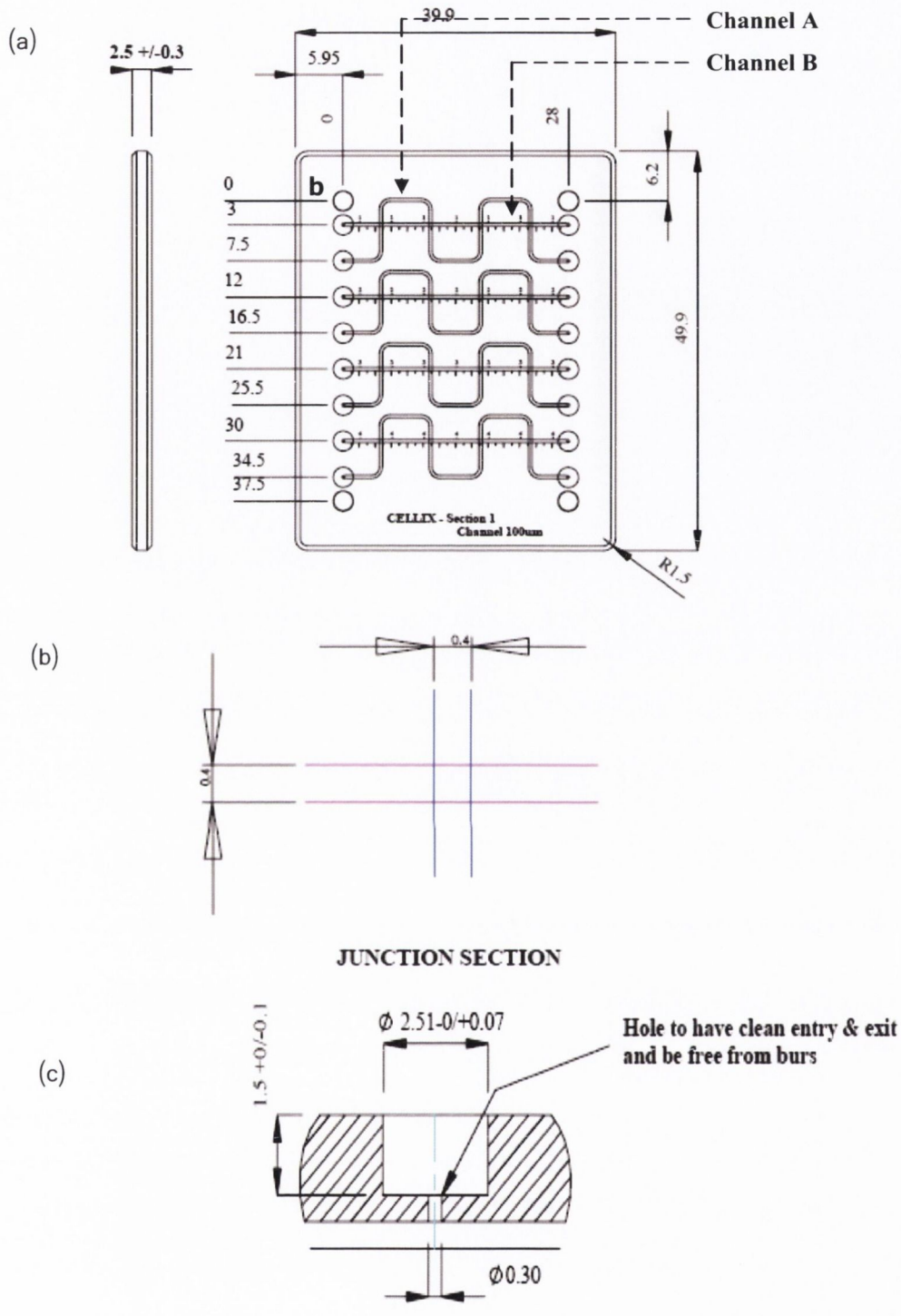

Figure 5-14: Schematic drawings showing the technical specifications of the Prototype 1. The general overview of the design of the chip is shown in figure (a). The dimensions of the intersection between the Channels A and B are given in figure (b). The technical specifications of the inlet/outlet ports "b" of the channels are presented in figure (c). Dimensions are given in mm.

5.2.2.2 Mathematical model applied to the Prototype 1

The volume of gel that could come into the Channel B of the Prototype 1 while the gel is dispensed in the Channel A can be firstly calculated as the average fluid velocity Q (cm^3/s) of water dispensed in Channel A using equation 5-3:

$$Q = \frac{\tau h^2 b}{6\eta}$$ Equation 5-3

$\tau = 1$ dyn/cm²

h = 0.01 cm

b = 0.04 cm

$\eta = 10^{-2}$ g/cm.s

$$Q = \frac{1 \times 0.01^2 \times 0.04}{6 \times 10^{-2}} = 66 \times 10^{-6}\ cm^3/s$$

where equation 5-5 is applied to calculate the difference of pressure ΔP between the inlet port and the outlet port of the Channel A while the gel was dispensed in it:

$$\Delta P = \frac{Q \times\ 128 \times \eta \times L}{\pi \times\ D^4}$$ Equation 5-5

$Q = 66.10^{-6}$ cm^3/s

L = 2 cm

D = (2x0.04x0.01)/(0.04+0.01) = $1.6x10^{-2}$ cm

$$\Delta P = \frac{66 \times 10^{-6}\ \times 128 \times 10^{-2} \times 2}{\pi \times\ (1.6 \times 10^{-2})^4} = 800\ dyn/cm^2 = 0.82 \times 10^{-7}\ N/cm^2$$

There it results that the variation in pressure between Channel A and Channel B is $\Delta P = 0.82 \times 10^{-7}$ N/cm².

Knowing ΔP, the volume that may seep into the top channel was estimated using equation 5-2:

$$\Delta V = \frac{V_0 \times \Delta P}{2P_0 + \Delta P}$$ Equation 5-2

$V_0 = 2 \times 0.04 \times 0.01 = 8 \times 10^{-4}$ cm^3

$P_0 = 1.013$ bar = 1.013×10^{-4} N/cm²

$\Delta P = 0.82 \times 10^{-3}$ bar = 0.82×10^{-7} N/cm²

$$\Delta V = \frac{8.10^{-4} \times 0.82 \times 10^{-7}}{2 \times 1.013 \times 10^{-4} + 0.82 \times 10^{-3}}$$

which results in a $\Delta V = 0.32$ nl.

The same calculations were done for the agarose gel 2 % and we obtained a volume $\Delta V = 164$ nl.

Therefore from the theoretical calculation the volume ΔV of the liquid that could seep into the Channel B is on the range of the nanolitre which results to be negligible in comparison with the total volume injected (10 µl).

5.2.2.3 Validation of the model

During the validation phase of the new channel prototype it was experienced that when the gel was pre-loaded into the syringe and then injected into the Channel A, the gel seeped into the Channel B for each attempt to entirely fill the volume of the Channel B. Solution to this problem was using manual syringe injection of the gel in the Channel A (Fig. 5-15) by a 10 µl pipette. This resulted to be effective and allowed the gel to only seep at the surrounding of the Channel A, where the excess of gel in the Channel B was removed by counter-injection by a 10 µl pipette of air or PBS. It is important to notice that by doing this, the injected-gel when approximating to the intersection of both channels was partially washed away and subsequently replaced by "air bubble" formation (Fig 5-15a). This was consistently seen across every experiments carried out. The phenomenon was highlighted by injecting fluorescent dyes (e.g. FITC-dextran) mixed with the gel and then imaged by optical microscopy (Fig. 5-15b). When the same experiment was carried out with shear stresses (0.1, 2 and 5 dyn/cm^2) applied in the Channel B by controlled pump injection, the decrease in fluorescence intensity in Channel A occurred within seconds which means that the concentration of FITC-dextran in the gel decreased and that fluorescent molecules have been washed away.

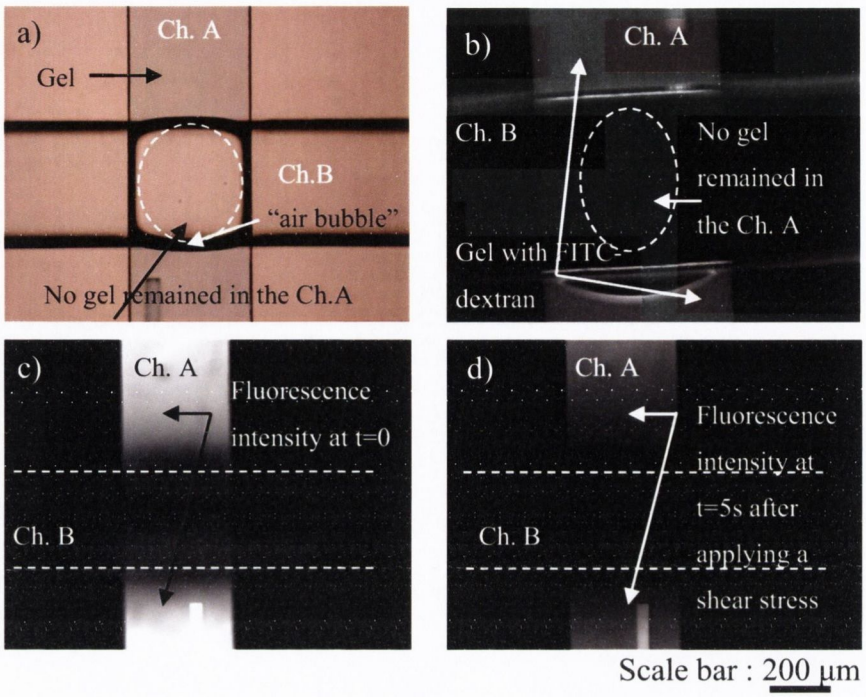

Figure 5-15: Photographs of the intersection of the channels of the Prototype 1 when the Channel A was filled with gel. Gel seeped from the Channel A (Ch. A) to the Channel B (Ch. B). When the excess of gel was washed away from the Channel B dispensing PBS with a pipette, the gel at the intersection of both channels within the Channel A was also washed away. (a) An "air bubble" was formed in the Channel A. (b) Under fluorescence observation; no visible gel was detected at the intersection of the channels. (c) Observation of the fluorescence intensity of the gel when the pump was used to remove the gel from the Channel B, a time t=0, (d) after applying PBS at 1 dyn/cm² for 5s.

The three types of gel mentioned earlier were used for this experiment. Working with collagen and ECM gels allowed us to wash out any excess gel from Channel B. However, agarose gel was not a viable procedure as agarose gel blocked the Channel B irreparably because of its greater viscosity when compared to the two other gels.

After the gel (either ECM or collagen) was removed from the Channel B, no gel remained in the Channel A, or at the intersection of both channels; that lack of gel created a "gap" which changed the flow path: the fluid dynamic was turbulent and not laminar.

These observations are clearly confirmed when cell-media injection were carried at variable shear stresses (0.1 and 1 dyn/cm^2). The results are shown on figure 5-16.

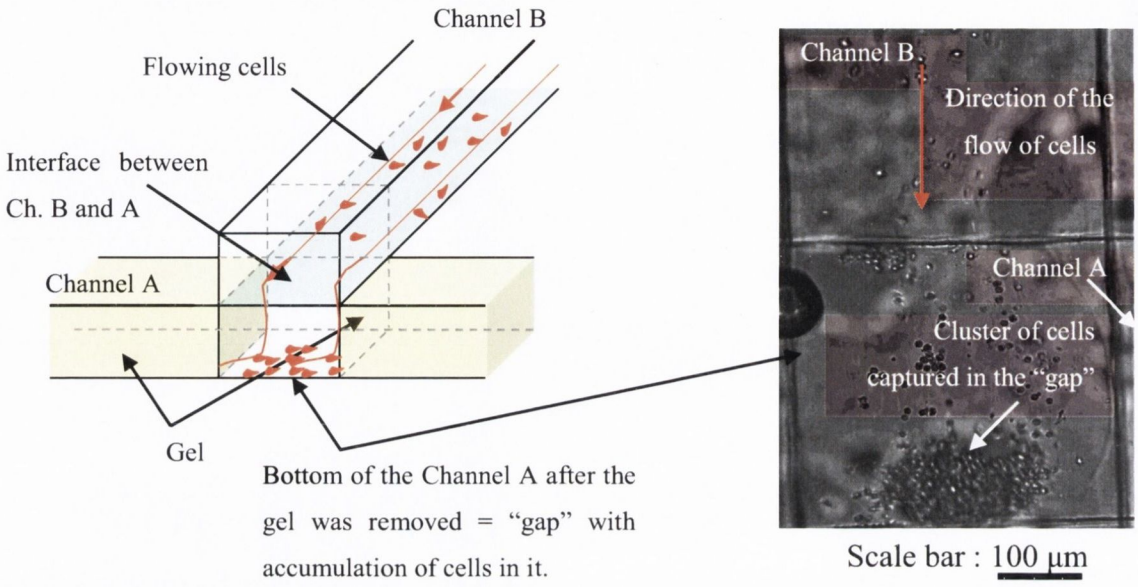

Figure 5-16: Experimental observation of the distribution of the cells in the Channel A at the intersection of both channels in the Prototype 1. The cells dispensed into the Channel B fell into the "gap" created in the Channel A by the lack of gel at the cross section area. The cells were captured in the "gap" and the regime of the fluid flow became turbulent.

The cells fell down into the "gap" formed by the lack of the gel at the cross section area in the Channel A. This "gap" led to the formation of a vortex (Fig. 5-17).

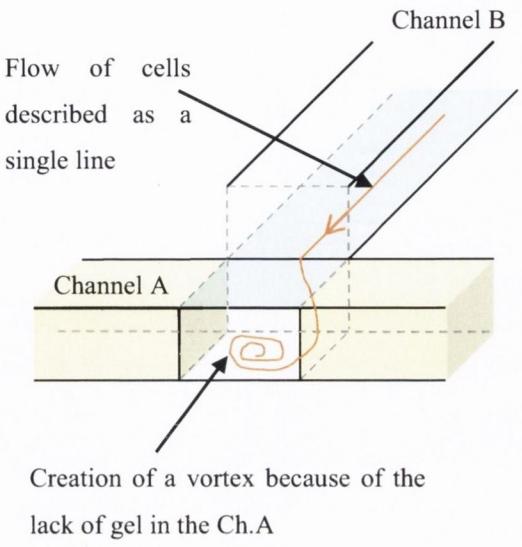

Figure 5-17: Schematic representation of the dynamic of the flow of cells in the Prototype 1. When the flow of cells (orange line) coming from the Channel B attains the intersection with the Channel A, the flow is trapped in the Channel A because of the lack of gel which creates a vortex.

Cells were not in a continuous flowing state anymore, but were continuously captured in the "gap" where a large cluster of cells was formed.

5.2.3 Results obtained using the Prototype 2

5.2.3.1 Design of the Prototype 2

The design of the Prototype 2 is presented in figure 5-18. This was achieved by designing a new chip with three Channels B connected to either four Channels A (Channels A_1, A_1', A_2, A_2') or two Channels A (A_1 and A_2).

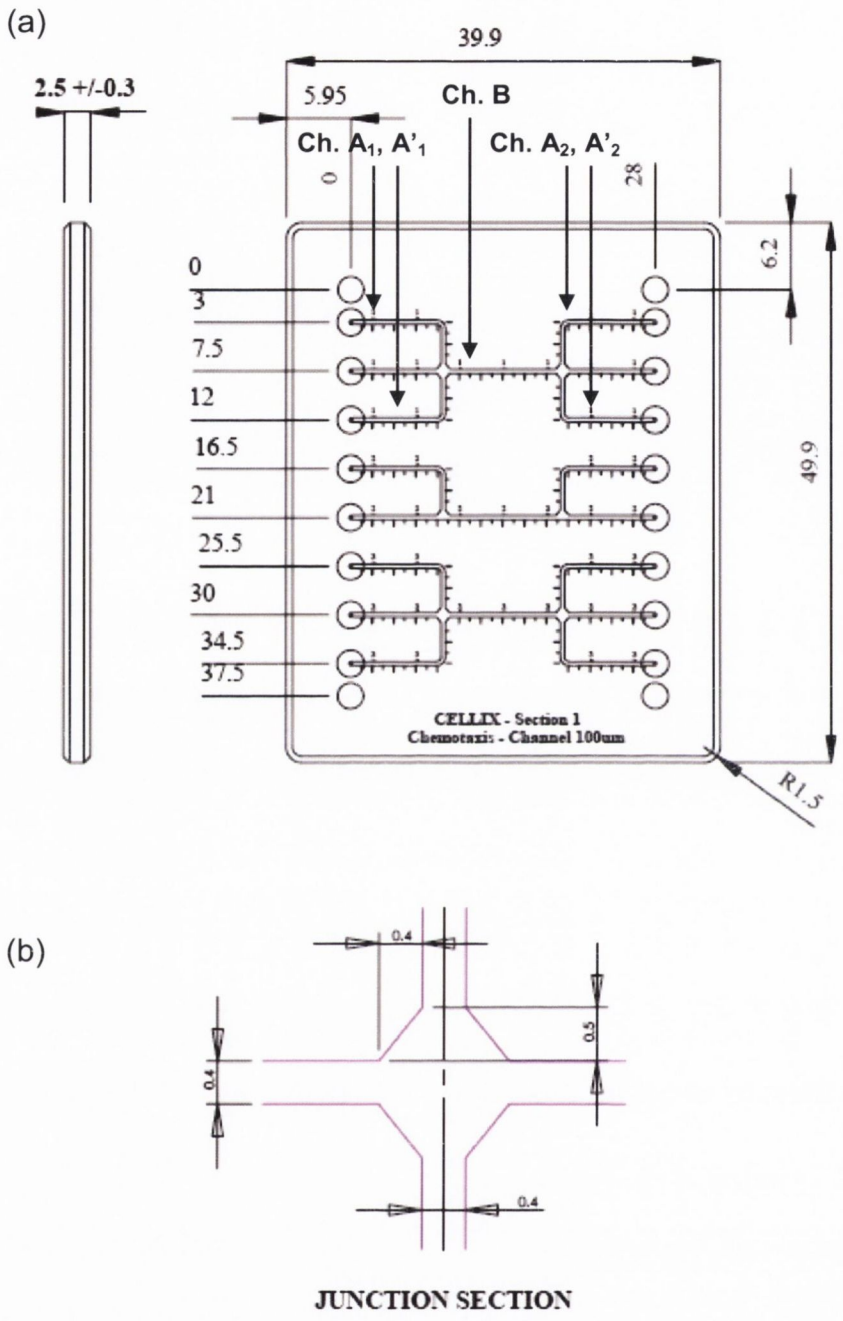

Figure 5-18: Schematic drawings showing the technical specifications of the Prototype 2. The general overview of the design of the chip is shown in figure (a). Detail of enlargement junction cross section: dimensions of the end of the Channels A at the intersection of both channels are given in figure (b). Dimensions are reported in mm.

As it is shown in figure 5-18b, the junction connection between Channels A and Channels B is purposely made not sharply straight with a 90 degree angle, but with wider enlargement at 45 degrees. The reason for such a design was in response to the experiments carried out with Prototype 1 where it was found that when a gel is

dispensed in a straight channel this create a prominent meniscus. However, with the configuration of the Prototype 2, having a channel with wider end allows the gel to create a flatter meniscus which would have an almost negligible impact on the resulting fluid dynamics of the channel.

5.2.3.2 Theoretical validation of Prototype 2 model

The theoretical prediction of the diffusion of chemokines in the Prototype 2 is presented in figure 5-19. From the implemented finite element model and solved mesh geometry (Fig. 5.8), it can be seen that the colour coded concentrations within each domain reflects the concentration of the flow of cells in mol/m^3. The concentration changes along the subdomain 1 due to the difference of pressure between the inlet and the outlet. The arrows depict the direction of the flow and the diffusion of molecules ($mol/m^2.s$) in subdomain 1 and subdomain 2 respectively. The red streamlines corresponded to the sum of the arrows in the subdomain 1. The blue streamlines were the representation of the dynamic of the gradient in the subdomain 2.

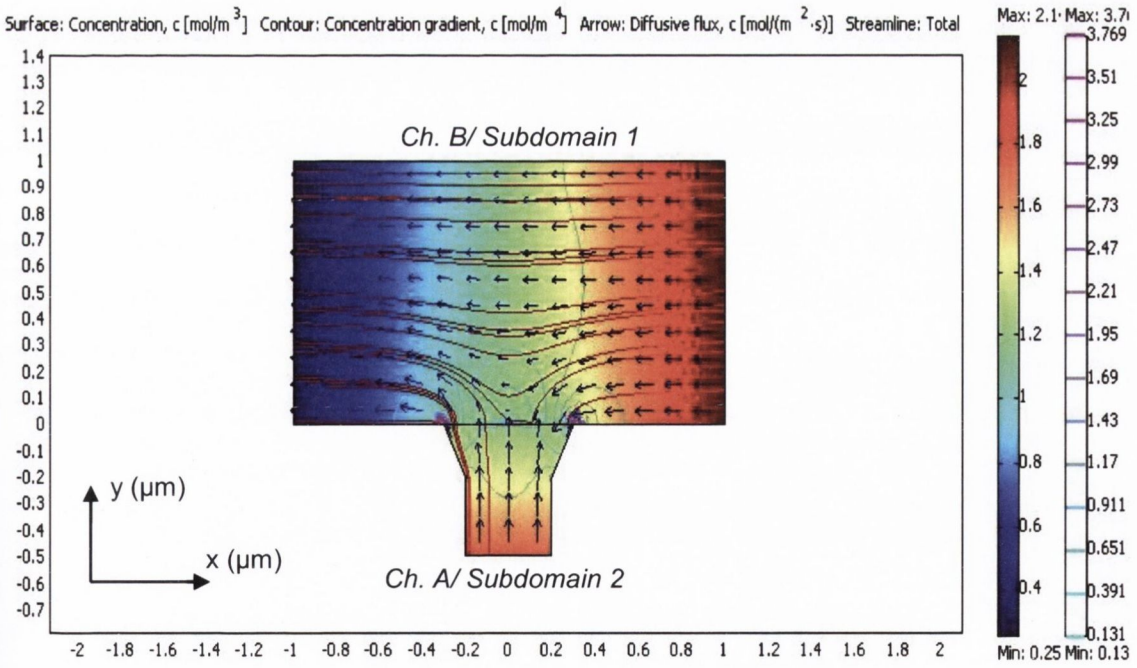

Figure 5-19: Theoretical model showing the dynamic of molecules and fluid in the Prototype 2. The model shows the result of the dynamic of the gradient of chemokines (blue streamlines) in response to the flow (red streamlines).

This theoretical model shows that the dynamics of the laminar flow changed when it is viewed at the channel intersection point and that it erodes the gel (arrows going into the subdomain 2). The erosion of the gel will induce a diffusion of chemokines only on the vicinity of the intersection (blue streamlines). In addition, as the gel gets eroded, the surface of the gel becomes not linear at both corners of the Channel A creating perturbation to the main laminar flow. Therefore, the corners encountered by the flow were an obstacle for both the flow and the gradient as it is shown in figure 5-19. This is why on both corners the streamlines of the concentration gradient were chaotic. This means that the observation of the cell migration should be observed after the T-junction where the cells are in laminar flow and where the chemokines are diffused.

5.2.3.3 Validation of the model

Prototype 2 was successfully manufactured following the specifications and protocols given in section 5.1.8. Protocol A, which consists of first coating Channel B with ligands and then filling Channel A with gel has shown drawbacks: a) the ligands dispensed in Channel B were also distributed in Channel A which made the surface of Channel A wet, b) the wet surface of Channel A made the filling of the gel irregular. Following to these observations, Protocol A was found to be unsuitable to be implemented on Prototype 2.

On the other hand, the advantage of Protocol B is that the surface of the Channel A was not wet during the gel dispensing, thus the filling resulted to be more effective than in Protocol A. However, if the gel seeped into Channel B, we observed that a layer of gel was left on the surface of the Channel B which made the dispensing of the ligands inhomogeneous. Nonetheless, Protocol B was chosen because it presented fewer drawbacks than Protocol A especially during the gel dispensing step.

When a gel is dispensed in Channel A, the gel seeps into the Channel B (Fig. 5-20a). The excess of gel is then removed by dispensing air or PBS with a pipette into Channel B. As mentioned before (§ 5.2.2.3), when ECM and collagen were used, it was possible to remove the gel in Channel B. Hence, the surface of the gel obtained at the intersection of both channels appeared flat (Fig. 5-20b). If the gel was dispensed just at the edge of the Channel A, the surface of the gel formed a meniscus (Fig. 5-20c). Even

in this case, Channel B was impossible to clean when the agarose gel was dispensed in Channel A; the agarose gel remained in the Channel B. In addition, due to the thermoplastic nature of the agarose polymer solution, which melts at around 85 °C (Chapter 3), it was only possible to pipette it from the stock solution to further dispense it into the channel when the temperature is above 50 °C (remark: the gel set within the pipette within 5 s). Contrastingly to the agarose solution, chemokines are denatured above such temperature (> 50 °C). Due to these contrasting thermal properties between agarose and chemokine, it was decided not to use the agarose gel as suitable matrix for chemokine diffusion.

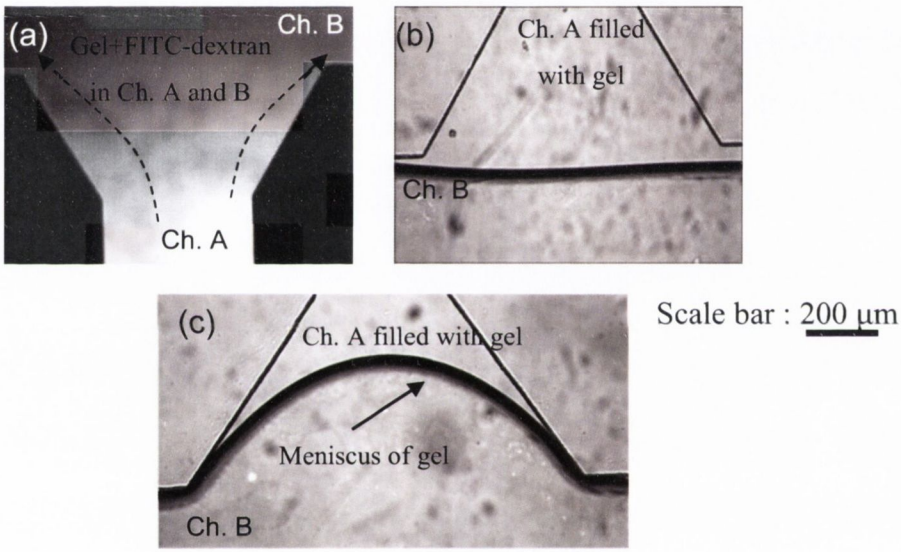

Figure 5-20: Images of Channel A filled with gel in the Prototype 2. Gel (ECM or collagen) is dispensed in Channel A. (a) Under fluorescence observation, the gel mixed with FITC-dextran seeped from Channel A to Channel B. (b) A flat surface of the gel is subsequently obtained to the washing of Channel B, (c) but a meniscus can also be obtained.

Although the gel was injected under controlled pressure in Channel A, the surface of the gel dispensed presented a meniscus. Consequently, the higher pressure derived from the fluid being under shear stress forced the gel to retract back into Channel A. This can be explained by the predominant shear force versus the injected force applied on the gel (Fig 5-21).

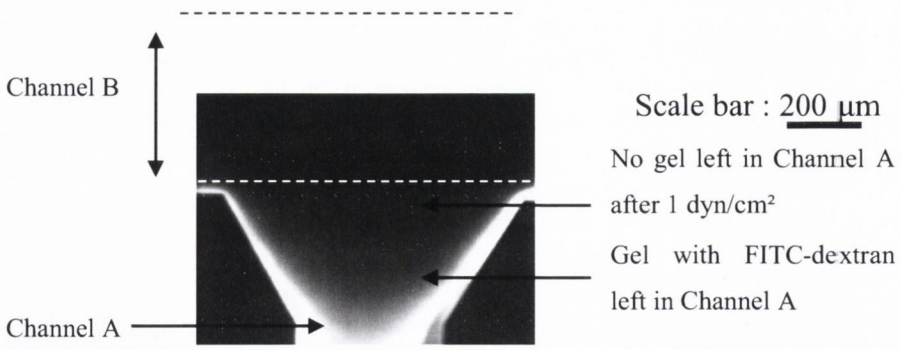

Figure 5-21: Photograph showing the dynamic of the gel to a shear stress in the Prototype 2. The gel was mixed with FITC-dextran and dispensed into the Channel A. The surface of the gel dispensed presented a meniscus. When a shear stress of 1 dyn/cm² was applied the gel was pushed back into Channel A.

The attempts to get a flat surface of the gel when the gel was dispensed in the design with Channels A_1/A'_1 and A_2/A'_2 have proven to be technically unfeasible. When the gel was dispensed in Channels A, the meniscus formed was removed by exerting a pressure to the gel to get a flat surface, but the gel from both Channels A was pushed into the Channel B which was subsequently blocked (Fig. 5-22).

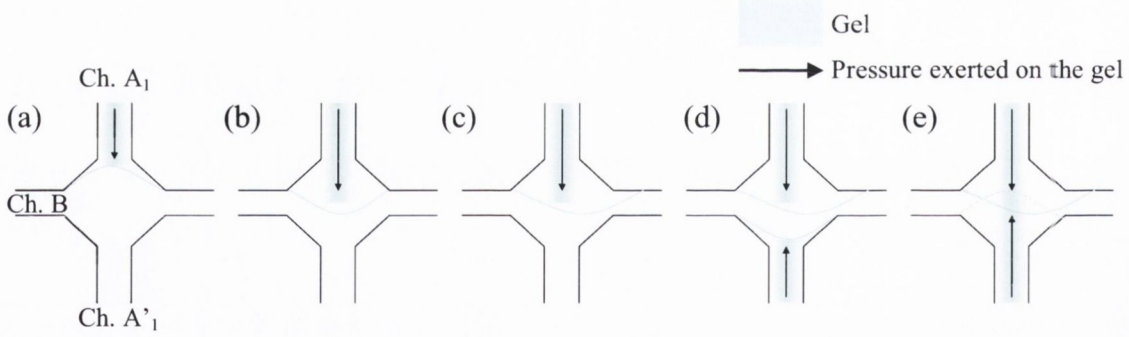

Figure 5-22: Schematic drawings of the issues met during the dispensation of the gel in the Prototype 2. Observation made when dispensing the gel in the Channels A_1/A'_1 and A_2/A'_2. For example, in Channels A_1/A'_1, the meniscus formed (a) was gently pushed (b) in order to get a flat surface. The pressure exerted on the gel (black arrow) kept pushing the gel towards the Channel B (c). Thus, when both Channels A were filled with the gel (d), the Channel B was blocked with the gel (e).

It resulted that working with Channel B which is connected only to Channels A_1 and A_2 was more successful to dispense the gel and subsequently washed the Channel B to get a flat surface of gel (Fig. 5-23).

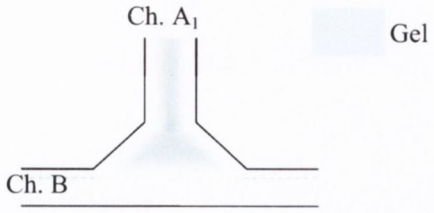

Figure 5-23: Schematic drawing showing the gel dispensed in Channel A_1 in the Prototype 2. The Channel B was connected only to the Channel A_1. When the gel was dispensed in the Channel A_1, a meniscus was formed, but when the Channel B was washed a flat surface was possible to obtain (dash line).

By using this experimental design it was difficult to account for any migrating cells towards the gradient of chemokines (Fig. 5-24). This could be mainly associated with a low concentration of chemokine diffusion.

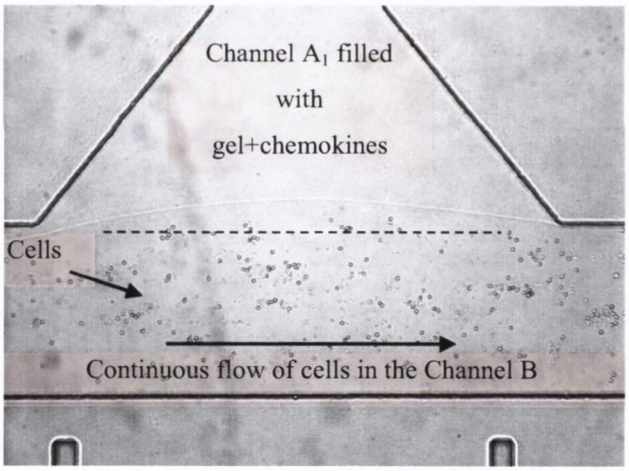

Figure 5-24: Experimental setup arrangement of a chemotactic assay run with Prototype 2. The gel mixed with chemokines was filled in the Channel A and the cells were continuously flowing in the Channel B. There was no significant migration of cells observed towards the gradient of chemokines.

The loading of the gel in Channel A is a very important issue during the experimental preparation. In fact, if the surface of the gel is not flat, the uniform distribution, and subsequent diffusion of the chemokine is not possible. As referred in the introduction, the surface does not need to be perfectly flat, but at least as smooth as possible to maintain a laminar flow within the chip. Therefore, wider and longer channels were two possible options to prevent the recurring problems encountered with Prototype 2, such

as vortexing and turbulence by non-laminar fluid flow condition. Also the avoidance of the obstruction of the Channel B with the gel would be another aspect to take into account during the designing phase of the chip. The modified design of the Prototype 2 is called Prototype *2m*.

5.2.4 Results obtained using the Prototype *2m*

5.2.4.1 Design modification on Prototype 2

The design of the Prototype 2 was subsequently modified in order to have only one intersection between Channels B and A. This design was named Prototype *2m*. The reason for such a design was to avoid the difficulties of filling the gel in Channel A. Therefore, the designs of these chips were done in such a way that Channels B were wider than in the first Prototype 2 (Fig. 5-25). With this new design, there was more control on the gel because the volume of the gel dispensed was greater than in the Prototype 2. Thus, if gel seeps into the Channel B, it will not obstruct it because of the wider Channel B.

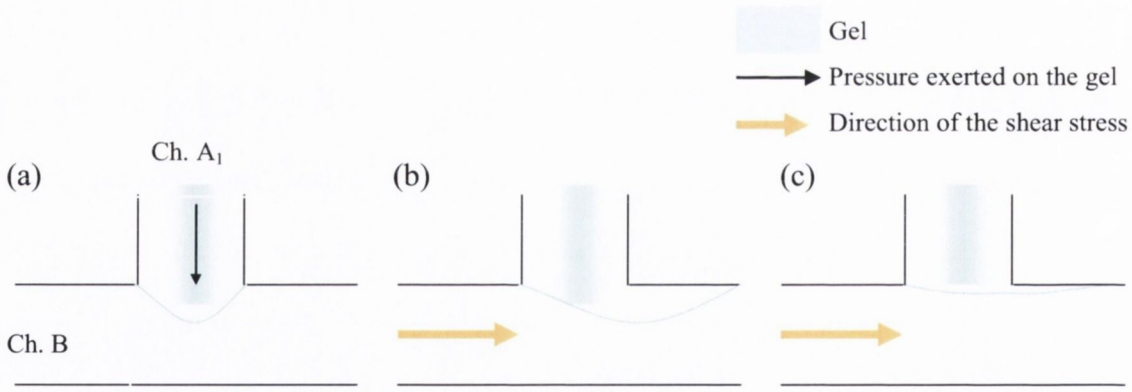

Figure 5-25: Schematic drawings showing the behaviour of the gel when dispensed in Prototype *2m*. The excess of gel in Channel B (a) was washed away when applying a shear stress (b) and a flat surface can be obtained (c).

Four new channel designs were developed with wider Channel B (1 mm or 1.5 mm) and with various patterns of the junction between Channels A and B (Fig 5-26).

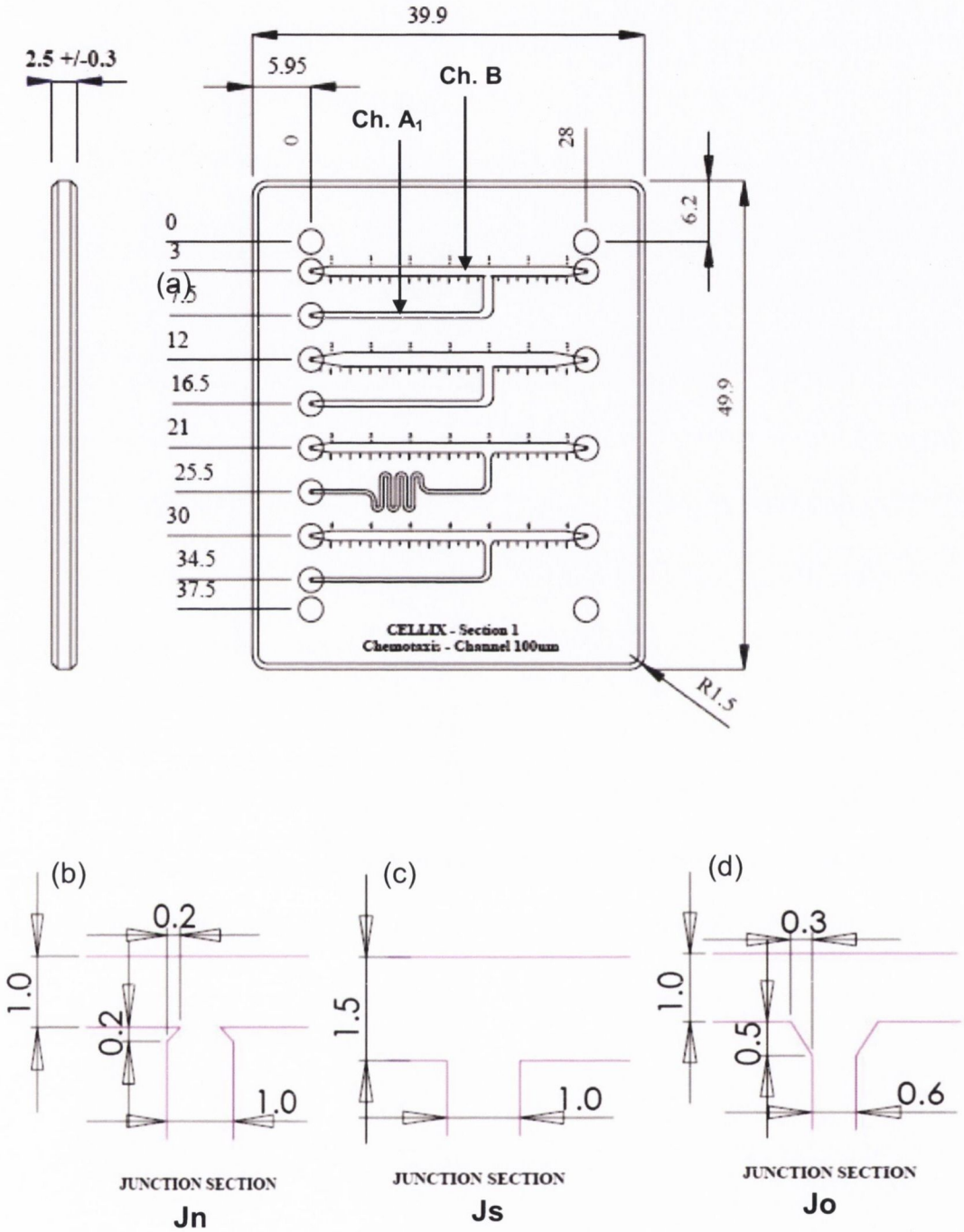

Figure 5-26: Schematic drawings showing the technical specifications of the Prototype *2m*. The general overview of the design of the chip is shown in figure (a). The dimensions (in mm) of the different junctions between the Channels A and B are given in figure b, c and d. The first junction is called Jn, the second Js and the third Jo.

5.2.4.2 Theoretical validation of Prototype *2m* model

The COMSOL simulations for the Prototype *2m* are presented in figures 5-27 and 5-28. The simulation of the design with Js junction shows that the flow will erode (red streamlines) less the gel than in the previous design (Fig. 5-19), and the simulation for Jn junction will exhibit more perturbations of the flow on one of the corners of the Channel A (Fig. 5-28).

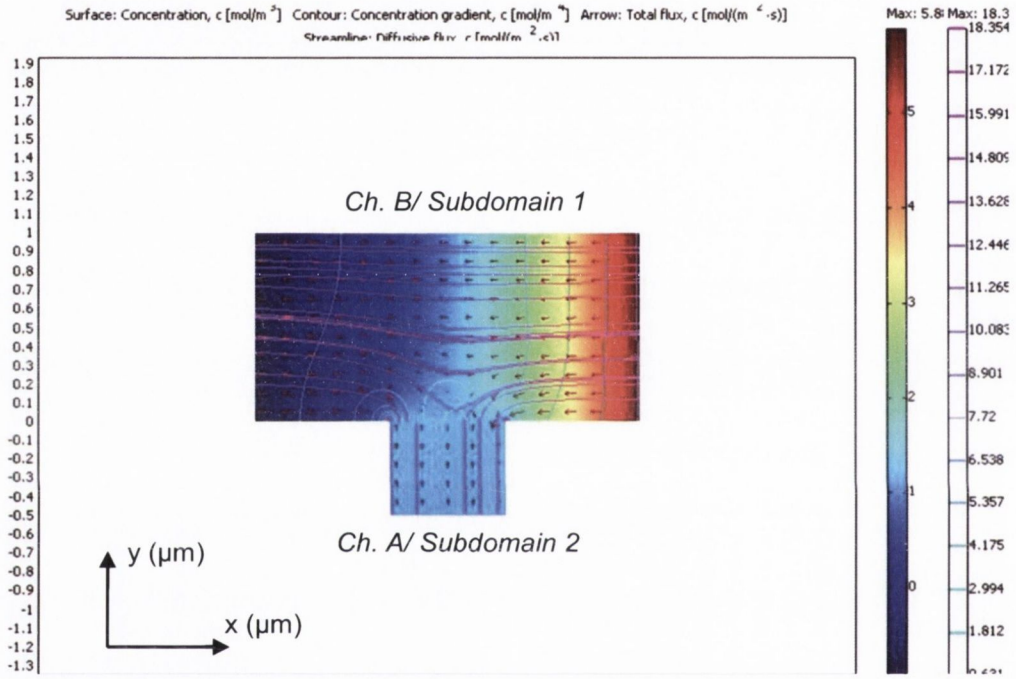

Figure 5-27: Theoretical model showing the dynamic of molecules and fluid in a Js junction in the Prototype *2m*. The model shows the result of the dynamic of the gradient of chemokines (blue streamlines) in response to the flow (red streamlines). The cell flow is not disturbing the surface of the gel and the gradient of chemokines is diffusing at the vicinity of Channel A but also into the Channel B.

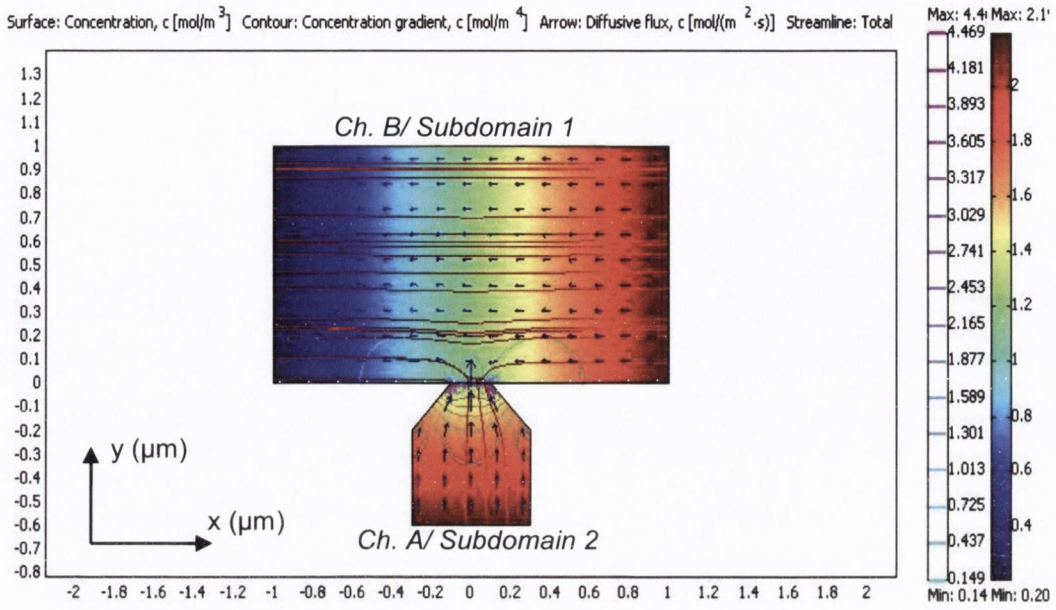

Figure 5-28: Theoretical model showing the dynamic of molecules and fluid in a Jn junction in the Prototype *2m*. The model shows the result of the dynamic of the gradient of chemokines (blue streamlines) in response to the flow (red streamlines). The streamlines of the flow show that the impact of the flow on the surface of the gel is negligible and that the gradient of chemokines is diffused at the near vicinity of the Channel A.

Here, the simulations show that the gradient (blue streamlines) is diffused across the surrounding area of the channel intersections. Therefore, in this particular case, the area to investigate and analyse when running a chemotactic assay is in Channel B right after either junction.

5.2.4.3 Validation of the model

When the gel with FITC-dextran was dispensed in the Jn junction, two different profiles of the surface of the gel were observed: 1) the gel either seeped into the Channel B (Fig. 5-29a) or 2) a meniscus at the end of the Channel A was formed (Fig. 5-29b). In the case of the Js junction, the gel systematically seeped into the Channel B (Fig. 5-29c). The excess of gel in Channel B was then washed but more pressure had to be applied to remove the gel from Channel B because the Channel B was wider than in the previous design and subsequently no gel remained in the Channel A (Fig. 5-30d). Furthermore, as previously mentioned, the microscopic irregularities on the surface of the channel did

not permit a linear washing of the gel (Fig. 5-29e); some gel was left on the surface of the Channel B.

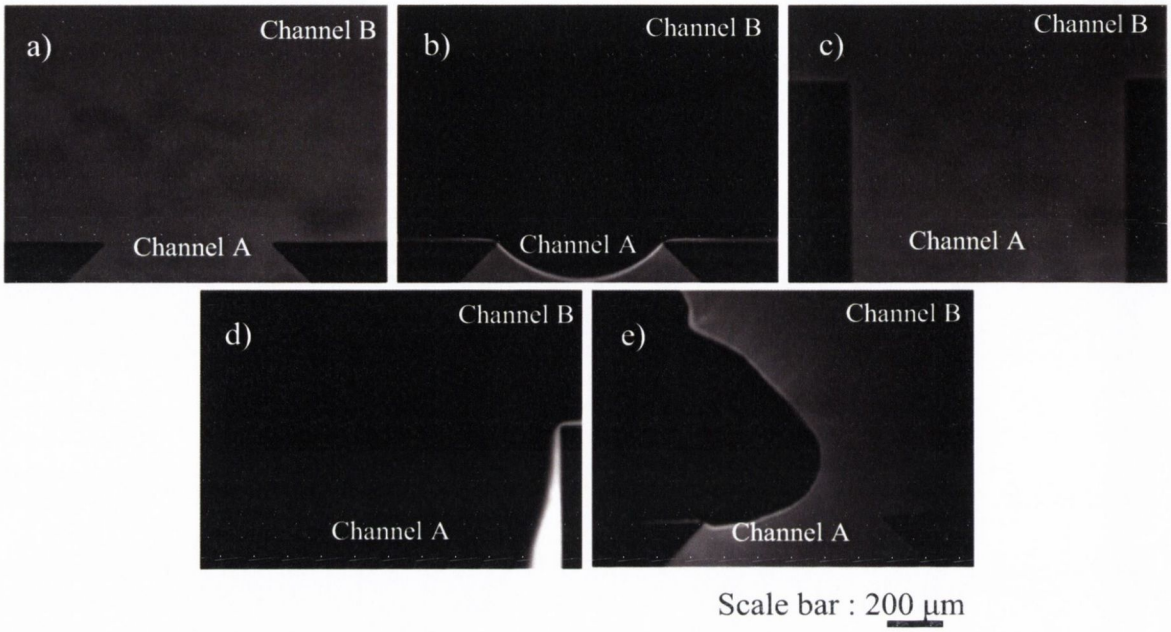

Figure 5-29: Photographs of the junction of the channels in the Prototype *2m* when the Channel A was filled with gel. In the Jn junction, the gel either seeped into the Channel B (a) or a meniscus was formed (b). In a Js junction, the gel systematically seeped into the Channel B (c). The excess of the gel in the Channel B was washed out but the gel kept being pushed back into the Channel A (d). It was noticed that the washing of the Channel B was not homogeneous (e). This can be explained by the irregularities on the surface of the channel.

Finally, the channel with a Jo junction did not show the same issue as the one previously described for the Jn and Js junctions. Even if the gel still seeped into the Channel B, as Channel B was wider, the filling of the gel was easier than in the Prototype 2 and a flat surface was possible to obtain when the Channel B was washed. Therefore, these channels were used for chemotactic assays because the flat surface of the gel was able to sustain a laminar flow of cells.

5.2.4.4 Chemotactic assays within Prototype *2m*

The results of the chemotactic assays carried out with the Prototype *2m* were processed using Image-Pro. There, the displacements of each cell were fully tracked. The graphs 5-2 and 5-3 show the final normalized track of each cell; the subtracks of each cell are described by the icons within the track (e.g. square, triangle). For an easier read out, 20

cells were randomly chosen. Images were acquired just after the junction of both channels where the gradient is diffused within the flow. It was expected that the cells will be influenced by the chemokines and will therefore be able to migrate against the flow towards the gradient which will be represented on the graph by an accumulation of tracks between the abscissa - 400 and 0. Therefore, the influence of the gradient of chemokines on the direction of migration of the cells was assessed by comparing the subtracks of the cells obtained from both experimental assays and control. The number of subtracks of the cells found between the abscissa - 400 and 0 were compiled in the tables 1 and 2.

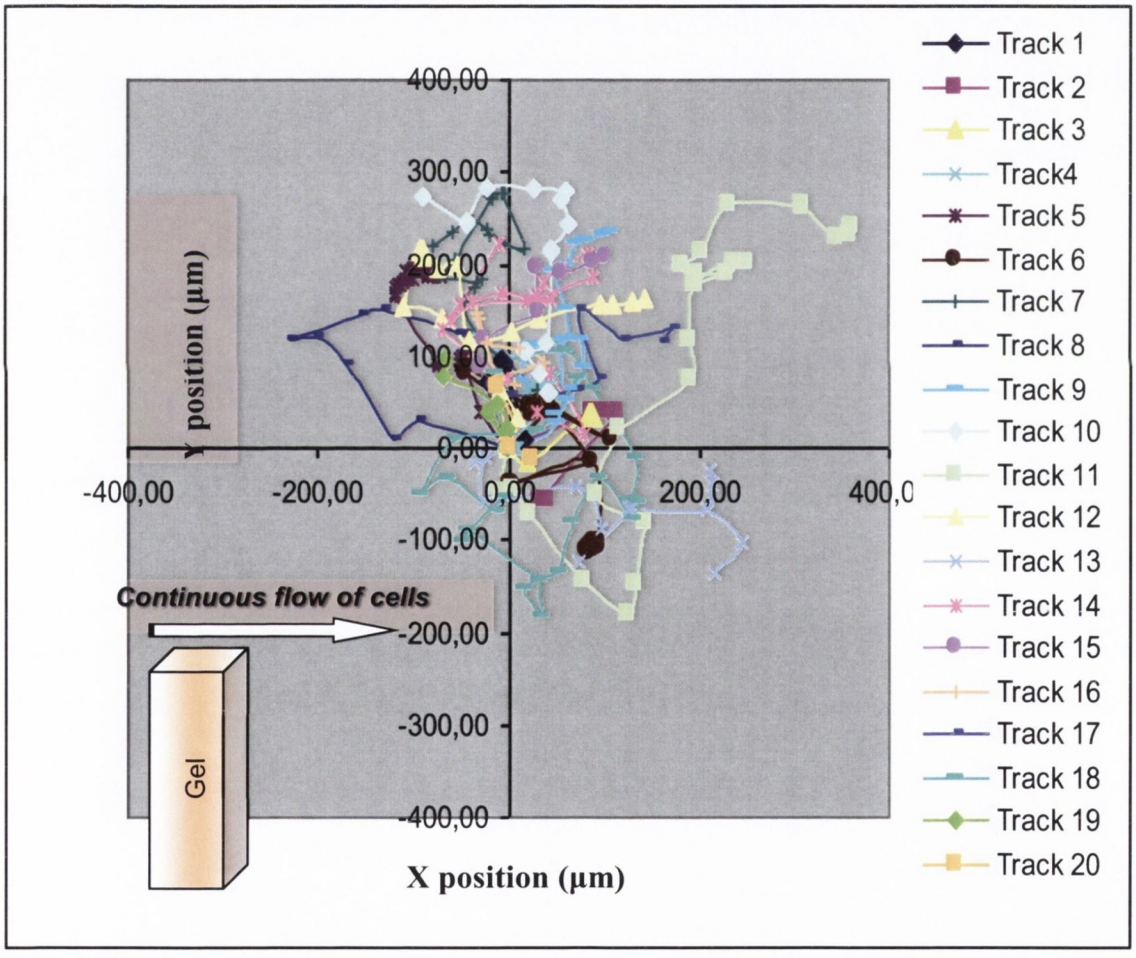

Graph 5-2: Graph showing the migration of PBL cells in the Prototype *2m* (control). The cells that had adhered on the surface of the channel were observed in real time under the microscope. The images of the migration of the cells were acquired after the junction of both channels. Each cell was tracked and the final normalized track of the migrating cells (n=20) shows that the cells are randomly distributed close to their initial position.

	Total number of subtracks	Number of subtracks between abscissa - 400 and 0	% of subtracks
Track 1	35.0	9.0	25.7
Track 2	35.0	35.0	100.0
Track 3	35.0	4.0	11.4
Track 4	35.0	8.0	22.9
Track 5	35.0	16.0	45.7
Track 6	35.0	2.0	5.7
Track 7	35.0	5.0	14.3
Track 8	35.0	8.0	22.9
Track 9	35.0	35.0	100.0
Track 10	35.0	2.0	5.7
Track 11	16.0	10.0	62.5
Track 12	35.0	9.0	25.7
Track 13	14.0	7.0	50.0
Track 14	35.0	6.0	17.1
Track 15	9.0	9.0	100.0
Track 16	10.0	8.0	80.0
Track 17	18.0	18.0	100.0
Track 18	6.0	6.0	100.0
Track 19	25.0	3.0	12.0
Track 20	7.0	7.0	100.0
		Average	**50.1**

Table 5-1: Table shows the quantification of the subtracks of the cells migrating against the flow in the Prototype *2m*. For each final track of the migrating cell, the number of subtracks positioned between the abscissa - 400 and 0 were quantified and it was found that 50.1% of the cells analysed migrated against the direction of the flow.

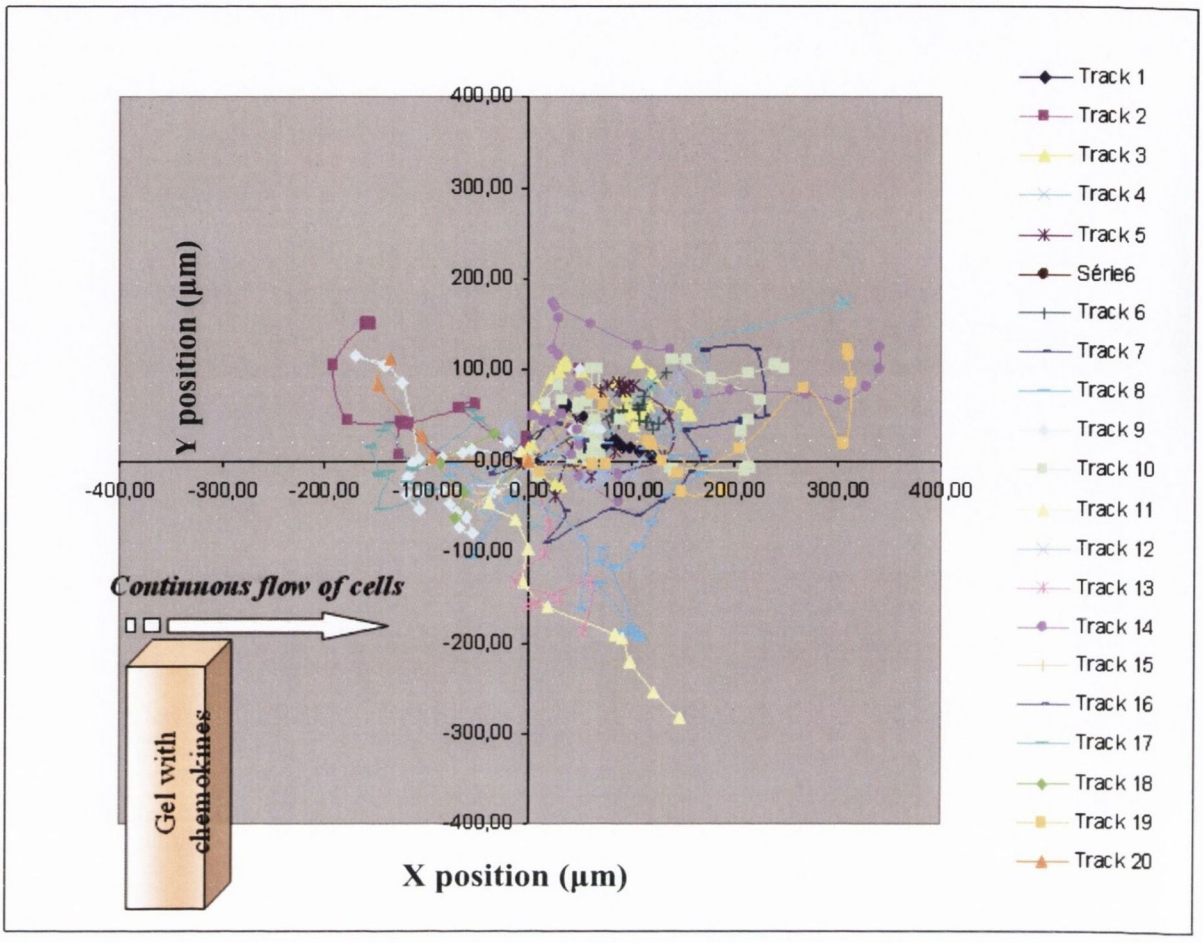

Graph 5-3: Graph showing the migration of PBL cells in response to a gradient of chemokines in the Prototype *2m*. The cells that had adhered on the surface of the channel were observed in real time under the microscope. The images of the migration of the cells were acquired after the junction of both channels. Each cell was tracked and the final normalized track of the migrating cells (n=20) shows that the tracks of the cells were mainly distributed between the abscissa 0-400, which means in the direction of the flow of cells, but not towards the gradient of chemokines.

	Total number of subtracks	Number of subtracks between abscissa - 400 and 0	% of subtracks
Track 1	41.0	40.0	97.6
Track 2	32.0	0.0	0.0
Track 3	41.0	2.0	4.9
Track 4	41.0	2.0	4.9
Track 5	41.0	41.0	100.0
Track 6	41.0	4.0	9.8
Track 7	41.0	34.0	82.9
Track 8	41.0	41.0	100.0
Track 9	21.0	5.0	23.8
Track 10	41.0	22.0	53.7
Track 11	41.0	5.0	12.2
Track 12	28.0	24.0	85.7
Track 13	18.0	5.0	27.8
Track 14	29.0	19.0	65.5
Track 15	11.0	3.0	27.3
Track 16	10.0	9.0	90.0
Track 17	14.0	5.0	35.7
Track 18	41.0	19.0	46.3
Track 19	7.0	7.0	100.0
Track 20	4.0	2.0	50.0
		Average	**50.90**

Table 5-2: Table shows the quantification of the subtracks of the cells migrating against the flow in presence of a gradient of chemokines in the Prototype *2m*. For each final track of the migrating cell, the number of subtracks positioned between the abscissa - 400 and 0 were quantified and it was found that 50.9 % of cells analysed migrated against the direction of the flow.

The diffusion of the chemokines into the channel did not influence the migration of cells because there was no significant difference in the direction of the migration of the cells against the flow between the control (50.1 %) and the chemotactic assay (50.9 %). However, the PBL "random" path in the chemotaxis assay was limited to +/- 100 µm on y-axis unlike the motility of cell in the control limited to +/- 200 µm on y-axis. Therefore, the gradient of chemokines diffused within the channel permitted to localize the migration of cells at the surroundings of the chemokines diffusion.

5.2.5 Results using the Prototype 3

The Prototype 3b (§ 5.1.6) which was composed of one chip with a flat surface assembled to a chip with etched channel is shown on figure 5-30a; a membrane was placed between these two chips. The two chips were then assembled on a frame kit to seal them together by pressure (Fig. 5-30b). By using this arrangement, the ability of the cells to stick onto the coated membrane when a shear stress is applied was assessed.

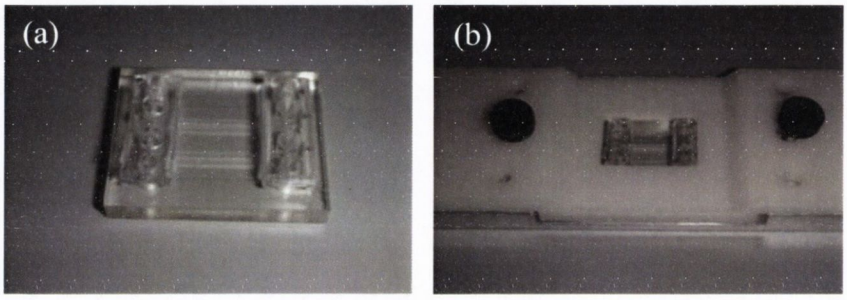

Figure 5-30: Photographs show the Prototype 3b. Two chips were assembled together (a) on a frame (b).

The cells that were flowing onto both fibronectin coated surface and non-coated surface were flowing on the same manner onto either surface. Flowing cells trapped into the membrane were shown by the decrease in the overall fluorescence intensity of all imaged cells at time t=10min (Fig. 5-31).

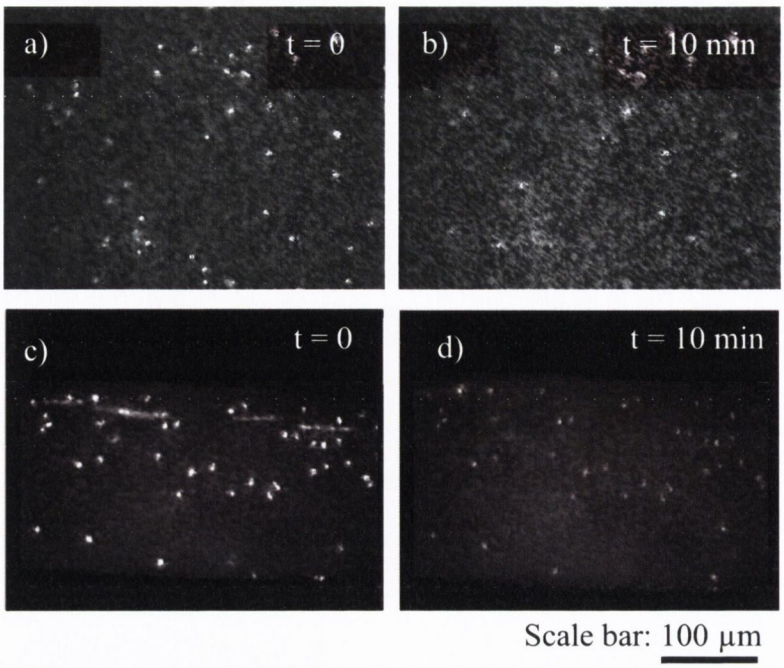

Figure 5-31: Fluorescence images of the flowing cells stained with green CellTracker on the surface of the porous membrane in Prototype 3b. The membrane was coated with fibronectin and the images were acquired at time t=0 (a) and t=10min (b). Control was performed on a non-coated membrane and images were acquired at t=0 (c) and t=10min (d).

By comparing the cells response between the different surfaces, it became clear that the experimental setup could be optimised. Therefore, additional experiments were conducted in the following fronts: a) a thin layer of collagen was coated on the membrane before assembling this membrane on the chip; b) endothelial cells were directly cultured on the surface of the bottom chip, or on a membrane or on a collagen layer. The observation made for each of this experiment is explained below:

a) Membrane coated with collagen: the issue observed was that the membrane was not homogeneously smooth after the gel was poured; and therefore when the membrane was placed in the Prototype 3a or 3b the cells were not flowing on a flat surface. At some stages, the channel was even sealed because of the unsmooth coated membrane.

b) Layer of endothelial cells: when the endothelial cells reached confluence on either the collagen layer or the membrane, the top channel was placed on top of that surface in the Prototype 3b. However, the cells were squeezed and there was not a smooth confluent layer of cells anymore. When the endothelial cells were directly cultured onto the surface of the chip, the cells did not grow.

5.3 Discussion

Four prototypes were designed, developed, tested and validated as viable platforms for chemotactic assays. First, the designs were studied and mathematical models were used to predict the behaviour of fluids within the chips.

In light of the results presented in the previous section, it was found that Prototype 1 was not a suitable design to be used for chemotactic assays because it did not comply with the required volume of chemokine-gel necessary to diffuse into the main-stream channel and significantly attract cells towards its generated gradient. One of the reasons behind this inefficacy is that the gel did not properly set while it was dispensed into Channel B. Another reason is linked to the nature of the polymer injected. In fact, the low volume of gel injected was highly thermosensitive to the ambient environment which made the control of this gel, when dispensed, difficult. Therefore, in each experiment with Prototype 1, excess of gel were found in the injection channel and when that excess was washed, no gel was found at the intersection of both channels. This resulted in a change of the flow path for the cells approximating to the junction of both channels due to the presence of an unexpected "void" created by gel washing out. From these considerations, it was sufficient to conclude that Prototype 1 was not a suitable solution to be used for chemotactic assay.

In light of the experience and knowledge generated from Prototype 1, Prototype 2 was subsequently designed and tested. There, the multiphysics simulations using COMSOL software were of importance to assess the combinatorial behaviour of the chemokine gradient in terms of diffusion of chemokines into the continuous flow of cells. The results from these simulations have shown that a chemokine gradient is diffused at the immediate vicinity of the T-junction section. Following to those conclusions, Prototype 2 was experimentally tested using a fluorescent staining (FITC-dextran) mixed in the gel. Different patterns of the surface of the gel, when it reached the intersecting channels, were possible which were either a meniscus or an excess of gel into the Channel B. From this evidence, the design of Prototype 2 was revised in several ways to finally design the Prototype *2m*. These modified prototype solutions derived from the analysis of the simulations with the aim to reduce the stagnation of the gel and subsequently increase the chemokine gradient to diffuse within the cell flowing channel.

Several solutions were attempted but in all these, one persisting problem was still very much occurring: the washing of the gel from the injection channel. From an in depth investigation, it was found that this problem is linked to the physical properties of the gel used as a vector for the chemokine gradient diffusion and by the micro irregularties in the channel surface which acted as a further constrain to the gel injection (Fig 5-29e).

When the chemotactic assays were performed with the latter designs, no significant difference was found between the control and the experimental assays. These results were confirmed by carrying out a random-walk motion plotting. It was found that in both systems cells migrated with a full random pattern. A further investigation highlighted that the chemokine diffusion was seriously limited to immediate proximity of the intersection of the injection channel into the main stream flow. The problem there was due to the contrasting pushing action of the mainstream shear stress on the injected gel surface. Another reason is that the diffusion of chemokines was washed away before the cells adhered onto the Channel B and therefore the cells did not have the opportunity to come in contact with the chemokines.

The last prototype, Prototype 3, was designed to be a very challenging configuration in which a porous membrane was placed between two chips to mimic, for example, the blood wall tissues. When the membrane was coated with fibronectin, or collagen or endothelial cells, no adherence of cells were observed on the coated surfaces.

The point of this study was to diffuse a gradient of chemokines on a similar manner as *in vivo*. Therefore, the next experiments were focused on the generation of a gradient of chemokines released from activated cells that will mimic a more physiological generation of chemokines.

Finally, there is a huge amount of information to be gathered from this study. Firstly, there is a substantial novelty in the design and development of a multichannel device in a single or multiple planes. Secondly, there is an increased interest in the use of gels for the diffusion of chemokines within a continuous flow of cells. Implementing chemotaxis assays within a 3D tissue-like environment has come to the attention of the research community relatively recently. Since then efforts have been made to develop more physiological *in vitro* models of the cell migration cascade. However, the

"homing" step which consists in the migration of cells from the blood flow through the tissue was not possible in standard 2D environment cell-based assays. Therefore, these assays are no longer sufficient to answer all the questions we have: for example, can the leukocytes migrate without the action of external chemical cues? Are there key signals generated *in vivo* which are not present in existing *in vitro* assays? This is why, new technologies should enable the development of a more complete and dynamic *in vitro* environment combining a natural gradient of chemokines diffused through a tissue-like matrix into the blood flow. Accordingly, gels have being optimised to be used more effectively thanks to their biocompatibility and ability to allow chemokines to diffuse at a constant rate such as happens within *in vivo* tissue.

I believe the questions and issued raised in this study relating to what is necessary to develop a physiologically relevant engineered microenvironment for leukocyte migration studies and generating a natural chemokine gradient in an artificial matrix while also considering the variables that shear flow brings to the problem, are crucial and should be taken into account when developing more physiological milieu for chemotactic assays (cf. Chapter 7).

6 Generation of a natural gradient of chemokines

In the previous chapter, the aim was to create a system where it was possible to observe cells responding as they would *in vivo* to a chemoattractant gradient diffused from a gel. However, the design limitations which we have outlined above did not permit us to observe the migration of cells towards the chemokines. One of the reasons is the difficulty in obtaining a homogeneous diffusion of chemokines due to the issues met with the gel (e.g. the interface between the flow of cells and the gel was not smooth).

An alternative method was studied in this chapter in an attempt to create a "natural" secretion and diffusion of chemokines. Lymphocyte function antigen-1α (LFA-1α) is a leukocyte integrin that mediates the adherence of activated leukocytes to endothelial ligands[88]. The mechanism of adhesion between activated LFA-1α on T-cells[118] and ligands induces a cascade of molecular signals such as the secretion of a range of cytokines (e.g. chemokines: TNF-α[18], MIP-1α[166], MIP-1β[167]). Therefore, a "natural" gradient of chemokines can be generated by artificially mimicking this integrin/ligand interaction.

Murphy *et al.* [105] shows that the presentation of the antibody to LFA-1α on a substrate such as sepharose beads promotes cell adhesion. When the cells adhere to the anti-LFA-1α coated beads, the cells are stimulated and secrete chemokines which, over time, create chemoattractant signals that stimulate the surrounding cells. The secretions of the chemokines MIP-1α and MIP-1β were investigated by incubating the cells with antibodies that neutralized those secretions. Under these conditions, the cells did not adhere onto the anti-LFA-1α coated beads which showed that the cells secreted chemokines which further stimulated the nearby cells. Therefore, these experiments were carried out in this chapter to generate a "natural" gradient of chemokines and an additional treatment of the cells with a microtubule inhibitor (Taxol) was performed to assess the ability of migration of cells towards anti-LFA-1α coated beads.

Based on the fact that cells stimulated by immobilized antibodies to LFA-1α secrete chemokines that subsequently mediate cells migration[105], an experiment with a confined area coated with anti-LFA-1α was developed using low-volume liquid handling devices. A line of anti-LFA-1α was coated in the middle of a well and the PBL cells were

dispensed into the well. As described, cells attached onto antibodies line will secret chemokines which will mediate cells migration towards the coated area. Therefore, it was expected to observe an accumulation of cells on the anti-LFA-1α coated line. If the results of these two experiments were validated, it would validate a new design that would be adapted for the diffusion of chemokines via an anti-LFA-1α coated substrate.

6.1 Materials and methods

6.1.1 Low-volume liquid dispensing

Equator GX8 system (Deerac Fluidics, Ireland) enables low-volume liquid handling using the Spot-on technology (Fig. 6-1). It consists of eight independent pipetting tips that are controlled via the Spot-on software. A volume of liquid from 50 nl up to 20 µl can be dispensed in a 96 well plate. A program is first developed in order to define the tasks that the tips had to perform (e.g. aspirate, dispense).

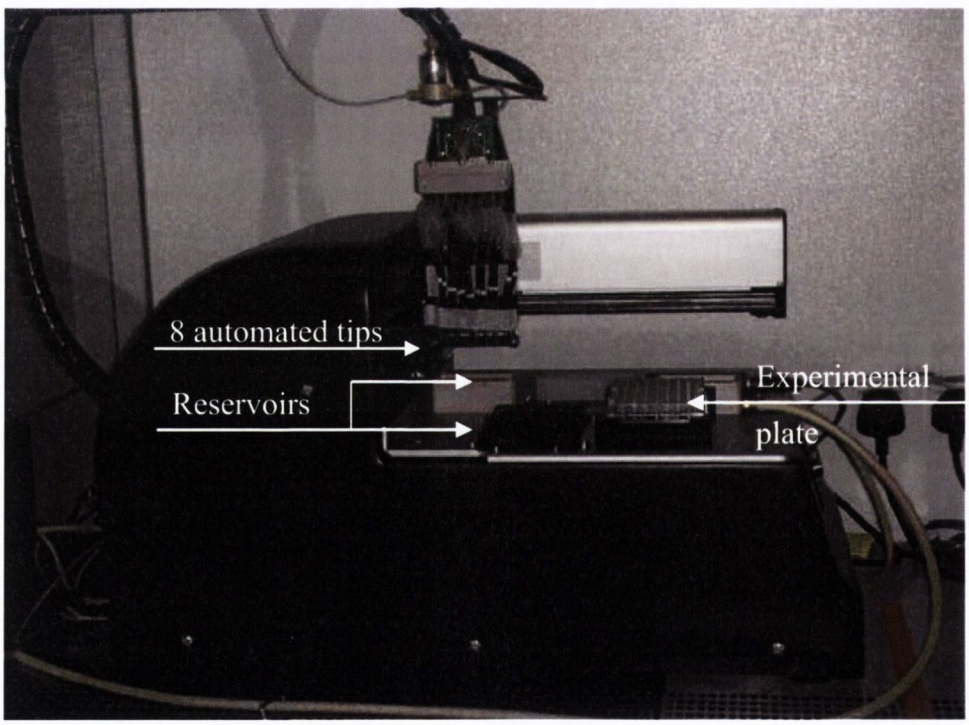

Figure 6-1: Photograph of the Equator GX8 equipment for low-volume liquid handling. This device consists of 8 automated controlled tips, a washing stage, and a reservoir from which the sample is aspirated. The sample can also be aspirated from a reservoir plate (Greiner, U bottom 96-well plate) and further dispensed into the experimental plate.

The tasks were programmed in such a way that two tips were selected to aspirate the liquid from the reservoir plate (96-well plate U bottom, Greiner) and to dispense it in the well of a 96-well plate (flat bottom, Nunc). The first tip aspirated a volume of 4 µl of anti-LFA-1α from the well A1 of the reservoir plate and the second tip aspirated simultaneously 4 µl of PBS from the well A2 (Fig. 6-2). Anti-LFA-1α was dispensed in four wells and PBS was dispensed in two wells.

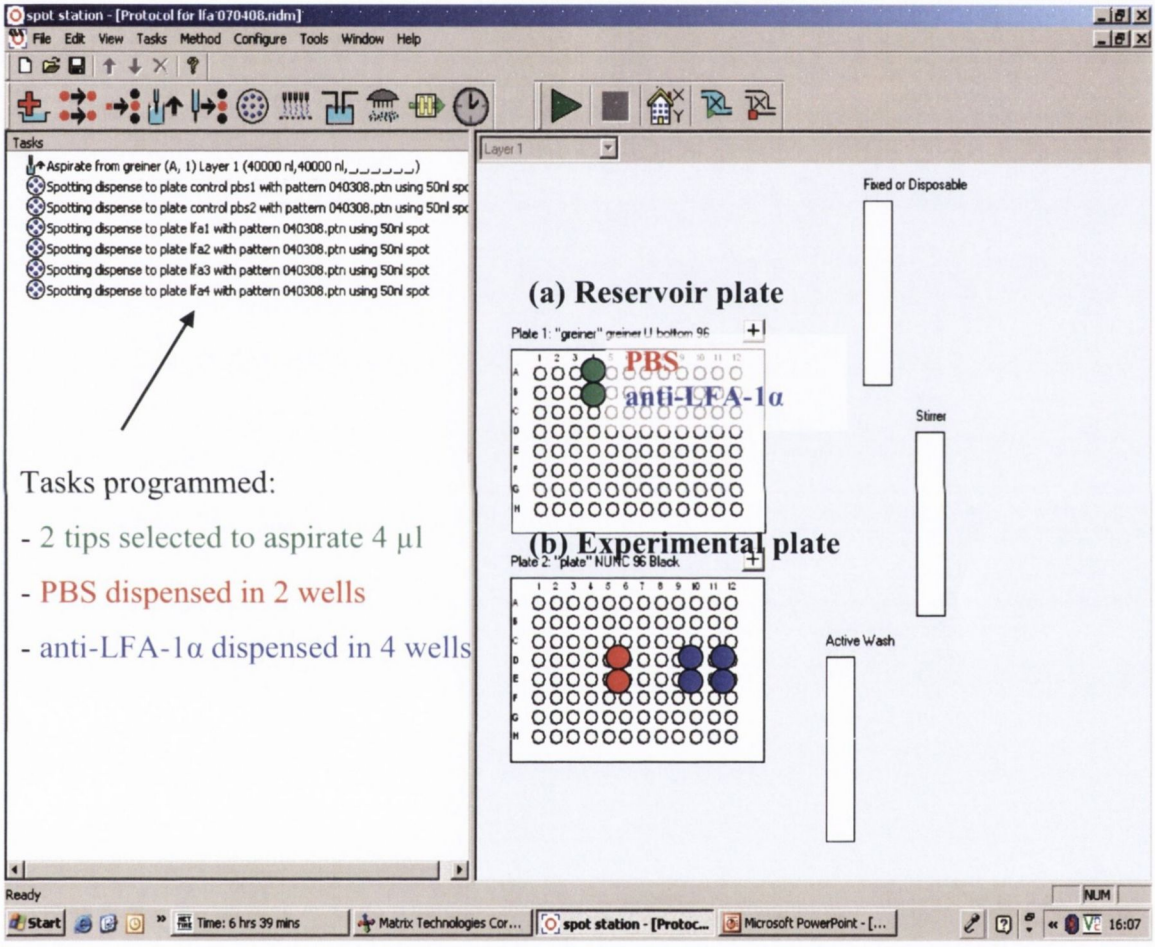

Figure 6-2: An example of the acquisition window of the Spot-on station software. The tasks programmed are referenced in the left side of the window. The tasks consisted in selecting one tip to aspirate 4 µl of anti-LFA-1α from the reservoir plate (a) and to dispense it in four wells in the 96-well plate (b). The same steps were performed to dispense the PBS in two different wells.

The sample was dispensed into the well according to the pattern designed in the Spot-on software which was a straight line of six droplets with a volume of 50 nl each, so a total volume of 300 nl (Fig. 6-3) was dispensed in the middle of a well.

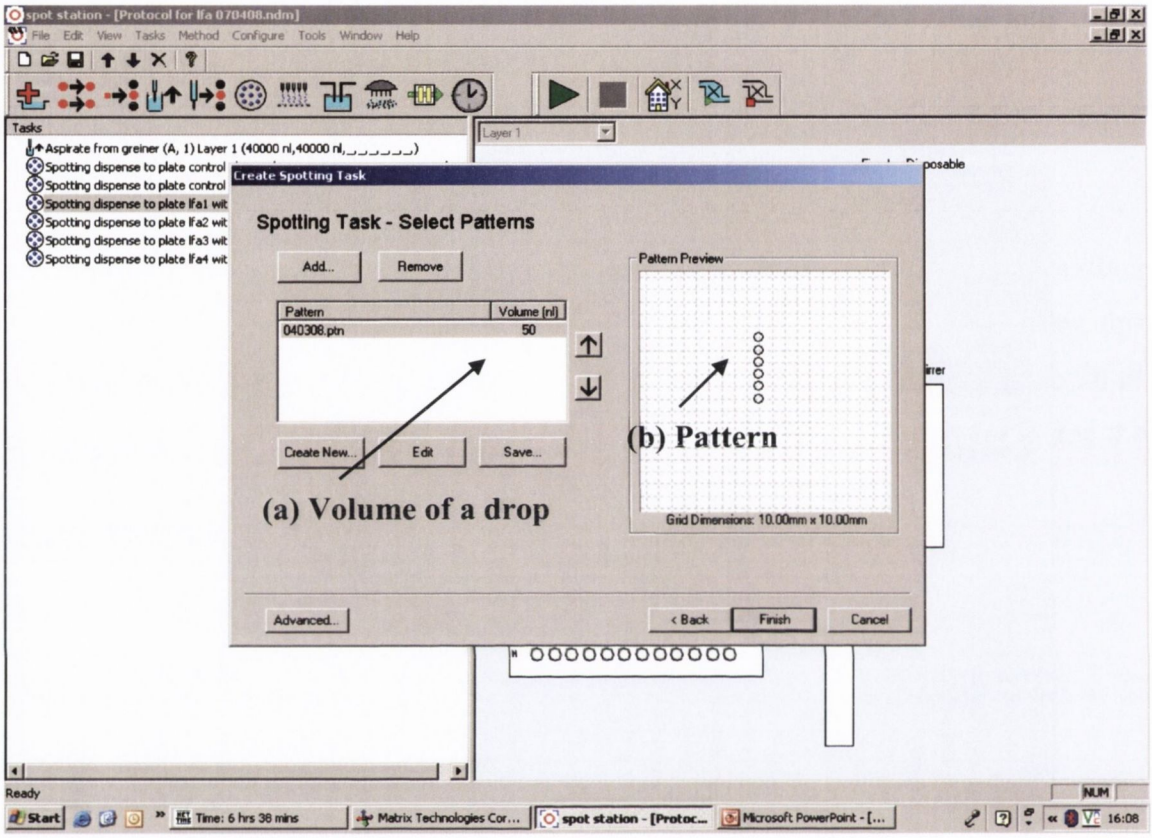

Figure 6-3: An example of the liquid dispensing pattern edited in Spot-on station software. (a) The volume of each drop was defined at 50 nl. (b) The pattern consists in a straight line of 6 drops.

6.1.2 Automated cell-based visualization

The IN Cell Analyzer 1000 (GE Healthcare, Ireland) is a rapid and automated image acquisition and analysis platform for cell-based assays. The IN Cell Analyzer comprises several core components including a Nikon microscope, high-resolution CCD camera, quality optics, laser auto-focus, and a motorized stage. All scanned cells within a sample are in focus due to the fast infrared laser autofocus system. Lens magnifications used are 4x and 10x. A temperature control module manages the microplate heat condition to maintain the live cell environment at 37 °C while under image acquiring process. The IN Cell Analyzer was used for the experiments with a line of anti-LFA-1α

and with the beads to record in real time the responses of the cells to the antibodies coated surfaces. The images were acquired every minute for a period of 6 hours at 37 °C. The images were acquired at four different spots chosen on the line of anti-LFA-1α and four random spots were chosen for the experiments with the beads. A total of 1440 images were recorded for each experiment.

6.1.3 Anti-LFA-1α handling assays

The *in vitro* cell-based assay developed consists in coating a line of anti-LFA-1α antibody (1:10 in PBS) on a well of a 96-well plate using Equator system. The plate was incubated for 30 min at 37 °C. The wells of the plate that were not used were filled with water in order to avoid the drying of the liquid dispensed. Then, anti-LFA-1α line was washed twice with PBS and 2% BSA was dispensed into the well and incubated for 5 min at 20 °C. The wells were washed twice with PBS and 5 x 10^4 PBL cells per well were dispensed and placed in the IN Cell Analyzer with the temperature set at 37 °C. There was no CO_2 control on the IN Cell Analyzer therefore the cells were resuspended in "activation buffer" (cf. § 3.1.1). The same steps of the protocol were followed to dispense PBS (control). The images were acquired with a 4x lens in order to visualize the line in its totality.

6.1.4 Generation of a gradient of chemokines using sepharose beads

Protein G sepharose beads (GE healthcare, Ireland) were used as a substrate for the presentation of ligands to the cells. The average beads size is 90 µm and the stock solution has a concentration of 900 000 beads/ml. The beads were diluted in order to have a range between 10 and 20 beads per well. Beads were first incubated with goat anti-mouse (IgG/Fc specific) antibody overnight at 4 °C and then coated with anti-LFA-1α. Beads are made of highly cross-linked agarose 4 % which means that beads are porous. Therefore, the concentration of ligands would be higher than for the coating of a surface of a plate. Hence, a titration of anti-LFA-1α was processed with a range of dilution of 1:1000, 5:1000 and 1:100 and the best dilution of anti-LFA-1α found to coat the beads was 1:100. Control was performed using non coated beads. The plates were either incubated in the IN Cell Analyzer for 6 hours or placed in the incubator for 24 hours. The purpose of carrying out the experiments in both the IN Cell

Analyzer and the incubator is that in the IN Cell Analyzer the focus is made automatically on the bottom of the plate while with the inverted microscope we can change the focus. Therefore, pictures were acquired on the inverted microscope a) on the bottom of the plate and b) on the side/top of the beads to observe the density of the cells that adhere onto the surface of the beads at time t=0 and t=24h.

To assess the ability of the cells to secrete chemokines such as macrophage inflammatory protein-1α (MIP-1α) and macrophage inflammatory protein-1β (MIP-1β), the cells were treated with two antibodies to neutralise MIP-1α and MIP-1β. Cells were pre-treated with antibodies at a concentration of 5 μg/ml for 15 min prior to chemotactic assays.

Cells were also treated with Paclitaxel (Taxol) which is a mitotic inhibitor which interferes with the normal function of microtubule breakdown by stabilizing microtubule structure. The ability of cell to use its cytoskeleton is destroyed. Therefore, this drug was used to block the capacity of cells to proliferate. The final concentration of Taxol dissolved in DMSO used for treatment of cells was 5 μM for 30 min at 37 °C and 5 % CO_2. The concentration of the stock solution concentration was 10 mM; hence 0.5 μl of stock solution was used per ml of cells.

The adhesion of the cells on the anti-LFA-1α coated beads was evaluated using Image-Pro in order to compare the massive data (1440 images) collected from each experiment. According to the images acquired of the beads shown in Murphy *et al.* paper, when there are no cells stick onto the surface of the beads, that surface is homogeneous and shown as smooth grey scale on the image, whereas when cells stick onto the beads, the outline of the cells is shown in a darker grey than the surface. Therefore, the more the cells adhere onto the surface of the beads, the more heterogeneous the surface is. Finally, as the outline of the cells was darker than the middle of the cells, we can say that the cells looked similar to "holes". Therefore, Image-Pro software was used to estimate the average of "holes" on the surface of each bead shown on each picture acquired. The filter applied was Holes (Fig.6-4) which is described as the number of holes within the selected object which was a bead.

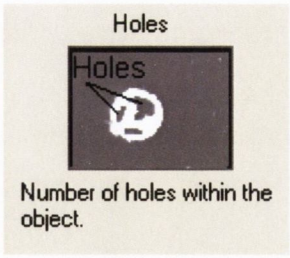

Figure 6-4: Algorithm of filter selection in Image-Pro application. Each microphotograph of beads assays was processed using the filter Holes. This filter enables to count the number of holes within a selected object which was the beads.

The data obtained with Image-Pro were exported into Excel sheet and the data were processed for each experiment.

6.2 Results

6.2.1 Evaluation of the migration of cells in response to an anti-LFA-1α coated line

The results of the responses of the cells to the anti-LFA-1α coated line at time t=0 and t=6h are shown on figure 6-5. An obvious line was observed representing the cells that had adhered onto the anti-LFA-1α coated line. This is explained by the fact that the cells that adhere onto antibodies can secrete biochemical signals which stimulate surrounding cells[105]. On the right side of the well, it was noticed that no cells remained after t=6h whereas on the left side of the well an accumulation of cells were observable.

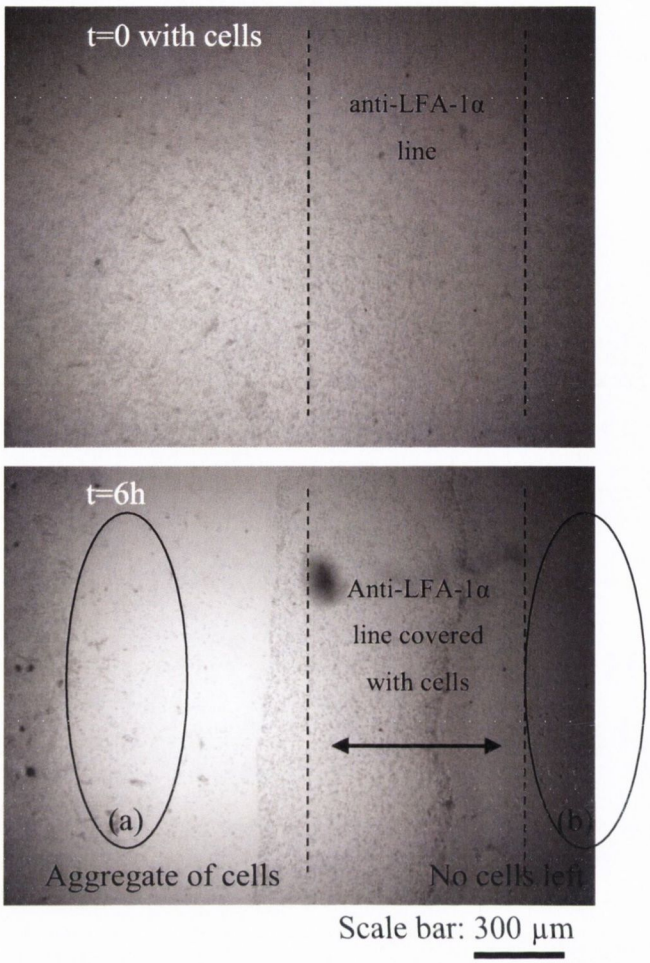

Figure 6-5: Images of the responses of the PBL cells to an anti-LFA-1α coated line. Observations were made at time t=0 and t=6h with a 4x lens. At time t=0, the surface of the well was homogeneously covered with PBL cells. At time t=6h, the anti-LFA-1α coated line was clearly covered with cells. On the left side of the image there was an aggregate of cells (a) whereas on the right side of the image no cells remained (b).

Images of control were acquired on the middle of the well (Fig. 6-6a) and it was noticed that no cells remained on the centre of the well where the line of PBS was coated. Nonetheless, an aggregate of cells were settled on the left side of the well (Fig. 6-6b).

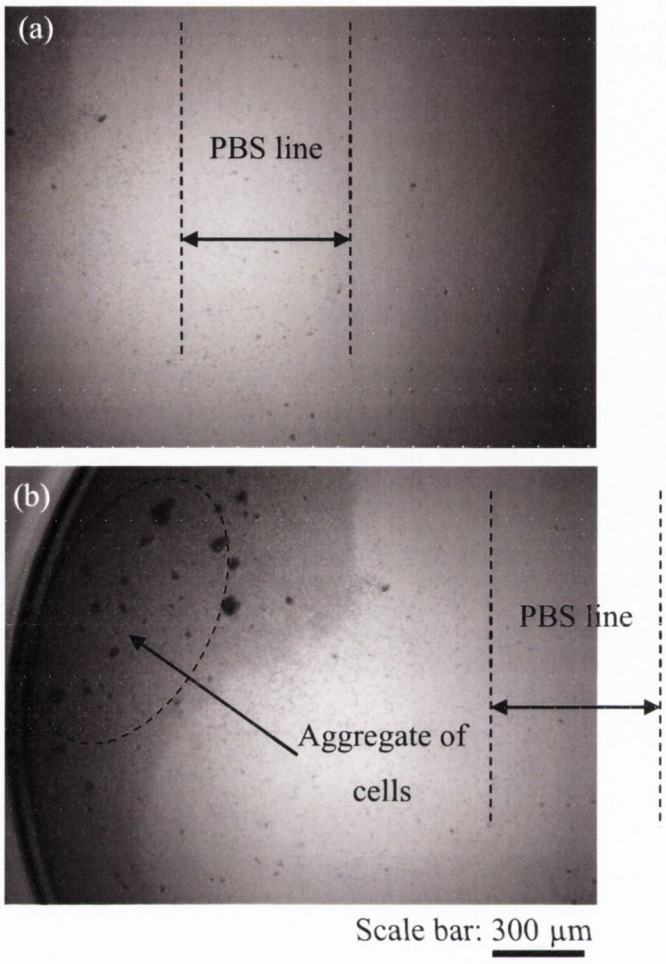

Figure 6-6: Images of the responses of PBL cells to a PBS coated line (control). Images were acquired at time t=6h in the middle of the well in the left side of the well with a 4x lens after 6h of incubation on the IN Cell analyzer. The cells did not attach to the PBS coated line (a) but they were aggregated in the left side of the well (b).

The same experiments were carried out directly on the surface of the plate (without BSA) or on poly-L-lysine coated surface in order to allow the cells to attach to the bottom of the well more firmly than on BSA due the higher electrostatic interaction. However, the same observations were made, the cells were "rolling" on the left side of the well. In order to eliminate the possibility that the IN Cell Analyzer plate was not aligned and that the cells were "rolling" from one side to the other, the plate was incubated at 37 °C with 5 % CO_2 in the incubator for 6 hours. In that case, the cells were homogeneously distributed on the surface of the plate and no significant differences were observed between control and the experimental assay because both PBS and antibodies coated lines were not covered with cells. Therefore, this setting was not optimum for the secretion of chemokines to further direct the migration of cells.

6.2.2 Evaluation of the migration of cells in response to anti-LFA-1α coated beads

The images acquired with the inverted microscope of the responses of the cells to anti-LFA-1α coated beads are shown on the figure 6-7.

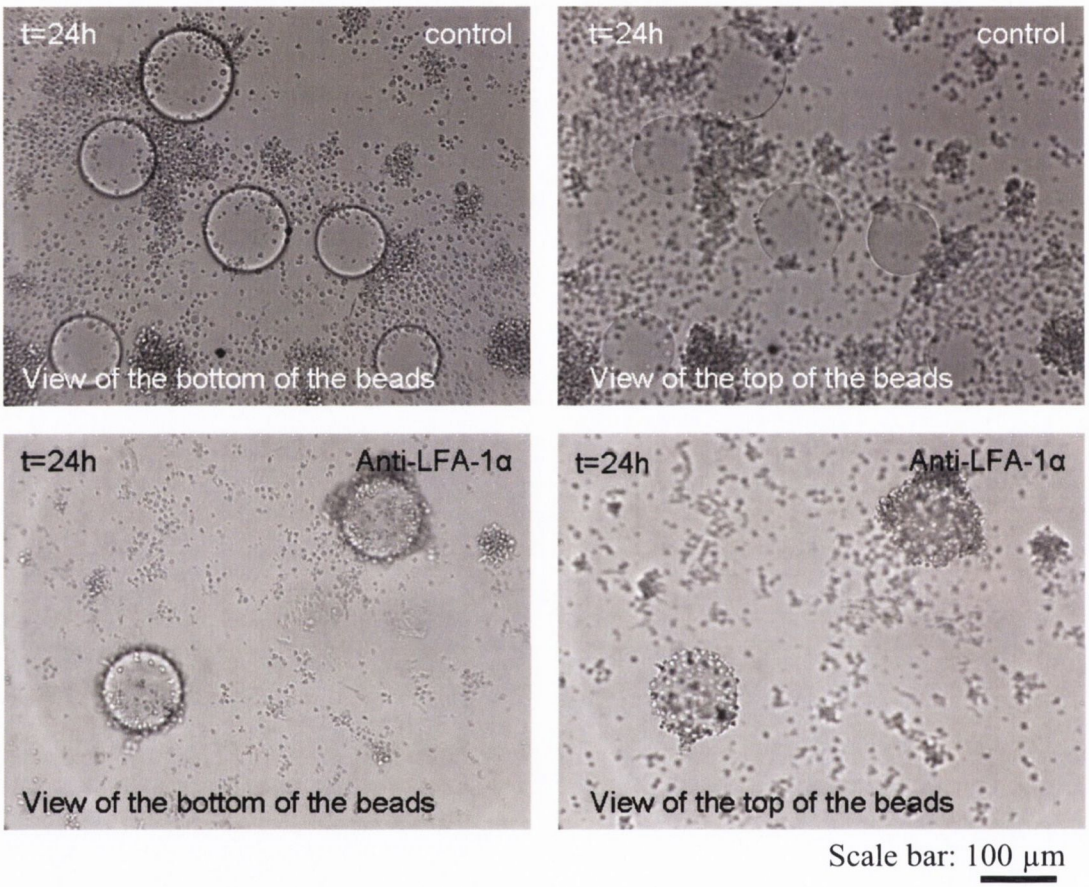

Figure 6-7: Images showing the responses of the cells to the anti-LFA-1α coated beads. Images were acquired on the bottom of the beads as well as on the side/top of the beads. After an incubation of 24 hours, the beads were covered with cells, whereas no cells adhered onto the non coated beads (control).

The beads coated with anti-LFA-1α were covered with cells after 24 hours of incubation. The control shows that the cells did not attach to the non coated beads. To explain the adhesion of cells to anti-LFA-1α coated beads, cells were incubated with antibodies to MIP-1α and MIP-1β to prove if the secretion of these two chemokines mediates cell migration towards the beads covered with cells.

An important remark is that the beads were randomly moving on the bottom of the plate; they were not stable, but were "rolling" on the surface of the plate.

The results obtained with the cells treated with antibodies that neutralise the secretion of MIP-1α and MIP-1β are shown on figure 6-8.

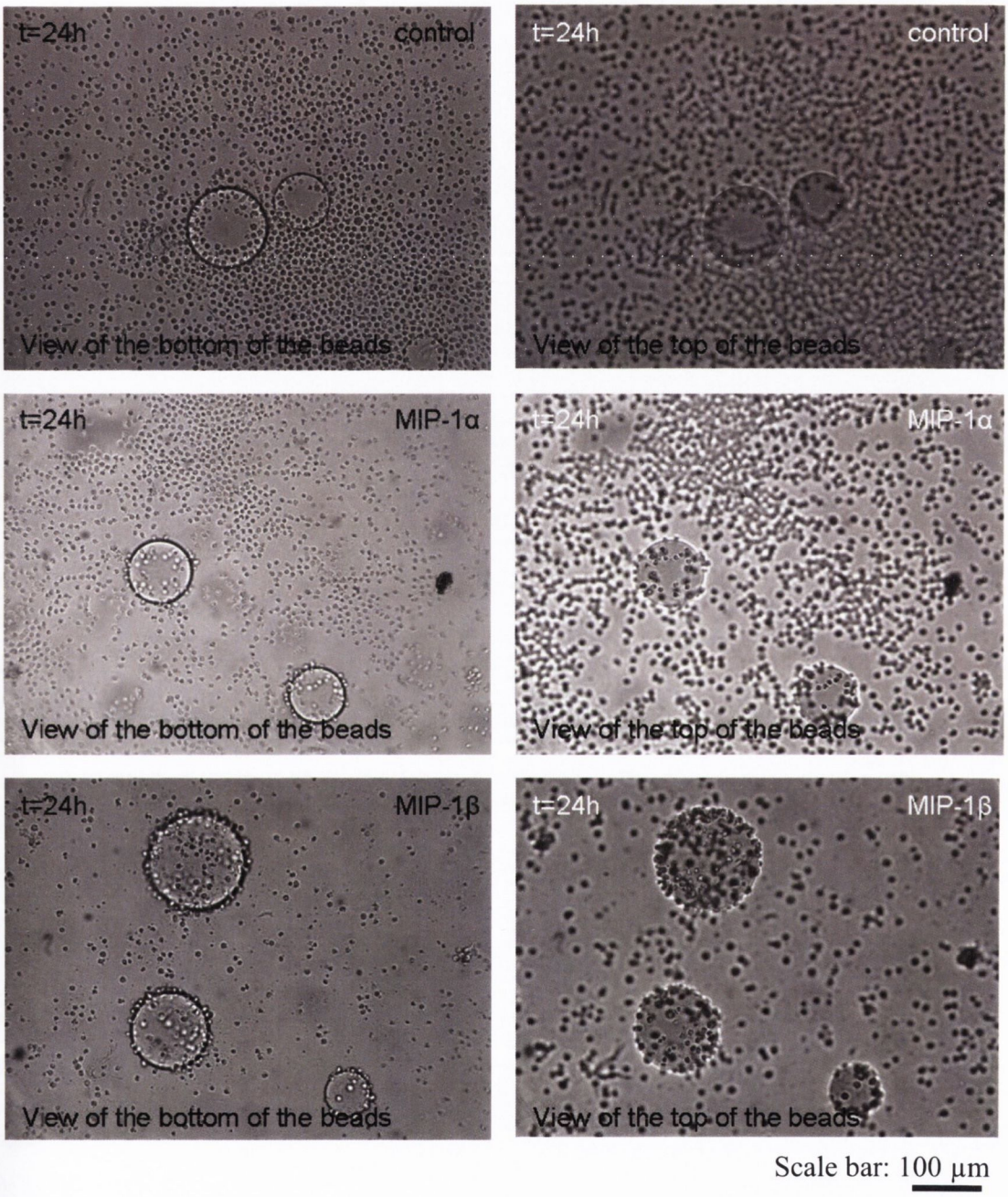

Figure 6-8: Images showing the responses of anti-MIP-1α and anti-MIP-1β treated cells to the anti-LFA-1α coated beads. Images were acquired on the bottom of the beads as well as on the side/top of the beads. After an incubation of 24 hours of the cells in presence with the anti-LFA-1α coated beads, the cells did not cover the beads.

The anti-LFA-1α coated beads were not entirely covered with cells when the cells were previously incubated with antibodies to MIP-1α and MIP-1β. These results prove that

the cells adhered to anti-LFA-1α coated beads secrete the chemokines MIP-1α and MIP-1β that subsequently promote cells migration towards the beads and cell adhesion onto the beads. To support these results, cells were treated with a microtubule inhibitor Taxol.

Pictures acquired of the bottom and the top of the beads incubated with cells treated with Taxol show that anti-LFA-1α coated beads were covered with cells (Fig. 6-9).

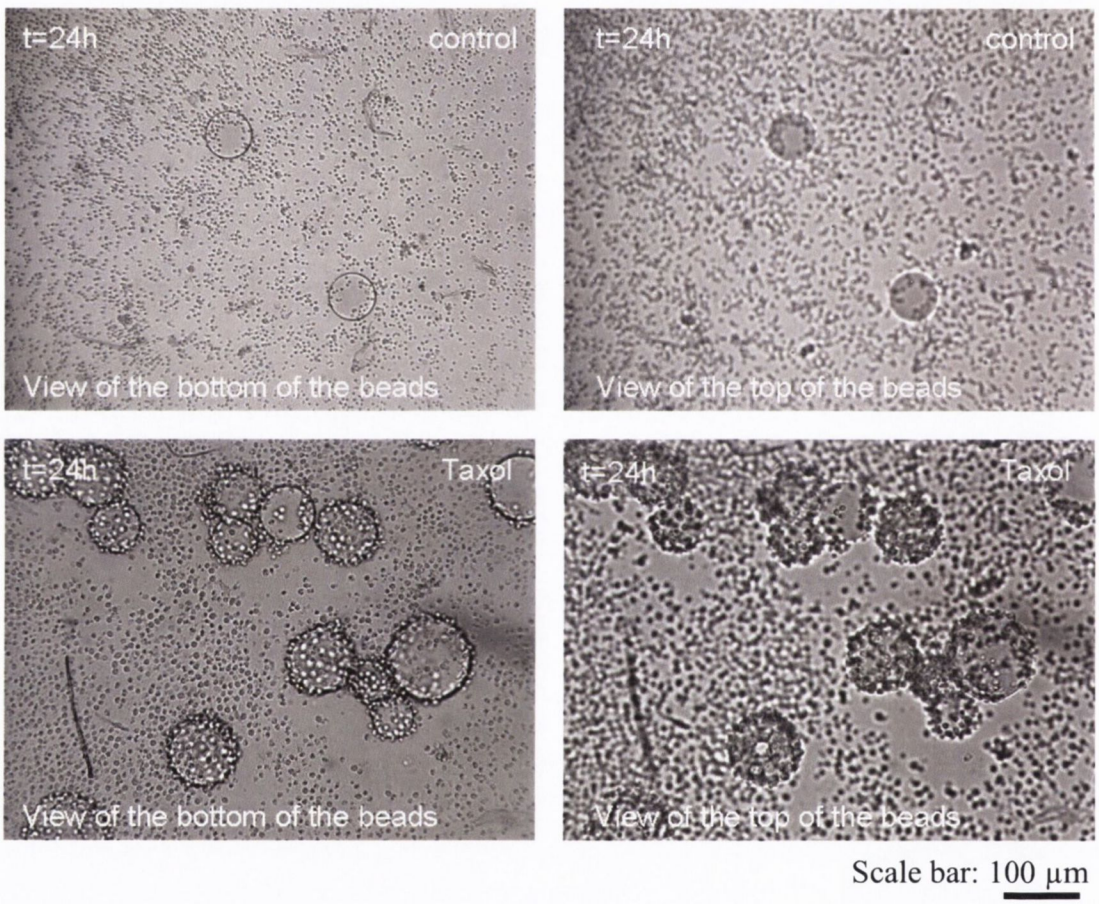

Figure 6-9: Images showing the responses of the Taxol treated cells to the anti-LFA-1α coated beads. Images were acquired on the bottom of the beads as well as on the side/top of the beads. After an incubation of 24 hours of the cells in presence with the coated beads, the cells covered the beads.

The inhibition of the microtubule did not inhibit the adherence of cells onto the beads (Fig. 6-9). Therefore, for the previous experiments with anti-LFA-1α coated beads, the mechanism by which the beads were covered with cells cannot be the migration. An explanation is that the cells were randomly picked up by the beads "rolling" on the bottom of the plate.

6.2.3 Quantification of the attachment of cells on coated beads

The results of the quantification of the attachment of cells onto the anti-LFA-1α coated beads depending on the treatment of the cells (antibodies to MIP-1α and MIP-1β, Taxol, and non treated cells) are shown on graph 6-1. Controls are performed for each cell treatment with non coated beads.

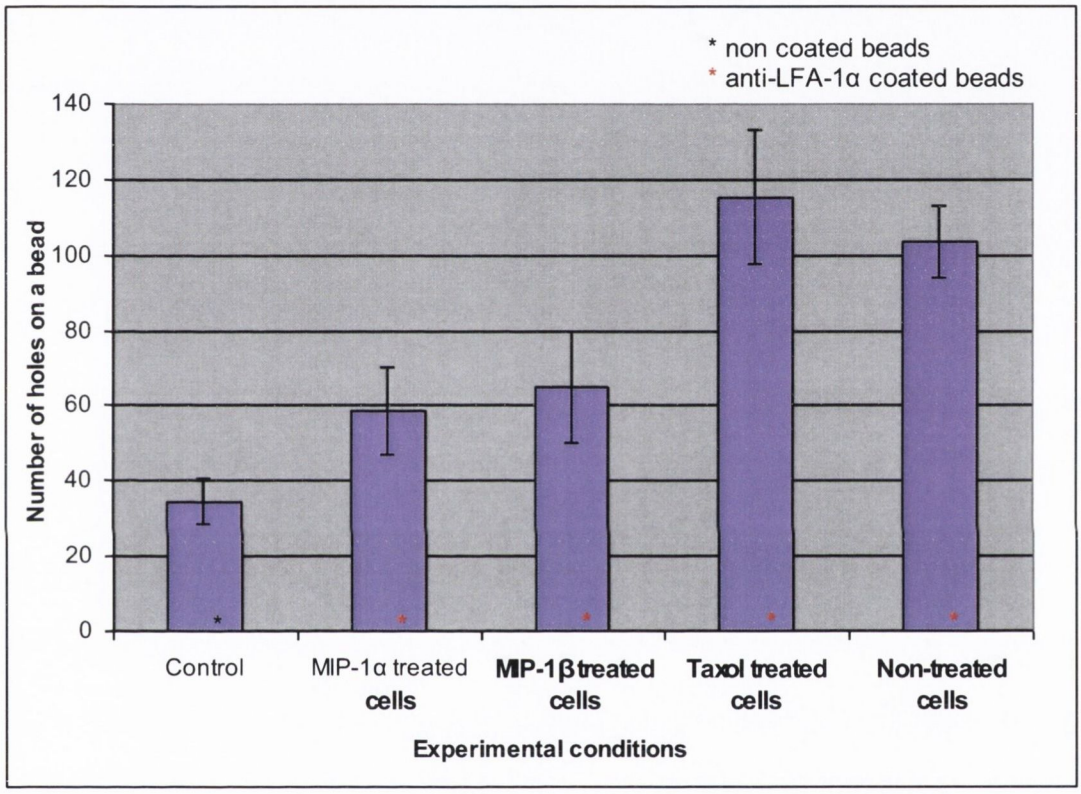

Graph 6-1: Quantification of the attachment of PBL cells onto anti-LFA-1α coated beads. The graph shows the results of the attachment of cells depending on the treatment of the cells (antibodies to MIP-1α and MIP-1β, Taxol, and non treated cells). Controls are performed with non coated beads with the same cell treatment than previously detailed.

The graph shows that between the experiments which involved anti-MIP-1α, anti-MIP-1β or the control and the experiments which involved Taxol treated cells or non treated cells; there was a difference in the number of holes of approximately 50 %. Less than half the cells were attached onto the surface of the beads in the control or cells treated with the antibodies than in the Taxol/non treated cells experiments, which confirms what was previously observed during the microscopic analysis.

6.3 Discussion

A method was investigated to generate a "natural" gradient of chemokines secreted by the stimulation of cells which was attached to anti-LFA-1α coated line or onto anti-LFA-1α coated beads. The PBL cells adhered onto the anti-LFA-1α coated line when the plate was placed in the IN Cell Analyzer as it was shown on figure 6-5. Since at the end of each experiment the majority of the non-adhered cells remained on the left side of the well, it was reasonable to stipulate that the plate on the IN Cell Analyzer was not precisely aligned. When the experiments were carried out in an incubator, the anti-LFA-1α coated line was not covered with cells. Therefore, the cells did not migrate towards the line. The fact that the line was covered with cells when the plate was placed in the IN Cell Analyzer demonstrated that a) the cells adhered onto the coated line when they were relocated from one side of the well to the other side because of the IN Cell Analyzer sample plate slightly unbalanced and that b) no directed migration of cells occurred due to the secretion of chemokines.

In the bead assays, as expected, the cells adhered onto anti-LFA-1α coated beads after 24 hours of incubation. According to Murphy *et al.*, this was first explained by the fact that the cells secreted chemokines that directed the migration of cells (e.g. MIP-1α, MIP-1β). To assess this statement, two antibodies were used to block the secretion of MIP-1α and MIP-1β. The cells were not able to adhere onto the anti-LFA-1α coated beads when they have previously been treated with antibodies to MIP-1α and MIP-1β. The results have shown that inhibiting the secretion of these chemokines decreased the quantity of adherent cells (Graph 6-1). A microtubule inhibitor (Taxol) was used to investigate the ability of cells to migrate towards the coated beads. The cells treated with Taxol adhered onto the beads in a similar manner than when the cells were not treated. The results on the graph 6-1 show that the Taxol treated cells adhered onto the beads as much as non-treated cells which means that the cells were not migrating towards the release of the chemokines at the surrounding of the beads. This is explained by the fact that the beads placed on the bottom of the plate were not immobilized but were "rolling" on the surface of the plate. It was shown that the cells did not migrate towards the beads; the cells were randomly "picked up" by the rolling beads.

Finally, these cell-based assays have shown that it would be of relevance for cell adherence assays but not for mediating directed cell migration. Therefore, there was no application of it in the context of this research.

7 General discussion of the full work presented in the thesis

Cellular chemotaxis is a fundamental molecular mechanism involved in various aspects of immunology. The ultimate mission of researchers is to identify new treatments that will address unmet medical needs. Principle among these goals is the desire to make treatments more effective through targeted drug delivery. Currently the two predominant research fields are oncology and immunology and within both fields the characteristics of white blood cells such as lymphocytes (T and B cells) are responsible for fighting bacterial and fungal infections. Cancer is a major cause of mortality and approximately 60 % of global cancer occurs in developed countries with probably 10 million new cases per year at present and is likely to double by 2020[171]. However, the problem with cancer treatment is that the body's immune system does not recognise cancer cells as abnormal and therefore cannot fight them. A major aspect of cancer is angiogenesis where blood vessels form within tumours providing the nutrients for continued growth. Drugs are currently being developed for the inhibition of adhesion and transmigration of metastatic cancer cells. The inhibition mechanism that these drugs utilise disrupt cell signalling pathways e.g. by proteolysis administrating a drug such as Velcade® (bortezomib) used for patients with multiple myelomas[168], by blocking cell adhesion molecule using Erbitux® (Cetuximab) resulting in inhibition of cell growth for patients with neck cancer[169], or the inhibition of the microtubule cytoskeleton for example by Taxol in patients with breast cancer is an alternative method to inhibit cell carcinoma migration[170]. These drugs, before being sold by pharmaceutical companies, have first to be tested in *in vitro* assays to evaluate their efficacy on cancer cells but also their toxicity on healthy cells. *In vivo* animal tests are also carried out before testing the drugs on volunteer patients in clinical trials. Although animal tests are still widely used they have high constraints: a) ethics approval which is time consuming to obtain, b) an important economic budget because of the high dose of drugs dispensed into the animals, and c) another constraint is the constant and massive sacrificing of animals for the sake of human beings. To avoid those disadvantages on animal trials, chemotaxis systems have widely been developed and used to elucidate the underlying biology of a process like cell migration.

Cell-based assays are concrete examples of pre-clinical studies. These assays were largely carried out for instance on plates coated with ECM-derived integrin ligands[172] to

describe cell adhesion and locomotion. These experimental models involving exposing cells to cell adhesion molecules immobilized on substrates demonstrated that collagens, laminins, arginine-glycine-aspartate called RGD-containing proteins (fibronectin, fibrin, vitronectin) also stimulate cells[173] by activating various signalling pathways and promoting cell-cell adhesion. In chapter 3, cell adhesion was mediated by coating the base of a plate with immunoglobulin superfamily proteins (VCAM-1, ICAM-1) and the antibody to LFA-1α. A range of concentration of these molecules was used to assess the ability of cells to migrate and polarize. This part of work was essential for the later chemotactic assays performed within a biochip design where cells were adhered onto a ligands coated channel.

Working in a physiologically relevant *in vivo* milieu is crucial when investigating chemotaxis. Initially, agarose has been the most used gel for mimicking the tissues because of its cost effectiveness, biocompatibility and its straight forward usability as it was shown in Chapter 3 with the under-agarose assay. This assay enabled us to observe the migration of cells towards a gradient of chemokines within a gel scaffold. The Dunn chamber is another well known assay in which cells migrate onto a cover glass in presence of a chemoattractant solution. These assays allow us to observe the responses of cells to a concentration of chemokines gradually diffused on a 2D plan. However, in *in vivo* conditions, the cells freely migrate within a 3D surrounding. Limitations in standard chemotaxis assays led biologists to jointly work with physicists, engineers and chemists to develop new microfluidic devices. Those devices were considered a relevant model for chemotaxis assays.

Current microfluidic platforms have certain advantages particular to their design and have achieved widespread use in biological assays. From simple microfluidic devices to highly advanced biochips, the researchers can at present use computer controlled flow devices and cell tracking software on almost any environment to study for e.g., the response of cells to chemokines diffused at a site of inflammation. To date, those devices had a common design which consisted of a main channel in which cells continuously flow as in blood vessel. Depending on the design of the device, a network of channels was dedicated to generate a gradient of chemokines that was directly injected into the main flow of cells. In those designs the gradient was mechanically controlled[70, 73] or passively diffused by contacting two fluid flows[174]. That gradient

could also be generated in a microstructure "gap"[100] or in a network of channels which were perpendicularly connected to the main channel[98]. These types of system allowed researchers to perform real time observations of leukocyte adhesion cascades, consisting of initial contact, slow rolling and adherence of cells on the surface of the biochips with different surface coatings. In Chapter 5 (§ 5.2.1), cell adhesion was shown to depend on the characteristics of ECM ligands (ICAM-1, VCAM-1) and in addition it has proven to be shear-rate-dependent[175]. We can say, at this time, "standard" microfluidic assays for chemotaxis which utilise shear flow, include controlled chemokine gradients and surfaces which are coated with ligands. However, this model system, for all its advantages, was incomplete as one important step was missing: that is the migration of cells through the endothelium into the tissues.

In this work, new microfluidic designs have been developed to study chemotactic assays using conventional soft lithography to fabricate soft polymer biochips. Three designs were produced in order to present a unique site in which chemokines were diffused from a gel matrix and from which cells could freely migrate into (Fig. 5-14, 5-18, 5-26). These designs did not allow us to investigate the influence of chemokines on the flowing cells. Multiple problems were initially determined: a) the filling of the gel in the Channel A was intrinsically due to the difficulty to dispense the low volume of gel, b) the interface of the gel with the flowing cells was either not flat or had a meniscus-like shape, and c) the diffusion of the chemokines into the Channel B was limited because it was either washed away in such manner that cells were not stimulated or because the gel kept being pushed back in the Channel A. The point of this study was to present a more physiologically relevant environment to the cells. However, the biochips which we developed are still different from the *in vivo* milieu because no consideration was made to mimic the physiological characteristics of the blood vessel, the diffusion of chemoattractant molecules through the vessel wall or the migration of cells from the flow through the blood vessel. Therefore, the validity of the responses of the cells acquired within soft polymer biochips could be truncated because some as yet uncharacterized intra- and extra-cellular mechanisms may not occur in a simplification of the *in vivo* milieu. The progress on the fabrication of microfluidic biochip evolves rapidly and since the beginning of this work, alternative material for the scaffold has been used instead of soft polymer.

The *in vivo* setting was widely reproduced utilising soft gel scaffolds for cell-based assays. Current improvements in biomaterials synthesis allow the researchers to use fine hydrogels[176-178]. Recently, by combining the advantages of both "under-agarose assays" and microfluidic biochips, hydrogel-based microfluidic devices have been developed to investigate chemotaxis. A hydrogel is a network of polymer chains that are water-insoluble in which water is the dispersion medium; agarose or collagen are common examples of such gels. The advantage of using synthetic polymeric scaffold is that it offers the capacity for rapid transport and exchange of materials. Diffusion of biochemical signal is then possible through the gel for cells feeding or stimulation of embedded cells[179]. Hydrogel-based microfluidic devices are relatively new, yet they have already shown much promise[180]. It is possible to observe in real time the morphogenesis of neurons in the presence of chemokine gradient in an ECM-like milieu under interstitial flow conditions[181]. The migration of cells towards a gradient of chemokines in a hydrogel scaffold has also been demonstrated[180]. Microfluidics technology offers a wide scope of applications for biomaterials, especially for medical and biological uses. However, biomaterials properties need to be optimised and functionally adjusted in order to mimic biological interfaces. Therefore, there is an increasing demand to develop and optimise new materials to address such problems in biology and medicine[182]. Different hydrogel polymers have also been used to develop microvascularised tissue[76] in the field of tissue engineering. Among some of the hydrogel polymers used, there are poly(ethylene) glycol, polysialic acid, poly(lactic-*co*-glycolic acid). Therefore, making a parallel with microfluidic biochips, tissue engineering applications provide a new method for the study of inflammatory diseases. Using MEMS technology to supply a support for the 3-dimensional scaffold,[183] artificial capillaries can be used for mimicking the *in vivo* conditions, for example to study the impact of shear stress on cells in a more physiological milieu. Therefore, merging of these technologies together provided the missing bridge between gel chemotaxis assays with no flow and 3D chemotaxis under flow conditions.

To summarize, the development of advanced devices for mimicking the *in vivo* conditions, for instance to study the behaviour of cancer cells when they migrate and disseminate to generate metastatic tumours, is essential to understand in order to develop strategies enabling to combat the increasing number of cancer patients worldwide. Relatively simple to manufacture and cheap devices offer a crucial

alternative as pre-clinical trial platforms to costly customised animal tests and can provide physiologically relevant data faster than animal tests with a lower volume of reagents. In this context, we developed and comprehensively evaluated four prototypes of new microfluidic biochips designs. We have concluded that these designs were not entirely suitable for sophisticated chemotactic assays; however we believe that we have significantly contributed to the progress in this challenging field during the course of the project. The meaning of the term research refers to a constant investigation based on an initial idea to determine information to confirm or invalidate these thoughts. From that, a method is elaborated and developed in order to study the parameters we want to evaluate. Therefore, although the results obtained in our study have not led to an immediate resolution of the issues with the creation of chemokine gradients under shear flow, the designs we had developed were innovative enough to enable us to collect valuable information and progress the future direction of microfluidic biochip design. Through these devices, the importance of designing ever more comprehensive imitations of the *in vivo* milieu in the context of chemotactic studies has been elucidated. There are currently a lot of "more physiological" microfluidic biochips designs in progress, which are made possible with hydrogel adapted for microfluidic conditions and with the potential use of tissue engineering as a support for the investigations of cells free to migrate in a 3D environment. As a consequence, further observations and interpretations of multimolecular mechanisms underlying cell adhesion, cell signalling pathways and dynamic changes of cell morphology, for example during cancer spreading and inflammatory processes, are to be expected using these types of devices in the future.

8 Conclusion

The new devices developed in the course of this study were expected to provide a better approximation of the *in vivo* physiological environment for cells and were designed to include many more *in vivo* parameters than are currently offered by standard microfluidic biochips. It has been shown that the prototype models developed were not directly applicable for advanced chemotaxis assays. Our chip designs were innovative and challenging as they took into account the diffusion of chemokines from and through the tissues into the flow of cells at a precise site and allowed the cells to freely migrate within a 3D plan. However, the complexity of the behaviour of the gel within the chip imposes a significant problem. In the Chapter 7 it has been shown that the progress in the development of microfluidic platforms with more physiological milieu evolves very quickly. Examples of next generation microfluidic platforms have been presented such as microfluidic hydrogels or engineered tissues that are expected to facilitate the elucidation of diverse biological processes involved at the site of inflammation.

Considering the complexity of the challenges taken up in this thesis across physics, engineering and immunology, I think the solutions and the results here presented are of considerable importance to the scientific and industrial research communities. Therefore as a concluding remark I feel that in the future advances in chemotaxis assay we can predict that chemotaxis assays based on hydrogels will be focused towards smart, injectable and highly physiologically adaptable scaffolds where vascularisation and chemokine gradients will be generated by the natural adaptive response of the *in vivo* surrounding tissue.

9 References

1. L. Stephens, L. Milne and P. Hawkins, *Curr Biol*, 2008, **18**, R485-494.
2. G. Cinamon, V. Grabovsky, E. Winter, S. Franitza, S. Feigelson, R. Shamri, O. Dwir and R. Alon, *J Leukoc Biol*, 2001, **69**, 860-866.
3. W. Savino, D. M. Villa-Verde, D. A. Mendes-da-Cruz, E. Silva-Monteiro, A. R. Perez, P. Aoki Mdel, O. Bottasso, N. Guinazu, S. D. Silva-Barbosa and S. Gea, *Cytokine Growth Factor Rev*, 2007, **18**, 107-124.
4. T. Sato, H. Thorlacius, B. Johnston, T. L. Staton, W. Xiang, D. R. Littman and E. C. Butcher, *J Immunol*, 2005, **174**, 277-283.
5. A. Chan, A. Filer, G. Parsonage, S. Kollnberger, R. Gundle, C. D. Buckley and P. Bowness, *Arthritis Rheum*, 2008, **58**, 707-717.
6. Y. Lu, J. Wang, Y. Xu, A. E. Koch, Z. Cai, X. Chen, D. L. Galson, R. S. Taichman and J. Zhang, *Mol Cancer Res*, 2008.
7. Y. Lu, Z. Cai, D. L. Galson, G. Xiao, Y. Liu, D. E. George, M. F. Melhem, Z. Yao and J. Zhang, *Prostate*, 2006, **66**, 1311-1318.
8. S. Shahrara, A. E. Proudfoot, C. C. Park, M. V. Volin, G. K. Haines, J. M. Woods, C. H. Aikens, T. M. Handel and R. M. Pope, *J Immunol*, 2008, **180**, 3447-3456.
9. B. Boldajipour, H. Mahabaleshwar, E. Kardash, M. Reichman-Fried, H. Blaser, S. Minina, D. Wilson, Q. Xu and E. Raz, *Cell*, 2008, **132**, 463-473.
10. R. Mohle, F. Bautz, S. Rafii, M. A. Moore, W. Brugger and L. Kanz, *Ann N Y Acad Sci*, 1999, **872**, 176-185; discussion 185-176.
11. P. Schaerli and B. Moser, *Immunol Res*, 2005, **31**, 57-74.
12. M. O'Hayre, C. L. Salanga, T. M. Handel and S. J. Allen, *Biochem J*, 2008, **409**, 635-649.
13. K. Nistala, H. Moncrieffe, K. R. Newton, H. Varsani, P. Hunter and L. R. Wedderburn, *Arthritis Rheum*, 2008, **58**, 875-887.
14. G. Li, H. Adesnik, J. Li, J. Long, R. A. Nicoll, J. L. Rubenstein and S. J. Pleasure, *J Neurosci*, 2008, **28**, 1085-1098.
15. W. Kessler, T. Budde, M. Gekle, A. Fabian and A. Schwab, *Pflugers Arch*, 2008, **456**, 813-823.
16. C. Weidt, B. Niggemann, B. Kasenda, T. L. Drell, K. S. Zanker and T. Dittmar, *Curr Stem Cell Res Ther*, 2007, **2**, 89-103.
17. M. Li and R. M. Ransohoff, *Prog Neurobiol*, 2008, **84**, 116-131.
18. J. R. Bradley, *J Pathol*, 2008, **214**, 149-160.
19. J. A. Carnegie, *Biol Reprod*, 1994, **50**, 413-420.
20. D. M. Rose, R. Alon and M. H. Ginsberg, *Immunol Rev*, 2007, **218**, 126-134.
21. T. M. Keenan and A. Folch, *Lab Chip*, 2008, **8**, 34-57.
22. T. W. Secomb, M. A. Konerding, C. A. West, M. Su, A. J. Young and S. J. Mentzer, *Proc Natl Acad Sci U S A*, 2003, **100**, 7231-7234.
23. M. Gouwy, S. Struyf, P. Proost and J. Van Damme, *Cytokine Growth Factor Rev*, 2005, **16**, 561-580.
24. A. Viola and A. D. Luster, *Annu Rev Pharmacol Toxicol*, 2008, **48**, 171-197.
25. X. Hu, S. D. Chakravarty and L. B. Ivashkiv, *Immunol Rev*, 2008, **226**, 41-56.
26. M. Moser, K. R. Legate, R. Zent and R. Fassler, *Science*, 2009, **324**, 895-899.
27. M. Nemethova, S. Auinger and J. V. Small, *J Cell Biol*, 2008, **180**, 1233-1244.
28. Y. Iwadate and S. Yumura, *J Cell Sci*, 2008, **121**, 1314-1324.
29. J. J. Grzesiak and M. D. Pierschbacher, *J Clin Invest*, 1995, **95**, 227-233.
30. B. Heit and P. Kubes, *Sci STKE*, 2003, **2003**, PL5.

31. R. Feynman, *Annual meeting of the American Physical Society, Caltech*, 1959.
32. A. K. Deisingh, *Analyst*, 2003, **128**, 9-11.
33. A. D. Livingston, C. J. Campbell, E. K. Wagner and P. Ghazal, *Genome Biol*, 2005, **6**, 112.
34. C. T. Nguyen, *IEEE Trans Ultrason Ferroelectr Freq Control*, 2007, **54**, 251-270.
35. D. L. Polla, A. G. Erdman, W. P. Robbins, D. T. Markus, J. Diaz-Diaz, R. Rizq, Y. Nam, H. T. Brickner, A. Wang and P. Krulevitch, *Annu Rev Biomed Eng*, 2000, **2**, 551-576.
36. G. Kotzar, M. Freas, P. Abel, A. Fleischman, S. Roy, C. Zorman, J. M. Moran and J. Melzak, *Biomaterials*, 2002, **23**, 2737-2750.
37. A. Long, S. Mitchell, D. Kashanin, V. Williams, A. Prina Mello, I. Shvets, D. Kelleher and Y. Volkov, *Ann N Y Acad Sci*, 2004, **1028**, 313-319.
38. R. Zaouk, B. Y. Park and M. J. Madou, *Methods Mol Biol*, 2006, **321**, 5-15.
39. L. Martynova, L. E. Locascio, M. Gaitan, G. W. Kramer, R. G. Christensen and W. A. MacCrehan, *Anal Chem*, 1997, **69**, 4783-4789.
40. J. Soo Ko, H. C. Yoon, H. Yang, H. B. Pyo, K. Hyo Chung, S. Jin Kim and Y. Tae Kim, *Lab Chip*, 2003, **3**, 106-113.
41. B. Ziaie, A. Baldi, M. Lei, Y. Gu and R. A. Siegel, *Adv Drug Deliv Rev*, 2004, **56**, 145-172.
42. A. L. Robinson, *Science*, 1984, **223**, 267-268.
43. M. Verzeano and J. D. French, *Electroencephalogr Clin Neurophysiol*, 1953, **5**, 613-616.
44. R. E. George, *Ann Phys Med*, 1956, **3**, 66-67.
45. A. Wixforth and J. Scriba, *GIT Labor-Fachzeitschrift*, 2002.
46. J. Vykoukal, *Micro Total Analysis Systems*, 2001, 72-74.
47. W. Papst, *Klin Monatsbl Augenheilkd*, 1983, **182**, 167-169.
48. D. A. Ogella, *J Indian Med Assoc*, 1999, **97**, 436-437, 441.
49. Tobias Lilliehorn, Ph.D. Thesis, Uppsala University 2003.
50. Y. Choi, J. Vukasinovic, A. Glezer and M. G. Allen, *Biomed Microdevices*, 2008.
51. K. M. Renshaw, D. E. Orr and K. J. L. Burg, *Biotechnol Prog.*, 2005, **21**, 538 - 545.
52. K. Chakrabarty and F. Su, 2005.
53. C. W. Frevert, G. Boggy, T. M. Keenan and A. Folch, *Lab Chip*, 2006, **6**, 849-856.
54. O. P. Kallioniemi, *Ann Med*, 2001, **33**, 142-147.
55. N. Broude, K. Woodward, R. Cavallo, C. Cantor and D. Englert, *Nucleic Acids Res.*, 2001, **29**.
56. L. C. Waters, S. C. Jacobson, N. Kroutchinina, J. Khandurina, R. S. Foote and J. M. Ramsey, *Anal. Chem*, 1998, **70**, 158 -162.
57. R. Liu, J. Yang, R. Lenigk, J. Bonanno and P. Grodzinski, *Anal Chem*, 2004, **76**, 1824-1831.
58. C. Thibault, V. L. Berre, S. Casimirius, Trévisiol, J. François and C. Vieu, *J Nanobiotechnology*, 2005.
59. Jordan S. Miller, Mathilde I. Bethencourt, Mariah Hahn, T. Randall Lee and J. L. West, *Wiley Periodicals*, 2005.
60. J.-Y. Cheng, C.-W. Wei, K.-H. Hsu and T.-H. Young, *Sensors and Actuators*, 2004, **99**, 186–196.
61. B. D. Ratner and S. J. Bryant, *Rev. Biomed. Eng.*, 2004.

62. A. Prina-Mello, Y. Volkov, D. Kelleher and P. J. Prendergast, *Ann Biomed Eng*, 2003, **31**, 1106-1113.
63. N. L. Jeon, H. Baskaran, S. K. W. Dertinger, G. M. Whitesides and L. V. D. Water, *Nature Biotechnology*, 2002, **20**, 826 - 830.
64. H. Mao, P. S. Cremer and M. D. Manson, *Proc Natl Acad Sci U S A*, 2003, **100**, 5449-5454.
65. T. Ahmed and R. Stocker, *Biophys J*, 2008.
66. S. K. Dertinger, X. Jiang, Z. Li, V. N. Murthy and G. M. Whitesides, *Proc Natl Acad Sci U S A*, 2002, **99**, 12542-12547.
67. J. S. Marcus, W. F. Anderson and S. R. Quake, *Anal Chem*, 2006, **78**, 956-958.
68. J. S. Marcus, W. F. Anderson and S. R. Quake, *Anal Chem*, 2006, **78**, 3084-3089.
69. F. Lin and E. C. Butcher, *Lab Chip*, 2006, **6**, 1462-1469.
70. D. Irimia, S. Y. Liu, W. G. Tharp, A. Samadani, M. Toner and M. C. Poznansky, *Lab Chip*, 2006, **6**, 191-198.
71. G. M. Walker, J. Sai, A. Richmond, M. Stremlere and C. Y. Chung, *Lab Chip*, 2005, **5**, 611-618.
72. C. Joanne Wang, X. Li, B. Lin, S. Shim, G. L. Ming and A. Levchenko, *Lab Chip*, 2008, **8**, 227-237.
73. Y. Liu, J. Sai, A. Richmond and J. P. Wikswo, *Biomed Microdevices*, 2008.
74. E. W. Young, A. R. Wheeler and C. A. Simmons, *Lab Chip*, 2007, **7**, 1759-1766.
75. C. Laudanna and R. Alon, *Thromb Haemost*, 2006, **95**, 5-11.
76. C. Fidkowski, M. R. Kaazempur-Mofrad, J. Borenstein, J. P. Vacanti, R. Langer and Y. Wang, *Tissue Eng*, 2005, **11**, 302-309.
77. U. Y. Schaff, M. M. Xing, K. K. Lin, N. Pan, N. L. Jeon and S. I. Simon, *Lab Chip*, 2007, **7**, 448-456.
78. E. Gutierrez and A. Groisman, *Anal Chem*, 2007, **79**, 2249-2258.
79. L. Kim, Y. C. Toh, J. Voldman and H. Yu, *Lab Chip*, 2007, **7**, 681-694.
80. B. M. Cooke, S. Usami, I. Perry and G. B. Nash, *Microvasc Res*, 1993, **45**, 33-45.
81. H. Wang, G. M. Riha, S. Yan, M. Li, H. Chai, H. Yang, Q. Yao and C. Chen, *Arterioscler Thromb Vasc Biol*, 2005, **25**, 1817-1823.
82. C. K. Prasad and L. K. Krishnan, *Acta Biomater*, 2008, **4**, 182-191.
83. P. Feugier, R. A. Black, J. A. Hunt and T. V. How, *Biomaterials*, 2005, **26**, 1457-1466.
84. S. Feng, X. Lu, J. C. Resendiz and M. H. Kroll, *Am J Physiol Cell Physiol*, 2006, **291**, C1346-1354.
85. G. Cinamon and R. Alon, *J Immunol Methods*, 2003, **273**, 53-62.
86. T. H. Schreiber, V. Shinder, D. W. Cain, R. Alon and R. Sackstein, *Blood*, 2007, **109**, 1381-1386.
87. M. J. Hickey, M. Forster, D. Mitchell, J. Kaur, C. De Caigny and P. Kubes, *J Immunol*, 2000, **165**, 7164-7170.
88. R. A. Warnock, S. Askari, E. C. Butcher and U. H. von Andrian, *J Exp Med*, 1998, **187**, 205-216.
89. W. Y. Lee and P. Kubes, *J Hepatol*, 2008, **48**, 504-512.
90. P. Kubes and S. M. Kerfoot, *News Physiol Sci*, 2001, **16**, 76-80.
91. F. W. Luscinskas, Y. C. Lim and A. H. Lichtman, *Nat Immunol*, 2001, **2**, 478-480.
92. C. Verdier, C. Couzon, A. Duperray and P. Singh, *J Math Biol*, 2008.

93. J. M. Rutkowski and M. A. Swartz, *Trends Cell Biol*, 2007, **17**, 44-50.
94. J. J. Campbell, J. Hedrick, A. Zlotnik, M. A. Siani, D. A. Thompson and E. C. Butcher, *Science*, 1998, **279**, 381-384.
95. R. Alon, D. A. Hammer and T. A. Springer, *Nature*, 1995, **374**, 539-542.
96. T. K. Hsiai, S. K. Cho, P. K. Wong, M. H. Ing, A. Salazar, S. Hama, M. Navab, L. L. Demer and C. M. Ho, *Ann Biomed Eng*, 2004, **32**, 189-201.
97. S. K. Murthy, A. Sin, R. G. Tompkins and M. Toner, *Langmuir*, 2004, **20**, 11649-11655.
98. W. Saadi, S. W. Rhee, F. Lin, B. Vahidi, B. G. Chung and N. L. Jeon, *Biomed Microdevices*, 2007, **9**, 627-635.
99. B. G. Chung, F. Lin and N. L. Jeon, *Lab Chip*, 2006, **6**, 764-768.
100. K. C. Chaw, M. Manimaran, F. E. Tay and S. Swaminathan, *Microvasc Res*, 2006, **72**, 153-160.
101. J. M. Schroder, *Mol Biotechnol*, 2001, **18**, 71-77.
102. P. Proost, A. Wuyts, R. Conings, J. P. Lenaerts, W. Put and J. Van Damme, *Methods*, 1996, **10**, 82-92.
103. G. J. Randolph and M. B. Furie, *J Immunol*, 1995, **155**, 3610-3618.
104. N. W. Lukacs, R. M. Strieter, V. Elner, H. L. Evanoff, M. D. Burdick and S. L. Kunkel, *Blood*, 1995, **86**, 2767-2773.
105. A. Murphy, A. Long, Y. Volkov and D. Kelleher, *Eur J Immunol*, 2000, **30**, 3006-3011.
106. D. Kelleher, A. Murphy, C. Feighery and E. B. Casey, *J Leukoc Biol*, 1995, **58**, 539-546.
107. Y. Korlann, T. Dertinger, X. Michalet, S. Weiss and J. Enderlein, *Opt Express*, 2008, **16**, 14609-14616.
108. J. S. Goodwin and A. K. Kenworthy, *Methods*, 2005, **37**, 154-164.
109. A. Lubelski and J. Klafter, *Biophys J*, 2008, **94**, 4646-4653.
110. G. S. Smith, J. H. Lumsden and B. P. Wilcock, *Can J Comp Med*, 1985, **49**, 43-49.
111. B. Mann, A. Gobin, A. T. Tsai, R. H. Schmedlen and J. L. West, *Biomaterials*, 2001, **22**, 3045-3051.
112. L. Soon, F. Braet and J. Condeelis, *Microsc Res Tech*, 2007, **70**, 252-257.
113. D. Lauffenburger, C. Rothman and S. H. Zigmond, *J Immunol*, 1983, **131**, 940-947.
114. D. Zicha, G. Dunn and G. Jones, *Methods Mol Biol*, 1997, **75**, 449-457.
115. I. Dransfield, C. Cabanas, A. Craig and N. Hogg, *J Cell Biol*, 1992, **116**, 219-226.
116. M. G. Narducci, E. Scala, A. Bresin, E. Caprini, M. C. Picchio, D. Remotti, G. Ragone, F. Nasorri, M. Frontani, D. Arcelli, S. Volinia, G. A. Lombardo, G. Baliva, M. Napolitano and G. Russo, *Blood*, 2006, **107**, 1108-1115.
117. B. Heit, P. Colarusso and P. Kubes, *J Cell Sci*, 2005, **118**, 5205-5220.
118. Y. Tanaka, S. Mine, C. G. Figdor, A. Wake, H. Hirano, J. Tsukada, M. Aso, K. Fujii, K. Saito, Y. van Kooyk and S. Eto, *Blood*, 1998, **91**, 3909-3919.
119. P. C. Wilkinson, J. M. Lackie, J. V. Forrester and G. A. Dunn, *J Cell Biol*, 1984, **99**, 1761-1768.
120. K. Nishinari, *Makrol. Chem.*, 1987, **188**, 1177-1186.
121. D. Kelleher, A. Murphy and D. Cullen, *Eur J Immunol*, 1990, **20**, 2351-2354.
122. E. B. Lomakina and R. E. Waugh, in *Biophys J*, 2004, pp. 1223-1233.
123. T. H. Howard, *Blood*, 1986, **67**, 1036-1042.

124. A. J. Millán, M. I. Nieto, C. Baudín and R. Moreno, *Journal of the European Ceramic Society*, 2002, **22**, 2217-2222.
125. V. E. Baracos, E. J. Wilson and A. L. Goldberg, *Am J Physiol*, 1984, **246**, C125-130.
126. T. J. Pucadyil and A. Chattopadhyay, *Journal of Fluorescence*, 2005.
127. P. G. Saffman and M. Delbrock, *Biophysics*, 1975, **72**, 3111-3113.
128. E. B. Walton, B. Oommen and K. J. Van Vliet, *Conf Proc IEEE Eng Med Biol Soc*, 2007, **2007**, 6419-6421.
129. J. A. Anta, I. Mora-Sero, T. Dittrich and J. Bisquert, *Phys Chem Chem Phys*, 2008, **10**, 4478-4485.
130. K. JACOBSON, D. O'DELL and J. T. AUGUST, *The Journal of Cell Biology*, 1984, **99**, 1624-1633.
131. H. Kang, K. J. Bayless and R. Kaunas, *Am J Physiol Heart Circ Physiol*, 2008, **295**, H2087-2097.
132. S. Ramanujan, A. Pluen, T. D. McKee, E. B. Brown, Y. Boucher and R. K. Jain, *Biophys J*, 2002, **83**, 1650-1660.
133. A. A. Tomei, F. Boschetti, F. Gervaso and M. A. Swartz, *Biotechnol Bioeng*, 2008.
134. K. Stuart and A. Panitch, *Biomacromolecules*, 2009, **10**, 25-31.
135. V. Di Felice, F. Cappello, A. Montalbano, N. M. Ardizzone, A. De Luca, F. Macaluso, D. Amelio, M. C. Cerra and G. Zummo, *Biol Cell*, 2007, **99**, 689-699.
136. S. Fernandez-Cossio, A. Leon-Mateos, F. G. Sampedro and M. T. Oreja, *Plast Reconstr Surg*, 2007, **120**, 1161-1169.
137. D. Lleres, S. Swift and A. I. Lamond, *Curr Protoc Cytom*, 2007, **Chapter 12**, Unit12 10.
138. M. E. van Royen, C. Dinant, P. Farla, J. Trapman and A. B. Houtsmuller, *Methods Mol Biol*, 2009, **505**, 69-96.
139. T.Chasteen, *http://www.shsu.edu/~chemistry/chemiluminescence/JABLONSKI.html*, .
140. Y. Chen, B. C. Lagerholm, B. Yang and K. Jacobson, *Methods*, 2006, **39**, 147-153.
141. A. Ekani-Nkodo and D. K. Fygenson, *PHYSICAL REVIEW*, 2003, **67**.
142. A. Christiaan and T. A. Maria, *http://mekentosj.com/science/frap/*.
143. P. S. Dittrich and P. Schwille, *Appl. Phys.*, 2001, **73**, 829-837.
144. J. Lippincott-Schwartz, N. Altan-Bonnet and G. H. Patterson, *Nat Cell Biol*, 2003, **Suppl**, S7-14.
145. S. J. Lockett, *Curr Protoc Cytom*, 2001, **Chapter 10**, Unit 10 10.
146. D. L. Kolin, S. Costantino and P. W. Wiseman, *Biophys J*, 2006, **90**, 628-639.
147. S. Jayaraman, N. S. Joo, B. Reitz, J. J. Wine and A. S. Verkman, *PNAS*, 2001, **98**, 8119-8123.
148. J. Labille, N. Fatin-Rouge and J. Buffle, *Langmuir*, 2007, **23**, 2083-2090.
149. B. L. Ziober, M. G. Mauk, E. M. Falls, Z. Chen, A. F. Ziober and H. H. Bau, *Head Neck*, 2008, **30**, 111-121.
150. D. A. Boy, F. Gibou and S. Pennathur, *Lab Chip*, 2008, **8**, 1424-1431.
151. X. Llopis, N. Ibanez-Garcia, S. Alegret and J. Alonso, *Anal Chem*, 2007, **79**, 3662-3666.
152. M. Gerard, A. Chaubey and B. D. Malhotra, *Biosensors and Bioelectronics*, 2002, **17**.
153. I. Wick and G. Hardiman, *Curr Opin Drug Discov Devel*, 2005, **8**, 347-354.
154. H. F. Li and J. M. Lin, *Anal Bioanal Chem*, 2009, **393**, 555-567.

155. M. Uttamchandani, J. L. Neo, B. N. Ong and S. Moochhala, *Trends Biotechnol*, 2009, **27**, 53-61.
156. L. J. Taite, M. L. Rowland, K. A. Ruffino, B. R. Smith, M. B. Lawrence and J. L. West, *Ann Biomed Eng*, 2006, **34**, 1705-1711.
157. E. Rondeau and J. J. Cooper-White, *Langmuir*, 2008, **24**, 6937-6945.
158. W. Zhu, W. Zhang, F. Han, X. Dong and X. Yan, *Biomed Microdevices*, 2005, **7**, 157-160.
159. *Comsol*, www.comsol.com.
160. Cellix, *http://www.cellixltd.com/*.
161. Epigem, *http://www.epigem.co.uk/*.
162. N. Midoux, 1993.
163. J. Berthier and P. Silberzan, 2006.
164. M. Gouwy, S. Struyf, S. Noppen, E. Schutyser, J. Y. Springael, M. Parmentier, P. Proost and J. Van Damme, *Mol Pharmacol*, 2008, **74**, 485-495.
165. S. Sheikh, G. E. Rainger, Z. Gale, M. Rahman and G. B. Nash, *Blood*, 2003, **102**, 2828-2834.
166. C. H. Hsieh, M. Frink, Y. C. Hsieh, W. H. Kan, J. T. Hsu, M. G. Schwacha, M. A. Choudhry and I. H. Chaudry, *J Immunol*, 2008, **181**, 2806-2812.
167. M. Abe, K. Hiura, S. Ozaki, S. Kido and T. Matsumoto, *J Bone Miner Metab*, 2009, **27**, 16-23.
168. H. Becker and C. Gartner, *Anal Bioanal Chem*, 2008, **390**, 89-111.
169. R. Schmidmaier and P. Baumann, *Curr Med Chem*, 2008, **15**, 978-990.
170. H. Thomadaki and A. Scorilas, *Biol Chem*, 2008, **389**, 1427-1434.
171. H. V. Fuentes and A. T. Woolley, *Anal Chem*, 2008, **80**, 333-339.
172. S. H. Zigmond, E. F. Foxman and J. E. Segall, *Curr Protoc Cell Biol*, 2001, **Chapter 12**, Unit 12 11.
173. R. Sackstein, *Curr Opin Hematol*, 2005, **12**, 444-450.
174. D. Irimia, G. Charras, N. Agrawal, T. Mitchison and M. Toner, *Lab Chip*, 2007, **7**, 1783-1790.
175. E. Bastida, L. Almirall, M. C. Bertomeu and A. Ordinas, *Int J Cancer*, 1989, **43**, 1174-1178.
176. S. Berski, J. van Bergeijk, D. Schwarzer, Y. Stark, C. Kasper, T. Scheper, C. Grothe, R. Gerardy-Schahn, A. Kirschning and G. Drager, *Biomacromolecules*, 2008, **9**, 2353-2359.
177. A. N. Buxton, J. Zhu, R. Marchant, J. L. West, J. U. Yoo and B. Johnstone, *Tissue Eng*, 2007, **13**, 2549-2560.
178. J. Zhang, A. Skardal and G. D. Prestwich, *Biomaterials*, 2008, **29**, 4521-4531.
179. W. J. Rosoff, J. S. Urbach, M. A. Esrick, R. G. McAllister, L. J. Richards and G. J. Goodhill, *Nat Neurosci*, 2004, **7**, 678-682.
180. S. Y. Cheng, S. Heilman, M. Wasserman, S. Archer, M. L. Shuler and M. Wu, *Lab Chip*, 2007, **7**, 763-769.
181. V. Vickerman, J. Blundo, S. Chung and R. Kamm, *Lab on a Chip*, 2008, **8**.
182. N. A. Peppas, Z. H. Hilt, A. Khademhosseini and R. Langer, *Adv Materials* 2006, **18**, 1345-1360.
183. H. Park, C. Cannizzaro, G. Vunjak-Novakovic, R. Langer, C. A. Vacanti and O. C. Farokhzad, *Tissue Eng*, 2007, **13**, 1867-1877.

10 Journal publication

The evolution of chemotaxis assays from static models to physiologically relevant platforms

Stephanie Toetsch,[a] Peter Olwell,[a] Adriele Prina-Mello[b] and Yuri Volkov*[a]

Received 21st August 2008, Accepted 6th October 2008
First published as an Advance Article on the web 12th December 2008
DOI: 10.1039/b814567a

The role of chemotactic gradients in the immunological response is an area which elicits a lot of attention due to its impact on the outcome of the inflammatory process. Consequently there are numerous standard *in vitro* designs which attempt to mimic chemotactic gradients, albeit in static conditions, and with no control over the concentration of the chemokine gradient. In recent times the design of the standard chemotaxis assay has incorporated modern microfluidic platforms, computer controlled flow devices and cell tracking software. Assays under fluid flow which use biochips have provided data which highlight the importance of shear stress on cell attachment and migration towards a chemokine gradient. However, the *in vivo* environment is far more complex in comparison to conventional cell assay chambers. The designs of biochips are therefore in constant flux as advances in technology permit ever greater imitations of *in vivo* conditions. Researchers are focused on designing a generation of new biochips and enhancing the physiological relevance of the current assays. The challenge is to combine a shear flow with a 3D scaffold containing the endothelial layer and permitting a natural diffusion of chemokines through a tissue-like basal matrix. Here we review the latest range of chemotaxis assays and assess the innovative features of their designs which enable them to better imitate the *in vivo* environment. We also present some alternative designs that were initially employed in tissue engineering which could potentially be used in the establishment of novel chemotaxis assays.

Introduction

The recruitment of leukocytes into tissues through endothelial cells lining the blood vessels is an essential step in the inflammatory response. Multiple biochemical signals are required to direct this process[1,2] which is relevant for all instances of inflammation.[3,4] Transendothelial migration (TEM) is the result of a multistep cascade in which different events culminate in the successful migration of a leukocyte through the endothelial wall and into the underlying tissue (Fig. 1A). The first step (a) is the margination of leukocytes from free flowing blood to the endothelial wall where they begin rolling on the surface of the endothelium. This rolling is promoted by the expression of selectins on endothelial surfaces. Selectins bind weakly to carbohydrate ligands on the surface of leukocytes causing them to roll on the surface of the endothelium. Cytokines induce the high affinity state of integrin receptors on the leukocytes and also stimulate the expression of matching integrin ligands on endothelial cells, which further slow leukocytes down (b). Cytokines, which are a family of proteins and peptides, also allow cells to communicate with each other.[5–18] Leukocytes which are adhered to the vessel wall (c), are stimulated to migrate across the endothelium into the tissues *via* a gradient of chemotactic cytokines (d) (chemokines).[19] Leukocytes which reach the tissue interstitium then bind to the extracellular matrix *via* a set of specific expressed integrins.[20]

Due to the essential role of leukocytes in inflammation, defects in leukocyte function often result in a decreased capacity for an inflammatory response with subsequent

[a] *Department of Clinical Medicine, Institute of Molecular Medicine, Trinity College Dublin, 8 Dublin, Ireland*
[b] *Centre for Research on Adaptative Nanostructures and Nanodevices (CRANN), Naughton Institute, Trinity College Dublin, 2 Dublin, Ireland. E-mail: yvolkov@tcd.ie; Fax: +353-1-4542043; Tel: +353-1-8963263*

Insight, innovation, integration

Inflammatory studies are carried out to understand how the immune system behaves when challenged. Limitations in existing biological assays led biologists to work conjointly with physicists, engineers, and chemists. This review shows the results of this multidisciplinary collaboration from standard chemotaxis assays to microfluidic platforms. Two parallel microfluidic technologies are outlined in this paper and biological processes involved at the site of inflammation using these platforms are highlighted. The purpose of this review is to show that more than two routes can be followed using alternate materials from separate fields of research. This review provides a novel point of view on current and prospective chemotaxis assays which fits in with the focus of Integrative Biology.

vulnerability to infection. Therefore, the leukocyte adhesion cascade is an important area of study when developing methods to control inflammation by modulating or blocking leukocyte adhesion to the endothelium. The development of anti-inflammatory drugs is largely dependent on research into inflammation using *in vitro* model systems and *in vivo* microcirculation studies. In the past few years, many *in vitro* studies[21] (*e.g.* Boyden chamber, Dunn chamber) have shown the pivotal role of the release of chemokines in leukocyte homing. These assays had significant limitations as experiments were performed in static environments without any shear stress, this is in contrast to *in vivo* conditions where cells are continually exposed to shear stress in flowing blood. New assays, based on the micro-electromechanical systems (MEMS), utilizing continuous-flow microfluidic biochips have been proposed to overcome these limitations. Human capillaries are mimicked within two-dimensional (2D) microfabricated channels in which continuous flow of cells and flow of chemokines are dispensed thanks to a microfluidic pump system. Cells are then free to migrate in 2D (only x–y axis) toward the gradient of chemokine. However, it is necessary to keep in mind that in the *in vivo* milieu, the leukocyte adhesion cascade is not taking place in a smooth environment as in the channel of a microdevice. The interface between the lumen and the underlying tissue is not a linear or flat surface (Fig. 1B), instead it presents a continually changing topography difficult to simulate in a model system. Epoxy resin casts of inflamed and non-inflamed blood vessels confirm this.[22] Thus, the diffusion of chemokines from the extracellular matrix to the lumen encounters a markedly different environment to that presented by *in vitro* models to date. Consequently, standardised microfluidic assays present a reductionist environment in which chemotaxis can be monitored. Hence, to reproduce realistic *in vivo* conditions, microfluidic biochips must present an environment capable of replicating the situation where a chemokine gradient is released from tissues through the endothelium such as at the inflammation site. Therefore, efforts are being made by researchers to enhance the next generation of microfluidic biochips in order to present more physiologically relevant 3D environments for cells to migrate in the x, y and z axes. This review gives a perspective of recent developments in this area, in particular, (1) standard chemotaxis assays, (2) MEMS, (3) microfluidic platforms, (4) shear stress and (5) tools for analysis and interpretation. In this paper, we also review current chemotaxis assay designs and comment on upcoming models which are currently being developed.

Standard chemotaxis assays

One of the most commonly used migration assays is the Boyden chamber/Transwell assay (Fig. 2). This system is used to quantify the migration of cells exposed to different chemokine concentrations. The chamber contains two compartments separated by a microporous filter (with commonly used pore sizes between 2 μm to 12 μm) through which cells migrate. The relevant chemoattractant solution is placed in the lower chamber to create a chemotactic gradient while leukocytes are incubated in the upper chamber. The cells need to squeeze

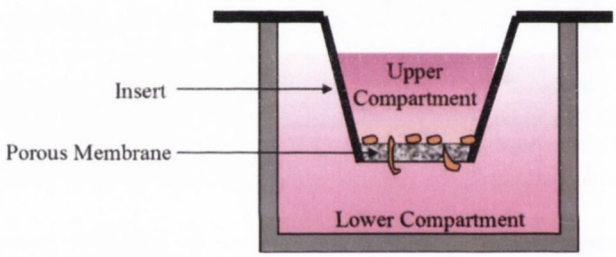

Fig. 2 The Boyden chamber assay is illustrated as two compartments separated with a porous membrane in which cells can migrate through. The lower compartment is filled with a chemoattractant solution creating a gradient by natural diffusion in the upper compartment which contains the cells. The gradient which is generated allows the cells to migrate through the porous membrane into the lower compartment.

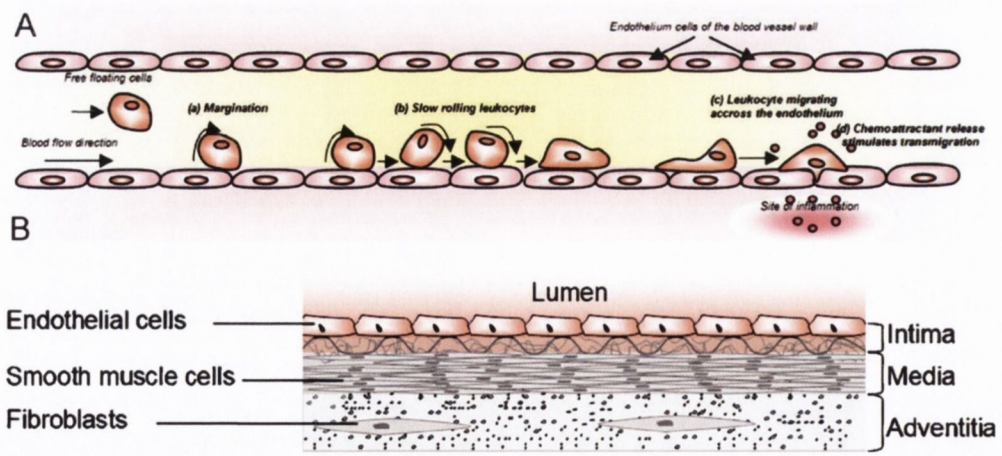

Fig. 1 Model of multistep leukocyte adhesion cascade resulting in transendothelial migration (A). The first step is the initial attachment of free floating leukocytes which leads to the transmigration (a). Interactions between endothelium integrins and cells ligands induce the slowing down of leukocyte (b) which further results in leukocytes migration across the endothelium (c) due to a gradient of chemokine (d). (B) Schematic model of the different layers of a human blood vessel tissue. The inner layer is called the intima. It is structured by a pavement of endothelium maintained by a layer of internal elastic lamina. The middle layer is called the media and is made of smooth muscle cells and elastic tissue. The outer layer is the adventitia which is mainly composed of connective tissue and fibroblasts.

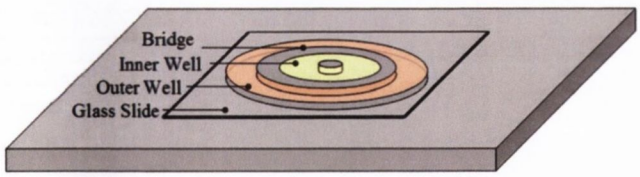

Fig. 3 The Dunn chamber consists of two concentric wells separated by a 20 μm glass bridge (image courtesy of Hawksley Medical and Laboratory Equipment, Lancing, Sussex, UK). Cells are seeded on a glass slide and placed inverted on top of the concentric wells. A gradient is created from the inner well to the outer well and the responses of cells can be visualized in the bridge region.

between the pores of the filter. In some cases endothelial cells are grown on the membrane to replicate the *in vivo* environment. The advantage of the Boyden chamber is that it facilitates the observation of the effect of chemokines on cells, allowing analysis of both chemokinetic (speed at which cells migrate) and chemotactic effects (direction in which cells migrate). One of the limitations of the Boyden chamber is that there is no reliable way to sustain the chemokine gradient. In a matter of hours the chemokine becomes homogeneously diffused in the upper chamber and the cells will no longer migrate through the pores. Another limitation with a Boyden chamber type assay is that there is no way to incorporate the effects of shear stress on the cells under investigation.

The agarose[23] or Dunn chamber assays are other standard chemotaxis assays which have been used to show the importance of chemokine gradients by evaluating leukocyte motility dependant on the concentration of specific chemokines (Fig. 3, 4). These static experiments were implemented predominantly to estimate the ability of particular cells to migrate towards a gradient of chemokines. However, they all have the same disadvantage; the cells are incubated in static conditions and not under hemodynamic shear stress conditions, as would be found as *in vivo*.

Micro-electromechanical systems

Micro-electromechanical systems (MEMS) technology was developed in the 1950s.[24–30] MEMS were facilitated by the development of microfabrication techniques[31–34] which were utilised in the design of the micro-electronic components (*e.g.* transistor, integrated circuit).[35–37] During the 1990s the novel aspects of MEMS were used to combine the mechanical and electronics micrometer elements on a common substrate. The size of these devices was so technologically attractive that, subsequently, many diverse areas of research became interested in miniaturization such as chemistry, biology, bioengineering and physics. Chemical reagents and markers for biomedical studies can be very costly and large volumes of each reagent were previously necessary for each experiment. That is why miniaturisation is a cost effective solution since it reduces the total sample volume from millilitre to nanolitre and maximise the usable surface area on which the reaction is carried out. It was seen as a means of miniaturising the laboratory. A subset of the MEMS devices appeared in the latter part of the 1980s termed "lab-on-a-chip". A wide range of novel mechanical systems emerged utilising new MEMS influenced designs which utilise low volume liquid handling devices[38–43] and biochip platforms.[30,44–46] There were a significant number of advantages in using these designs from the point of view of cost and time. For example, multiple parts of the same assay can be run in sequence; additionally, replicates can be included and run in parallel.[47–50] Biochips can be applied to various fields of medical research including immunology, genomic and proteomic research, as well as pharmacology and toxicology.

In the earliest biochip designs that utilised the effects of biological shear, the architecture of the channels had rectangular cross-sections which precluded laminar flow. More recent advances in soft polymer lithographical processing and design comprised of channels with "U-shape" cross-sections which are better suited for enabling laminar flow. Now, after half a

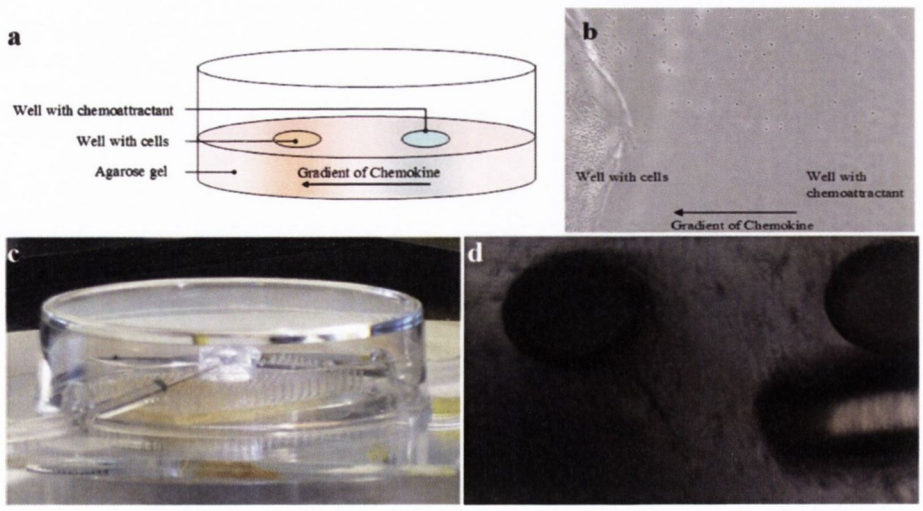

Fig. 4 (a) Schematic model of an under-agarose assay. Depending on the desired number of experimental set points, two or more wells can be punched into the agarose gel. Cells are seeded in one well and a chemoattractant solution is placed in the second well. (b) Cells are then exposed to a gradient of chemokine and are able to migrate under the agarose gel (Source: Cell signalling lab, TCD, 2007). (c) Example of microfluidic biogel. Agarose gel base on vertical PDMS macrofluidic pillar template. Horizontal chemokine gradient generated by opposite side microinjection. (d) Magnification of microneedle chemical injection and PDMS pillar structure (pillar diameter, ϕ = 10 μm). (Courtesy of Dr Adriele Prina-Mello—CRANN—IMM-TCBE (TCD, Dublin); microscope magnification ×10).

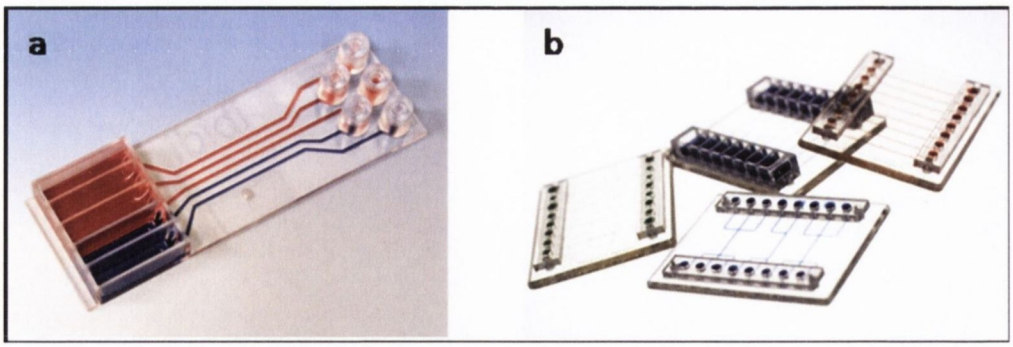

Fig. 5 Examples of commercially available microfluidic biochips. (a) μ-Slide V from the μ-Slide family chip of IBIDI GmbH (Germany) for parallel immunoassays. (b) Different designs of Cellix biochips (Ireland). Each chip contains enclosed microcapillaries that can be coated with different antibodies.

century since the original development of MEMS technology, designs are more advanced and processes of microfabrication are better understood (Fig. 5). As a consequence of this, the layout of a biochip can rapidly be redesigned and that design can be subsequently manufactured with much more ease and at a lower cost. Soft polymer and MEMS technologies can be used for chemotaxis assays and allow detailed dissection of disease processes at the cellular level in a disposable biochip.

Microfluidic platforms

Microfluidic biochips are typically made to mimic human capillaries using a specific channel network. These systems are essential for the study of basic cell signalling related phenomena, such as T-cell chemotaxis,[51,52] bacterial chemotaxis,[53,54] morphogenesis,[30,55] and regulation of gene expression.[56,57] Channels are usually coated with proteins present in extracellular matrix or endothelial cells.

A continuous flow with varying shear stresses can be applied in closed-channels using a precisely controlled microlitre injection or dispensing system.[30,40,41,58,59] The advantage of such devices is that the control of the gradient of chemokines in these channels is predictable, reproducible and easily quantified.[60,61] There are limited reports in the literature of microfluidic devices where tunable concentration gradients can be produced.

The gradient of chemokines in such dual channel microfluidic biochips is created not by physiological means but by the exogenous addition of the chemokine of choice,[60] by alternating gradients,[62] or by natural diffusion between two continuous flows.[58] This is a disadvantage as it does not mimic physiologically relevant concentrations or patterns of release. Even if the surface of the channel is coated with extracellular proteins, it still can not imitate the diffusion of chemokines from the tissue at the site of inflammation, nor the leukocytes migration through the endothelium.

One attractive design option is to grow a confluent layer of endothelial cells on a coated channel. Then, a continuous flow of cells is dispensed over the endothelial cells and the adhesive properties of these cells on the endothelial layer can be observed using standard microscopic procedures.[63]

In a recent review, Keenan and Folch[21] have summarised the technical aspects of current microfluidic biochips in which a gradient of chemokines could be mechanically controlled. The designs which are now possible using advanced computer-aided design (CAD), moulding and manufacturing techniques are limited only by the creativity of researchers. Both biologists and physicists have focused on improving microfluidic biochips, this cross disciplinary collaboration is essential for the successful creation of new model systems. The advantage of this complimentary research is clear and many of the interesting recent designs described below have come from this interdisciplinary approach.

Shear stress

Under different physiological conditions blood vessels are subjected to differing shear stresses. Shear stress is defined as the tangential force per unit area that is exerted by the flowing fluid on the surface of the conduit tube. Shear stress is a potent facilitator of integrin conformational changes during leukocyte arrest on blood vessels and antigen-presenting cells.[64] The magnitude of shear stress is proportional to the velocity gradient near the tube wall, *i.e.* it is dependent on the speed of the flowing blood. Shear stress is expressed in dyne cm^{-2}. The physiological range of shear stresses varies considerably depending on the type of vessel and its inflammatory state (Table 1), typically more than 10 dyn cm^{-2} in arteries and 1 dyn cm^{-2} to 5 dyn cm^{-2} in postcapillary venules.[65] The physiological range of shear stresses for leukocyte recruitment close to the postcapillary venules is usually around 1 to 6 dyn cm^{-2}.[66,67]

Different model systems have shown mechanisms of leukocyte transmigration and described the multistep paradigm for leukocyte recruitment.[68–70] However, recently substantial evidence has been accumulated highlighting the impact of shear stress[71–73] on the induction and enhancement of T cell migration. In that work, shear stress was applied to the cells which would encounter flow physiologically and significant avidity and response differences were detected.[74,75] Due to these innovative *in vitro* methods, leukocyte capture and subsequent rolling are known to be mediated by shear stress.[66,76–78] Transendothelial migration has been reproduced *in vitro* using these biochip designs highlighting the hitherto unknown importance of shear in transmigration due to its ability to modulate the activity of many of the cell

Table 1 Microfluidic shear flow conditions for different type of cells (modified from Kim *et al.*)

Cell type	Shear stress/dyn cm^{-2}	Surface/coating assay	Assay conditions	Ref.
Vascular endothelial cells	10–100		*in vivo*	103
	0.6–22	Gelatin	*in vitro*	104
Hepatocytes	<2	Collagen type I	*in vivo*	103
Mouse embryonic stem cells	6.5–16	Collagen type I	*in vitro*	103, 105
Human umbilical vein endothelial cells (HUVECs)	4–25	Gelatin Collagen type I/III	*in vitro*	103, 106, 107
Bovine/porcine aortic endothelial cells (BAEC-PAEC)	4–25	Fibronectin Collagen type I	*in vitro*	103, 108
HeLa cells	4–25		*in vitro*	103
Chinese hamster ovary (CHO)	2–25	von Willebrand factor	*in vitro*	109
Leukocytes	0.5–10	HUVEC monolayer Fibronectin HUVECs	*in vitro*	72, 61, 110
Neutrophils	0.72–6.2	Human fibrinogen	*in vitro*	74

bound proteins and their ligands involved in the extravasation process.[58,59,79–81]

Tools for analysis and interpretation

There are a wide variety of image analysis software packages available to researchers and these can be used to assess and quantify the morphometric parameters of cells. The commonly used and relevant packages are ImageJ (National Institute of Health),[58] ImagePro (MediaCybernetics), Volocity (ImproVision), Cell (Olympus), Analysis Pro (Analysis), MetaMorph (Molecular Devices). Many of these applications emerged from researchers and spin out companies, for example CellTrek from the University of Virginia. Such software applications are now *de rigueur* in labs which need to track multiple fast-moving cells over a selected area for a fixed time period. Cell-tracking software is necessary for the analysis of the large data sets which are generated from any experiment which involves the tracking of cells in a flow environment. Some software packages are also used for mathematical modelling of proposed chip designs to approximate their expected efficacy.[58,66]

It is beneficial to have mathematical modelling of a continuous flow of cells concurrent with the data which describes the diffusion of a gradient of chemokines, correlating to the experimental data obtained. It enables the researcher to anticipate the movement of the chemokine gradient in response to flow and thus aids in the rationalisation of the design. MatLab (from Mathworks) is one of the most powerful software packages for numerical computing and modelling. As many non-programmers have to work with these packages, the utilization of this kind of software has become easier and more accessible to a wider range of users. Thus, the interface of the software has become more intuitive over time. Comsol Multiphysics (previously femlab, from ComsolLab) is a fully developed Matlab platform integrated in a user-friendly Finite Element Analysis (FEA) Graphic User Interface (GUI). Comsol extensively covers the majority of advanced multiple physics applications in a modular software package; among these there are dedicated modules for fluidodynamics problems. The user friendly interface of this package effectively removes all programming steps from the design process to the post-processing simulation.

Optimised microfluidic systems

Modified Boyden chamber

Some of the researchers are focused on implementing modifications to the existing systems, such as a modified Boyden chamber setup.[82] This design was developed in order to study the effects of shear stress on leukocyte trans-endothelial migration in real time under flow conditions (Fig. 6). Here, the effects of both apical and sub-endothelial chemokines were examined concurrently. The membrane was coated with fibronectin and human umbilical vascular endothelial cells (HUVECs) were cultured on this surface. It had been shown that the chemokine CXCL12 is expressed by the vascular endothelium and is a key regulator of the recruitment of leukocytes from the bloodstream through the endothelium.[83–85] The chemokine CCL5 is released by platelets[86] and is also produced by many cells in the extracellular compartment (basal layer) beneath the endothelium. Thus, cells were loaded at a physiological shear stress of 2 dyn cm^{-2}, and experiments run under continuous flow over a period of time in the presence of both chemokines. Under these conditions there was a significant increase in the number of cells migrating through the HUVEC cell layer in shear conditions compared to shear free conditions. Strikingly, a combination of CCL5 and CXCL12 caused a significant increase in migration, more than would be observed when combining the effect of the individual chemokines. Most interestingly, this observed increase in migration due to combining the effects of both chemokines was only observed under flow conditions. This indicates that the optimal efficacy of chemokines in

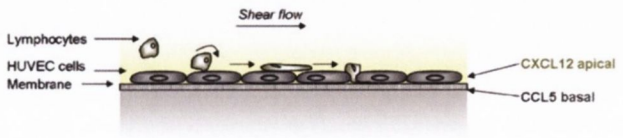

Fig. 6 Representation of the modified Boyden chamber of Schreiber *et al.*[82] for studying the transmigration of lymphocyte under flow conditions. Cells are migrating through the endothelial cells coated membrane undergoing a physiological shear flow.

promoting extravasation through the endothelium is dependent on shear stress.

The advantage of the model described above is that it allows the observer to evaluate the different responses of lymphocytes to chemokines and shear stress in real time. The principle steps of the leukocyte adhesion cascade; rolling, capture and transmigration, can be visually observed and recorded through the endothelial layer. Combinations of chemokines can be presented to the cells and the synergistic effects of apical and sub-endothelial release of chemokines can be evaluated.

However, chemokines loaded in the bottom compartment are in solution. That means that the diffusion of chemokine through the insert is from liquid to liquid. Although this system has yielded interesting results by releasing a combination of chemokine, the conditions of this assay are still far from ideal.

Ladder chamber

Saadi *et al.*[79] described a device which allows the study of migration of cells towards a gradient of chemokines (Fig. 7). An interesting aspect in this design is that the gradient of chemokines originates from a "reservoir" and is diffused through a collagen type I gel dispensed in the microgrooves. These microgrooves connect the "reservoir" channel with a channel in which cells are continuously flowing. Channels were coated with fibronectin in order to mimic the presentation ligands on the endothelium. A steady state gradient was set up in 15 to 18 min and could be maintained for 3 h. Once the gradient was established, experiments were run with neutrophils and interleukin-8 (IL-8) was dispensed in the "reservoir" channel. Neutrophils were then dispensed in the continuous flow channel. Once the cells reached a microgroove containing collagen/IL-8 they migrated through the collagen in the direction of the IL-8 gradient.

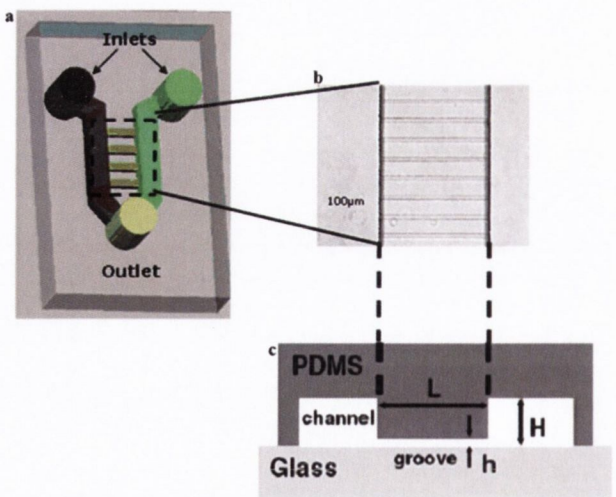

Fig. 7 Design of the Ladder chamber (a) for generating a diffusion of chemokines from the right channel (chemokine) to the left channel (cells). Both channels are connected by horizontal microgrooves (b) of 3–10 µm height (c), ten times bigger than both main channels (100 µm). With kind permission from Springer Science + Business Media: *Biomed. Microdevices*, Generation of stable concentration gradients in 2D and 3D environments using a microfluidic ladder chamber, **9**, 2007, 627–635, Saadi, W. *et al.*, figure 1.

This inventive chamber design is useful for studying the ability of cells to migrate towards a gradient of chemokines found at areas of inflammation throughout the tissue. In previous microfluidic assays, cells were exposed to a shear stress that can influence the migration of cells in the direction of the flow. In the Ladder chamber, the diffusion of chemokines from the microgrooves allows cells to move perpendicular to the central flow. The chemotactic ability of multiple chemokines can be assessed using this design in the presence or absence of shear stress.

One notable drawback, the authors point out, is that only the cells which are localized close to the border of the microgroove can "feel" the gradient of chemokine. The gradient is not dispensed into the main flow of cells as *in vivo* but is only next to the microgroove. This means that the amount of cells which may actually have the potential to migrate toward such a gradient is considerably diminished and solely dependent on their position in the channel.

It is interesting to point out that a parallel study was carried out in a similar channel network[87] in which microchannels laterally constrain cell morphology. This system allows localised drug delivery to the anterior and posterior regions of locomoting neutrophils. This results in observable mechanical changes in the leading or trailing edges of motile cells visualized using optical microscopy. Localization of actin and microtubules was tracked in live cells providing real time observation of the cytoskeletal dynamics. This assay enables precise characterisation of the morphology of the cells crawling towards a gradient of chemokine under complex mechanical constrains imposed, for example, by human connective tissue. A drawback of that device is that cells are constrained in hard polymer and not in soft flexible tissue as in *in vivo*. Therefore, some reservations can be made regarding direct extrapolation of these cytoskeletal changes on the cells migrating in an extracellular matrix-like environment.

Hydrogels in microfluidics

Microfluidics technology offers a wide scope of applications for biomaterials, especially for medical and biological uses. However, biomaterials properties need to be optimised and functionally adjusted in order to mimic biological interfaces. Therefore there is an increasing demand in developing and optimising new materials to address such problems in biology and medicine.[88] One of the promising solutions is presented by the use of hydrogels. A hydrogel is a network of polymer chains that are water-insoluble in which water is the dispersion medium; agarose or collagen are common examples of such gels. The advantage of using a synthetic polymeric scaffold is that it offers the capacity for rapid transport and exchange of materials. Diffusion of a biochemical signal is then possible through the gel for cells feeding or stimulation of embedded cells.[89]

Hydrogel-based microfluidic devices are relatively new, yet they have already shown much promise and produced some interesting results which will be outlined below. The idea of a hydrogel based design, as with the other microfluidic designs

we have described, is to reproduce an environment which presents the same *in vivo* properties of blood vessels. It has previously been shown that cells are able to migrate under an agarose gel toward a gradient of chemokines.[23] Unfortunately, these agarose assays enable no fine control of the generation of the gradient of chemokines and cells move under static conditions. Recently, by combining the advantages of both "under-agarose assays" and microfluidic biochips, hydrogel-based microfluidic devices have been developed to investigate chemotaxis.

Microfluidic polymeric networks can be fabricated by using conventional soft lithography stamping as reported in the literature.[64,90–92] Several techniques are applied depending on the rheological properties of the polymers used. We will now discuss a subsection of microfluidic devices which are composed almost entirely of hydrogels.

Hydrogel-based microfluidic device

In one example of a microfluidic hydrogel device,[93] Cheng *et al.* based their research on the design of the "under-agarose assay" using standard molding processes and three channels composed of agarose were molded on a fibronectin-coated glass side (Fig. 8).

The diffusion coefficient of FITC-Dextran in agarose is well established[60,94,95] and is used to investigate putative generation of a gradient of chemokines in many systems. A fluorescein solution was loaded in the source channel of the design outlined in Fig. 8 and the center channel and sink channel were loaded with PBS. The difference in intensity of FITC-dextran in the three channels enabled Cheng *et al.*[93] to show that a concentration gradient is formed from the source to the sink channel within 10 min.

These researchers have met the challenge of developing a microchannel composed of hydrogel. The system is stable and a gradient of chemokines can be produced through the gel enabling cells to migrate from the centre channel loaded with cells toward the chemokine gradient.

Cheng *et al.* are presently addressing the challenge of implementing their microfluidic channels with continuous physiological flow. They have already tested the application of shear stress in the centre channel which had been coated with endothelial cells. This hydrogel channel system would be a more physiologically relevant environment for chemotaxis than hard plastic designs as it more accurately mimics the extracellular matrix beneath the endothelium of blood vessels. If this device can be refined to allow creation of relevant shear stresses, it could represent a dramatic departure for chemotaxis assays in general and allow the investigation of some interesting sub-endothelial events post-extravasation.

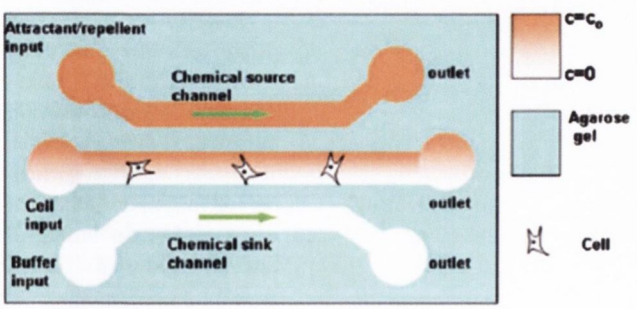

Fig. 8 Representation of a hydrogel channel network by Cheng *et al.*[93] composed of three independent channels molded in an agarose gel matrix. The upper channel is the reservoir that contains chemokine which is diffused through the agarose gel. A gradient of chemokine is generated in the center channel which contains cells. *Reproduced by permission of The Royal Society of Chemistry.*

Microfluidic hydrogel using a sacrificial element

Another example of a microfluidic hydrogel network[96] is the model described by Golden and Tien based on sacrificial layer microfluidic fabrication methods.[97] Standard microfluidic techniques are used to develop a polydimethylsiloxane (PDMS) stamp in order to mould a channel network in gelatine. Then, a hydrogel is dispensed on top of the gelatine channels. The gelatine can be easily flushed away with PBS, leaving behind the hydrogel cast, by applying heat to the plate. This works because hydrogel jellifies at room temperature and gelatine melts at 37 °C, leaving only a hydrogel channel network remains (Fig. 9).

Different hydrogels can be used to form microfluidic gel channels (Matrigel, collagen, fibrin) (Fig. 10(a)) and a combination of gel layers can be used (Fig. 10(b)). Thus, depending on the experimental conditions a specific gel can be the substrate while another type of gel can be used to form the top layer (Fig. 10(c)). The diffusion of macromolecules into the gel is possible by applying differential pressures between the inlet and the outlet of the channel. The biocompatibility of such gels is high enough to enable the viability of embedded cells under a perfusion procedure. Endothelial cells were also able to grow in a collagen network (Fig. 10(d)). Cells can also be embedded in the matrix, for instance collagen can be mixed, before casting, with fibroblast (Fig. 10(e)).

The advantage of this hydrogel networks is very broad. Hydrogels are biocompatible and cells grow easily in such a matrix. The diffusion of molecule into gel shows that perfusion conditions could be created in such an environment. It is possible to envisage growing cells in the channel and then perfuse the gel with a chemokine prior to inserting in into the channel. The natural diffusion of chemokine in a collagen or agarose gel is well established.[98–100] If a continuous flow of T-cells are running into a coated channel in a natural-like environment with a diffusion of chemokine, it might be

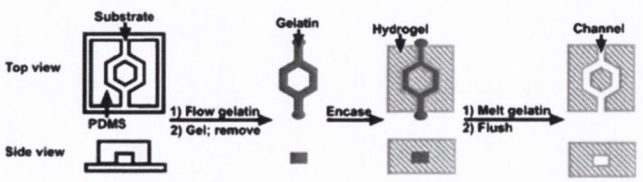

Fig. 9 Illustration of the fabrication of microfluidic hydrogels network by Golden and Tien[96]. In brief, a PDMS stamp is sealed on a substrate creating microfluidic architecture. The introduction of sacrificial gelatine at 4 °C and further gelation at 23 °C creates a gelatine mesh. The mesh is then encapsulated in hydrogel (type collagen, fibrinogen, Matrigel) and polymerized. The sacrificial gelatine is flushed away after melting at 37 °C creating an open microchannel in a hydrogel environment. *Reproduced by permission of The Royal Society of Chemistry.*

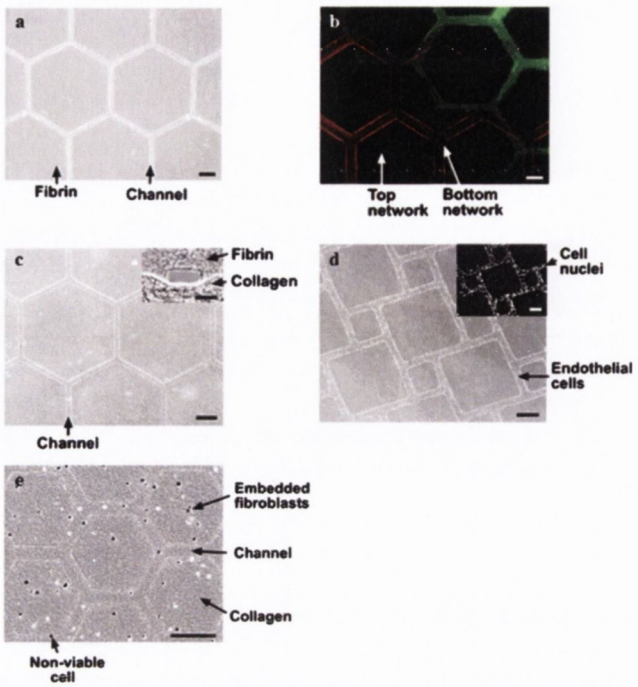

Fig. 10 Sample of microfluidic hydrogels. (a) A hexagonal channel network encasted in a fibrin gel. (b) Fluorescence images of superposed collagen gel layers. (c) Phase contrast image of a network channel designed on a combination of collagen (bottom layer) and fibrin (top layer). (d) Monolayer of endothelial cells growing in the collagen channel. (e) Embedded fibroblasts in collagen gel with nuclei stained in blue (Hoechst 33342). *Reproduced by permission of The Royal Society of Chemistry.*

interesting in considering that this device could be used as an implemented chemotaxis assay.

"Gel" cage in microfluidic device

A 3D gel scaffold[101] has been developed in a creative microdevice (Fig. 11) for the study of the morphogenesis of endothelial cells (EC) under physiological shear stresses in ECM-like environment. Two parallel channels controlling fluid flow are connected to a central "gel" cage for 3D cell culture. That cage presents a PDMS wafer design providing a mechanical support for hydrogels such as collagen. Pro-angiogenic gradient is diffused through the matrix under static flow and is stable for up to 40 h. However, to get a constant gradient over a longer period of time a slow flow is established in the two microchannels to generate interstitial flow through the cage. Encapsulated or monolayer endothelial cells were cultured in collagen for up to seven days. Time lapse images shows EC sprouting mechanisms over 40 h from initial root-like structure to lumen-like structure. The morphology of EC changes depending on the presence or absence of an interstitial pro-angiogenic gradient. An isolated ring-like configuration was formed with no gradient, while cellular cords or lumen-like structures were observed in the presence of a gradient.

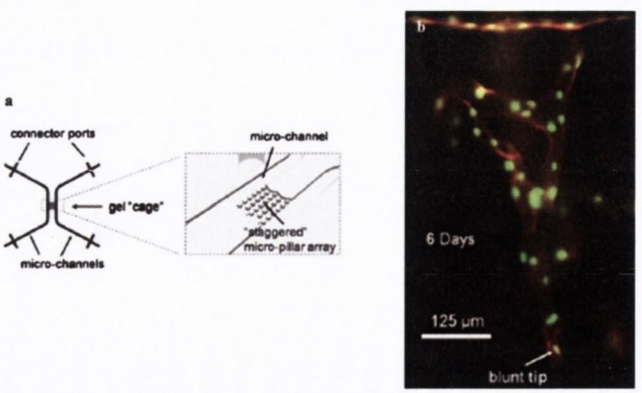

Fig. 11 Schematic of the microfluidic device by Vickerman *et al.*[101] consisting of two parallel channels and a central "gel" cage. PDMS micropillars provide a mechanical support to collagen. An endothelial cell monolayer cultured for six days presents a capillary-like structure. *Reproduced by permission of The Royal Society of Chemistry.*

The advantages of such 3D devices in the research of angiogenesis are considerable. Such an approach consolidates the main factors that an ideal *in vitro* model system should contain. Cells encapsulated in the "gel" cage undergo a physiological shear stress but, to date, the generation of interstitial shear has not been possible. So far, in the examples used, physiological shear stress has been considered. Interstitial flow is also important as it corresponds to the mechanical changes within the human tissue due to the blood flow. Therefore, interstitial stress is an important parameter to take into account during studies of cell migration into tissue. The gel cage has proven its efficacy for growth of endothelial cells, but other cells can be encapsulated in the hydrogel matrix. The behaviour of leukocytes under continuous shear stress, with or without gradient of chemokine, has been widely studied. However, a key step in leukocyte homing is the migration of cells within tissue. Working with this device could elucidate a number of cell signalling interactions which occur between tissue and leukocyte morphology under interstitial flow, as many of these mechanisms still remain unclear.[102]

3D extracellular matrices

Native tissues are rich in fibrous materials such as fibrin, collagen, fibronectin, laminin and others, therefore presenting heterogeneous properties. Synthesized matrices have already been widely used to study tissue morphogenesis and the interaction between cells and ECM. However, these matrices present isotropic properties in which cells are randomly distributed. Gillette *et al.* have microfabricated three-dimensional cell-seeded matrices[103] for a physiologically relevant *in vitro* environment. They have demonstrated *in situ* collagen fibre assembly creating three-dimensional matrices which contain collagen I, Matrigel, fibrin or alginate. Different matrices can be seeded with cells such as human umbilical vein endothelial cells (HUVECs). Matrices laced with collagen have shown encouraging results in mediating collagen fibres at the interface of two phases, and also present a stable environment for multicellular structures. HUVECs seeded in matrices containing collagen completely filled the channels. So far, microfluidic biochips have only been coated with cells on their surface but have not yet organised to form a capillary structure. The varieties of ECM composition that have been

developed present a simple approach to interface multiple 3D matrices for tissue engineering but also for biological studies. HUVEC-seeded collagen within hydrogel scaffolds can be used as an enhanced environment for the study of cell–cell interaction.

Potential alternative microfluidic models

Tissue engineering is a relatively new and dynamic research field; nonetheless, it is an exceptionally challenging and promising research area for the future. Despite enormous advances in tissue engineering, which include the clinical approval of tissue engineered skin, a number of scientific barriers still prevent the fabrication of more complex organs. Hydrogels have also been used as templates for immuno-isolation and microencapsulation technology.[104] Therefore, to engineer functional tissues it is important to engineer a vascular network that can perform a similar function to *in vivo* tissue. Several studies have used biological hydrogels to mimic this complex *in vivo* environment.[65,104–107] Developing microvascularised tissue is an important goal in tissue engineering.

Natural materials have also been used in conjunction with tissue-engineering scaffolds to provide more support for cell growth. For example, fibrin-filled poly(lactic-*co*-glycolic acid) or PLGA scaffolds have been used to modulate tissue invasion *in vivo* for bone regeneration.[107] Fibroblasts, osteoblasts, vascular smooth muscle cells, and chondrocytes successfully attach and grow to these hydrogel scaffolds. Poly(ethylene) glycol (PEG) is another polymer widely used in tissue engineering to improve the biocompatibility of implanted medical devices and also used as an extracellular matrix (ECM) model.[108,109] In recent work, it has been used in combination with other polymers for the synthesis of copolymers based on disulfide-containing PEG diacrylate (PEGDA)[110] to crosslink thiol-modified hyaluronan and gelatine macromonomers (natural components of *in vivo* ECM). In another study, a network is developed with PEGDA and PEG to study the influence of artificial matrices on human stem cells.[111] Polysialic acid is a polymer known to play a regulatory role in neurogenesis and neural functions. Based on that, a promising polysialic acid-based hydrogel[112] has been developed which has successful biocompatibility and stable properties under physiological conditions.

Using a combination of microfluidic channel technology and soft lithography patterning of hydrogels, these scaffolds can localise the delivery of cell growth-factor and increase the cell surface binding reaction. Therefore, making a parallel with microfluidic biochips, tissue engineering applications provide a new method for the study of inflammatory diseases. Using MEMS technology to supply a support for the three-dimensional scaffold,[105] artificial capillaries can be used to study the impact of shear stress on cells in a more physiological milieu and could potentially form the nucleus of groundbreaking applications in the development of chemotaxis assays.

Fidkowski *et al.* reported experimental results achieved by using a biodegradable and biocompatible microvasculature network[65] developed in poly(glycerol sebacate) (PGS). Different steps are necessary to build up this artificial capillary. A silicon wafer is processed by standard lithography techniques[96] and then spin coated with sucrose solution. PGS prepolymer is poured over the coated wafer and cured. After the dissolution of the sucrose layer, the patterned PGS film is released and placed between a glass slide and a flat PGS layer. It is cured several times to facilitate the bonding between the two layers. The moulding process results in a transparent capillary network capable of resisting the effect of a flow rate of 100 $\mu L\ h^{-1}$. Thus, endothelial cells can be grown in this network under perfusion culture condition for a period up to 4 weeks. Confluency is reached after 14 days. This device is suitable for tissue engineering because of the biocompatible network developed in PGS. It is important that such material provides an environment that can support physiological flow and mass transport. Its *in vivo* compatibility makes it an interesting model for use during a chemotaxis assay. This network can be bonded to a well which has previously been loaded with a chemokine. PGS has similar mechanical properties to blood vessels such as the ability to permit transport of oxygen and carbon dioxide. Chemokines could thus be diffused through a PGS network creating a chemotactic gradient in a physiologically relevant environment.

Using chemotaxis systems to elucidate the underlying biology

Cell–extracellular matrix interactions are essential for the control of cell adhesion in many fundamental biological processes such as angionenesis, apoptosis and inflammation. They can also have a profound impact on normal and tumor cell signal transduction cascades. The results of the studies on cell functions during the tissue-specific homing process indicate that mechanical properties of the surrounding microenvironment are critical for regulating cell-ECM interactions.[113–115]

Relevant cell-based assays can be carried out on plates coated for example, with ECM-derived integrin ligands.[116] Thus, the experimental models implementing cell exposure to molecules adsorbed on substrates enabled to demonstrate that collagens, laminins, 'RGD'-containing proteins (fibronectin, fibrin, vitronectin) as well as immunoglobulin superfamily proteins (VCAM, ICAMs) are capable of mediating cell adhesion.[117]

Working in a physiologically relevant *in vivo* milieu is crucial. The environment for cell-based assays is widely imitated utilising soft gel scaffolds. Initially, agarose has been the most used soft gel, because of its cost effectiveness. Current improvements in biomaterials synthesis allow the researchers to use fine ECM-like matrices (*i.e.* hydrogels). Biochemical signals are diffused through these gels and a library of chemokines and chemokine receptors has been built up.[118,119]

Parallel to advances in other biological assays, microfluidic platforms presented a challenging new setting for cells to evolve in. It was possible with these types of systems to perform real time observations of leukocyte adhesion cascades, consisting of initial contact, slow rolling and adherence of cells on the surface of the biochips with different surface coatings. Cell adhesion has been shown to depend on the characteristics of ECM and in addition it has proven to be

shear-rate-dependent.[120] However, this model system, for all its advantages, is incomplete as one important step is missing. That is, the migration of cells through the endothelium to the tissue.

It is at this juncture in general biochip development that the researchers were able to combine the technologies of gel chemotaxis and microfluidic assays to further develop the *in vitro* model. It has previously been shown that it is possible to observe the real time morphogenesis of neurons in the presence of chemokine gradient in an ECM-like milieu under interstitial flow conditions.[101] The migration of cells towards a gradient of chemokine in a hydrogel scaffold has also been demonstrated.[93] Therefore, merging of these technologies together provided the missing bridge between gel chemotaxis assays with no flow and 3D chemotaxis under flow conditions. As a consequence, further observations and interpretations of multimolecular mechanisms underlying cell adhesion, cell signalling pathways and dynamic changes of cell morphology during inflammation process are expected to be seen using these types of devices.

Conclusions

Studies focused on inflammation-associated phenomena are widely carried out by biologists to better understand how the immune system responds to foreign bodies and pathogens. Limitations in standard chemotaxis assays inspired the biologists to work jointly with physicists, engineers and chemists. In this review, we have shown the evolution of this multidisciplinary area, presenting some examples of next generation microfluidic platforms, in order to elucidate diverse biological processes developing at the inflammation site.

Current microfluidic platforms have certain advantages particular to their design and have achieved widespread use in biological assays. From simple microfluidic devices to highly advanced biochips, the researchers at present, can use computer controlled flow devices and cell tracking software in the most sophisticated experimental environments under study, such as for example, the models imitating the progress of inflammation. However, even the ideal situation in an *in vitro* environment by default is still far from the realistic *in vivo* scenario because *in vivo* conditions are much more complex than those found in conventional 2D biochips. Therefore, the new challenge for researchers is to combine a shear flow environment with a 3D endothelial layer which allows a natural diffusion of chemokines through a tissue-like basal matrix. The new devices described here are expected to provide a better approximation of the *in vivo* physiological environment for cells and are intended to include many more *in vivo* related parameters than are currently offered by standard microfluidic biochips.

We also show that tissue engineering, traditionally a separate area of research, is now providing leads to the development of new chemotaxis assays. The central idea of this work is to design capillaries which mimic the microvasculature capable of withstanding physiological flow rates.[65]

It is an interesting exercise to chart the evolution of microfluidic platforms. It started with simple straight channels connected to a pump to deliver a controlled shear stress to specific type of cells. Since it has been established how important shear stress is for leukocyte homing, attempts were made to introduce finely controlled chemokine gradients. The more progress has been made, the more it was noticed that it was difficult to include all the important *in vivo* parameters in a single chip. It is possible, of course, to work on different parameters at different times. But presently it is understood the challenge is to work on multiple and competing parameters simultaneously. We can say, at this time, standard microfluidic assays for chemotaxis which utilise shear flow, include controlled chemokine gradients and surfaces which are coated with ligands.

Would it be realistic and honest to say that with these parameters we are closer to an *in vivo* model? In reality, we feel much work needs to be done. For this purpose, we need to keep in mind that being focused on one area of a research field is not always helpful when developing new assays. However, every researcher needs to revisit and rethink existing designs in order to enable new assays to evolve in this area. That is why we have included the current progress made in tissue engineering. The goal of tissue engineering in this area is to develop vascularised tissues as well as mimicking the complex structure and architecture of the surrounding biological tissues. Therefore, synthetic and natural hydrogels are important milestones to develop biomaterials that are capable of being treated by physiological flow, which respond in a physiological manner and are capable of facilitating extravasation.

In light of this, we can predict that advanced research in chemotaxis assay based on hydrogels will be focused towards smart, injectable and highly physiologically adaptable scaffolds where vascularisation and chemokine gradients will be generated by the natural adaptive response of the *in vivo* surrounding tissue.

Acknowledgements

ST and PO were supported by the grants from Science Foundation of Ireland and Health Research Board of Ireland.

References

1 L. Stephens, L. Milne and P. Hawkins, *Curr. Biol.*, 2008, **18**, R485–R494.
2 G. Cinamon, V. Grabovsky, E. Winter, S. Franitza, S. Feigelson, R. Shamri, O. Dwir and R. Alon, *J. Leukocyte Biol.*, 2001, **69**, 860–866.
3 W. Savino, D. M. Villa-Verde, D. A. Mendes-da-Cruz, E. Silva-Monteiro, A. R. Perez, P. Aoki Mdel, O. Bottasso, N. Guinazu, S. D. Silva-Barbosa and S. Gea, *Cytokine Growth Factor Rev.*, 2007, **18**, 107–124.
4 T. Sato, H. Thorlacius, B. Johnston, T. L. Staton, W. Xiang, D. R. Littman and E. C. Butcher, *J. Immunol.*, 2005, **174**, 277–283.
5 A. Chan, A. Filer, G. Parsonage, S. Kollnberger, R. Gundle, C. D. Buckley and P. Bowness, *Arthritis Rheum.*, 2008, **58**, 707–717.
6 Y. Lu, J. Wang, Y. Xu, A. E. Koch, Z. Cai, X. Chen, D. L. Galson, R. S. Taichman and J. Zhang, *Mol. Cancer Res.*, 2008.
7 Y. Lu, Z. Cai, D. L. Galson, G. Xiao, Y. Liu, D. E. George, M. F. Melhem, Z. Yao and J. Zhang, *Prostate*, 2006, **66**, 1311–1318.

8 S. Shahrara, A. E. Proudfoot, C. C. Park, M. V. Volin, G. K. Haines, J. M. Woods, C. H. Aikens, T. M. Handel and R. M. Pope, *J. Immunol.*, 2008, **180**, 3447–3456.
9 B. Boldajipour, H. Mahabaleshwar, E. Kardash, M. Reichman-Fried, H. Blaser, S. Minina, D. Wilson, Q. Xu and E. Raz, *Cell*, 2008, **132**, 463–473.
10 R. Mohle, F. Bautz, S. Rafii, M. A. Moore, W. Brugger and L. Kanz, *Ann. N. Y. Acad. Sci.*, 1999, **872**, 176–185, discussion 185-176.
11 P. Schaerli and B. Moser, *Immunol. Res.*, 2005, **31**, 57–74.
12 M. O'Hayre, C. L. Salanga, T. M. Handel and S. J. Allen, *Biochem. J.*, 2008, **409**, 635–649.
13 K. Nistala, H. Moncrieffe, K. R. Newton, H. Varsani, P. Hunter and L. R. Wedderburn, *Arthritis Rheum.*, 2008, **58**, 875–887.
14 G. Li, H. Adesnik, J. Li, J. Long, R. A. Nicoll, J. L. Rubenstein and S. J. Pleasure, *J. Neurosci.*, 2008, **28**, 1085–1098.
15 W. Kessler, T. Budde, M. Gekle, A. Fabian and A. Schwab, *Pfluegers Arch.*, 2008, **456**, 813–823.
16 C. Weidt, B. Niggemann, B. Kasenda, T. L. Drell, K. S. Zanker and T. Dittmar, *Curr. Stem Cell Res. Ther*, 2007, **2**, 89–103.
17 M. Li and R. M. Ransohoff, *Prog. Neurobiol.*, 2008, **84**, 116–131.
18 J. R. Bradley, *J. Pathol.*, 2008, **214**, 149–160.
19 J. A. Carnegie, *Biol. Reprod.*, 1994, **50**, 413–420.
20 D. M. Rose, R. Alon and M. H. Ginsberg, *Immunol. Rev.*, 2007, **218**, 126–134.
21 T. M. Keenan and A. Folch, *Lab Chip*, 2008, **8**, 34–57.
22 T. W. Secomb, M. A. Konerding, C. A. West, M. Su, A. J. Young and S. J. Mentzer, *Proc. Natl. Acad. Sci. U. S. A.*, 2003, **100**, 7231–7234.
23 B. Heit and P. Kubes, *Sci. STKE*, 2003, **2003**, PL5.
24 R. P. Feynman, presented at the Annual meeting of the American Physical Society, Caltech, 1959 (http://www.zyvex.com/nanotech/feynman.html).
25 A. K. Deisingh, *Analyst*, 2003, **128**, 9–11.
26 A. D. Livingston, C. J. Campbell, E. K. Wagner and P. Ghazal, *Genome Biol.*, 2005, **6**, 112.
27 C. T. Nguyen, *IEEE Trans. Ultrason. Ferroelectr. Freq. Control*, 2007, **54**, 251–270.
28 D. L. Polla, A. G. Erdman, W. P. Robbins, D. T. Markus, J. Diaz-Diaz, R. Rizq, Y. Nam, H. T. Brickner, A. Wang and P. Krulevitch, *Annu. Rev. Biomed. Eng.*, 2000, **2**, 551–576.
29 G. Kotzar, M. Freas, P. Abel, A. Fleischman, S. Roy, C. Zorman, J. M. Moran and J. Melzak, *Biomaterials*, 2002, **23**, 2737–2750.
30 A. Long, S. Mitchell, D. Kashanin, V. Williams, A. Prina Mello, I. Shvets, D. Kelleher and Y. Volkov, *Ann. N. Y. Acad. Sci.*, 2004, **1028**, 313–319.
31 R. Zaouk, B. Y. Park and M. J. Madou, *Methods Mol. Biol.*, 2006, **321**, 5–15.
32 L. Martynova, L. E. Locascio, M. Gaitan, G. W. Kramer, R. G. Christensen and W. A. MacCrehan, *Anal. Chem.*, 1997, **69**, 4783–4789.
33 J. Soo Ko, H. C. Yoon, H. Yang, H. B. Pyo, K. Hyo Chung, S. Jin Kim and Y. Tae Kim, *Lab Chip*, 2003, **3**, 106–113.
34 B. Ziaie, A. Baldi, M. Lei, Y. Gu and R. A. Siegel, *Adv. Drug Delivery Rev.*, 2004, **56**, 145–172.
35 N. L. Mills, N. Amin, S. D. Robinson, A. Anand, J. Davies, D. Patel, J. M. de la Fuente, F. R. Cassee, N. A. Boon, W. Macnee, A. M. Millar, K. Donaldson and D. E. Newby, *Am. J. Respir. Crit. Care Med.*, 2006, **173**, 426–431.
36 M. Verzeano and J. D. French, *Electroencephalogr. Clin. Neurophysiol.*, 1953, **5**, 613–616.
37 R. E. George, *Ann. Phys. Med.*, 1956, **3**, 66–67.
38 A. Wixforth and J. Scriba, *GIT Labor-Fachzeitschrift*, 2002.
39 J. Vykoukal, *Micro. Total Anal. Syst.*, 2001, 72–74.
40 W. Papst, *Klin. Monatsbl. Augenheilkd.*, 1983, **182**, 167–169.
41 D. A. Ogella, *J. Indian Med. Assoc.*, 1999, **97**, 436–437, 441.
42 Tobias Lilliehorn, Ph.D. Thesis, Uppsala University, 2003.
43 Y. Choi, J. Vukasinovic, A. Glezer and M. G. Allen, *Biomed. Microdevices*, 2008.
44 K. M. Renshaw, D. E. Orr and K. J. L. Burg, *Biotechnol. Prog.*, 2005, **21**, 538–545.
45 K. Chakrabarty and F. Su, 2005.
46 C. W. Frevert, G. Boggy, T. M. Keenan and A. Folch, *Lab Chip*, 2006, **6**, 849–856.
47 O. P. Kallioniemi, *Ann. Med.*, 2001, **33**, 142–147.
48 N. Broude, K. Woodward, R. Cavallo, C. Cantor and D. Englert, *Nucleic Acids Res.*, 2001, 29.
49 L. C. Waters, S. C. Jacobson, N. Kroutchinina, J. Khandurina, R. S. Foote and J. M. Ramsey, *Anal. Chem.*, 1998, **70**, 158–162.
50 R. Liu, J. Yang, R. Lenigk, J. Bonanno and P. Grodzinski, *Anal. Chem.*, 2004, **76**, 1824–1831.
51 A. Prina-Mello, Y. Volkov, D. Kelleher and P. J. Prendergast, *Ann. Biomed. Eng.*, 2003, **31**, 1106–1113.
52 N. L. Jeon, H. Baskaran, S. K. W. Dertinger, G. M. Whitesides and L. V. D. Water, *Nat. Biotechnol.*, 2002, **20**, 826–830.
53 H. Mao, P. S. Cremer and M. D. Manson, *Proc. Natl. Acad. Sci. U. S. A.*, 2003, **100**, 5449–5454.
54 T. Ahmed and R. Stocker, *Biophys. J.*, 2008.
55 S. K. Dertinger, X. Jiang, Z. Li, V. N. Murthy and G. M. Whitesides, *Proc. Natl. Acad. Sci. U. S. A.*, 2002, **99**, 12542–12547.
56 J. S. Marcus, W. F. Anderson and S. R. Quake, *Anal. Chem.*, 2006, **78**, 956–958.
57 J. S. Marcus, W. F. Anderson and S. R. Quake, *Anal. Chem.*, 2006, **78**, 3084–3089.
58 F. Lin and E. C. Butcher, *Lab Chip*, 2006, **6**, 1462–1469.
59 D. Irimia, S. Y. Liu, W. G. Tharp, A. Samadani, M. Toner and M. C. Poznansky, *Lab Chip*, 2006, **6**, 191–198.
60 G. M. Walker, J. Sai, A. Richmond, M. Stremlere and C. Y. Chung, *Lab Chip*, 2005, **5**, 611–618.
61 C. Joanne Wang, X. Li, B. Lin, S. Shim, G. L. Ming and A. Levchenko, *Lab Chip*, 2008, **8**, 227–237.
62 Y. Liu, J. Sai, A. Richmond and J. P. Wikswo, *Biomed. Microdevices*, 2008.
63 E. W. Young, A. R. Wheeler and C. A. Simmons, *Lab Chip*, 2007, **7**, 1759–1766.
64 C. Laudanna and R. Alon, *Thromb. Haemostasis*, 2006, **95**, 5–11.
65 C. Fidkowski, M. R. Kaazempur-Mofrad, J. Borenstein, J. P. Vacanti, R. Langer and Y. Wang, *Tissue Eng.*, 2005, **11**, 302–309.
66 U. Y. Schaff, M. M. Xing, K. K. Lin, N. Pan, N. L. Jeon and S. I. Simon, *Lab Chip*, 2007, **7**, 448–456.
67 E. Gutierrez and A. Groisman, *Anal. Chem.*, 2007, **79**, 2249–2258.
68 R. A. Warnock, S. Askari, E. C. Butcher and U. H. von Andrian, *J. Exp. Med.*, 1998, **187**, 205–216.
69 W. Y. Lee and P. Kubes, *J. Hepatol.*, 2008, **48**, 504–512.
70 P. Kubes and S. M. Kerfoot, *News Physiol. Sci.*, 2001, **16**, 76–80.
71 F. W. Luscinskas, Y. C. Lim and A. H. Lichtman, *Nat. Immunol.*, 2001, **2**, 478–480.
72 C. Verdier, C. Couzon, A. Duperray and P. Singh, *J. Math. Biol.*, 2008.
73 J. M. Rutkowski and M. A. Swartz, *Trends Cell Biol.*, 2007, **17**, 44–50.
74 G. Cinamon and R. Alon, *J. Immunol. Methods*, 2003, **273**, 53–62.
75 J. J. Campbell, J. Hedrick, A. Zlotnik, M. A. Siani, D. A. Thompson and E. C. Butcher, *Science*, 1998, **279**, 381–384.
76 R. Alon, D. A. Hammer and T. A. Springer, *Nature*, 1995, **374**, 539–542.
77 T. K. Hsiai, S. K. Cho, P. K. Wong, M. H. Ing, A. Salazar, S. Hama, M. Navab, L. L. Demer and C. M. Ho, *Ann. Biomed. Eng.*, 2004, **32**, 189–201.
78 S. K. Murthy, A. Sin, R. G. Tompkins and M. Toner, *Langmuir*, 2004, **20**, 11649–11655.
79 W. Saadi, S. W. Rhee, F. Lin, B. Vahidi, B. G. Chung and N. L. Jeon, *Biomed. Microdevices*, 2007, **9**, 627–635.
80 B. G. Chung, F. Lin and N. L. Jeon, *Lab Chip*, 2006, **6**, 764–768.
81 K. C. Chaw, M. Manimaran, F. E. Tay and S. Swaminathan, *Microvasc. Res.*, 2006, **72**, 153–160.
82 T. H. Schreiber, V. Shinder, D. W. Cain, R. Alon and R. Sackstein, *Blood*, 2007, **109**, 1381–1386.
83 M. Kucia, K. Jankowski, R. Reca, M. Wysoczynski, L. Bandura, D. J. Allendorf, J. Zhang, J. Ratajczak and M. Z. Ratajczak, *J. Mol. Histol.*, 2004, **35**, 233–245.
84 M. Irigoyen, E. Anso, E. Martinez, M. Garayoa, J. J. Martinez-Irujo and A. Rouzaut, *Biochim. Biophys. Acta*, 2007, **1773**, 880–890.
85 L. Yao, O. Salvucci, A. R. Cardones, S. T. Hwang, Y. Aoki, M. De La Luz Sierra, A. Sajewicz, S. Pittaluga, R. Yarchoan and G. Tosato, *Blood*, 2003, **102**, 3900–3905.

86 M. B. Rookmaaker, M. C. Verhaar, H. C. de Boer, R. Goldschmeding, J. A. Joles, H. A. Koomans, H. J. Grone and T. J. Rabelink, *Am. J. Physiol.*, 2007, **293**, F624–630.
87 D. Irimia, G. Charras, N. Agrawal, T. Mitchison and M. Toner, *Lab Chip*, 2007, **7**, 1783–1790.
88 N. A. Peppas, Z. H. Hilt, A. Khademhosseini and R. Langer, *Adv. Mater. (Weinheim, Ger.)*, 2006, **18**, 1345–1360.
89 W. J. Rosoff, J. S. Urbach, M. A. Esrick, R. G. McAllister, L. J. Richards and G. J. Goodhill, *Nat. Neurosci.*, 2004, **7**, 678–682.
90 H. Becker and C. Gartner, *Anal. Bioanal. Chem.*, 2008, **390**, 89–111.
91 H. V. Fuentes and A. T. Woolley, *Anal. Chem.*, 2008, **80**, 333–339.
92 A. Prina-Mello, Ph.D. Thesis, Trinity College Dublin, 2003.
93 S. Y. Cheng, S. Heilman, M. Wasserman, S. Archer, M. L. Shuler and M. Wu, *Lab Chip*, 2007, **7**, 763–769.
94 T. J. Pucadyil and A. Chattopadhyay, *J. Fluoresc.*, 2005.
95 S. Jayaraman, N. S. Joo, B. Reitz, J. J. Wine and A. S. Verkman, *Proc. Natl. Acad. Sci. U. S. A.*, 2001, **98**, 8119–8123.
96 A. P. Golden and J. Tien, *Lab Chip*, 2007, **7**, 720–725.
97 B. A. Peeni, M. L. Lee, A. R. Hawkins and A. T. Woolley, *Electrophoresis*, 2006, **27**, 4888–4895.
98 S. Liang, J. Xu, L. Weng, H. Dai, X. Zhang and L. Zhang, *J. Controlled Release*, 2006, **115**, 189–196.
99 J. Gutenwik, B. Nilsson and A. Axelsson, *J. Chromatogr., A*, 2004, **1048**, 161–172.
100 S. Ramanujan, A. Pluen, T. D. McKee, E. B. Brown, Y. Boucher and R. K. Jain, *Biophys. J.*, 2002, **83**, 1650–1660.
101 V. Vickerman, J. Blundo, S. Chung and R. Kamm, *Lab Chip*, 2008, **8**.
102 L. Flaishon, G. Hart, E. Zelman, C. Moussion, V. Grabovsky, G. Lapidot Tal, S. Feigelson, R. Margalit, A. Harmelin, T. Avin-Wittenberg, D. Shoseyov, R. Alon, J. P. Girard and I. Shachar, *Blood*, 2008.
103 B. M. Gillette, J. A. Jensen, B. Tang, G. J. Yang, A. Bazargan-Lari, M. Zhong and S. K. Sia, *Nat. Mater.*, 2008, **7**, 636–640.
104 S. Lahooti and M. V. Sefton, *Cell Transplant*, 2000, **9**, 785–796.
105 H. Park, C. Cannizzaro, G. Vunjak-Novakovic, R. Langer, C. A. Vacanti and O. C. Farokhzad, *Tissue Eng.*, 2007, **13**, 1867–1877.
106 D. J. Beebe, J. S. Moore, J. M. Bauer, Q. Yu, R. H. Liu, C. Devadoss and B. H. Jo, *Nature*, 2000, **404**, 588–590.
107 J. M. Karp, F. Sarraf, M. S. Shoichet and J. E. Davies, *J. Biomed. Mater. Res., Part A*, 2004, **71**, 162–171.
108 J. Y. Jang, D. Y. Lee, S. J. Park and Y. Byun, *Biomaterials*, 2004, **25**, 3663–3669.
109 G. P. Raeber, M. P. Lutolf and J. A. Hubbell, *Biophys. J.*, 2005, **89**, 1374–1388.
110 J. Zhang, A. Skardal and G. D. Prestwich, *Biomaterials*, 2008, **29**, 4521–4531.
111 A. N. Buxton, J. Zhu, R. Marchant, J. L. West, J. U. Yoo and B. Johnstone, *Tissue Eng.*, 2007, **13**, 2549–2560.
112 S. Berski, J. van Bergeijk, D. Schwarzer, Y. Stark, C. Kasper, T. Scheper, C. Grothe, R. Gerardy-Schahn, A. Kirschning and G. Drager, *Biomacromolecules*, 2008, **9**, 2353–2359.
113 E. A. Cavalcanti-Adam, A. Micoulet, J. Blummel, J. Auernheimer, H. Kessler and J. P. Spatz, *Eur. J. Cell Biol.*, 2006, **85**, 219–224.
114 E. B. Walton, B. Oommen and K. J. Van Vliet, *Conf. Proc. IEEE Eng. Med. Biol. Soc.*, 2007, **2007**, 6419–6421.
115 D. G. Stupack, *Cell Death Differ.*, 2005, **12**, 1021–1030.
116 S. H. Zigmond, E. F. Foxman and J. E. Segall, *Curr. Protoc. Cell Biol.*, 2001, ch. 12, Unit 12 11.
117 R. Sackstein, *Curr. Opin. Hematol.*, 2005, **12**, 444–450.
118 K. A. Papadakis, *Curr. Allergy Asthma Rep.*, 2004, **4**, 83–89.
119 S. Mahalingam and G. Karupiah, *Immunol. Cell Biol.*, 1999, **77**, 469–475.
120 E. Bastida, L. Almirall, M. C. Bertomeu and A. Ordinas, *Int. J. Cancer*, 1989, **43**, 1174–1178.